

UC Santa Barbara

UC Santa Barbara Electronic Theses and Dissertations

Title

Advancing Control in Polymer Chemistry

Permalink

<https://escholarship.org/uc/item/8xv1r35x>

Author

Mattson, Kaila Marie

Publication Date

2016

Peer reviewed|Thesis/dissertation

University of California
Santa Barbara

Advancing Control in Polymer Chemistry

A dissertation submitted in partial satisfaction
of the requirements for the degree

Doctor of Philosophy
in
Chemistry

by

Kaila Marie Mattson

Committee in charge:

Professor Craig J. Hawker, Chair
Professor Javier Read de Alaniz
Professor Ram Seshadri
Professor Song-I Han

September 2016

The Dissertation of Kaila Marie Mattson is approved.

Professor Javier Read de Alaniz

Professor Ram Seshadri

Professor Song-I Han

Professor Craig J. Hawker, Committee Chair

September 2016

Advancing Control in Polymer Chemistry

Copyright © 2016

by

Kaila Marie Mattson

Dedicated to my incredible parents, Sharon and Gary Mattson.

Mom and Dad, thank you for everything. I love you!

Acknowledgements

First and foremost, I would like to extend my sincere gratitude to my advisor, Craig Hawker. I am deeply grateful for the opportunity to pursue my graduate research in his laboratory. Craig's vision and generosity are second to none. He has worked tirelessly to remove barriers and create an atmosphere of innovation and collaboration. By encouraging me to pursue diverse research topics and giving me the freedom to explore my own ideas, he has helped me become a well-trained and independent research scientist. Craig, I cannot thank you enough.

Ram, you have been simply amazing. From informally adopting me into your research group to teasing me about "The President," you have become more than a mentor – at this point, you're family. Thank you for the years of support, advice, and frequent check-ups that I am working hard enough. Thanksgiving won't be the same without you.

Javier, your patience and kindness are limitless. Thank you for teaching me organic chemistry and answering each of my seemingly infinite questions about reaction mechanisms. Your enthusiasm for science and dedication to mentoring are truly inspiring.

Song-I, thank you for the many helpful discussions and useful advice. When Allegra decided she wanted to gain experience in synthesis, you directed her to me. Thank you so much for facilitating that collaboration.

Thank you to the wonderful MRL staff. You keep things running like a well-oiled machine and are always willing to help. You are the reason I lovingly refer to my workplace as "Happy MRL Land." Thank you especially to Sylvia Vogel, Rachel Behrens, Samantha Cardillo, Jerry Hu, Joni Schwartz, Julie Standish, Dorothy Pak, Krystyna Brzezinska, Joe Doyle, and everyone else at the MRL.

To the Hawker group, thank you for making graduate school so fun. From scientific collaborations to many entertaining beer nights, you all have been fantastic. In particular, I'd like to thank Frank Leibfarth for helping me navigate the oftentimes murky waters of being a first year graduate student. I truly appreciate your patience and willingness to help. Max Robb and Brett Fors, your yin and yang mentoring styles helped me learn and improve. Thank you for being your wonderful selves. Alaina McGrath, thank you for helping me through some of my toughest stretches in graduate school. I appreciate not only your scientific advice, but also your continued friendship. Jetsuda Areephong, thank you for making the three-weeks we spent in the middle of winter in Midland, Michigan such a blast. A special thanks to Will(a) Gutekunst for his advice on both chemistry and beer alike.

During my tenure in the Hawker Group, I benefited from working alongside so many fun and gifted individuals, including Hazel and Johannes Sprafke, SangHo Lee, Emre Discekici, Sarah and David Lunn, Daniel Klinger, Jason Spruell, Yingdong Luo, Nate Lynd, Saemi Oh, Edward Toumayan, Brenden McDearmon, Cynthia Wang, Eric Pressly, and many others. Thank you all for making my life at UCSB so enjoyable.

I have had the great privilege to work with numerous talented undergraduate students. I am thankful for the time I spent with all of them. I consider myself extremely fortunate to have worked with both Allegra Latimer and Andy Hsueh for well over a year each. Allegra and Andy, you are two of the sweetest and most dedicated people I could have ever hoped to mentor. While I taught you, thank you for also teaching me.

Though I graduated years ago, I am forever grateful to my University of South Alabama Chemistry "family." Their willingness to go above and beyond the call of duty continues to impress and inspire me. In particular, thank you to James Davis, Richard O'Brien, Arsalan Mirjafari, Alexandra Stenson, David Forbes, and Robert Barletta.

Jake, though you will inevitably call me “Rd.” instead of “Dr.” and continue chastising me for not discovering a way for you to teleport (which I still argue is unreasonably far beyond the scope of polymer chemistry), I know you always have my back. Thank you for being a fantastic big brother. Your ability to bring levity to any situation and willingness to do anything for a laugh are truly remarkable. We tease each other mercilessly, but I hope you know how much I love you and appreciate all the guidance and support you’ve provided me throughout the years. The next time you come visit, I promise I’ll try not to shatter my nose on a surfboard within 12 hours of your arrival.

Christian, though we’ve been together for years, your infectious smile, kind eyes, and silly antics continue to give me butterflies. Thank you for encouraging me to pursue my dreams and for supporting me every step of the way. Each day, without even trying, you make me a better person. Your sincerity is unrivaled, and I consider myself truly blessed to know you. As we embark on the next stage of our respective careers, there are many unknowns. However, of this I am certain — there is no one I would rather have by my side. I look forward to tackling life with you. *Ich liebe dich mein Christian.*

Lastly, it is my great privilege to acknowledge my absolutely incredible parents. Mom and Dad, I dedicate this thesis to you. I could not and would not be where I am without your constant support, endless encouragement, and unconditional love. Throughout my life, you’ve led by example. You taught me to always give my best effort, persevere through adversity, surround myself with good people, remain humble, and to find joy and humor in everything. Your love knows no bounds. Thank you for being not only my parents, but also my biggest role models and best friends. I love you!

Kaila Marie Mattson

Curriculum Vitæ

RESEARCH SUMMARY I am working at the interface of organic and polymer chemistry to develop design principles for the synthesis of well-defined macromolecular architectures both in solution and on surfaces.

EDUCATION **University of California, Santa Barbara**, Santa Barbara, CA
Ph.D., Chemistry **September 2016**
• Advisor: Prof. Craig J. Hawker

University of South Alabama, Mobile, AL
B.Sc., Chemistry **May 2011**
• *Magna cum laude*, with University Honors
• Minor in general business

HONORS AND AWARDS

- Denice Denton Emerging Leaders Workshop (invitation-only workshop) 2016
- Materials Research Laboratory Outreach Award 2014–2015
- Dow Materials Institute Travel Fellowship 2013, 2015
- Robert H. DeWolfe Outstanding Teaching Assistant in Organic Chemistry Fellowship 2012–2015
- NSF Graduate Research Fellowship 2011–2014
- NSF ConvEne IGERT Associate 2012–2013
- Mortar Board Foundation National Fellowship 2011
- Barry M. Goldwater Scholarship 2010
- University of South Alabama Presidential Scholarship 2007–2011
- Federal Robert C. Byrd Honors Scholarship 2007–2011
- Distinguished Young Woman of Wisconsin 2007

PROFESSIONAL EXPERIENCE **University of California, Santa Barbara**, Santa Barbara, CA
Graduate Research Assistant **September 2011–present**
• Advisor: Prof. Craig J. Hawker
• Synthesis of polymers with controlled architecture and functionality

BASF, Ludwigshafen, Germany
BASF International Summer Course **August 2016**
• Selected to participate in the 131st BASF International Summer Course

The Dow Chemical Company, Midland, MI

High Throughput Campaign

December 2013

- Dow host and collaborator: Dr. John W. Kramer
- Investigated new mediators for controlled radical polymerizations

University of South Alabama, Mobile, AL

Undergraduate Research Assistant

September 2007–May 2011

- Advisor: Prof. James H. Davis, Jr.
- Design and elucidation of structure-property relationships in lipid-inspired ionic liquids

Ruhr-Universität Bochum, Bochum, Germany

Visiting Researcher

May 2010–June 2010

- Supervisor: Prof. Anja-Verena Mudring
- Synthesis and characterization of ionic liquid crystals

Friedrich-Alexander-Universität Erlangen-Nürnberg, Erlangen, Germany

Visiting Researcher

June 2010–August 2010

- Supervisor: Prof. Peter Wasserscheid
- Improved synthetic routes toward ionic liquid precursors

PUBLICATIONS

- [14] **K. M. Mattson**, C. W. Pester, W. R. Gutekunst, A. T. Hsueh, E. H. Discekici, Y. Luo, B. V. K. J. Schmidt, A. J. McGrath, P. G. Clark, C. J. Hawker, Metal-free removal of polymer chain ends using light. *Macromolecules* **2016**, in press.
- [13] C. W. Pester, B. Narupai, **K. M. Mattson**, D. P. Bothman, D. Klinger, K. W. Lee, E. H. Discekici, C. J. Hawker, Engineering surfaces through sequential stop-flow photopatterning. *Adv. Mater.* **2016**, in press.
• Published as VIP article (“Very Important Paper”) (top 5%)
- [12] S. O. Poelma, G. L. Burnett, E. H. Discekici, **K. M. Mattson**, N. J. Treat, Y. Luo, Z. H. Hudson, S. L. Shankel, P. G. Clark, J. W. Kramer, C. J. Hawker, J. Read de Alaniz, Chemoselective radical dehalogenation and C–C bond formation on aryl halide substrates using organic photoredox catalysts. *J. Org. Chem.* **2016**, *81*, 7155–7160.
- [11] E. H. Discekici, C. W. Pester, N. J. Treat, J. Lawrence, **K. M. Mattson**, B. Narupai, E. P. Toumayan, Y. Luo, A. J. McGrath, P. G. Clark, J. Read de Alaniz, C. J. Hawker, Simple benchtop approach to polymer brush nanostructures using visible-light-mediated metal-free atom transfer radical polymerization. *ACS Macro Lett.* **2016**, *5*, 258–262.
- [10] J. Areephong, **K. M. Mattson**, N. J. Treat, S. O. Poelma, J. W. Kramer, H. A. Sprafke, A. A. Latimer, J. Read de Alaniz, C. J. Hawker, Triazine-mediated controlled radical polymerization: New unimolecular initiators. *Polym. Chem.* **2016**, *7*, 370–374.

- [9] **K. M. Mattson**, A. A. Latimer, A. J. McGrath, N. A. Lynd, P. Lundberg, Z. M. Hudson, C. J. Hawker, A facile synthesis of catechol-functionalized poly(ethylene oxide) block and random copolymers. *J. Polym. Sci., Part A: Polym. Chem.* **2015**, *53*, 2685–2692.
- [8] E. H. Discekici, N. J. Treat, S. O. Poelma, **K. M. Mattson**, Z. H. Hudson, Y. Luo, C. J. Hawker, J. Read de Alaniz, A highly reducing metal-free photoredox catalyst: Design and application in radical dehalogenations. *Chem. Commun.* **2015**, *51*, 11705–11708.
- [7] J. K. Sprafke, J. M. Spruell, **K. M. Mattson**, D. Montarnal, A. J. McGrath, R. Pötzsch, D. Miyajima, J. Hu, A. A. Latimer, B. I. Voit, T. Aida, C. J. Hawker, Revisiting thiol-yne chemistry: Selective and efficient monoaddition for block and graft copolymer formation. *J. Polym. Sci., Part A: Polym. Chem.* **2015**, *53*, 319–326.
- [6] R. A. O'Brien, A. Mirjafari, **K. M. Mattson**, S. M. Murray, N. Mobarrez, E. A. Salter, A. Wierzbicki, J. H. Davis, K. N. West, The effect of sulfur position on the melting points of lipidic 1-methyl-3-thiaalkylimidazolium ionic liquids. *J. Phys. Chem. B* **2014**, *118*, 10232–10239.
- [5] R. A. O'Brien, C. W. West, B. E. Hollingsworth, A. C. Stenson, C. B. Henderson, A. Mirjafari, N. Mobarrez, K. N. West, **K. M. Mattson**, E. A. Salter, A. Wierzbicki, J. H. Davis, A simple and rapid route to novel tetra(4-thiaalkyl)ammonium bromides. *RSC Adv.* **2013**, *3*, 24612–24617.
- [4] F. A. Leibfarth, **K. M. Mattson**, B. P. Fors, H. A. Collins, C. J. Hawker, External regulation of controlled polymerizations. *Angew. Chem. Int. Ed.* **2012**, *52*, 199–210.
- [3] A. Mirjafari, R. A. O'Brien, S. M. Murray, **K. M. Mattson**, N. Mobarrez, K. N. West, J. H. Davis, Lipid-inspired ionic liquids containing long-chain appendages: Novel class of biomaterials with attractive properties and applications. In: *Ionic Liquids: Science and Applications*. **January 1, 2012**, 199–216. (Peer-reviewed book chapter.)
- [2] S. M. Murray, R. A. O'Brien, **K. M. Mattson**, C. Ceccarelli, R. E. Sykora, K. N. West, J. H. Davis, The fluid-mosaic model, homeoviscous adaptation, and ionic liquids: Dramatic lowering of the melting point by side-chain unsaturation. *Angew. Chem. Int. Ed.* **2010**, *49*, 2755–2758.
- Highlighted in C&E News, “New chains for ionic liquids.”
Chem. Eng. News, **2010**, 88 (11), p 11.
- [1] T. Rüter, T. D. Huynh, J. Huang, A. F. Hollenkamp, E. A. Salter, A. Wierzbicki, **K. M. Mattson**, A. Lewis, J. H. Davis, Stable cycling of lithium batteries using novel boronium-cation-based ionic liquid electrolytes. *Chem. Mater.* **2010**, *22*, 1038–1045.

**INTELLECTUAL
PROPERTY**

- [1] **K. M. Mattson**, C. J. Hawker, C. W. Pester, W. R. Gutekunst, B. V. K. J. Schmidt, “Catalytic polymer modification.” U.S. Patent Application No. 62/363552, filed July 18, 2016.

**INVITED
LECTURES AND
PRESENTATIONS**

- [6] K. M. Mattson, C. J. Hawker, Bioinspired “sticky” polyethers. **Materials Research Outreach Program**, Santa Barbara, CA; February 2016.
- [5] K. M. Mattson, C. J. Hawker, Engineering functional polymers by controlled radical polymerization. **University of Texas at El Paso–Partnership for Research and Education in Materials (UTEP–PREM)/UCSB Workshop on Materials Chemistry**, Santa Barbara, CA; November 2015.
- [4] K. M. Mattson, C. J. Hawker, Facile synthesis of catechol-functionalized polyethers: Development and applications. **Jackson State University**, Jackson, MS; July 2015.
- [3] K. M. Mattson, B. F. Fors, J. E. Poelma, C. J. Hawker, Turning polymerizations “on” and “off” using visible light: Developments and applications. **California State Polytechnic University Pomona**, Pomona, CA; May 2014.
- [2] K. M. Mattson, B. F. Fors, C. J. Hawker, Frontiers in polymer chemistry: Externally regulated polymerizations. **University of South Alabama**, Mobile, AL; March 2014.
- [1] K. M. Mattson, C. J. Hawker, Lessons from the other side: Planning and preparation for graduate school. **University of South Alabama**, Mobile, AL; March 2014.

**CONFERENCE
CONTRIBUTIONS**

- [6] K. M. Mattson, A. A. Latimer, A. J. McGrath, N. A. Lynd, P. Lundberg, Z. M. Hudson, C. J. Hawker, A facile synthesis of catechol-functionalized poly(ethylene oxide) block and random copolymers. **The 251st ACS National Meeting**, San Diego, CA, March 2016; *Oral Presentation*.
- [5] K. M. Mattson, J. Areephong, S. O. Poelma, J. W. Kramer, J. Read de Alaniz, C. J. Hawker, Controlling radical polymerizations using next-generation triazine-based unimolecular initiators. **Edward J. Kramer Memorial Symposium**, Santa Barbara, CA, January 2016; *Poster Presentation*.
- [4] K. M. Mattson, J. Areephong, N. J. Treat, S. O. Poelma, J. W. Kramer, H. A. Sprafke, J. Read de Alaniz, C. J. Hawker, Triazine-mediated controlled radical polymerization: New unimolecular initiators. **Polymers Gordon Research Conference**, Mount Holyoke, MA, June 2015; *Poster Presentation*.
- [3] K. M. Mattson, J. Areephong, N. J. Treat, S. O. Poelma, J. W. Kramer, H. A. Sprafke, J. Read de Alaniz, C. J. Hawker, Introducing new mediators for controlled radical polymerizations: Triazine-based unimolecular initiators. **The 248th ACS National Meeting**, San Francisco, CA, August 2014; *Poster Presentation*.

[2] K. M. Mattson, J. Heo, T. Kang, S. G. Jang, D. S. Hwang, E. P. Toumayan, K. Killops, H. Waite, C. J. Hawker, A facile and efficient strategy for the preparation of marine-inspired wet adhesive materials using protected catechol-functionalized polymers. **Polymers Gordon Research Conference**, Mount Holyoke, MA, June 2013; *Poster Presentation*.

[1] K. M. Mattson, R. A. O'Brien, A. Mirjafari, J. L. McDonald, S. M. Murray, M. La, K. N. West, J. H. Davis, Thiol-ene coupling reactions as a method to prepare functionalized ionic liquids. **The 4th International Congress on Ionic Liquids (COIL-4)**, Washington, D.C., June 2011; *Poster Presentation*.

MENTORSHIP: **Andy Hsueh** **January 2015–April 2016**
UNDERGRADUATE STUDENTS

- UCSB Honors Chemistry Program
- Research Internships in Science and Engineering (RISE)

Allegra Latimer **January 2013–June 2014**

- UCSB Honors Chemistry Program
- McNair Scholars Program
- Research Internships in Science and Engineering (RISE)

Currently a graduate student at Stanford University

Andrea Rivas **Summer 2013**

- Summer Applied Biotechnology Research Experience (SABRE)

Currently an Associate Development Engineer at AdvanDx

Adrian Figg **Fall 2012**

- UCSB Honors Chemistry Program

Currently a graduate student at the University of Florida

TEACHING EXPERIENCE

University of California, Santa Barbara, Santa Barbara, CA

Co-Lecturer **Fall 2015**

- CHEM 285: Synthetic Chemistry of Macromolecules
 - Graduate-level course in polymer synthesis
 - Main instructor: Prof. Craig J. Hawker

Teaching Assistant **Spring 2013**

- CHEM 2AL: Organic Chemistry Laboratory (II)

Teaching Assistant **Winter 2012**

- CHEM 1BL: General Chemistry Laboratory (II)

Teaching Assistant **Fall 2012**

- CHEM 1AL: General Chemistry Laboratory (I)

**SERVICE AND
OUTREACH
ACTIVITIES**

2016 Johns Hopkins Center for Talented Youth: Family Academic Programs
“Engineering Next Generation Materials”

- Hosted a workshop for students and their parents introducing them to soft matter and polymeric materials.

2015 UCSB Materials Research Laboratory Science Teacher Workshop

“No child left out of STEM: STEM and NGSS for Science Teachers”

- Hosted a workshop introducing approximately 80 junior high and high school teachers to polymer chemistry and recent advances in controlled radical polymerizations.

Dow-UCSB Safety Initiative

- Attended a two-day safety workshop at Dow Chemical in Midland, Michigan and spearheaded the formation of an interdepartmental team of graduate students, postdoctoral researchers, and faculty members who work together to develop departmental safety programs.
- Highlighted in C&E News, “Dow Chemical teams up with universities on laboratory safety”
Chem. Eng. News, **2012**, 90 (44) pp 21–23.

Graduate Students for Diversity in Science (GSDS), UCSB

- Participated in this student organization committed to recognizing and promoting diversity in the sciences through lectures series, outreach programs, and policy considerations. (2012–present)

“It’s a Material World!” Elementary School Outreach

- Participated in numerous workshops focused on engaging students and their parents in learning through hands-on activities highlighting Materials Science. (2012–present)

“Build a Buckyball” Workshop

- Volunteered with multiple workshops for K-12 students in which we helped them discover the beauty of molecules and the relationships between molecular structures and properties by helping them build their own six-inch Buckminsterfullerene (Buckyball) molecular model.

UCSB Materials Research Outreach Program (MROP) Symposium

- Organized and planned a poster session at both the 2012 and 2015 MROP Symposia in Santa Barbara, showcasing the work of over 40 graduate students and postdoctoral fellows in diverse fields of study.

Abstract

Advancing Control in Polymer Chemistry

by

Kaila Marie Mattson

Controlling molecular weight, architecture, and comonomer incorporation in polymers is of paramount importance for the preparation of functional materials. This dissertation will highlight the development of three strategies that improve control in macromolecular synthesis, ranging from initial polymerization to macromolecular post-modification.

Controlled radical polymerization is a well-established platform for macromolecular engineering. However, many techniques require metal or sulfur additives and yield macromolecules with chain ends that are chemically reactive and thermally unstable. This dissertation presents a light-mediated method for the removal of such end groups, which is effective for a variety of chain ends as well as polymer families, both in solution and with spatial control on surfaces. Polymers with improved thermal and chemical stability can now be obtained under mild, metal-free conditions and with external regulation.

To circumvent the presence of such reactive chain ends altogether, triazine-based unimolecular initiators were developed. These metal- and sulfur-free mediators are shown to control the radical polymerization of several monomer classes.

Generally, the distribution of functional groups throughout the macromolecular backbone is important for numerous applications. An efficient and high-yielding strategy for the functionalization of well-defined polyethers is described herein. By controlling both the number and location of underwater adhesive catechol groups, these biomimetic macromolecules may facilitate future insights into the mechanics of mussel and underwater adhesion, and related antifouling materials.

Contents

Dedication	iv
Acknowledgements	v
Curriculum Vitae	viii
Abstract	xiv
1 Introduction	1
1.1 Radical Chain Polymerization	1
1.1.1 Challenges of Radical Polymerization	3
Inability to Achieve Targeted Molecular Weights	3
Limited Architectural Control	4
1.2 Controlled Radical Polymerization	5
1.2.1 Nitroxide Mediated Polymerization	6
1.2.2 Reversible Addition-Fragmentation Chain Transfer Polymerization	7
1.2.3 Atom Transfer Radical Polymerization	8
1.2.4 Surface-Initiated Controlled Radical Polymerization	9
1.3 Externally Regulated Polymerization	10
1.4 “Living” Anionic Polymerization	11
1.5 Post-Polymerization Functionalization	12
2 Metal-Free Removal of Polymer Chain Ends Using Light	15
2.1 Abstract	15
2.2 Introduction	16
2.3 Solution Dehalogenations	17
2.3.1 Impact on Thermal Stability	19
2.3.2 Extension to Other Polymer Systems	20
2.4 Surface Dehalogenations	21
2.4.1 Uniform Dehalogenation of Surface-Tethered Monolayers	22
2.4.2 Spatially Controlled Dehalogenation of Monolayers	23
2.4.3 Spatially Controlled Dehalogenation of Polymer Brushes	24

2.5	Conclusion	25
2.6	Experimental	25
2.6.1	Materials	25
2.6.2	General Analytical Information	26
2.6.3	Light Sources	27
2.6.4	Methods	27
2.7	Supplemental Results	33
2.7.1	Demonstration of the Necessity of Both Light and PTH	33
2.7.2	Debromination of Poly(<i>tert</i> -butyl acrylate)-Br	35
2.7.3	Dehalogenation of Polystyrene-Cl	36
2.7.4	Removal of RAFT Chain End	37
3	Triazine-Mediated Controlled Radical Polymerization	38
3.1	Abstract	38
3.2	Introduction	39
3.3	Results and Discussion	41
3.3.1	Polymerization of Styrene	43
3.3.2	Demonstrations of Chain End Fidelity	45
3.3.3	Functional Group Tolerance — Copolymerizations	47
3.4	Conclusion	49
3.5	Experimental	50
3.5.1	Materials and Equipment	50
3.5.2	General Procedure for the Preparation of Benzoyl Hydrazine 1(a-c)	50
3.5.3	General Procedure for the Preparation of Benzohydrazonoyl Chloride 2(a-c)	52
3.5.4	General Procedure for the Preparation of Benzo-1,2,4-triazinyl Radical 3(a-c)	53
3.5.5	General Procedure for the Preparation of Triazine Unimolecular Initiators 4(a-c)	55
3.5.6	General Procedure for Styrene Polymerization	58
4	Catechol-Functionalized Polyethers	63
4.1	Abstract	63
4.2	Introduction	64
4.3	Results and Discussion	65
4.3.1	“Clickable” Catechols	65
4.3.2	Small Molecule Characterization	67
4.3.3	Early Studies — Small Molecule Optimization	69
4.3.4	Synthesis of Polyethers	71
4.3.5	Polymer Functionalization	72
4.4	Conclusion	75

4.5	Experimental	75
4.5.1	Materials	75
4.5.2	Instrumentation	76
4.5.3	Methods	76
4.5.4	Representative Procedure for Synthesis of Triblock Copolymers	79
4.5.5	Representative Procedure for Thiol-ene Coupling of Catechols to Copolymers	81
4.5.6	Representative Procedure for Deprotecting Catechol-Functionalized Polymers	83
	Appendix	83
A	External Regulation of Controlled Polymerizations	84
B	Revisiting Thiol-yne Chemistry: Selective and Efficient Monoaddition for Block and Graft Copolymer Formation	97
C	A Highly Reducing Metal-Free Photoredox Catalyst: Design and Application in Radical Dehalogenations	106
D	Simple Benchtop Approach to Polymer Brush Nanostructures Using Visible-Light-Mediated Metal-Free Atom Transfer Radical Polymeriza- tion	111
E	Chemoselective Radical Dehalogenation and C–C Bond Formation on Aryl Halide Substrates Using Organic Photoredox Catalysts	117
F	Engineering Surfaces Through Sequential Stop-Flow Photopatterning	124

Chapter 1

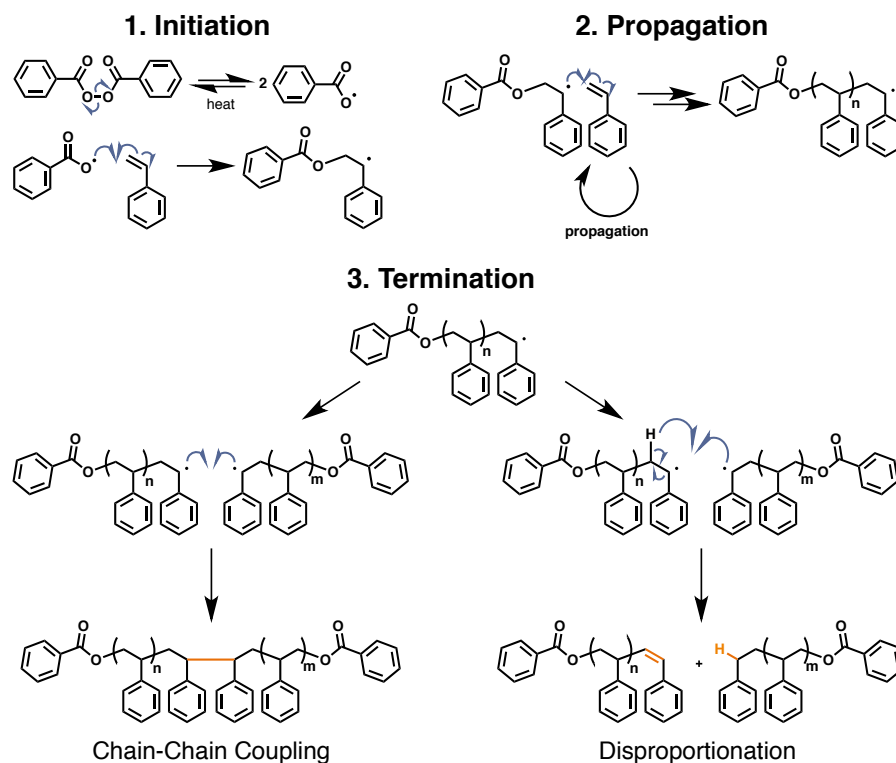
Introduction

1.1 Radical Chain Polymerization

Polymers are omnipresent in today’s society. Each year, an estimated 200 million tons of synthetic polymers are produced worldwide.^[1] These materials percolate through our lives in both obvious (plastic bags, packaging materials, and rubber tires) and more subtle (additives in medication, dental fillings, and insulating wiring coatings) ways. Macromolecules can be synthesized by either “step growth”[‡] or “chain growth” mechanisms.^[2] An example for chain growth is radical polymerization, which accounts for approximately 40–50% of all synthetic polymers produced.^[3]

An exemplary mechanism for the radical polymerization of styrene is shown in Scheme 1. The process can be dissected into three key steps: initiation, propagation, and termination.^[2] The most common method to generate initiating radicals is the homolytic dissociation of the initiator species, which yields two short-lived and highly reactive radicals. Approximately 1 ms after formation, this radical will react with a nearby species,

[‡]Step growth polymerizations, also called condensation polymerizations, inherently yield polymers with broad molecular weight distributions and are therefore not addressed in this dissertation. Readers are directed to Odian’s *Principles of Polymerization*^[2] for further details of the step growth mechanism.



Scheme 1 Representative mechanism for the radical polymerization of styrene using the thermal radical initiator benzoyl peroxide.

in most instances, a monomer. Addition of monomer (propagation) is repeated until the polymer chain is terminated by recombination (chain-chain coupling) or disproportionation (Scheme 1). Termination occurs approximately one second after initiation.^[1,2,4]

There following are general characteristics of *uncontrolled* radical polymerization:^[1,2,5]

1. Initiation is slow and happens continuously throughout the polymerization.
2. Chain propagation is rapid. After initiation, high molecular weight species are formed almost instantaneously (see Figure 1.1).
3. Termination rates are diffusion-controlled and occur approximately one second after initiation.

4. Once a polymer chain has been terminated, there is very limited possibility for re-initiation or introduction of chain end functionality.

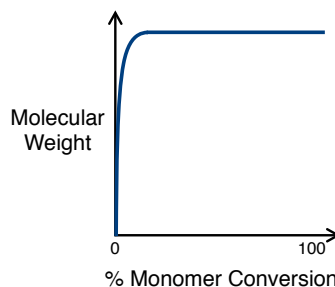


Figure 1.1 In radical polymerization, high molecular weight polymers are formed almost immediately. Despite increasing monomer conversion over time, molecular weight remains relatively unchanged.

1.1.1 Challenges of Radical Polymerization

Though a powerful and industrially employed technique, traditional radical polymerizations suffer from various drawbacks that limit the design of materials properties.

Inability to Achieve Targeted Molecular Weights

Most of the hallmark properties of polymeric materials arise from the polymers' large sizes. A classic example is the relationship between polymer molecular weight and mechanical strength (Figure 1.2). Mechanical strength initially rises rapidly with molecular weight. However, above a certain threshold, there are diminishing returns and marginal improvements in mechanical strength are accompanied by dramatic increases in viscosity, processability challenges, and processing costs.^[2,6] Thus, the ability to target specific molecular weights is considered highly advantageous for scientists and industrial manufacturers alike.

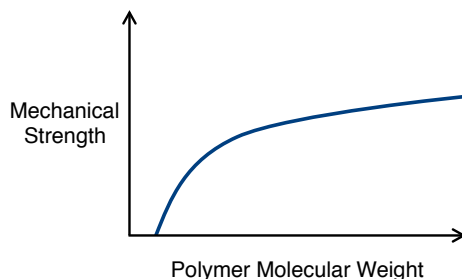


Figure 1.2 Mechanical strength increases with polymer molecular weight. Figure adapted from Reference 2 © 2004 John Wiley & Sons, Inc.

Limited Architectural Control

An impressive array of macromolecular properties is accessible through a very diverse scope of monomers. 100 million tons of polymers are produced annually with “thousands of different compositions” using radical polymerization.^[5] However, radical polymerization has very limited ability to produce macromolecules with targeted architecture or specific monomer sequence — two features that can have dramatic effects on physical properties.

One example for such advanced architectures are block copolymers, which are comprised of two or more covalently linked macromolecules. By joining polymers of disparate physical and chemical properties, materials with new and useful attributes can be designed.^[7-9] For example, poly(styrene-*b*-1,3-butadiene-*b*-styrene) (SBS) is an elastomer found in consumer products ranging from the rubber soles of shoes to automobile tires.^[10,11] The incompatibility of the blocks results in microphase separation, creating a thermoplastic elastomer which merges the flexibility of polybutadiene with the mechanical toughness of polystyrene. Vital to the preparation of such block copolymer materials is the ability to (1) sequentially add a second monomer to a polymerization after the first monomer has been consumed, (2) re-initiate a previously grown homopolymer in the presence of a second, different monomer, or (3) perform post-polymerization modifica-

tion (e.g. to facilitate polymer coupling). Traditional uncontrolled radical polymerization offers none of these benefits.

1.2 Controlled Radical Polymerization

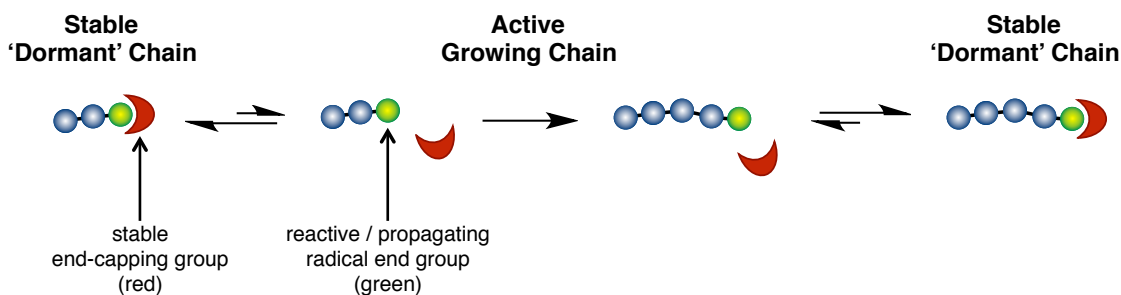


Figure 1.3 In general, most methods for establishing control in radical polymerizations involve reversible activation of growing polymer chain ends, with the equilibrium shifted heavily towards the dormant state. The low concentration of propagating radicals limits the probability of bimolecular termination reactions.

The attempt to address the aforementioned challenges led to the development of controlled radical polymerization (CRP).^[12] Gaining control over the polymerization process is generally achieved by reducing the concentration of (propagating) radicals to minimize termination reactions (Figure 1.3). A number of CRP techniques have been developed that all follow the same basic principle: introduction of a stable, inactive (“dormant”) state that is non-propagating. It reduces the effective radical concentration and thereby suppresses bimolecular termination events (Scheme 1).^[2]

A majority of become propagating species become “active” at the same time through **fast and quantitative initiation**. A mediating species promptly **reversibly deactivates these propagating radicals**. The exchange between active and inactive states is rapid, with the equilibrium shifted heavily towards the inactive state. Once re-activated, and throughout the polymerization process, propagating chains grow at approximately the same linear rate (Figure 1.4). This *linear relationship between monomer conver-*

sion and polymer size is a hallmark of CRP, and demonstrates the concentration of propagating radicals remains constant throughout the polymerization. It also facilitates production of macromolecules with targeted molecular weights (cf. Figure 1.1). The dynamic equilibrium between active and dormant states is predicated upon **retention of active/mediating polymer chain ends** throughout the reaction. These chain ends not only allow for controlled polymerization, but also allow for subsequent functionalization and chain-extension to form block copolymers.^[2] Overall, the combination of fast initiation, constant radical concentration, and minimal termination events means that nearly all propagating chains have similar lifetimes, yielding macromolecules with a *narrow distribution of molecular weights*.

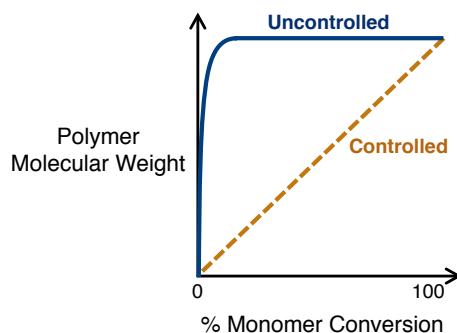


Figure 1.4 Polymer molecular weight versus monomer conversion for traditional free radical polymerization (solid blue line) and controlled radical polymerization (dashed orange line).

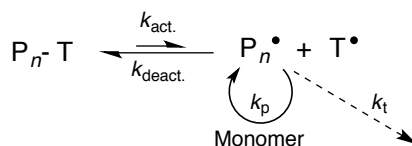
The three most commonly used CRP techniques: Nitroxide mediated polymerization (NMP),^[13] atom transfer radical polymerization (ATRP),^[14,15] and reversible addition-fragmentation chain transfer (RAFT)^[16] polymerization will be discussed in the following.

1.2.1 Nitroxide Mediated Polymerization

Nitroxide mediated polymerization was the first reported CRP, and provides control by utilizing a stable nitroxide radical to reversibly cap and deactivate growing polymer

chain.^[17,18] Initially requiring two components (a radical initiator and a stable radical), Hawker revolutionized the technique in 1994 by combining them into one elegant species.^[13] Upon thermal activation, each unimolecular initiator dissociates into one initiating radical and one stable radical (T^\bullet). This makes NMP the most operationally simple CRP, requiring only monomer and a unimolecular initiator.^[19] It is important to note that the stable radical is not capable of initiating polymerization itself. Instead, it helps maintain a low reactive radical concentration by reversibly deactivating growing polymer chains (P_n^\bullet) (see Scheme 2).

Compared to ATRP and RAFT, NMP benefits from avoiding metal or sulfur-containing agents, but suffers from limited monomer scope.^[20] In an attempt to address this challenge, metal- and sulfur-free triazine-based unimolecular initiators were developed within the framework of this dissertation (**Chapter 3**).



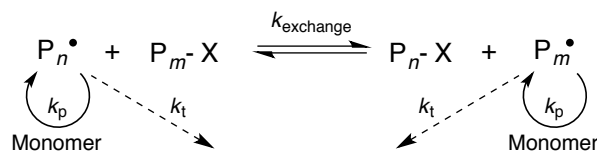
Scheme 2 Schematic representation of the mechanism for nitroxide mediated polymerization. The stable radical (T^\bullet) reversibly deactivates the growing polymer chain end (P_n^\bullet). Reproduced from Reference 21 © 2005, with permission from Elsevier.

1.2.2 Reversible Addition-Fragmentation Chain Transfer Polymerization

First reported in 1998,^[16] RAFT requires (in addition to monomer) both a separate radical source, e.g. azobisisobutyronitrile (AIBN), as well as a chain transfer agent, generally in the form of a thiocarbonylthio compound (commonly referred to as a RAFT agent).^[22] Selection of this RAFT agent is crucial, as its structure dictates the poly-

merization kinetics and the products' molecular weight distribution. Control is realized through a combination of (1) low radical concentration and (2) reversible trapping and transfer of propagating radicals (Scheme 3). In a two-step addition-fragmentation process, propagating radicals (P_n^\bullet) are first "trapped" through addition to the RAFT agent (X), forming an intermediate radical which subsequently fragments, yielding a RAFT-capped polymer (P_n-X) and a new propagating radical (P_m^\bullet). The diversity of commercially available and synthetically accessible RAFT agents makes this one of the most versatile CRP techniques.

However, the use of thiocarbonylthio groups as chain ends produces macromolecules that are often highly colored or can degrade and produce unpleasant odors (thiols). As a result, the transformation of RAFT chain ends to more stable groups has been the source of extensive research.^[23] **Chapter 2** presents a novel, externally regulated, and mild method for their complete removal.

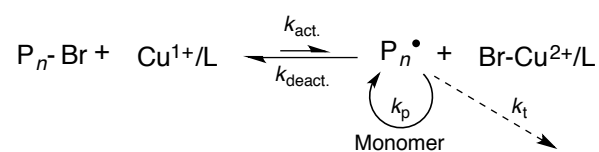


Scheme 3 Schematic representation of the mechanism of reversible addition-fragmentation chain transfer (RAFT) polymerization, in which "X" is a RAFT agent, P_n^\bullet and P_m^\bullet are propagating radicals, k_p is the rate of monomer addition, and k_t is the rate of bimolecular termination. Reproduced from Reference 21 © 2005, with permission from Elsevier.

1.2.3 Atom Transfer Radical Polymerization

Atom transfer radical polymerization was independently discovered by Sawamoto^[15] and Matyjaszewski^[14] in 1995, and is arguably the most complex CRP technique.^[4,5] ATRP requires (in addition to solvent and polymerizable monomer) an alkyl-halide initiator, a redox-active transition metal (commonly copper, Cu), and a ligand (L) to sol-

utilize the metal and form a catalyst complex.^[4] As shown in Scheme 4, a transition metal complex in its lower oxidation state (Cu^{1+}/L) undergoes a one-electron oxidation process and abstracts a halogen atom from the dormant species ($\text{P}_n\text{-Br}$), yielding a propagating radical ($\text{P}_n\bullet$), and a halide anion coordinated to the higher oxidation state metal complex ($\text{Br-Cu}^{2+}/\text{L}$). This reversible oxidation/reduction of the transition metal allows the bromines to reversibly cap radical chain ends.



Scheme 4 Schematic representation of the mechanism of atom transfer radical polymerization (ATRP) using one of the most common transition metal catalysts, CuBr and a ligand (L). Adapted from Reference 21 © 2005, with permission from Elsevier.

ATRP's broad monomer scope and use of commercially available, inexpensive reagents is in direct contrast to NMP and RAFT, which both require more specialized mediating agents. However, its adoption into more widespread industrial applications has been limited by difficulties associated with metal contamination.^[6,12] Significant efforts have been expended towards reducing the amount of transition metal catalyst needed during polymerization and completely removing it from polymers thereafter,^[24-27] leading to the development of metal-free ATRP in 2014.^[28,29]

1.2.4 Surface-Initiated Controlled Radical Polymerization

Surface-tethered macromolecules (polymer brushes) are used to modify the properties of surfaces. They are formed either by immobilizing macromolecules onto a substrate (i.e. a "grafting-to" approach) or by polymerizing monomers directly from surface-tethered initiators (i.e. "growing-from").^[30,31] Though nearly all CRP techniques have been adapted

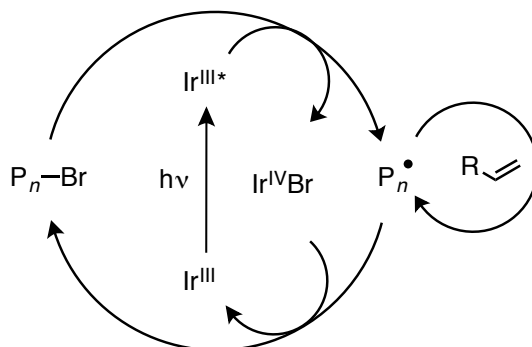
to surfaces, this dissertation will deal exclusively with surface-initiated ATRP (SI-ATRP) (**Chapter 2** and **Appendix D**).^[30–37]

1.3 Externally Regulated Polymerization

Although CRP facilitates preparation of polymers with targeted size, composition, and architecture, there is little opportunity to “pause” the reaction once a polymerization has begun. Gaining the ability to turn polymerizations *both* “on” and “off” has recently been the subject of significant research. The reader is referred to **Appendix A: External Regulation of Controlled Polymerizations**^[38] for an overview of progress and remaining challenges in the field.

Indeed, in a 2012 seminal report, Fors and Hawker extended the CRP platform to include temporal control.^[39] They demonstrated visible light-mediated CRP of methyl methacrylate using a commercially available *fac*-[Ir(ppy)₃] catalyst. Unlike previous reports in which only the initiation step was mediated by light, this process offered photocontrol over each step in the polymerization (Scheme 5).^[40] Visible light irradiation induces an excited state, *fac*-[Ir(ppy)₃]*, which reduces the alkyl bromide initiator (or polymer chain end), generating a reactive radical and a highly oxidizing Ir^{IV}Br complex. The latter subsequently reacts with the radical to regenerate the initial *fac*-[Ir(ppy)-₃] complex and return the polymer chain end to its dormant state. Upon removal of the light source, all radicals are efficiently and rapidly returned to their stable, inactive state.^[39] The useful ability to modulate both wavelength and intensity of light has led to the adoption of light-mediation by nearly every CRP technique.^[3,40–45]

Both conventional and light-mediated ATRP techniques have been successfully translated to surfaces.^[32,34,37,46,47] The use of light as an external regulator facilitates production of patterned surfaces by irradiation through photomasks. However, preparation of



Scheme 5 Proposed mechanism of light-mediated polymerization. Reproduced from Reference 39 © 2012 WILEY-VCH Verlag GmbH & Co. KGaA, Weinheim.

highly complex, hierarchically-patterned polymer brushes has been precluded by the prohibitively challenging nature of realigning or replacing photomasks with micron-precision. The development of *Solution Exchange Lithography* represents a significant advancement in the field and a solution to this challenge. Spatial decoupling of light source from photomask, combined with light-mediated passivation facilitates unprecedented access to complex polymer brush patterns in two- and three-dimensions (see **Chapter 2** and **Appendix F**).

1.4 “Living” Anionic Polymerization

CRP techniques control polymerization by reducing the radical concentration, thereby *minimizing* termination reactions. Anionic polymerization follows a chain-growth mechanism and imparts control by *eliminating* termination reactions.^[10,11] First reported by Szwarc in 1956,^[48,49] this technique utilizes propagating species that are incapable of recombining — anions. In the absence of impurities, termination and transfer reactions are effectively nonexistent. Even at 100% monomer conversion, active chain ends are

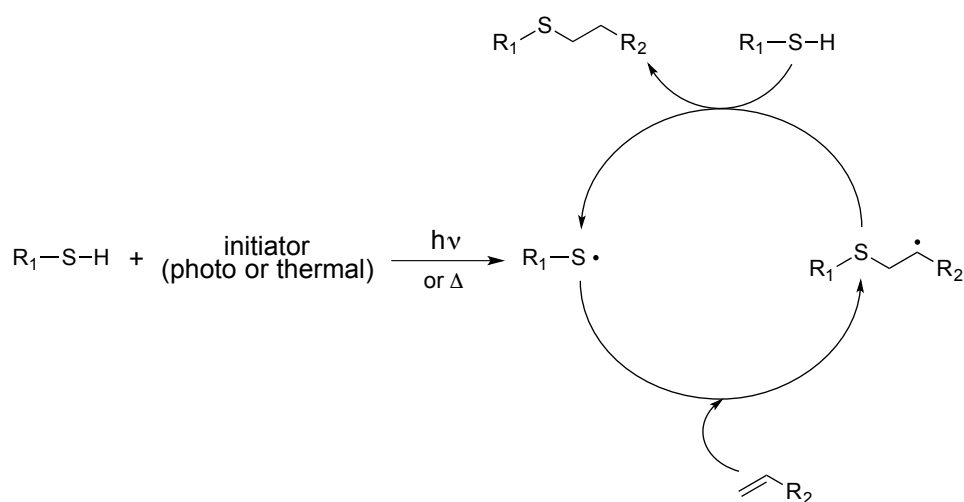
retained, enabling formation of well-defined block copolymers via sequential monomer addition.^[2,11,48,49] These traits make anionic a so-called “living” polymerization.^[48,49]

Certain monomers (e.g. ethylene oxide) cannot be polymerized by radical techniques, but are highly amenable to anionic polymerization. However, compared to CRP, the monomer scope for anionic polymerization more limited, as dictated by strict mechanistic requirements for stabilization of propagating anionic species. Many functional groups are chemically incompatible with anionic processes, and must be protected before polymerization or introduced through post-polymerization modification (see Section 1.5). Nonetheless, when conducted under well-chosen reaction conditions using materials of high purity, living anionic polymerization affords polymers with unparalleled control over molecular weight, extraordinarily narrow molecular weight distributions, and essentially quantitative retention of chain end functionality. Thus, living anionic polymerization remains the preferred method for the precision preparation of large, extremely well-defined macromolecules. Materials synthesized using living anionic polymerization are utilized in **Chapter 4**.

1.5 Post-Polymerization Functionalization

Some macromolecules contain functional handles that provide the opportunity to perform post-polymerization modifications. These reactions often serve to impart additional functionality, alter existing chemistries, and tailor the properties of the resulting polymer.^[50,51] However, a major challenge in modifying macromolecules is the requirement for highly efficient, and sometimes orthogonal, reactions. A number of “click” reactions address both of these needs. In 2001, Sharpless and co-workers established the following criteria for a reaction to be considered “click chemistry:” *“The reaction must be modular, wide in scope, give very high yields, [and] generate only inoffensive byproducts.”* They

further parameterized operationally simple reaction conditions, which utilize only readily available materials, and can be conducted in either the bulk or an easily removable and benign solvent.^[52] Detailed description of the myriad applications for “click” reactions in polymer chemistry is beyond the scope of this work. The reader is referred to recent publications for a thorough review of the topic.^[50,51,53–57] This dissertation will focus on one subset of this efficient reaction family: Thiol-ene coupling.



Scheme 6 Mechanism for thiol-ene coupling. Reproduced from Reference 57 © 2010 Wiley Periodicals, Inc.

Thiol-ene addition reactions are initiated by radicals, which can be generated by either heat or light (Scheme 6).^[57] The initiator radical abstracts a hydrogen from a thiol compound to generate a thiyl radical, which adds across the carbon–carbon double bond (alkene, or “ene”) in an anti-Markovnikov fashion. Subsequently, this carbon-centered radical abstracts a hydrogen from another thiol, thereby regenerating the thiyl radical and forming the thiol-ene product.^[55,57–59] The net reaction is simply the radical addition of a thiol across a carbon–carbon double bond.

Owing to its mild reaction conditions and diversity of both thiols and alkenes, thiol-ene coupling has found widespread use in macromolecular synthesis. However, for the

functionalization of macromolecules, 1:1 stoichiometry of reactants is typically insufficient and frequently leads to side reactions.^[59] Such undesired reaction pathways can be suppressed by using an excess of one reagent (generally the thiol). While thiol-ene coupling does fulfill many of the “click” criteria, the possibility for side reactions and the required use of excess reagents have sparked debate regarding its status as a true “click” reaction.^[59,60] Nevertheless, thiol-ene radical addition is a robust and versatile tool for the functionalization of macromolecules both in solution (see **Chapter 4** and **Appendix B**) and on surfaces (**Appendix F**).

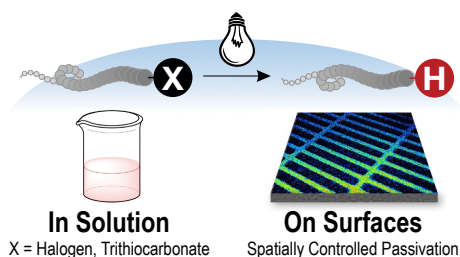
Chapter 2

Metal-Free Removal of Polymer Chain Ends Using Light

2.1 Abstract

A light-mediated method for the facile removal of polymer end groups that are common to controlled radical polymerization techniques is presented. This metal-free strategy is effective for a number of different chain end groups (e.g. chlorine,

bromine, and thiocarbonylthio moieties) as well as polymer families (styrenic, acrylic, methacrylic). In addition to solution reactions, this process is readily translated to thin films, where light-mediation allows the straightforward production of hierarchically-patterned polymer brushes.



2.2 Introduction

Controlled radical polymerization techniques,^[5,12,61,62] such as atom transfer radical polymerization (ATRP)^[5] and Reversible Addition-Fragmentation chain Transfer (RAFT)^[16] polymerization have been successfully used to commercially produce polymers from readily-available starting materials under mild conditions.^[5,6,21,22] Both ATRP and RAFT processes require the presence of chain ends that can undergo reversible activation to give propagating radicals as a prerequisite for control. These chain ends are chemically reactive and thermally unstable, which negatively influences long-term stability and is problematic for polymer processing.^[23,63–67] For example, the elimination of toxic and corrosive hydrobromic (HBr) or hydrochloric acid (HCl) from thermal decomposition of ATRP polymer chain ends leads to a range of issues, including acid-catalyzed ester degradation or corrosion of metals.^[64] Challenges related to polymerization-active chain ends also extend beyond solution-processed materials. The fabrication of patterned, functional polymer surfaces serves as an example where chain end removal with spatial control is often desirable for surface passivation and long-term stability.^[30,46,68]

In previous work, spatial control has been achieved in the production of surface-grafted polymer brushes through deactivation by particle beams,^[69] UV-irradiation,^[70–73] or light-mediated atom transfer radical addition (ATRA).^[74,75] However, the former methods are considered high-cost, low throughput, and destructive. The latter method (ATRA) does not remove the halogen, but merely changes its reactivity.

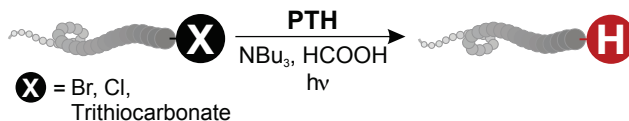


Figure 2.1 Graphical representation of the metal-free removal of terminal polymer chain end groups common to controlled radical polymerizations.

A reducing photoredox catalyst — 10-phenylphenothiazine (PTH) was recently used for the dehalogenation of small molecule halides.^[76,77] In this dissertation, that approach is applied to efficiently remove the chain ends that are common to controlled radical polymerizations (see Figure 2.1). This mild, metal-free, and operationally simple method is applicable to a number of different polymer classes and is compatible with diverse chemical functionalities. Rigorous deoxygenation, anhydrous conditions, and elevated temperatures are all rendered unnecessary. In addition, the use of visible light as an external stimulus for catalyst activation allows spatial control and localized dehalogenation of surface-grafted polymer brushes. As a consequence, a much greater range of materials systems can be used in the preparation of soluble and grafted polymer chains.

2.3 Solution Dehalogenations

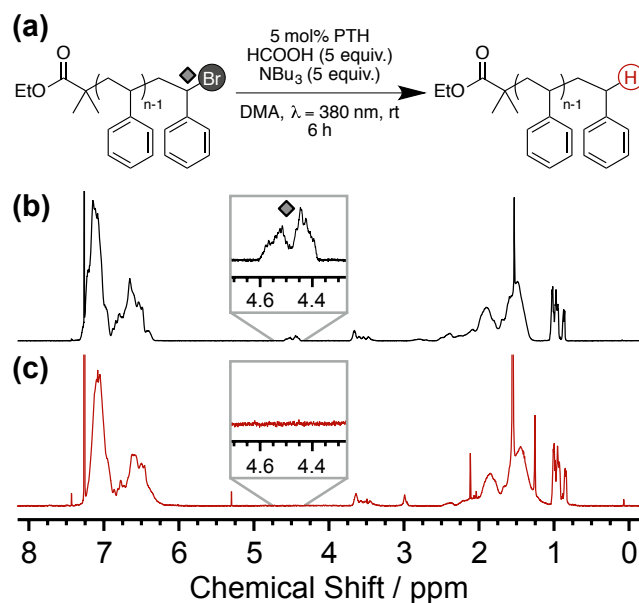


Figure 2.2 (a) Synthetic strategy for debromination of linear polystyrene. (b) ¹H-NMR spectrum of polystyrene-Br, and (c) ¹H-NMR spectrum of the dehalogenated polymer. Insets emphasize the loss of the α-Br proton signal, indicative of successful dehalogenation.

To initially demonstrate this metal-free chain end removal strategy, 5 mol% of PTH in the presence of formic acid and tributylamine was used to debrominate a linear polystyrene–Br derivative (PS–Br, Figure 2.2a). Efficient chain end removal was confirmed via analysis of the characteristic $^1\text{H-NMR}$ signal at $\delta(\text{CH-Br}) = 4.5$ ppm. As evident from Figure 2.2b and c, this key peak, corresponding to the methine proton on the terminal styrene unit adjacent to the ω -end C–Br bond, was no longer detectable after six hours of reaction.

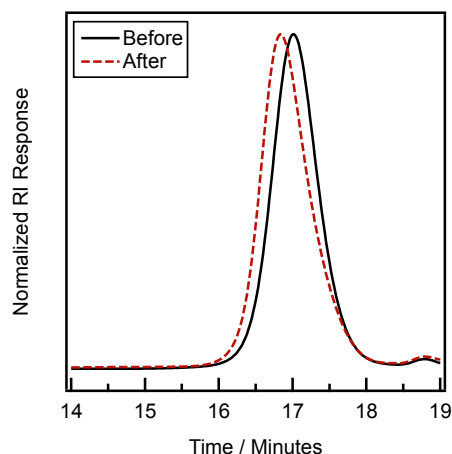


Figure 2.3 SEC traces showing PS–Br (solid black line, reaction time = 0 hours, $M_n = 1.6 \text{ kg}\cdot\text{mol}^{-1}$, $M_w/M_n = 1.11$) and the dehalogenated product PS–H (dashed red line, reaction time = 6 hours, $M_n = 1.9 \text{ kg}\cdot\text{mol}^{-1}$, $M_w/M_n = 1.10$).

Size Exclusion Chromatography (SEC) showed no appreciable changes in molecular weight or polydispersity (Figure 2.3),[‡] indicating the absence of undesired side reactions (e.g., polymer degradation, chain scission, chain-chain coupling) with Field-Desorption Mass Spectrometry (FD-MS) providing additional evidence for quantitative hydrogenation (Figure 2.4). Prior to dehalogenation (Figure 2.4a), the absolute mass of each peak corresponds to a polystyrene chain with ethyl isobutyrate at the α -end and bromine at the ω -end. After reaction (Figure 2.4b), the spectrum was shifted by $m/z = 78.9$ (loss

[‡] M_n is the number-average molecular weight and M_w is the weight-average molecular weight. M_n and M_w/M_n were determined using SEC, relative to linear polystyrene standards.

of Br and addition of H) reaffirming the successful removal of the bromine chain end and full retention of polymer structure. Control experiments under the same conditions, either in the absence of PTH or light, showed no dehalogenation, even after 24 hours with analysis by $^1\text{H-NMR}$ revealing only starting material (see Figure 2.11).

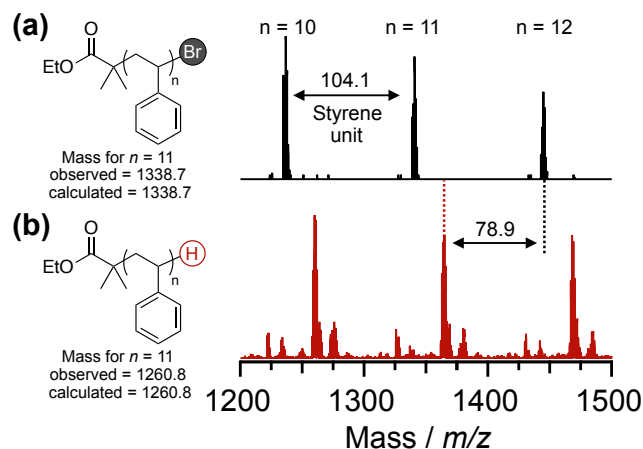


Figure 2.4 FD-MS spectra of (a) the unmodified PS-Br polymer and (b) dehalogenated PS-H confirmed the loss of bromine chain ends.

2.3.1 Impact on Thermal Stability

The removal of dormant Br-chain ends is not only of considerable importance for chemical, but also for thermal stability and related polymer processing (vide supra). Indeed, thermogravimetric analysis (Figure 2.5) showed increased thermal stability for the dehalogenated PS-H when compared to the initial PS-Br. In direct contrast to PS-Br, which lost 7 wt% at $T = 215^\circ\text{C}$ (corresponding to HBr) with the onset of complete decomposition at $T = 390^\circ\text{C}$, the dehalogenated PS-H polymer was thermally stable even above 325°C with the onset of degradation for PS-H being delayed until $\sim 400\text{--}420^\circ\text{C}$.

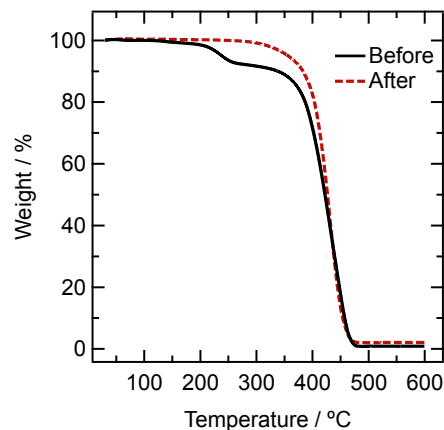
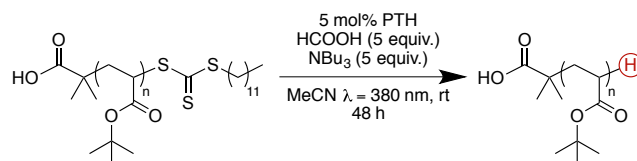


Figure 2.5 Thermogravimetric analysis (TGA) of polystyrene with bromine chain end (solid black line) and after dehalogenation (red dashed line).

2.3.2 Extension to Other Polymer Systems

The versatility of PTH-based chemistry for chain end removal was reinforced by its successful implementation with other polymer families. For the dehalogenation of poly(*tert*-butyl acrylate)-Br, loss of the halogen chain end was confirmed by the disappearance of the ^1H -NMR signal at $\delta = 4.4$ ppm (CH-Br) (Figure 2.12). Again, no precautions were taken to ensure an inert environment during the reaction. Similar reactivity was observed for the removal of chloro-based chain ends (Figure 2.14). Significantly, macromolecules synthesized via RAFT polymerization with thiocarbonylthio RAFT chain ends also underwent facile deactivation and conversion to hydrogen (see Scheme 7 and Figure 2.15). In the latter case, the UV activity of the thiocarbonylthio moiety (absorption maximum, $\lambda_{max} = 310$ nm) served as a marker to monitor the progress of this reaction via SEC (Figure 2.16). Again, SEC indicated no appreciable change in molecular weight or dispersity for all samples studied, reaffirming the mild and non-destructive nature of this process.



Scheme 7 Synthetic strategy for the facile deactivation and conversion of thiocarbonylthio RAFT chain ends to hydrogen.

2.4 Surface Dehalogenations

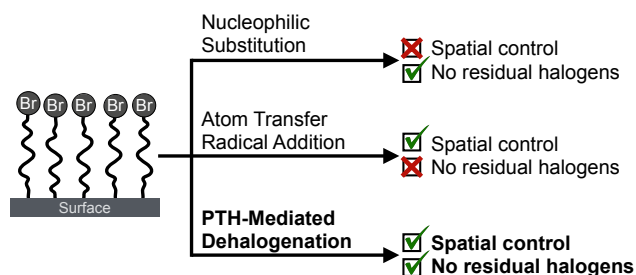


Figure 2.6 Comparison of the visible light-mediated dehalogenation strategy, which combines both spatially and chemically controlled removal of reactive halogens, with traditional approaches based on nucleophilic substitution and ATRA chemistry.

Having demonstrated applicability to a wide range of polymeric starting materials in solution, attentions were turned to the passivation of polymer brushes. The ability to pattern surfaces and remove reactive chains ends would be useful for a variety of applications and therefore it was envisioned that translation of this chemistry to surfaces would be further enabled by the robust reaction conditions.

For the formation of complex 2-D and 3-D grafted polymer brushes, the selective termination of polymer chain ends allows for hierarchical patterning via surface-initiated ATRP (SI-ATRP).^[37,46,68,74,78] Figure 2.6 summarizes the advantages and disadvantages of common techniques for modulating the reactivity of polymer brushes through nucleophilic substitution^[30,79–81] and ATRA.^[74,75] This comparison with the PTH-based dehalogenation strategy described above clearly illustrates the potential advantages of this robust and spatially controlled alternative for polymer brush deactivation.

2.4.1 Uniform Dehalogenation of Surface-Tethered Monolayers

Initial experiments were directed towards the uniform debromination of a silicon oxide substrate functionalized with the ATRP initiator undecyl 2-bromoisobutyrate (see Figure 2.7). X-ray photoelectron spectroscopy (XPS) was employed to detect the presence of bromine-containing functional groups on the substrate. For the substrate functionalized with immobilized ATRP initiators (Figure 2.7c), the bromine $3d$ orbital contains two components: the $3d_{5/2}$ and $3d_{3/2}$ doublet at binding energies BE = 69 eV and BE = 70 eV, respectively, as a result of spin orbit splitting. Figure 2.7d illustrates disappearance of this Br $3d$ peak, confirming that irradiation at $\lambda = 405$ nm in the presence of PTH was capable of removing the halogen from the ATRP initiating layer.

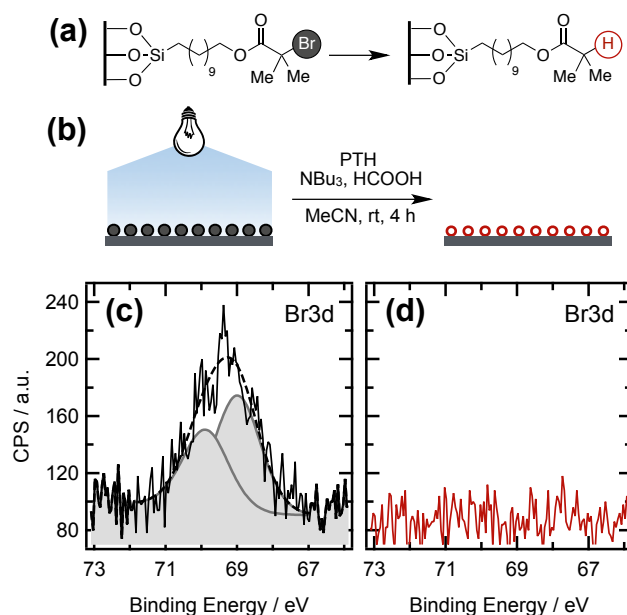


Figure 2.7 (a) Synthetic strategy and (b) schematic representation showing the uniform dehalogenation of α -bromoisobutyrate functionalized silicon surfaces. High-resolution XPS scans provided evidence for (c) the brominated ATRP initiator for the untreated substrates and (d) the absence of Br-signals after PTH-catalyzed dehalogenation. Gaussian bell curves (c) correspond to the Br $3d_{5/2}$ and Br $3d_{3/2}$ orbitals. The dashed line represents the sum of both bell curves.

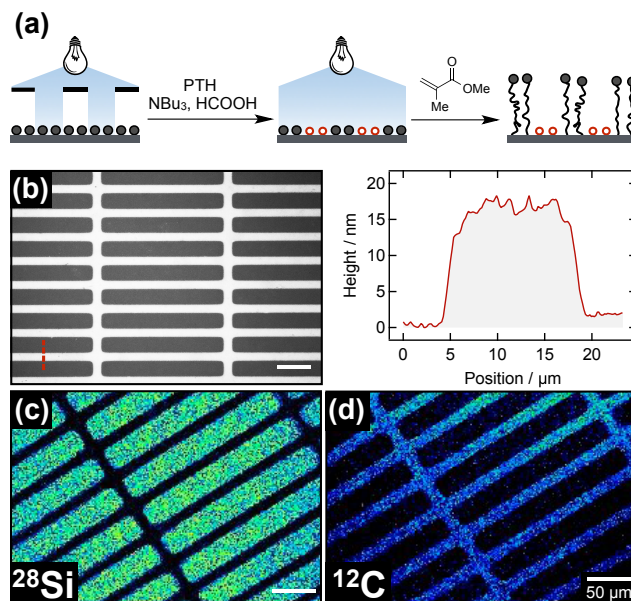


Figure 2.8 (a) Spatially confined dehalogenation of α -bromoisobutyrate functionalized silicon substrates by irradiation through a binary photomask with $20 \times 200 \mu\text{m}^2$ clear rectangles, followed by subsequent homogeneous irradiation and light-mediated polymerization of MMA. (b) Optical micrograph (left) of the resulting patterned PMMA brushes confirmed the absence of polymer growth within the dehalogenated rectangles. AFM (right) indicated 15 nm polymer brush height and provided additional evidence for the absence of polymer in dehalogenated areas. SIMS chemical maps for (c) silicon and (d) carbon fragments confirmed spatially confined polymerization. All scale bars are 50 μm .

2.4.2 Spatially Controlled Dehalogenation of Monolayers

To illustrate the spatial fidelity of this light-mediated process, localized debromination of ATRP-initiator functionalized wafers was investigated by irradiation through a photomask with $20 \times 200 \mu\text{m}^2$ clear rectangles. The photomask was subsequently removed and poly(methyl methacrylate) (PMMA) polymer brushes grown via light-mediated radical polymerization.^[39,47] Optical microscopy, Secondary Ion Mass Spectrometry (SIMS), and Atomic Force Microscopy (AFM) confirmed spatially confined growth of polymer brushes exclusively in areas which were not previously irradiated/dehalogenated in the presence of PTH (Figure 2.8).

2.4.3 Spatially Controlled Dehalogenation of Polymer Brushes

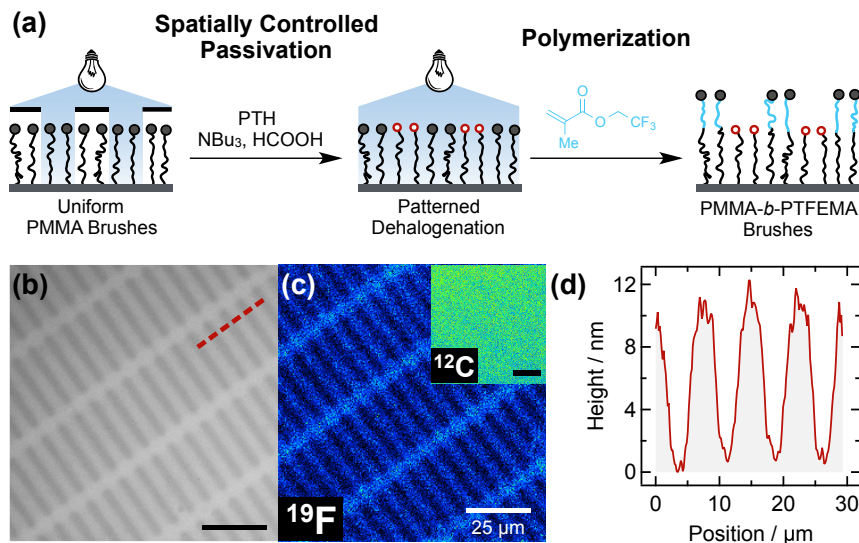


Figure 2.9 (a) Patterned diblock copolymer brush formation via spatially controlled dehalogenation and subsequent uniform polymerization of TFEMA. (b) Optical micrograph of the patterned polymer brushes. (c) ^{19}F fluorine and (inset) ^{12}C carbon SIMS scans confirmed localized presence of fluorine (PMMA-*b*-PTFEMA brushes) atop a uniform MMA polymer brush layer. (d) AFM height profile of the patterned PTFEMA brushes along the dashed line in (b) confirmed patterning and allowed quantification of brush height increase after block copolymerization. Scale bars in (b–c) are $25\ \mu\text{m}$.

The utility of this process was further demonstrated by transitioning from the debromination of monolayers to the dehalogenation of surface-grafted polymer brush chain ends. As illustrated in Figure 2.9a, a uniform PMMA brush layer was initially grown (thickness $39 \pm 2\ \text{nm}$), followed by spatially controlled dehalogenation by irradiation through a binary photomask with $2.5 \times 25\ \mu\text{m}^2$ clear rectangles. Removal of the photomask and homogeneous polymerization of a second monomer, 2,2,2-trifluoroethyl methacrylate (TFEMA), resulted in a chemically patterned surface composed of PMMA homopolymer and PMMA-*b*-PTFEMA diblock brushes. Both optical microscopy (Figure 2.9b) and SIMS (Figure 2.9c) confirmed successful patterning via spatially controlled dehalogenation and subsequent polymer brush extension. Detection of fluorine (^{19}F) and carbon

(^{12}C) fragments in SIMS confirmed the spatial confinement of TFEMA exclusively in areas with PMMA-*b*-PTFEMA diblock copolymer brushes (Figure 2.9c).

2.5 Conclusion

This chapter describes a fully organic, light-mediated approach for the efficient removal of ATRP (Br, Cl) or RAFT (thiocarbonylthio) polymer chain ends for a number of different polymer classes. The facile and robust nature of this approach does not require elevated temperatures or inert reaction conditions, occurring with high efficiency under ambient conditions. Further, dehalogenation of both ATRP initiator monolayers and surface-grafted polymer brushes affords a novel and versatile procedure for surface patterning. Soluble and supported polymers with improved thermal and chemical stability can now be obtained under mild, metal-free conditions and with external regulation.

2.6 Experimental

2.6.1 Materials

All reagents were purchased from Sigma-Aldrich and used as received, unless stated otherwise. RuPhos Precatalyst (Chloro-(2-dicyclohexylphosphino-2',6'-diisopropoxy-1,1'-biphenyl)[2-(2-aminoethyl)phenyl]palladium(II) – methyl-*t*-butyl ether adduct) was purchased from Strem Chemicals Inc. Azobisisobutyronitrile (AIBN) was recrystallized twice in methanol before use. Methyl methacrylate (MMA), styrene, *tert*-butyl acrylate, and 2,2,2-trifluoroethyl methacrylate (TFEMA) were filtered through a plug of basic alumina immediately preceding use. All reactions were carried out at room temperature (ca. 23 °C), unless otherwise noted. Silicon substrates with 100 nm of oxide were purchased from Silicon Quest International.

2.6.2 General Analytical Information

Nuclear magnetic resonance (NMR) spectra were recorded on a VNMRs 600 MHz spectrometer at room temperature using an acquisition time of 3.4 seconds, a 10 second relaxation delay, and at least 64 scans. Unless otherwise stated, all ^1H -NMR spectra are reported in parts per million (ppm), and were measured relative to the signal for residual chloroform in the deuterated solvent (7.26 ppm). A Micromass QTOF2 Quadrupole/Time-of-Flight Tandem mass spectrometer was used for mass analysis using field desorption (FD). Size exclusion chromatography (SEC) was performed at ambient temperature using chloroform with 0.25 wt% triethylamine as the mobile phase in a Water 2695 separation module with a Waters 2414 refractive index detector. Number average molecular weights (M_n) and weight average molecular weights (M_w) were calculated relative to linear polystyrene standards. Values for each sample's polydispersity (D) are reported as the quotient of M_w/M_n . Film thicknesses were measured with a Filmetrics F20 optical reflectometer ($\text{RI}_{\text{PMMA}} = 1.485$) by setting silicon oxide (100 nm) as the first layer and polymer as a second layer. Optical micrographs were captured using a Nikon Eclipse E600 optical microscope. X-ray photoelectron spectroscopy (XPS) measurements were performed using a Kratos Axis Ultra Spectrometer (Kratos Analytical, Manchester, U.K.) with a monochromatic Aluminum K_α X-ray source (1486.6 eV) operating at 225 W under a vacuum of 10^{-8} Torr. Tapping mode AFM data was acquired on a MFP-3D system (Asylum Research, Santa Barbara, CA) using commercial Si cantilevers. Dynamic Secondary Ion Mass Spectrometry (SIMS) imaging was performed using a Cameca IMS 7f system (Cameca SAS, Gennevilliers, France). A 10 kV Cs^+ ion beam and 5 kV negative sample potential were used, for a total impact energy of 15 kV. The 150 pA primary beam was focused to a spot size of approximately 2 μm , and rastered over a 100 μm area. Pho-

tomasks containing clear rectangles of $2.5 \times 25 \mu\text{m}^2$ and $20 \times 200 \mu\text{m}^2$ were purchased from Photonics, Inc.

2.6.3 Light Sources

Solution Experiments: LED strips ($\lambda = 380 \text{ nm}$) were purchased from Elemental LED (www.elementalled.com) and used to line the inside of a Corning crystallization dish. The light intensity was measured to be $1.8 \mu\text{W}/\text{cm}^2$.

Surface Reactions: A collimated LED light ($\lambda = 405 \text{ nm}$) was purchased from Thor Labs (part number M405L2-C1). Reactions were placed approximately 1.5 cm below light source, where the light intensity was measured to be $1.1 \text{ mW}/\text{cm}^2$.

2.6.4 Methods

Preparation of Polystyrene-Br

Styrene (20 mL, 174 mmol, 50 equiv) was passed through basic alumina to remove inhibitor and transferred to a 50 mL schlenk flask containing ethyl bromoisobutyrate (512 μL , 3.5 mmol, 1 equiv) and *N,N,N',N',N''*-pentamethyldiethylenetriamine (PMDETA) (146 μL , 0.7 mmol, 0.2 equiv). The reaction mixture was degassed using freeze-pump-thaw three times, frozen once more, uncapped and CuBr (100 mg, 0.7 mmol, 0.2 equiv) was added on top of the frozen mixture. While still frozen, the flask was evacuated and backfilled with argon three times, then warmed to room temperature. The flask was placed into an oil bath set to $100 \text{ }^\circ\text{C}$ for 3 hours. Then, the flask was rapidly cooled in liquid nitrogen and opened to air to oxidize the catalyst. The crude polymer was diluted with dichloromethane and passed through neutral alumina to remove the copper catalyst. The filtered solution was concentrated *in vacuo* and precipitated twice into methanol to

isolate polystyrene–Br as a white solid.

$$M_n \text{ (SEC)} = 1.6 \text{ kg}\cdot\text{mol}^{-1}; M_w/M_n = 1.11$$

Preparation of Poly(*tert*-butyl acrylate)–Br

tert-Butyl acrylate (17 mL, 117 mmol, 150 equiv) was passed through basic alumina to remove inhibitor and transferred to a 40 mL vial with septum containing ethylene carbonate (3.5 g), ethyl bromoisobutyrate (114 μ L, 0.78 mmol, 1 equiv) and PMDETA (163 μ L, 0.78 mmol, 1 equiv). The reaction mixture was degassed using freeze-pump-thaw three times, frozen once more, uncapped and CuBr (112 mg, 0.78 mmol, 1 equiv) was added on top of the frozen mixture. While still frozen, the flask was evacuated and backfilled with argon three times, then warmed to room temperature. The flask was placed into an oil bath set to 70 °C for 30 minutes. Then, the flask was rapidly cooled in liquid nitrogen and opened to air to oxidize the catalyst. The crude polymer was diluted with diethyl ether and passed through neutral alumina to remove the copper catalyst. The filtered solution was concentrated in vacuo and precipitated twice into a cold methanol/water (3:1) mixture to isolate poly(*tert*-butyl acrylate)–Br.

$$M_n \text{ (SEC)} = 6.5 \text{ kg}\cdot\text{mol}^{-1}; M_w/M_n = 1.18$$

Preparation of Polystyrene–Cl

Styrene (20 mL, 174 mmol, 50 equiv) was passed through basic alumina to remove inhibitor and transferred to a 50 mL schlenk flask containing ethyl 2-chloropropionate (445 μ L, 3.5 mmol, 1 equiv) and PMDETA (146 μ L, 0.7 mmol, 0.2 equiv). The reaction mixture was degassed using freeze-pump-thaw three times, frozen once more, uncapped and CuCl (69 mg, 0.7 mmol, 0.2 equiv) was added on top of the frozen mixture. While still frozen, the flask was evacuated and backfilled with argon three times, then warmed to room temperature. The flask was placed into an oil bath set to 100 °C for 20 hours.

Then, the flask was rapidly cooled in liquid nitrogen and opened to air to oxidize the catalyst. The crude polymer was diluted with dichloromethane and passed through neutral alumina to remove the copper catalyst. The filtered solution was concentrated in vacuo and precipitated twice into methanol to isolate polystyrene-Cl as a white solid.

$$M_n \text{ (SEC)} = 4.1 \text{ kg}\cdot\text{mol}^{-1}; M_w/M_n = 1.48$$

Preparation of Poly(*tert*-butyl acrylate)-RAFT

2-(Dodecylthiocarbonothioylthio)-2-methylpropionic acid (DMP) was obtained according to a literature procedure.^[82,83] *tert*-Butyl acrylate (3.00 g, 23.41 mmol, 41.8 equiv), DMP (203.0 mg, 0.56 mmol, 1.0 equiv), AIBN (18.3 mg, 0.11 mmol, 0.2 equiv) and ethyl acetate (5.5 mL) were charged into a reaction tube. The tube was sealed with a septum and the mixture bubbled with argon for 30 minutes. Subsequently, the reaction mixture was stirred in an oil bath at 60 °C for 1 hour. Afterwards, the mixture was cooled, opened to air and the product precipitated in a mixture of deionized water/methanol (3:1) to yield the polymer as a yellow solid.

$$M_n \text{ (SEC)} = 3.4 \text{ kg}\cdot\text{mol}^{-1}; M_w/M_n = 1.12$$

Synthesis of 10-phenylphenothiazine (PTH)^[76]

To a vial equipped with a magnetic stir bar was added sodium *tert*-butoxide (134 mg, 1.4 mmol), phenothiazine (199 mg, 1 mmol), RuPhos Precatalyst (14 mg, 0.02 mmol, 2 mol%), and RuPhos (2-dicyclohexylphosphino-2',6'-diisopropoxybiphenyl) (8 mg, 0.02 mmol, 2 mol %). The vial was evacuated and backfilled with argon three times, then backfilled with argon once more. Anhydrous dioxane (1 mL) was charged to the vial, followed by anhydrous chlorobenzene (143 μ L, 1.4 mmol). The vial was then placed into an oil bath at 110 °C and allowed to react for 5 hours. The reaction mixture was then cooled to room temperature, diluted with CH₂Cl₂, washed with water, washed with

brine, then dried over Mg_2SO_4 . It was subsequently passed through a plug of silica gel (5% EtOAc/hexanes as eluent) and dried under reduced pressure to afford the title compound.

Yield: 267 mg, white solid (97%).

$^1\text{H-NMR}$ (600 MHz, CDCl_3): δ (ppm) = 7.60 (t, J = 8 Hz, 2 H), 7.49 (t, J = 8 Hz, 1 H), 7.40 (d, J = 7 Hz 2 H), 7.02 (d, J = 8 Hz, 2 H), 6.86–6.79 (m, 4 H), 6.20 (d, J = 8 Hz, 2 H).

$^{13}\text{C-NMR}$ (150 MHz, CDCl_3): δ (ppm) = 144.5, 141.2, 131.1, 130.9, 128.4, 127.0, 126.9, 122.7, 120.4, 116.3.

HR-ESI $\text{C}_{18}\text{H}_{13}\text{NS}$: calculated 275.0769, found 275.0753.

Representative Procedure for Chain End Removal in Solution

0.025 mmol polymer (1.0 equiv with respect to the polymer chain end) was weighed into a 1 dram glass vial (“VWR Vial Borosilicate Glass, with Phenolic Screw Cap, 1 dram”). A 0.50 mL aliquot of a stock solution of 1.1 mg PTH (0.00125 mmol, 0.05 equiv) in 1.62 mL solvent (0.34 mg PTH/ 0.5 mL solvent) was added to the vial, along with a micro stir bar. 4.7 μL (0.125 mmol, 5.0 equiv) of formic acid was added to the vial, followed by 29.7 μL (0.125 mmol, 5.0 equiv) tributylamine. Please note that, depending on the substrate’s solubility, either acetonitrile (MeCN) or *N,N*-dimethylacetamide (DMA) was used as the solvent. The vial was capped with a “Thermo Scientific™ National™ PTFE/Silicone Septa for Sample Screw Thread Cap” and gently shaken until the run mixture was homogenous. The vial’s cap was removed to take an NMR sample for $T = 0$ minutes. (NMR samples prepared using 50 μL aliquot of crude reaction mixture and 0.50 mL CDCl_3). The cap was replaced and the vial was placed in a Corning dish lined with 380 nm LED lights. A small piece of tape from the outside of the light dish to the top of the vial ensured the vial did not move away from the lights during the reaction. Throughout the reaction,

the solution was rapidly stirred, and cooled to room temperature by a constant stream of air being blown into the middle of the light setup.

Preparation of Uniformly Functionalized Alkyl Bromide Silicon Surfaces^[47]

A 25 mL schlenk flask, equipped with a magnetic stir bar and a rubber septum, was evacuated, backfilled with argon, then charged with undec-10-enol (2.50 mL, 12.5 mmol, 1.0 equiv), pyridine (1.07 mL, 13.3 mmol, 1.1 equiv), and tetrahydrofuran (50 mL). Over a ten-minute period, 2-bromoisobutyryl bromide (1.55 mL, 12.5 mmol, 1.0 equiv) was added to the reaction mixture in a dropwise fashion. The solution was stirred overnight at room temperature, then diluted with hexanes, washed with 1M HCl, dried with MgSO₄ and concentrated in vacuo. The crude product was purified using flash chromatography on silica gel (25:1 hexanes:ethyl acetate) to afford undec-10-en-1-yl 2-bromo-2-methylpropanoate as a colorless oil.

A 10 mL schlenk flask, equipped with a magnetic stir bar and a rubber septum, was evacuated, and backfilled with nitrogen. It was then charged with an aliquot of the aforementioned undec-10-en-1-yl 2-bromo-2-methylpropanoate (1.35 g, 4.2 mmol), trichlorosilane (4.2 mL, 42.6 mmol), and a solution of Karstedt's catalyst in xylene (5 μ L, 2 wt% platinum in xylene). The solution was stirred at room temperature for two hours, at which point ¹H-NMR indicated the reaction had reached full conversion. The crude mixture was then concentrated under reduced pressure to give 11-(trichlorosilyl)undecyl 2-bromo-2-methylpropanoate as a clear oil, which was used without further purification.

Representative Procedure for Dehalogenation of Surfaced-Tethered Initiators and Brushes

As shown in a recent publication from the Hawker group, a simple benchtop apparatus comprised of a modified Petri dish with a covering glass slide can be used instead

of a glovebox for PTH surface reactions. Accordingly, this “benchtop apparatus” was used interchangeably with the glovebox. For a more detailed description, please see Discekici and co-workers’ recent publication.^[37] A stock solution was prepared by thoroughly mixing 1.4 mg PTH, 19 μ L HCOOH, 0.12 mL NBU₃, and 1.0 mL MeCN (due to the monomer/polymer solubility, *N,N*-dimethylacetamide was used as the solvent for reactions with polymer brushes) in a 1 dram vial. The solution was added dropwise to cover the entire surface of the functionalized silicon wafer substrate. The substrate was covered with either a coverslip or a photomask and irradiated with 405 nm collimated light for a predetermined time.

2.7 Supplemental Results

2.7.1 Demonstration of the Necessity of Both Light and PTH

As controls, portions of the same PS–Br were subjected to the optimized reaction conditions, excluding either PTH or light. Though the dehalogenation has been shown to be complete within six hours in the presence of light, after 24 hours, both reactions yielded polymers with fully intact chain ends. This demonstrates that both the PTH catalyst and light are necessary for the dehalogenation reaction to proceed, and that no deleterious side reactions occur with or without light.

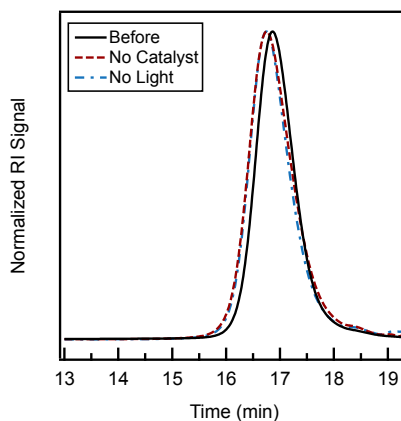


Figure 2.10 Overlaid SEC traces showing no change in PS–Br before (solid black line, reaction time = 0 hours, $M_n = 1.6 \text{ kg}\cdot\text{mol}^{-1}$, $M_w/M_n = 1.11$), or after being exposed to optimized reaction conditions for 24 hours either *excluding PTH* (red dashed line, $M_n = 1.7 \text{ kg}\cdot\text{mol}^{-1}$, $M_w/M_n = 1.22$), or *in the dark* (blue dotted line, $M_n = 1.7 \text{ kg}\cdot\text{mol}^{-1}$, $M_w/M_n = 1.20$).

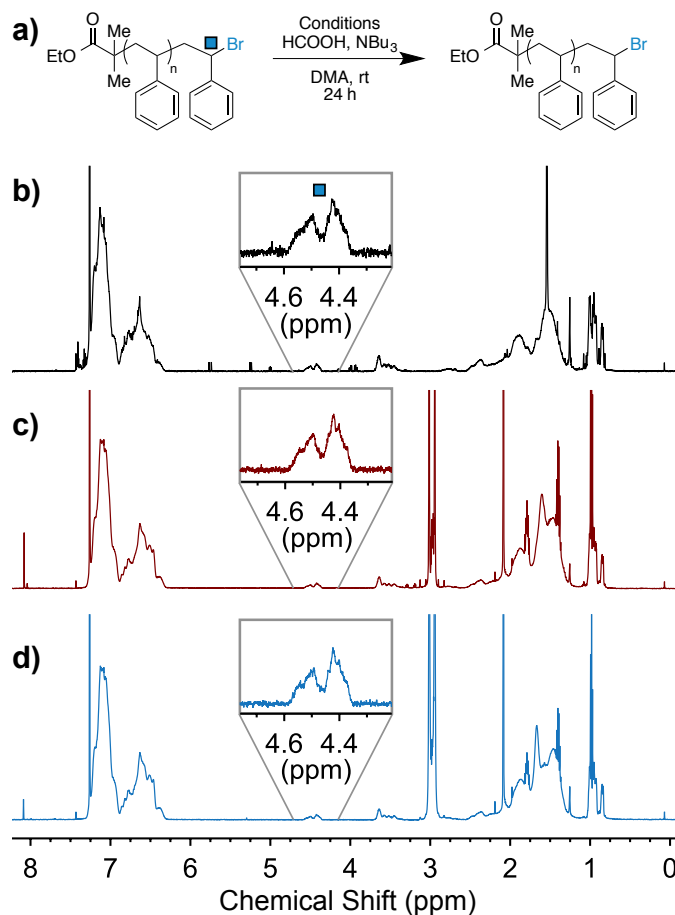


Figure 2.11 (a) General reaction scheme for control reactions. All control reactions were run for 24 hours. ¹H-NMR spectra showing (b) unmodified PS-Br, (c) PS-Br after being subjected to optimized dehalogenation reaction conditions *excluding PTH*, and (d) PS-Br after being subjected to optimized dehalogenation conditions *excluding light*. Insets present to emphasize the signature chain-end signal. In the absence of either PTH or light, there is no change in the polymer chain end.

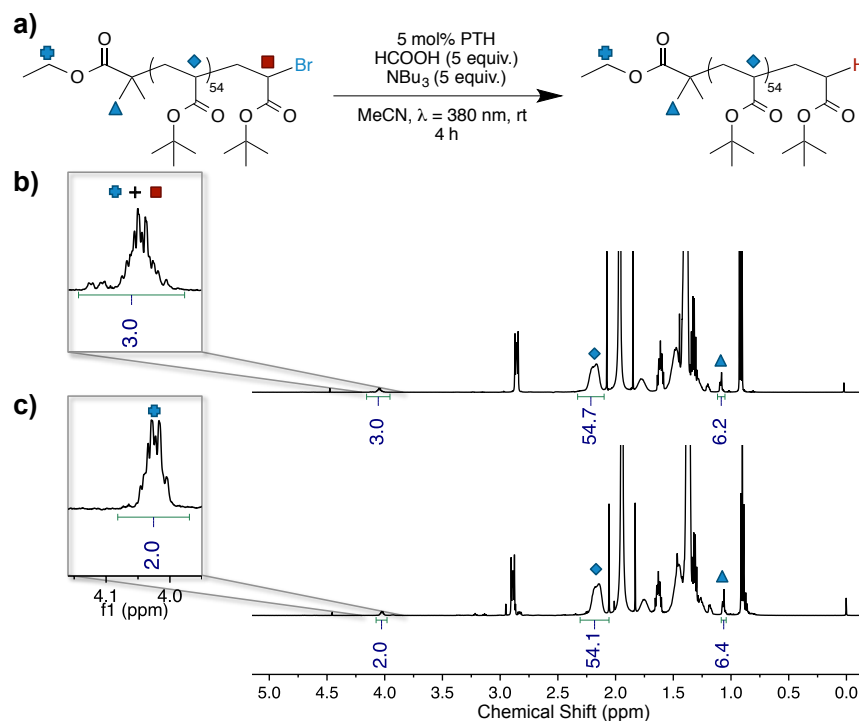
2.7.2 Debromination of Poly(*tert*-butyl acrylate)-Br

Figure 2.12 (a) Reaction scheme for the air-insensitive dehalogenation of poly(*tert*-butyl acrylate)-Br. ¹H-NMR spectra annotated to show the diagnostic peaks (b) before and (c) after dehalogenation.

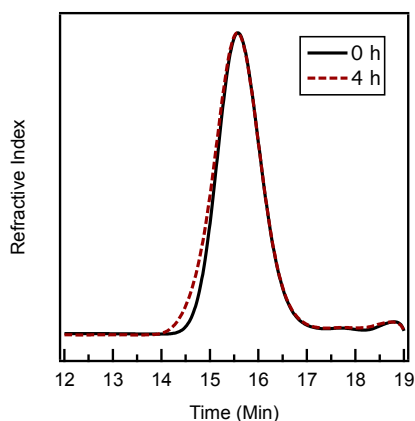


Figure 2.13 SEC traces of the initial poly(*tert*-butyl acrylate)-Br before reaction (solid black line, reaction time = 0 hours, $M_n = 6.5 \text{ kg}\cdot\text{mol}^{-1}$, $M_w/M_n = 1.18$), and the dehalogenated sample (dashed red line, reaction time = 4 hours, $M_n = 6.6 \text{ kg}\cdot\text{mol}^{-1}$, $M_w/M_n = 1.21$).

2.7.3 Dehalogenation of Polystyrene-Cl

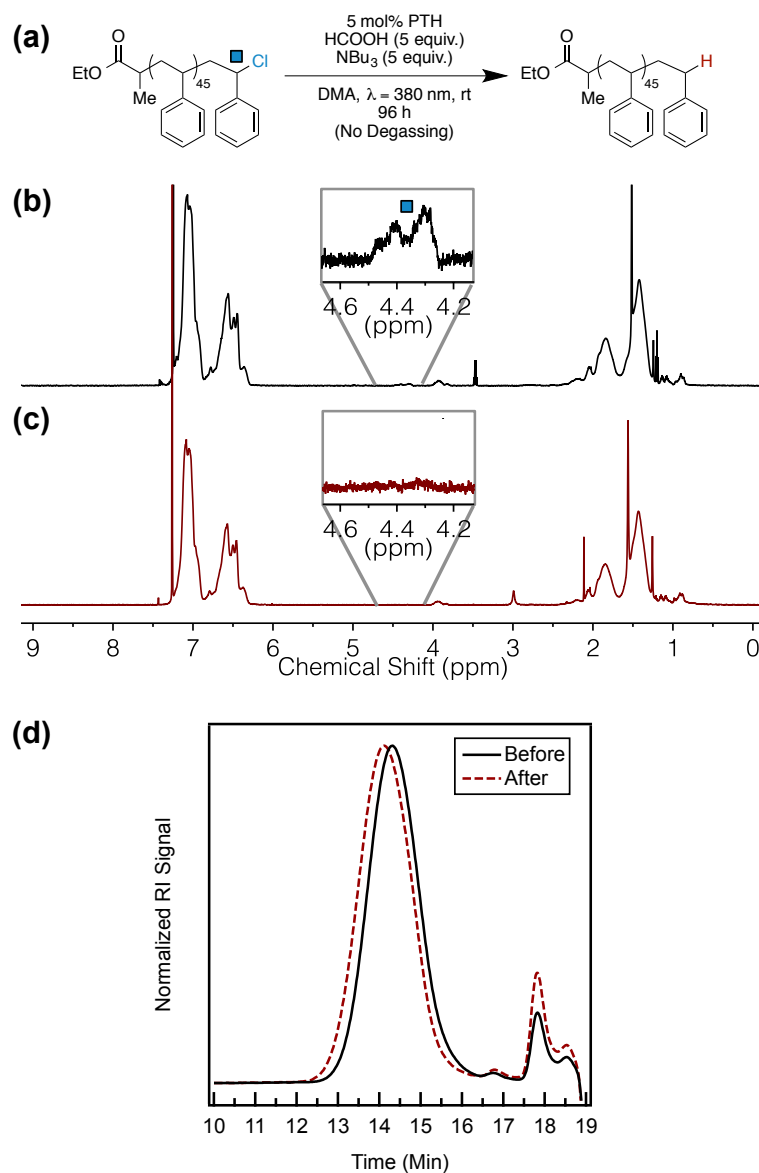


Figure 2.14 (a) Reaction scheme for the dechlorination of PS-Cl, (b) ¹H-NMR spectrum of PS-Cl before dehalogenation, (c) ¹H-NMR spectrum of the dehalogenated polymer. (d) SEC traces showing PS-Cl before (solid black line, $M_n = 4.1 \text{ kg}\cdot\text{mol}^{-1}$, $M_w/M_n = 1.48$) and after (dashed red line, $M_n = 5.1 \text{ kg}\cdot\text{mol}^{-1}$, $M_w/M_n = 1.48$).

2.7.4 Removal of RAFT Chain End

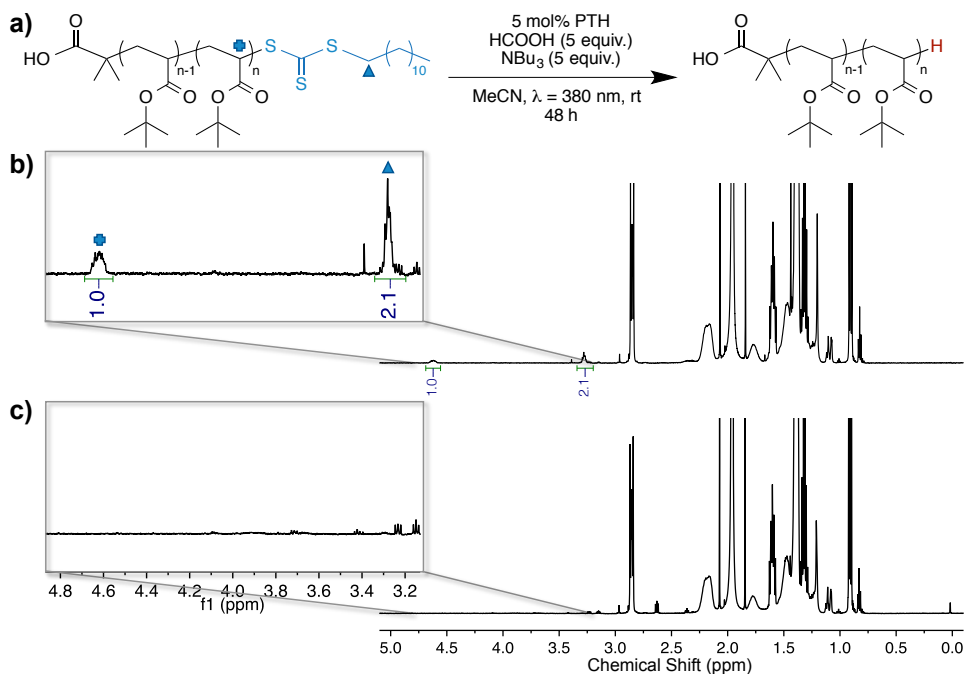


Figure 2.15 (a) Reaction scheme (top) and ¹H-NMR spectra highlighting (b) the presence of signals from RAFT chain end protons before reaction and (c) the corresponding disappearance of those peaks, indicative of chain end removal.

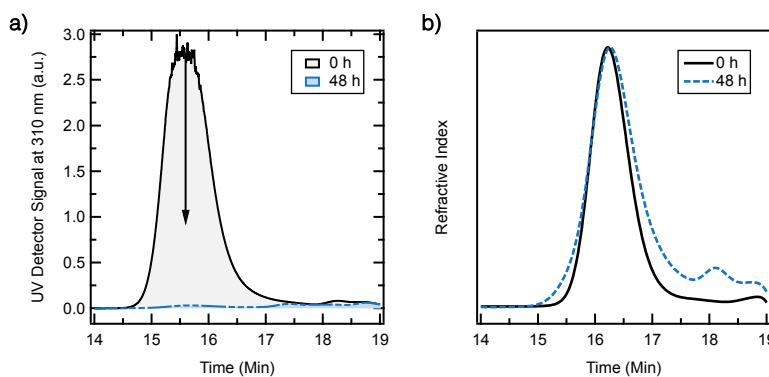


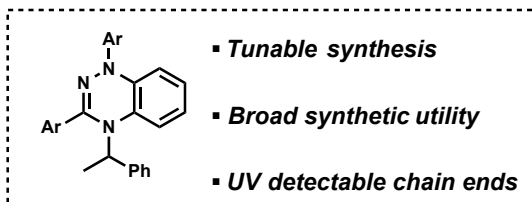
Figure 2.16 SEC traces showing the poly(*tert*-butyl acrylate)-RAFT polymer before and after chain end removal. (a) UV detector signal at 310 nm showing the presence of the strongly absorbing RAFT chain end (black, reaction time = 0 hours), and its disappearance after the reaction (blue, reaction time = 48 hours). (b) SEC chromatograms showing the starting polymer (black solid line, $M_n = 3.4 \text{ kg}\cdot\text{mol}^{-1}$, $M_w/M_n = 1.12$) and the chain end removed sample after 48 hours (dashed blue line, $M_n = 3.3 \text{ kg}\cdot\text{mol}^{-1}$, $M_w/M_n = 1.17$).

Chapter 3

Triazine-Mediated Controlled Radical Polymerization[‡]

3.1 Abstract

Triazine-based unimolecular initiators are shown to mediate the controlled radical polymerization of several monomer classes, yielding polymers with low dispersities, targeted molecular weights, and active chain ends.



This chapter reports the modular synthesis of structurally and electronically diverse triazine-based unimolecular initiators and demonstrate their ability to efficiently control the radical polymerization of modified styrene monomers. Copolymerizations of styrene with butyl acrylate or methyl methacrylate were conducted to highlight the monomer family tolerance of this system. Notably, in the case of methyl methacrylate and styrene, up to 90 mol% methyl methacrylate comonomer

[‡]Reproduced from J. Areephong, K.M. Mattson, N.J. Treat, S.O. Poelma, J.W. Kramer, H.A. Sprafke, A.A. Latimer, J. Read de Alaniz, C.J. Hawker, *Polym. Chem.* **2016**, *7*, 370–374 with permission from the Royal Society of Chemistry.

loadings could be achieved while maintaining a controlled polymerization, allowing the synthesis of a range of block copolymers. This class of triazine-based mediators has the potential to complement current methods of controlled radical polymerization and marks an important milestone in ongoing efforts to develop initiators and mediators with high monomer tolerance that are both metal and sulfur-free.

3.2 Introduction

While there are a variety of controlled radical polymerization (CRP) techniques,^[84–86] three dominate due to their simplicity and functional group tolerance: atom transfer radical polymerization (ATRP),^[4,87] reversible addition-fragmentation chain transfer polymerization (RAFT),^[62] and nitroxide-mediated polymerization (NMP).^[18,61] Of these, NMP is particularly useful because of both its inherent simplicity (i.e. needing only monomer and unimolecular initiator) and its avoidance of sulfur and metal catalysts found in the RAFT and ATRP processes.^[18] This is achieved through the use of a stable nitroxide radical (Figure 3.1a) that reversibly caps the growing polymer chain end, establishing a low radical concentration in solution, and minimizing deleterious termination events (Figure 3.2a). Over the last 20 years, NMP has evolved to be a viable technique for the production of a variety of functional materials.^[18,88–93] However, limitations still exist. For example, NMP’s monomer scope does not match those of RAFT and ATRP, with the controlled polymerization of methacrylates only recently being reported using specialized mediators.^[94–96] In hopes of overcoming these issues, many other stable radicals have been evaluated for controlled polymerization, including (aryloxy)oxy,^[97] borinate,^[98] triazolinylyl,^[99–102] and verdazyl^[103–107] radicals. Of these, only triazolinylyl and verdazyl radicals have been shown to control polymerizations, and these only for styrene and acrylates. Thus, there is significant potential for the development of new radical

mediators that may overcome limitations of NMP and expand the field of controlled radical polymerizations. With this in mind, the search for a new radical mediator began, eventually leading to the benzo-1,2,4-triazinyl (triazine) moiety first reported by Blatter in 1968 as a highly stable radical (Figure 3.1b).^[108]

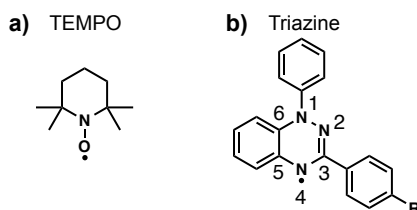


Figure 3.1 (a) 2,2,6,6-tetramethylpiperidinyl-1-oxyl (TEMPO) and (b) benzo-1,2,4-triazinyl (triazine) stable radicals.

The triazine moiety was of particular interest because it had previously been explored for controlled radical polymerization in combination with thermal initiators, but the performance of the corresponding unimolecular initiator and associated structural variations had not been studied.^[109] Further, the triazine unit is a versatile building block, easily tunable from a synthetic standpoint, and triazine-mediated polymerizations would be analogous to NMP in avoiding sulfur and metal contamination (Figure 3.2).

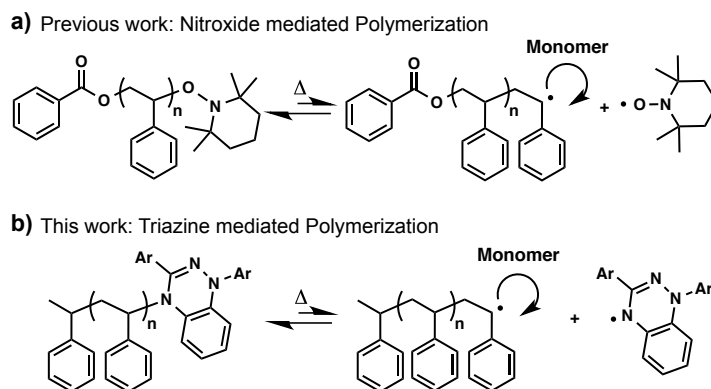
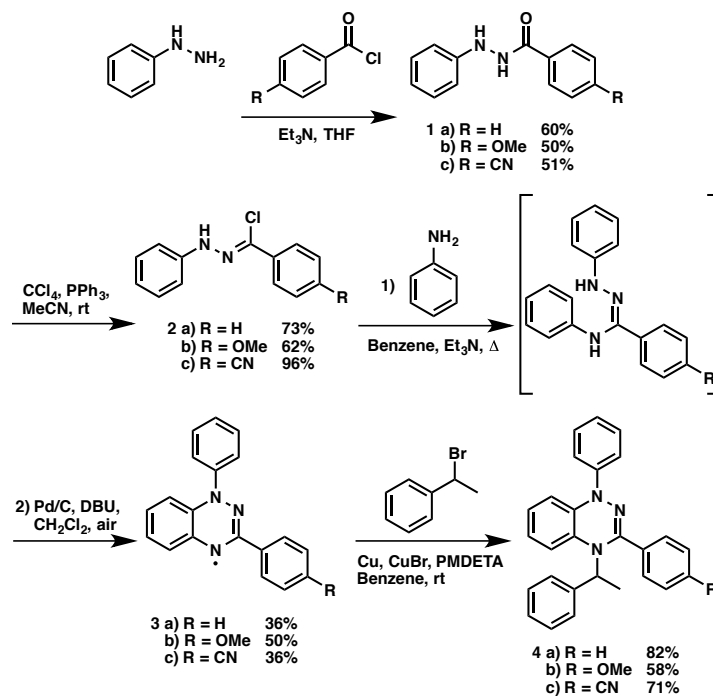


Figure 3.2 (a) Mechanism of NMP. (b) Proposed mechanism for triazine-mediated polymerization.

3.3 Results and Discussion

After identifying the triazine radical as a nitroxide equivalent in an NMP-like system, synthesis of the stable radical **3a** (Scheme 8) was achieved in three steps starting from low cost commercially available phenyl hydrazine and benzoyl chloride. For an initial screen, **3a** was combined with styrene and benzoyl peroxide at 125 °C. At low conversions, controlled polymerization was observed with good agreement between theoretical and experimental molecular weights, as well as low dispersities (see Table 3.3). However, at conversions above ca. 14%, the polymerization became uncontrolled. To overcome this, atom transfer radical addition was carried out to convert triazine radical **3a** into the unimolecular initiator (**4a**, see Scheme 8) in analogy with NMP literature where unimolecular initiators exhibit improved polymerization behavior over their stable free radical counterparts.^[13,19] Accordingly, the parent triazine-based unimolecular initiator **4a** displays superior control over the bulk polymerization of styrene up to high conversions (~80%), with low dispersities ($M_w/M_n = 1.15\text{--}1.23$, see Table 3.4). These initial results encouraged preparation of a series of triazine-based unimolecular initiators and exploration of their potential in controlled radical polymerizations.

In a systematic study examining the influence of the electronic nature of the triazine radical, unimolecular initiators **4b** and **4c** were synthesized (Scheme 8). The synthesis was analogous to that of **1a** but used para-substituted benzoyl chlorides in the initial condensation step to obtain **1b–c**. Treatment of **1b–c** with triphenylphosphine and carbon tetrachloride gave the corresponding chlorohydrazones **2b–c**, which were then condensed with aniline to give the desired stable triazine radical following oxidative cyclization.^[110] Coupling with (1-bromoethyl)benzene under a modified atom transfer radical addition step then provides the corresponding unimolecular initiators **4a–c** in



Scheme 8 Synthetic platform for triazine unimolecular initiators.

moderate to high yields. Single crystal X-ray analysis of **4a** confirmed the attachment of the 2-methyl benzyl unit on the *N*-4 position (Figure 3.3).

It is important to note that this synthetic strategy provides a platform for producing a wide variety of triazine structures, many of which may be easily accessible from the large number of commercially available aryl amines and substituted benzoyl chlorides and acids. Further, these molecules are inherently chromophoric (Figure 3.13). Both the electron-neutral and donating (**4a–b**) triazines have absorption maxima (λ_{max}) of 315 nm, while the electron-withdrawing derivative (**4c**) has a significant red-shift ($\lambda_{max} = 430$ nm) (see Figure 3.13). Compared to other CRP techniques, these tunable chromophoric properties are a distinct advantage as they allow for facile chain-end verification via UV-vis spectroscopy. They also provide application capabilities for optical imaging and biological signal enhancement.^[111]

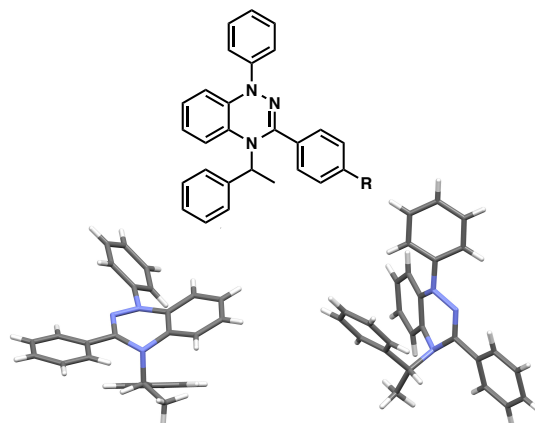


Figure 3.3 Top: General structure of triazine-based unimolecular initiator. Bottom: Crystal structure of triazine unimolecular initiator **4a** determined by X-ray crystallography.

3.3.1 Polymerization of Styrene

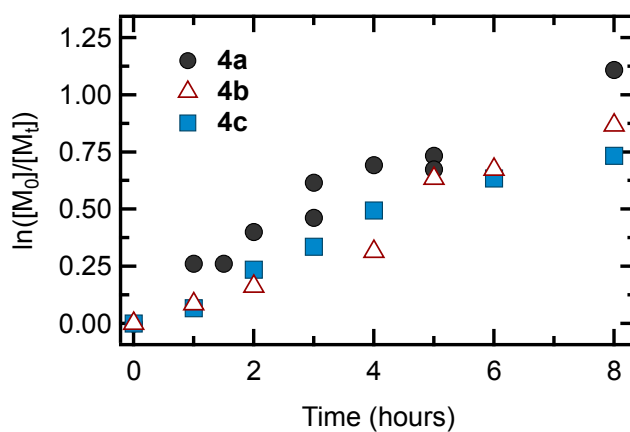


Figure 3.4 a) Kinetic plot $\ln([M_0]/[M_t])$ versus time for bulk polymerization of styrene at 125 °C with triazine unimolecular initiators **4a** (filled black circles), **4b** (open red triangles), and **4c** (filled blue squares).

Following the synthesis of unimolecular initiators **4a–c**, bulk polymerization of styrene was investigated at 125 °C, thoroughly monitoring the reaction progress over time. Significantly, controlled behavior was observed for each triazine derivative, as indicated by a linear increase in molecular weight with conversion, and low dispersities ($M_w/M_n = 1.1–1.3$) (Figure 3.5a–b). Additionally, the linear semi-logarithmic plot of $\ln([M_0]/[M_t])$

versus time (Figure 3.4) indicates first order reaction kinetics and a constant radical concentration over the course of the polymerization. Interestingly, introducing electron-donating (**4b**, OMe) or electron-withdrawing (**4c**, CN) groups into the *C*-3 position (Figure 3.1b) gave very little difference in the polymerization kinetics or control, though they do provide a valuable handle for tuning chain-end absorption properties (vide supra). Controlled polymerization was also observed at temperatures as low as 110 °C (Table 3.4), although a marked decrease in rate occurred.

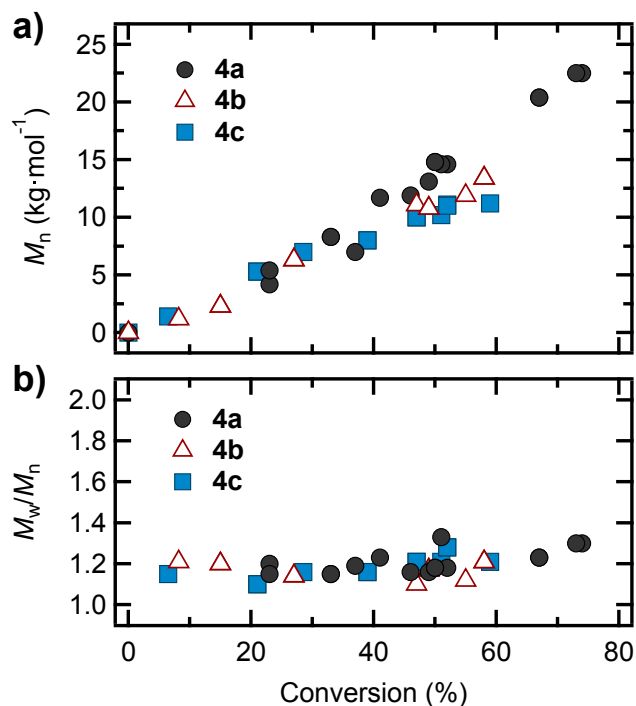


Figure 3.5 (a) Evolution of experimental molecular weight versus conversion for the polymerization of styrene using unimolecular initiators **4a**, **4b**, and **4c** and (b) the corresponding M_w/M_n values demonstrate controlled polymerization for all triazines tested.

Having established a controlled chain-growth process for unimolecular initiators **4a**–**4c**, a range of molecular weights were targeted by adjusting the ratio of **4a** to styrene (1–45 $\text{kg}\cdot\text{mol}^{-1}$, Figure 3.6 and Table 3.5). Indeed, low dispersity and good agreement between experimental and theoretical molecular weights were consistently observed under

bulk conditions. This demonstrates the ease in preparation of a range of materials, and provides evidence for the potential of triazine-mediated controlled polymerization.

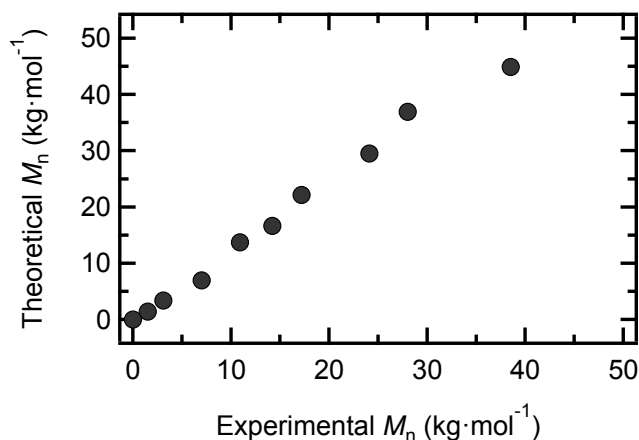


Figure 3.6 Relationship between experimental and theoretical molecular weights for the polymerization of styrene targeted at different molecular weights, initiated with **4a**, run at 125 °C for 8 hours.

3.3.2 Demonstrations of Chain End Fidelity

To further illustrate the living radical nature of this process, chain end control was thoroughly studied. First, a polystyrene homopolymer was grown using unimolecular initiator **4b** and investigated by ¹H-NMR. The methoxy group of **4b** has a diagnostic ¹H-NMR signal at 3.8 ppm, which was used as a handle for molecular weight calculation (Figure 3.7). The theoretical molecular weight as well as experimental molecular weights determined by both ¹H-NMR and SEC were all in good agreement, verifying controlled polymerization and high retention of the triazine chain ends. Moreover, SEC monitoring of UV-vis absorption and comparison of RI and UV-vis detection confirmed that the triazine moiety was present across the entire weight-range (Figure 3.8).

Excellent chain end fidelity naturally led to examining the use of these homopolymers as stable macroinitiators for block copolymer formation. Unimolecular initiator **4a** was employed to extend isolated polystyrene homopolymers to give poly(styrene-*b*-styrene)

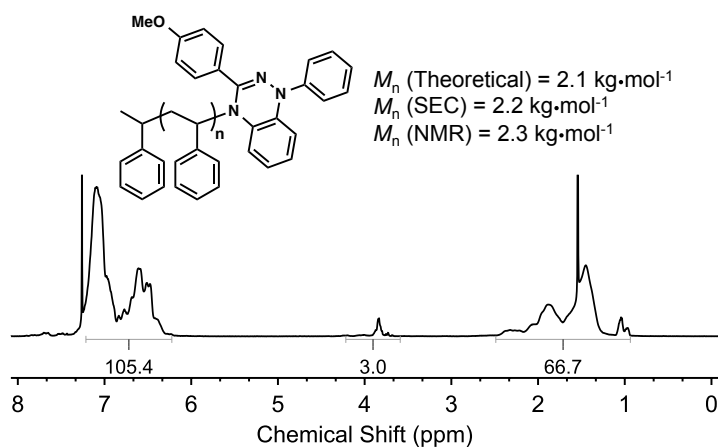


Figure 3.7 ¹H-NMR spectrum of polystyrene synthesized using triazine unimolecular initiator **4b** demonstrating high retention of triazine chain ends.

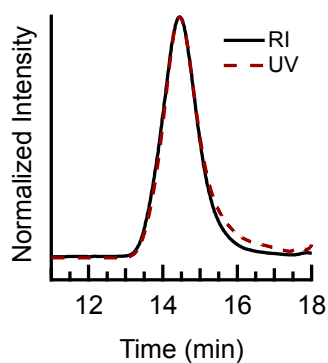


Figure 3.8 Overlaid refractive index (solid black line) and UV detector (350 nm, dashed red line) SEC traces of polystyrene terminated with triazine unimolecular initiator **4a**, $M_n = 5.5 \text{ kg}\cdot\text{mol}^{-1}$, $\bar{D} = 1.13$. The UV trace has been shifted by 14 seconds to account for the detector offset.

and poly(styrene-*b*-4-vinylanisole) diblock copolymers (Figure 3.9) with minimal tailing in the low molecular weight region of their respective SEC chromatographs, validating the retention of triazine end-groups throughout the polymerization. These experiments clearly demonstrate that a living process is occurring, and that triazine-based mediators have the ability to control the synthesis of multiblock copolymers.

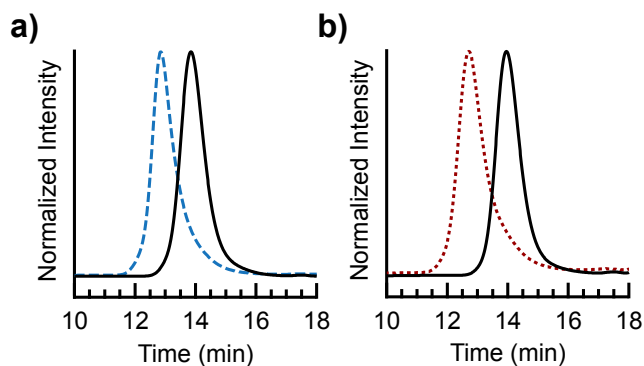


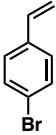

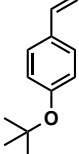
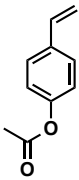
Figure 3.9 SEC traces of block copolymer syntheses: (a) (black solid line) polystyrene macroinitiator ($M_n = 13.1 \text{ kg}\cdot\text{mol}^{-1}$, $M_w/M_n = 1.16$), (blue dashed line) poly(styrene-*b*-styrene) ($M_n = 25.1 \text{ kg}\cdot\text{mol}^{-1}$, $M_w/M_n = 1.26$); (b) (black solid line) polystyrene macroinitiator ($M_n = 11.9 \text{ kg}\cdot\text{mol}^{-1}$, $M_w/M_n = 1.16$), (red dotted line) poly(styrene-*b*-4-vinylanisole) ($M_n = 28.5 \text{ kg}\cdot\text{mol}^{-1}$, $M_w/M_n = 1.27$).

3.3.3 Functional Group Tolerance — Copolymerizations

The triazine system was then evaluated for functional group tolerance through copolymerization experiments, with a focus on comonomers containing functional groups commonly used for post-polymerization modifications (Table 3.1). Thus, using unimolecular initiator **4a**, copolymerizations with styrene were conducted with high comonomer loadings (50–90 mol%) of halogenated styrenics, including chlorides and bromides, as well as protected phenols. In all cases, polymerizations showed controlled behavior. Subsequently, homopolymerization of the same functional monomers were examined, and again low dispersities were observed (Table 3.1), further demonstrating the robust nature of triazine-mediated polymerizations.

These initial results using functional styrene monomers encouraged the exploration of triazine-based unimolecular initiators for the polymerization of other monomer families. Consequently, a series of copolymerizations of styrene with butyl acrylate and methyl methacrylate were conducted. When butyl acrylate was copolymerized with styrene in bulk at 125 °C employing the unimolecular initiator **4a**, well-defined polymers with low dispersities were observed up to 50 mol% acrylate loadings (Table 3.2). Loadings of

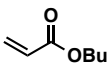
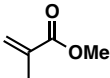
Table 3.1 Dispersities and experimental molecular weights (M_n) for bulk random copolymerizations of styrene and styrenic derivatives in the presence of **4a**.

Comonomer	Molar ratio of styrene/co-monomer	M_n (kg·mol ⁻¹)	M_w/M_n
	50/50	15.4	1.32
	10/90	15.5	1.38
	0/100	14.7	1.34
	50/50	12.5	1.27
	10/90	13.0	1.27
	0/100	12.2	1.47
	50/50	21.3	1.24
	10/90	17.6	1.26
	0/100	19.3	1.26
	50/50	13.0	1.35
	10/90	15.0	1.43
	0/100	15.3	1.47

Reaction conditions: Unimolecular initiator **4a** (1.0 equivalent), monomer (200 equivalents), in bulk at 125 °C for 12 hours. M_n and M_w/M_n determined using SEC, relative to linear polystyrene standards.

> 50 mol% butyl acrylate dramatically reduced the rate of polymerization. Further work is needed to fully understand the mechanism behind this behavior. However, in contrast to the butyl acrylate system, copolymerizations of styrene with methyl methacrylate resulted in a controlled system at up to 90 mol% methyl methacrylate ($M_w/M_n = 1.1$ – 1.34). In stark contrast to NMP, triazine-mediated polymerizations do not suffer from termination by disproportionation of chain ends, as indicated by an absence of peaks in the 5.50–6.20 ppm region of the ¹H-NMR spectrum (Figure 3.15).^[95,112] Although homopolymerization of butyl acrylate and methyl methacrylate currently do not show controlled behavior, these initial results suggest that triazines may be further developed to control polymerization of these important monomer families.

Table 3.2 Dispersities and experimental molecular weights (M_n) for the bulk random copolymerizations of styrene and butyl acrylate or methyl methacrylate in the presence of **4a**.

Comonomer	Molar ratio of styrene/co-monomer	M_n (kg·mol ⁻¹)	M_w/M_n
	90/10	16.8	1.17
	80/20	14.8	1.18
	60/40	15.6	1.27
	50/50	14.8	1.32
	90/10	11.6	1.11
	60/40	16.4	1.16
	40/60	16.9	1.22
	20/80	14.4	1.27
	10/90	11.1	1.34

Reaction conditions: Unimolecular initiator **4a** (1.0 equivalent), 200 total monomer equivalents, in bulk, at 125 °C for 8 hours. M_n and M_w/M_n determined using SEC.

3.4 Conclusion

Triazine-based stable radicals have been developed for controlled radical polymerization. A tunable synthesis allowed for the production of a variety of unimolecular initiators and their ability to mediate the polymerization of styrene was demonstrated with a linear increase in molecular weight with conversion and first order kinetics. A variety of functional styrenic derivatives could be homopolymerized and the copolymerization of styrene with butyl acrylate or methyl methacrylate resulted in well-defined polymers. Control over chain ends was demonstrated via UV-vis, NMR, and block copolymerization experiments. These initial results demonstrate the utility of triazine derivatives as stable radicals for controlling the polymerization of vinyl monomers.

3.5 Experimental

3.5.1 Materials and Equipment

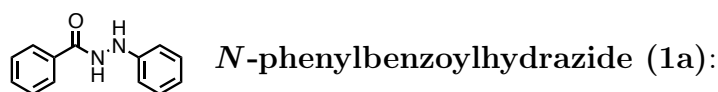
All reactions were conducted under Argon unless noted. Benzoyl peroxide (BPO, 97%), *N,N,N',N',N''*-pentamethyldiethylenetriamine (PMDETA) (99%), Cu(0) (99%), and CuBr (99.999%) were purchased from Sigma Aldrich and used as received. Monomers were passed through a column of basic alumina to remove inhibitors before use. Nuclear magnetic resonance (NMR) spectra were recorded on a Varian 400 MHz, Varian 500 MHz, or a Varian 600 MHz instrument. All ^1H -NMR experiments are reported in δ units, parts per million (ppm), and were measured relative to the signals for residual chloroform (7.26 ppm) in the deuterated solvent, unless otherwise stated. All ^{13}C -NMR spectra are reported in ppm relative to deuterated chloroform (77.23 ppm), unless otherwise stated, and all were obtained with ^1H decoupling. VG70 Magnetic Sector and Waters GCT Premier TOF instruments were used for low- and high-resolution mass analysis by electron ionization (EI). A Micromass QTOF2 Quadrupole/Time-of-Flight Tandem mass spectrometer was used for high-resolution mass analysis using electrospray ionization (ESI). Size exclusion chromatography (SEC) was performed on a Waters 2695 separation module with a Waters 2414 refractive index detector in chloroform with 0.25% triethylamine. Number average molecular weights (M_n) and weight average molecular weights (M_w) were calculated relative to linear polystyrene standards.

3.5.2 General Procedure for the Preparation of

Benzoyl Hydrazine 1(a-c)

Benzoyl hydrazine was synthesized using a modified literature procedure.^[113] Briefly, triethylamine (12.8 mL, 92.5 mmol) was added to a solution of phenylhydrazine (5 g,

46.3 mmol) in THF (60 mL) at 0 °C. The resulting mixture was stirred at 0 °C for 10 min and a solution of benzoyl chloride (46.3 mmol) in THF (30 mL) was added dropwise. The reaction mixture was stirred for 18 h while allowing it to slowly warm to room temperature. The solvent was evaporated under reduced pressure and the residue was dissolved in ethyl acetate (EtOAc) (150 mL), washed with water (2 × 100 mL), then dried over MgSO₄. The solvent was removed in vacuo. Recrystallization from a minimum amount of dichloromethane gave rise to **1a**, **1b** and **1c**.



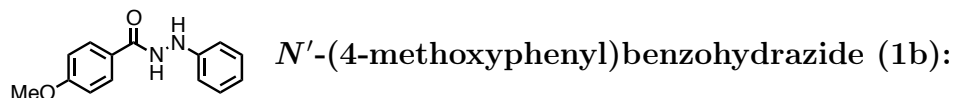
Yield: Colorless solid (60 %).

¹H-NMR (500 MHz, DMSO-d₆): δ (ppm) = 10.35 (d, J = 2.7 Hz, NH, 1 H), 7.90 (m, 2 H), 7.88 (d, J = 2.6 Hz, NH, 1 H), 7.56 (m, 1 H), 7.49 (m, 2 H), 7.14 (dd, J = 8.5, 7.2 Hz, 2 H), 6.78 (m, 2 H), 6.70 (m, 1 H).

¹³C-NMR (125 MHz, DMSO-d₆): δ (ppm) = 166.8, 150.0, 133.5, 132.1, 129.2, 128.9, 127.7, 119.1, 112.8.

IR (neat): $\tilde{\nu}$ (cm⁻¹) = 3268, 3056, 1642, 1600, 1494, 1481, 1303, 1205, 901, 750.

HR-ESI C₁₃H₁₂N₂O (M+Na)⁺: calculated 235.0847, found 235.0832.



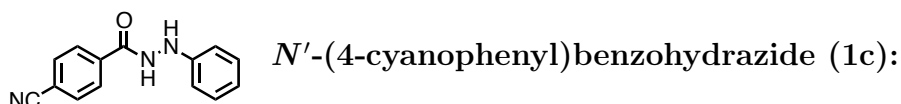
Yield: Colorless solid (50 %).

¹H-NMR (500 MHz, CDCl₃): δ (ppm) = 7.91 (br, NH, 1 H), 7.81 (d, J = 8.8 Hz, 2 H), 7.24 (m, 2 H), 6.96–6.91 (m, 5 H), 6.34 (br, NH, 1 H), 3.86 (s, 3 H).

¹³C-NMR (150 MHz, CDCl₃): δ (ppm) = 162.7, 148.2, 129.2, 129.0, 124.4, 121.3, 114.0, 113.8, 55.4.

IR (neat): $\tilde{\nu}$ (cm⁻¹) = 3261, 1636, 1601, 1494, 1247, 1172, 1027, 903, 843, 751.

HR-ESI $C_{14}H_{14}N_2O_2$ (M)+: calculated 242.1055, found 242.1065.



Yield: Yellow solid (51 %).

$^1\text{H-NMR}$ (500 MHz, DMSO-d_6): δ (ppm) = 10.59 (d, J = 2.7 Hz, NH, 1 H), 8.05 (d, J = 8.4 Hz, 2 H), 7.98 (d, J = 8.3 Hz, 3 H), 7.14 (dd, J = 8.5, 7.2 Hz, 2 H), 6.78 (d, J = 7.3 Hz, 2 H), 6.72 (dd, J = 7.3, 1.1 Hz, 1 H).

$^{13}\text{C-NMR}$ (125 MHz, DMSO-d_6): δ (ppm) = 165.5, 149.6, 137.5, 133.1, 129.2, 128.6, 119.3, 118.7, 114.5, 112.8.

IR (neat): $\tilde{\nu}$ (cm^{-1}) = 3243, 2232, 1648, 1600, 1493, 1307, 1250, 904, 862, 747.

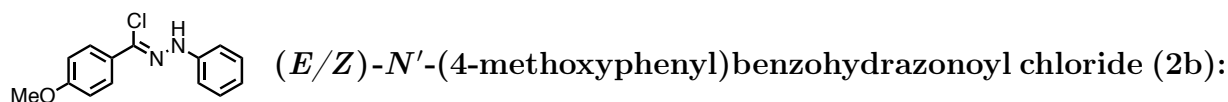
HR-ESI $C_{14}H_{11}N_3O$ (M+Na)+: calculated 260.0794, found 260.0791.

3.5.3 General Procedure for the Preparation of Benzohydrazonoyl Chloride 2(a–c)

To a dried flask was added a suspension of **2a–c** (22.0 mmol), triphenylphosphine (27.2 mmol), and anhydrous carbon tetrachloride (27.2 mmol) in anhydrous acetonitrile (60 mL). The mixture was stirred overnight at room temperature. Afterwards, solvent was evaporated under reduced pressure and the crude product was purified by chromatography on silica gel (see below).



Compound **2a** was obtained according to literature procedure.^[114]



Compound **2b** was obtained following the general procedure (EtOAc:hexanes, 1:30).

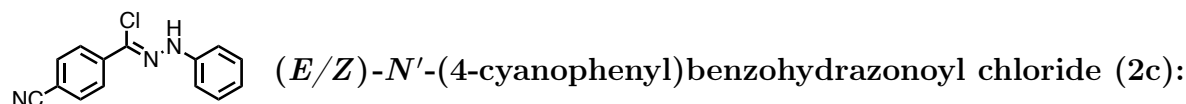
Yield: Colorless solid (62 %).

¹H-NMR (500 MHz, CDCl₃): δ (ppm) = 7.94 (br, NH, 1 H), 7.86 (d, J = 8.9 Hz, 2 H), 7.31 (m, 2 H), 7.16 (d, J = 7.7 Hz, 2 H), 6.93 (d, J = 8.9 Hz, 2 H), 3.85 (s, 3 H).

¹³C-NMR (150 MHz, CDCl₃): δ (ppm) = 160.5, 143.6, 132.1, 132.0, 131.9, 129.3, 128.5, 128.4, 127.9, 127.1, 124.7, 120.8, 113.8, 113.3, 55.4.

IR (neat): $\tilde{\nu}$ (cm⁻¹) = 3314, 1600, 1500, 1434, 1259, 1109, 940, 825, 754.

HR-ESI C₁₄H₁₃N₂OCl (M)⁺: calculated 260.0716, found. 260.0717.



Compound **2c** was obtained following the general procedure (EtOAc:hexanes, 1:30).

Yield: yellow solid (96 %).

¹H-NMR (500 MHz, CDCl₃): δ (ppm) = 8.21 (s, NH, 1 H), 8.01 (d, J = 8.5 Hz, 2 H), 7.68 (d, J = 8.6 Hz, 2 H), 7.34 (dd, J = 8.6, 7.3 Hz, 2 H), 7.24 (m, 2 H), 7.01 (m, 1 H).

¹³C-NMR (125 MHz, CDCl₃): δ (ppm) = 142.5, 138.5, 132.2, 132.1, 132.1, 129.5, 128.6, 128.5, 126.5, 122.4, 122.1, 118.6, 113.7, 112.1.

IR (neat): $\tilde{\nu}$ (cm⁻¹) = 3288, 2219, 1601, 1544, 1495, 1237, 1164, 947, 833, 736.

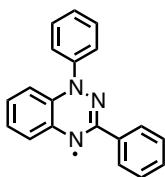
HR-ESI HC₁₄H₁₀N₃Cl (M+Na)⁺: calculated 278.0461, found 278.0454.

3.5.4 General Procedure for the Preparation of

Benzo-1,2,4-triazinyl Radical **3(a-c)**

Benzo-1,2,4-triazinyl radical **3(a-c)** was prepared following a modified literature procedure.^[110] A solution of **2a** (1.50 g, 5.70 mmol), aniline (0.57 mL, 6.27 mmol) and TEA

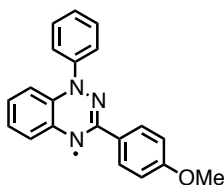
(1.20 mL, 8.65 mmol) in 25 mL benzene was refluxed overnight. The solvent was removed under reduced pressure and the mixture was diluted with CH₂Cl₂ before extracting with 50 mL cold water. The organic phase was then washed with brine and dried over MgSO₄ before concentration under reduced pressure. The residue was treated with Pd/C (9.5 mg, 1.6 mol%) and 1,8-diazabicycloundec-7-ene (DBU) (0.8 mL) in CH₂Cl₂ (50 mL). The reaction mixture was stirred in air at room temperature for 3 h until thin layer chromatography (TLC) showed the presence of a new fast running brown compound (CH₂Cl₂/hexanes 1/1). The solvent was evaporated under reduced pressure, and the residue was purified by silica gel column chromatography (EtOAc:hexanes, 5:95) to give **3a** as a black solid.



1,3-Diphenyl-1,4-dihydro-1,2,4-benzotriazin-4-yl (3a):

Yield: black solid (36 %).

HRMS C₁₉H₁₄N₃ (M)⁺: calculated 284.1188, found 284.1175.

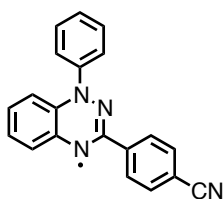


1-Phenyl-3-(4-methoxyphenyl)-1,2,4-benzotriazin-4-yl (3b):

Yield: black solid (50 %).

IR (neat): $\tilde{\nu}$ (cm⁻¹) = 1606, 1479, 1390, 1247, 1167, 1026, 837, 753.

HRMS C₂₀H₁₇N₃O (M+H)⁺: calculated 315.1372, found 315.1359.



1-Phenyl-3-(4-cyanophenyl)-1,2,4-benzotriazin-4-yl (3c):

Yield: dark green solid (36 %).

IR (neat): $\tilde{\nu}$ (cm⁻¹) = 3044, 2227, 1592, 1482, 1385, 1207, 1079, 858, 735.

HRMS C₂₀H₁₃N₄ (M)⁺: calculated 309.1140, found 309.1130.

3.5.5 General Procedure for the Preparation of Triazine Unimolecular Initiators 4(a–c)

A solution of benzene (20 mL) was sparged with argon for 30 minutes. CuBr (2.6 mmol, 0.37 g), PMDETA (5.2 mmol, 1.09 mL), and Cu(0) (2.6 mmol, 0.17 g) were placed into a schlenk flask which was subsequently evacuated and backfilled with argon three times. **3a** (1.75 mmol, 500 mg) and 1-bromoethylbenzene (1.5 equiv, 2.6 mmol, 0.36 mL) were diluted with 10 mL of degassed benzene and transferred to the schlenk flask. The reaction mixture was stirred at room temperature for 24 h. The solution was then filtered, diluted with CH₂Cl₂ (50 mL), and washed with deionized water (3 × 50 mL) to remove the copper complex. The organic layer was dried over anhydrous MgSO₄. The solvent was removed under reduced pressure, and the crude product was purified by silica gel column chromatography (EtOAc:hexanes, 5:95) to give **4a** as a yellow powder.

1,3-diphenyl-4-(1-phenylethyl)-1,4-dihydro-1,2,4-benzotriazine (4a):

Yield: yellow powder (82 %).

¹H-NMR (500 MHz, CDCl₃): δ (ppm) = 7.91 (m, 2 H), 7.40 (m, 3 H), 7.33 (t, J = 7.8 Hz, 2 H), 7.24 (m, 3 H), 7.19 (m, 4 H), 7.13 (m, 1 H), 6.84 (m, 2 H), 6.75 (m, 1 H), 6.52 (d, J = 5.0 Hz, 1 H), 4.66 (q, J = 7.0 Hz, 1 H), 1.75 (d, J = 7.1 Hz, 3 H).

¹³C-NMR (150 MHz, CDCl₃): δ (ppm) = 149.4, 144.0, 143.3, 141.5, 134.5, 130.4, 129.3, 128.8, 128.4, 127.9, 127.6, 127.6, 127.5, 125.1, 124.5, 124.4, 123.3, 122.5, 111.9, 61.2, 19.7.

IR (neat): $\tilde{\nu}$ (cm⁻¹) = 2982, 1586, 1486, 1293, 1053, 757.

HR-ESI C₂₇H₂₃N₃ (M)⁺: calculated 389.1892, found 389.1900.

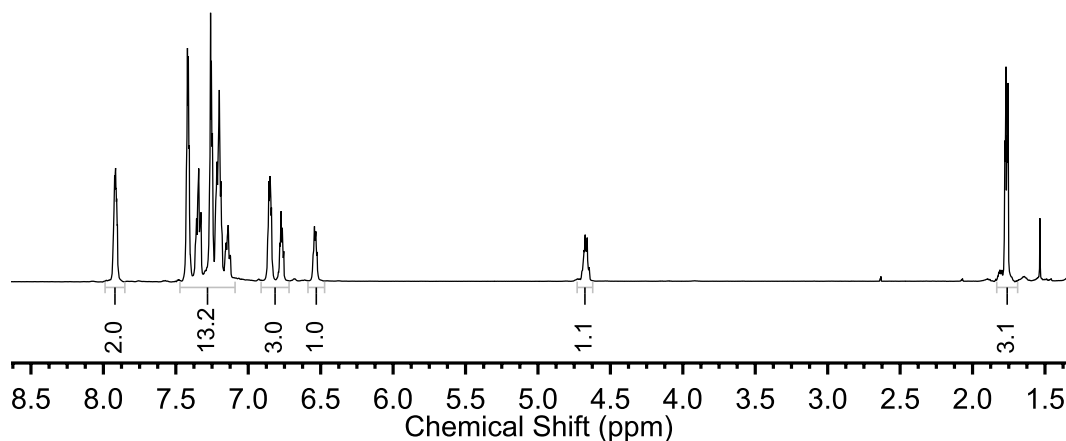


Figure 3.10 ^1H -NMR spectrum of triazine unimolecular initiator **4a**.

1-Phenyl-3-(4-methoxyphenyl)-4-(1-phenylethyl)-1,4-dihydro-1,2,4-benzotriazine (4b):

Yield: yellow powder (58 %).

^1H -NMR (500 MHz, CDCl_3): δ (ppm) = 7.84 (d, $J = 9.0$ Hz, 2 H), 7.32 (dd, $J = 8.4$, 7.2 Hz, 2 H), 7.24 (m, 3 H), 7.19 (m, 4 H), 7.11 (t, $J = 7.3$ Hz, 1 H), 6.94 (m, 2 H), 6.83 (m, 2 H), 6.74 (m, 1 H), 6.53 (m, 1 H), 4.68 (q, $J = 7.1$ Hz, 1 H), 3.86 (s, 3 H), 1.75 (d, $J = 7.1$ Hz, 3 H).

^{13}C -NMR (125 MHz, $\text{DMSO}-d_6$): δ (ppm) = 160.9, 150.2, 143.7, 143.3, 141.8, 130.9, 129.4, 129.3, 128.4, 127.9, 127.5, 126.2, 125.6, 124.7, 124.2, 123.1, 122.8, 114.5, 111.8, 60.8, 55.7, 20.4.

IR (neat): $\tilde{\nu}$ (cm^{-1}) = 2832, 1602, 1452, 1252, 1166, 1038, 841, 737.

HRMS $\text{C}_{28}\text{H}_{26}\text{N}_5\text{O}_3$ ($\text{M}+\text{H}$) $^+$: calculated 420.2076, found 420.2057.

1-Phenyl-3-(4-cyanophenyl)-4-(1-phenylethyl)-1,4-dihydro-1,2,4-benzotriazine (4c):

Yield: orange powder (71 %).

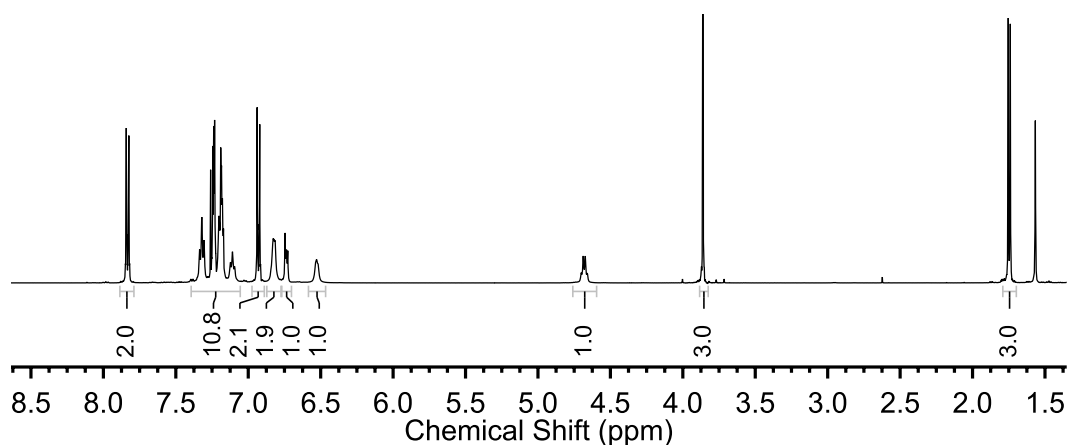


Figure 3.11 ^1H -NMR spectrum of triazine unimolecular initiator **4b**.

^1H -NMR (500 MHz, CDCl_3): δ (ppm) = 7.99 (d, $J = 8.4$ Hz, 2 H), 7.65 (d, $J = 8.4$ Hz, 2 H), 7.33 (m, 2 H), 7.28–7.14 (m, 4 H), 7.12–7.04 (m, 4 H), 6.96–6.81 (m, 3 H), 6.48 (dd, $J = 8.0, 1.4$ Hz, 1 H), 4.47 (q, $J = 7.1$ Hz, 1 H), 1.73 (d, $J = 7.1$ Hz, 3 H).

^{13}C -NMR (125 MHz, CDCl_3): δ (ppm) = 146.2, 143.8, 142.7, 140.8, 139.6, 132.2, 129.5, 129.0, 128.0, 127.9, 127.6, 127.6, 125.6, 125.3, 125.3, 123.8, 123.3, 118.9, 112.2, 112.1, 62.4, 19.7.

IR (neat): $\tilde{\nu}$ (cm^{-1}) = 2930, 2224, 1588, 1485, 1293, 846, 755.

HRMS $\text{C}_{28}\text{H}_{22}\text{N}_4$ ($\text{M}+\text{H}$) $^+$: calculated 415.1923, found 415.1906.

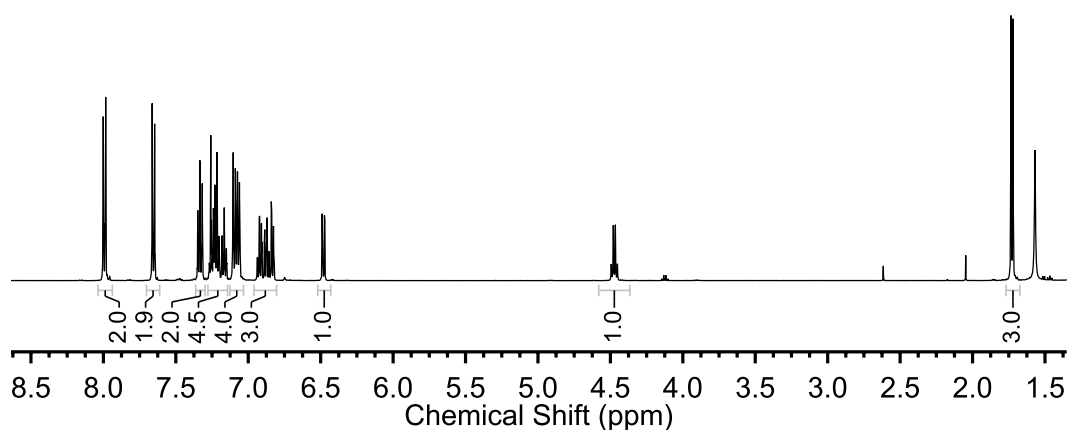


Figure 3.12 ^1H -NMR spectrum of triazine unimolecular initiator **4c**.

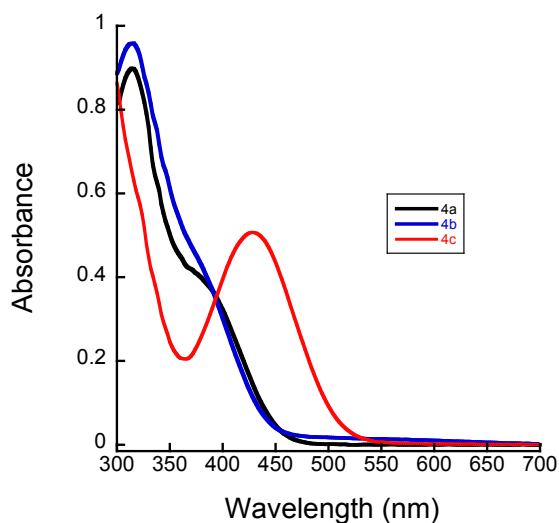


Figure 3.13 UV-vis spectra of triazine unimolecular initiators **4a–c** in CH₂Cl₂.

3.5.6 General Procedure for Styrene Polymerization

A vial equipped with a magnetic stir bar and fitted with a teflon screw cap septum was charged with desired triazine unimolecular initiator **4** (10 mg, 0.025 mmol, 1 equiv) and styrene (0.74 mL, 6.4 mmol, 250 equiv). The solution was degassed using three freeze-pump-thaw cycles. The vial was then backfilled with argon and stirred at 125 °C for 6 h. The reaction mixture was dissolved in dichloromethane (1 mL) and precipitated in MeOH. The resulting solid was dried, redissolved, and precipitated a second time into MeOH. After drying, the polymers were analyzed by SEC to give the number average M_n , M_w and dispersity (M_w/M_n) of the polymer.

Table 3.3 Polymerization of styrene (250 equivalents) at 125 °C in bulk, and mediated by triazinyl radical **3(a–c)**.

Entry	Conditions	Time (h)	Conversion ^a (%)	M_n^b (kg·mol ⁻¹)	$M_n(\text{theoretical})^c$ (kg·mol ⁻¹)	\bar{D}^b
1	3a	5	< 5	nd	nd	nd
2	3a BPO (0.5 equiv)	1	–	–	–	–
		2	–	–	–	–
		3	14	4.2	3.6	1.16
		4	17	9.2	4.4	1.24
		5	23	11.2	5.9	1.35
		7	29	15.1	7.6	1.53
		9	31	16.0	8.0	1.65
		12	36	16.3	9.5	1.68
3	3b	5	< 5	nd	nd	nd
4	3b , BPO (0.5 equiv)	7	19	11.8	7.1	1.44
5	3c	1	–	–	–	–
		3	–	–	–	–
		5	3	2.6	0.8	1.08
		7	12	5.4	3.0	1.14
		9	20	7.8	5.3	1.33
		11	22	7.7	5.8	1.42
		13	22	7.9	5.8	1.53
6	3c , BPO (0.5 equiv)	1	–	–	–	–
		2	–	–	–	–
		3	–	–	–	–
		5	7	5.4	1.8	1.17
		7	12	8.3	3.1	1.44
		10	15	9.1	4.0	1.54
		12	20	10.0	5.2	1.61

^aConversion determined by ¹H-NMR, ^bdetermined by SEC analysis relative to linear polystyrene standards, ^ctheoretical molecular weight calculated on the basis of monomer conversion, ndnot determined.

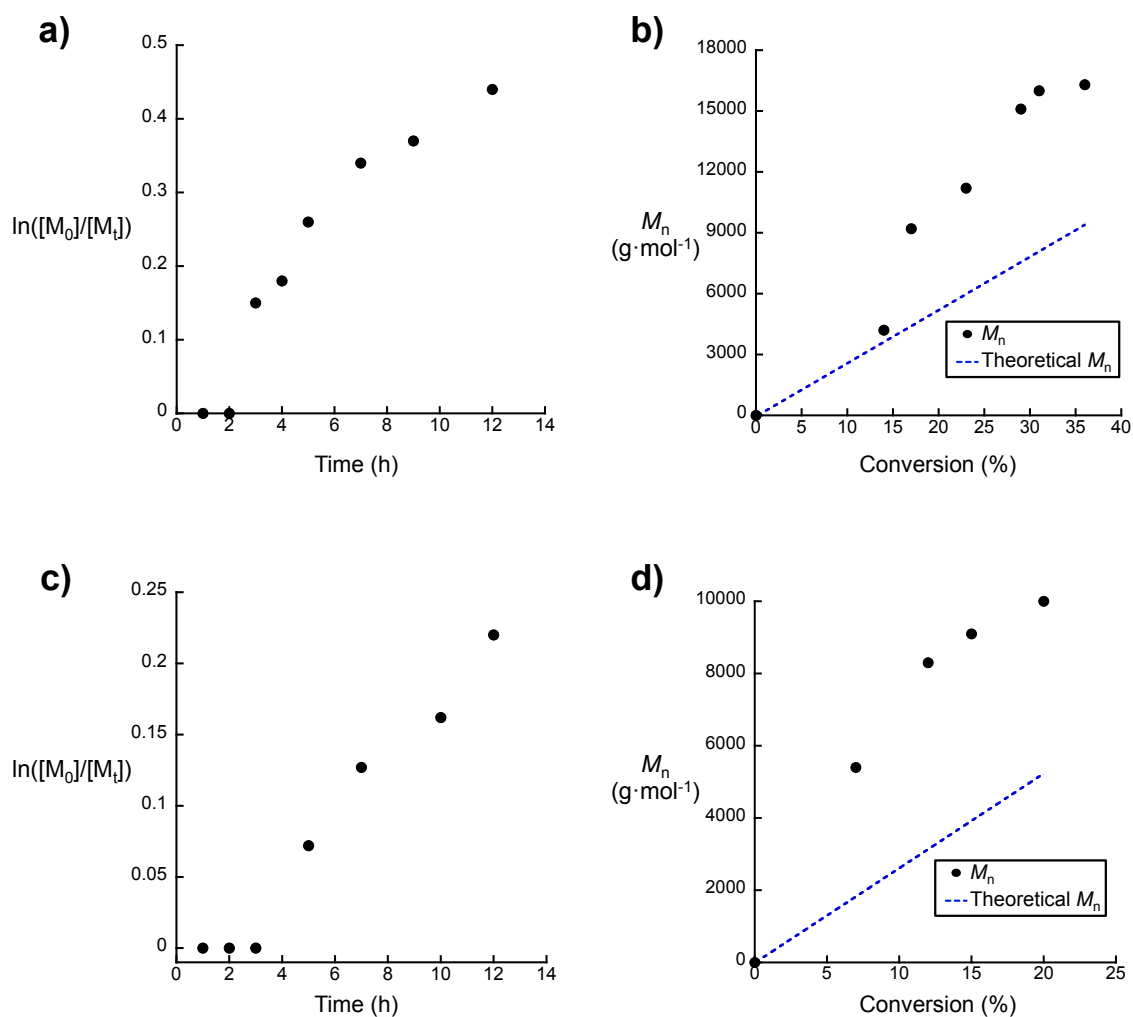


Figure 3.14 a) Kinetic plot $\ln([M_0]/[M_t])$ versus time for bulk polymerization of styrene at 125 °C with triazinyl radical **3a** and BPO (0.5 equivalents). b) Evolution of molecular weight (M_n) **3a** versus conversion for triazine mediated polymerization. c) Kinetic plot $\ln([M_0]/[M_t])$ versus time for bulk polymerization of styrene at 125 °C in the presence of triazinyl radical **3c** and BPO (0.5 equivalents); d) Evolution of molecular weight (M_n) **3c** versus conversion for triazine mediated polymerization.

Table 3.4 Bulk polymerization of styrene (250 equivalents) at 125 °C, and mediated by triazine unimolecular initiator **4(a–c)**.

Entry	Unimolecular Initiator	Time (h)	Conversion ^a (%)	M_n^b (kg·mol ⁻¹)	$M_n(\text{theoretical})^c$ (kg·mol ⁻¹)	\bar{D}^b
1	4a	1	23	5.4	6.0	1.15
		2	33	8.3	8.7	1.15
		4	50	14.8	13.0	1.18
		8	67	20.4	17.4	1.23
2	4b	2	15	2.3	3.9	1.20
		4	27	6.3	7.0	1.14
		6	49	10.8	12.8	1.17
		8	58	13.4	15.1	1.21
3	4c	2	21	5.3	5.6	1.15
		4	39	8.0	10.1	1.16
		6	47	10.0	12.2	1.21
		8	52	11.1	13.5	1.28
4	4a^d	6	21	5.4	5.3	1.25

^aConversion determined by ¹H-NMR, ^bdetermined by SEC analysis relative to linear polystyrene standards, ^ctheoretical molecular weight calculated on the basis of monomer conversion, ^dreaction run at 110 °C using 240 equivalents of styrene to **4a**.

Table 3.5 Polymerization of Styrene targeted at different molecular weights, 125 °C, 8 hours, mediated by triazine unimolecular initiator **4a**.

Entry	[Sty] ₀ /[4a] ₀	Conversion ^a (%)	M_n^b (kg·mol ⁻¹)	$M_n(\text{theoretical})^c$ (kg·mol ⁻¹)	\bar{D}^b
1	25/1	54	1.5	1.4	1.24
2	50/1	65	3.1	3.4	1.18
3	100/1	67	5.3	7.0	1.17
4	250/1	67	17.4	20.4	1.23
5	400/1	67	20.5	28.5	1.19
6	600/1	67	35.1	42.3	1.20
7	1000/1*	50	49.5	52.0	1.40

^aConversion determined by ¹H-NMR, ^bdetermined by SEC analysis, ^ctheoretical molecular weight calculated on the basis of monomer conversion (* in 50% v/v NMP).

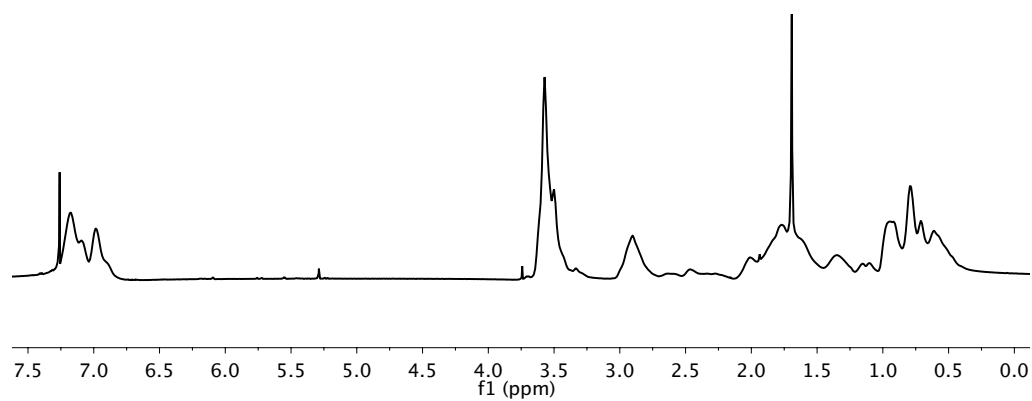


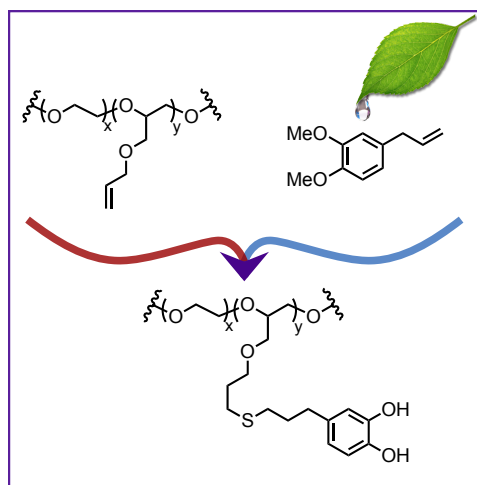
Figure 3.15 $^1\text{H-NMR}$ spectrum of PS-*r*-PMMA (monomer ratio = 20:80 styrene:methyl methacrylate).

Chapter 4

Catechol-Functionalized Polyethers[‡]

4.1 Abstract

This chapter describes a facile synthetic strategy for the functionalization of well-defined polyether copolymers with control over the number and location of catechol groups. Previously, the functionalization of polyethylene oxide (PEO)-based polymers with catechols has been limited to functionalization of the chain ends only, hampering the synthesis of adhesive and antifouling materials based on this platform. To address this challenge,



an efficient and high-yielding route to catechol-functionalized polyethers was developed, which could allow the effects of polymer architecture, molecular weight, and catechol incorporation on the adhesive properties of surface-anchored PEO to be studied.

[‡]Reproduced with permission: K.M. Mattson, A.A. Latimer, A.J. McGrath, N.A. Lynd, P. Lundberg, Z.M. Hudson, C.J. Hawker, *J. Polym. Sci., Part A: Polym. Chem.* **2015**, *53*, 2685–2692. © 2015 Wiley Periodicals, Inc. CCC License Number 3932101147554.

4.2 Introduction

Polyethylene oxide (PEO) is used widely as a thickening and lubricating agent in food products, cosmetics, and pharmaceuticals.^[115,116] Its simple chemical structure belies its wide-ranging and versatile properties, including good aqueous and organic solubility, low immunogenicity and toxicity, and large aqueous exclusion volume.^[116,117] These qualities make PEO an attractive candidate for use in polymer surface coatings.^[118–120] Grafted PEO can impart a surface with biological stealth, fouling resistance, and water solubility.^[121–123] Contact lenses, for example, can be coated with PEO to enhance their hydrophilicity and reduce biofouling.^[115,116,121]

In spite of its many applications, non-covalent grafting of PEO to a variety of different surfaces has been a challenge, as only chain end groups are available for reaction, and adhesive functional units strong enough to operate in aqueous environments are limited.^[116,117,123]

Functionalization of PEO with multiple catechol units presents a potential solution to this problem. Marine organisms, such as mussels, exploit catechol-modified proteins to adhere to a wide variety of surfaces in mechanically and chemically hostile aqueous environments. In these systems, catechols are introduced through the selective hydroxylation of tyrosine residues to give dihydroxyphenyl alanine (DOPA) units, which are believed to be at least partially responsible for the impressive binding strength of mussels on submerged surfaces.^[121–124] Furthermore, catechols are exceptionally versatile; not only can they bind to a variety of metals and metal-oxides, such as titania, silica, gold, and iron, but they can also adhere firmly to both biological tissue and bone.^[123,125–129]

While catechols have previously been employed to tether PEO to surfaces,^[122,130–141] their use has been complicated by an inability to vary the number and location of the catechol residues on the polyether backbone. In contrast to mussel foot proteins in which

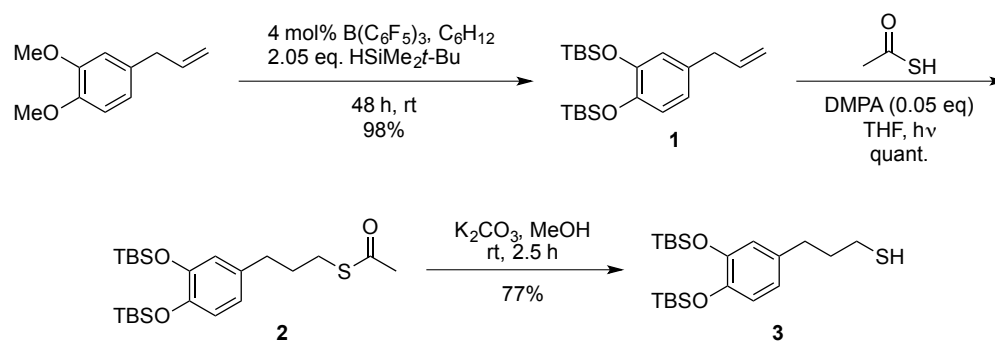
numerous DOPA residues are arrayed along the protein backbone, synthetic PEO-based materials have relied almost exclusively on solitary catechol units at one or both ends of the polymer chain. Additionally, a limited number of reports have described the incorporation of up to four catechol units at a single PEO chain end.^[133,135,137,138] Given the host of applications for surface-anchored PEO, an inexpensive and versatile method that provides control over the number and location of catechol units on a PEO backbone is needed.

PEO/catechol-based materials that more closely mimic adhesive proteins in the number and distribution of catechol units along the backbone would also facilitate fundamental studies on adhesion in aquatic organisms. It is known that catechol incorporation is just one of many factors contributing to mussel adhesion; the binding of synthetic bioinspired adhesives has been shown to depend on pH, polymer molecular weight, and chemical environment.^[127,142–146] However, the degree to which these factors play a role in adhesion has been difficult to evaluate experimentally, and has therefore remained relatively unexplored. A modular synthesis of catechol-functionalized PEO amenable to the preparation of large-scale samples that could facilitate the systematic evaluation of biomimetic adhesive materials is needed. This dissertation presents a modular strategy starting from readily available methyl eugenol to embed protected catecholic moieties at controlled levels within polyether backbones synthesized using anionic polymerization.

4.3 Results and Discussion

4.3.1 “Clickable” Catechols

This versatile, straightforward, and high-yield synthetic strategy allows access to a wide variety of well-defined catechol-functionalized polyethers. Key to this strategy is



Scheme 9 Synthetic strategy for thiol-terminated protected catechol.

the synthesis of a protected catechol with a thiol functional handle conducive to facile coupling onto polymers with pendent alkenes.

Prior work has highlighted the oxidative instability of catechol units during the multi-step functionalization of various materials. When exposed to neutral and basic conditions, the catechol can readily oxidize to its quinone form, which not only substantially decreases its adhesive capabilities but also allows for unwanted cross-linking and addition reactions.^[147,148] For this reason, a robust precursor with a protected catechol functionality was sought. Methyl eugenol, a common phenylpropanoid found in many plants,^[149] is an ideal starting material because it is both inexpensive and readily available. Direct use of methyl eugenol and methyl ether protection of the eugenol group is not viable as traditional methods for deprotecting methyl ethers can prove challenging, involving harsh conditions incompatible with numerous functional group types.^[150] For this reason, a hydro-silylation reaction catalyzed by tris(pentafluorophenyl)borane ($B(C_6F_5)_3$) was employed to exchange both methyl ether protecting groups with the synthetically more versatile *tert*-butyldimethylsilyl (TBS) groups (Scheme 9). This gives the protected product **1** in 98% yield, which is stable under ambient conditions for extended periods. Radical addition of thioacetic acid across the allyl unit of **1** facilitated installation of an acetyl-protected thiol, **2**. Treatment with mild base selectively cleaves the acetyl protecting

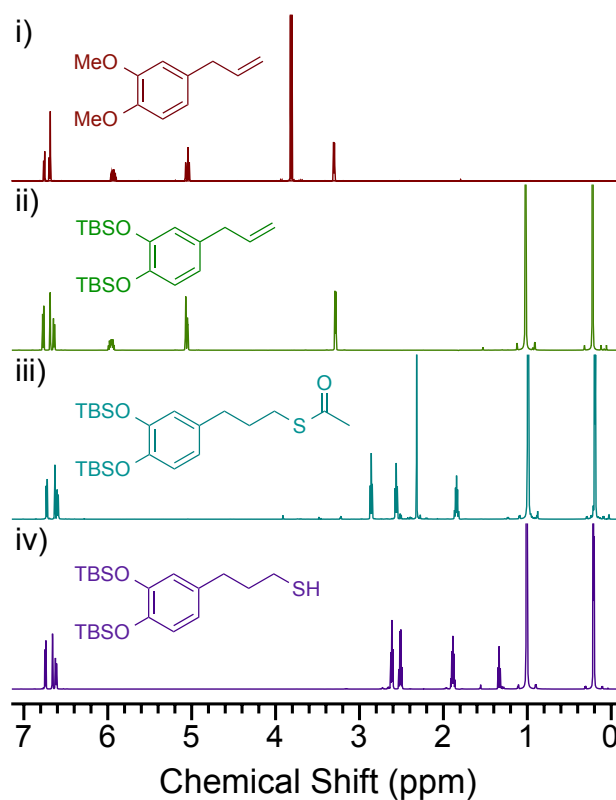


Figure 4.1 ¹H-NMR spectra showing the progression from (i) methyl eugenol to (ii) TBS-protected catechol **1**, (iii) thioacetate-terminated catechol **2**, to (iv) the thiol-functionalized protected catechol product **3**.

group, yielding the desired silyl-protected catechol derivatized with a thiol functional handle **3**. Significantly, the synthesis of **3** from methyl eugenol can be performed efficiently on a large, multi-gram scale and results in an overall yield of 75%.

4.3.2 Small Molecule Characterization

¹H-NMR shows the progression from methyl eugenol to the final product **3** (Figure 4.1). Briefly, the signature changes include the disappearance of the methyl ether signals ($\delta = 3.82$ ppm) and the corresponding appearance of the *tert*-butyl and dimethyl signals ($\delta = 1.02$ and 0.22 ppm). Quantitative installation of the *S*-acetyl protected thiol **2** is confirmed by the loss of olefin peaks ($\delta = 6.01$ – 5.91 ppm and 5.10 – 5.02 ppm), shifts in

the alkyl region, and appearance of the thioacetate methylene singlet ($\delta = 2.32$ ppm). Finally, selective cleavage of the thioacetate group in the presence of TBS is evidenced by the disappearance of the aforementioned thioacetate methylene singlet and emergence of the thiol triplet ($\delta = 1.34$ ppm) with no significant change in the TBS or aromatic regions.

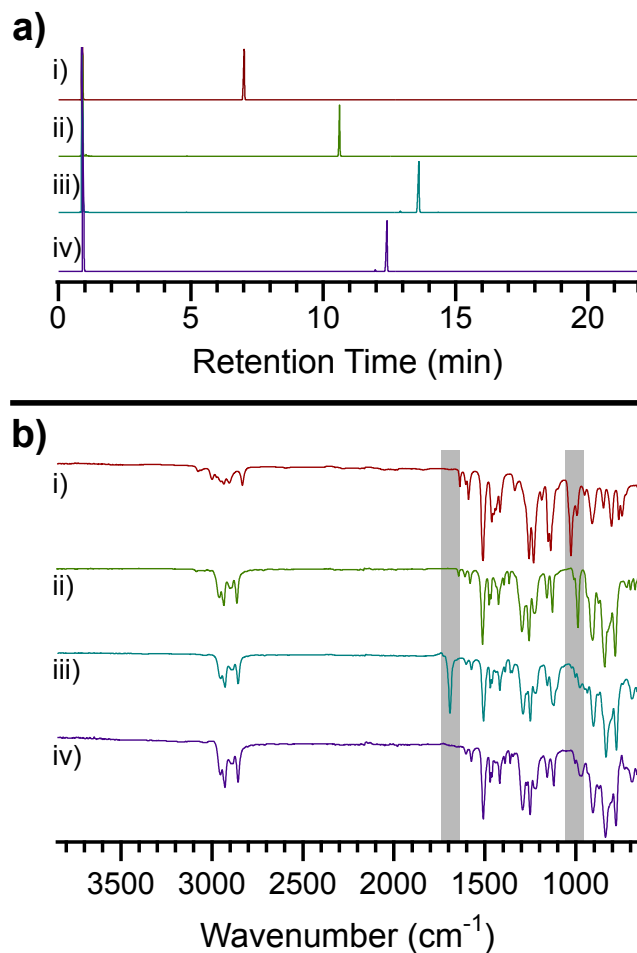


Figure 4.2 (a) Gas chromatograms depicting the progression from (i) starting material methyl eugenol to (ii) TBS-protected intermediate **1**, (iii) *S*-acetyl functionalized **2**, and (iv) silyl-protected thiol-derivatized catechol **3**. The signal at 1 minute is acetone, the solvent used for GC analysis. (b) FT-IR of (i) methyl eugenol, (ii) compound **1**, (iii) **2**, and (iv) **3**. Boxes present to emphasize the signature changes indicative of successful transformation.

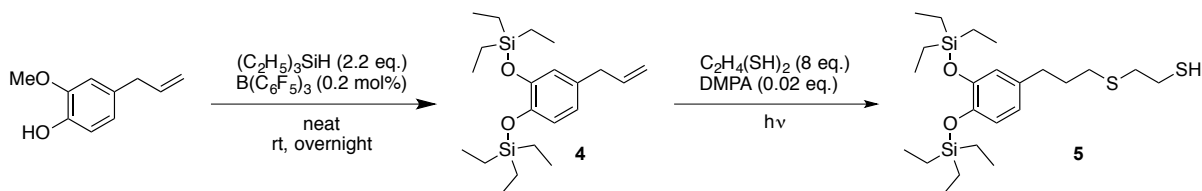
Gas chromatography (GC) further corroborates the success of each reaction shown in Scheme 9 (Figure 4.2a). Each intermediate has a distinct and unique GC profile,

confirming not only the completeness of the reaction, but also the purity of the product. Crucially, the TBS protecting groups remain intact throughout the protocol and there are no appreciable byproducts (from oxidation, disulfide formation, or otherwise).

Figure 4.2b shows the FT-IR spectra of methyl eugenol and compounds **1–3**. In the top two spectra, a strong alkene signal is clearly visible around $\tilde{\nu} = 1000 \text{ cm}^{-1}$. This signal is then replaced by the carbonyl signal at $\tilde{\nu} = 1694 \text{ cm}^{-1}$, indicating incorporation of the thioacetate. Successful cleavage of the *S*-acetyl protecting group is evidenced by the complete disappearance of the aforementioned carbonyl signal.

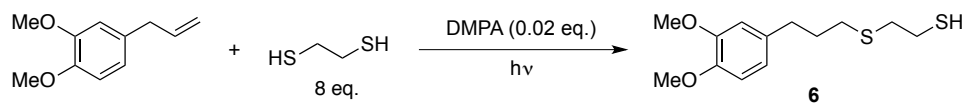
4.3.3 Early Studies — Small Molecule Optimization

The design of small molecule **3** was originally inspired by previously published work from the Hawker group.^[151] In that report, triethylsilane (TES) was used to derivatize 4-allyl-2-methoxyphenol, and then reacted with commercially available poly[(mercapto-propyl)methylsiloxane], yielding catechol-functionalized polysiloxanes. For this work, initial efforts focused on adapting this small-molecule chemistry for polyether functionalization (Scheme 10). After derivatizing the TES-protected catechol, making it amendable to thiol-ene chemistry (**5**),^[152] it was coupled to a P(EO-*co*-AGE)-*b*-PEO-*b*-P(EO-*co*-AGE) triblock copolymer.



Scheme 10 Synthesis of thiolated TES-catechol **5**.^[152]

Unfortunately, size exclusion chromatography (SEC) showed a dramatic increase in dispersity as well as the formation of a significant amount of high molecular weight byproduct (Figure 4.3a). Passing the unfunctionalized polymer through a plug of silica



Scheme 11 Synthesis of thiolated methoxy-catechol **6**.

gel before use improved the result; however, the high molecular weight peak persisted (Figure 4.3b). This peak was attributed to polymer chain-chain coupling and expended significant efforts probing its origins. The most dramatic improvement (Figure 4.3c) was realized by replacing the TES protecting groups (**5**) with methoxy groups (**6**), which are neither acid nor base labile (Scheme 11).

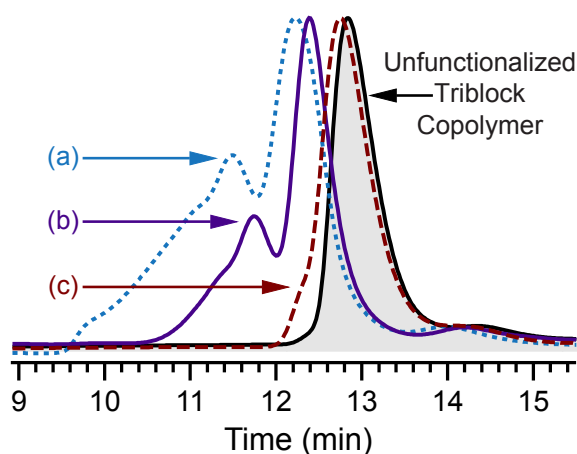


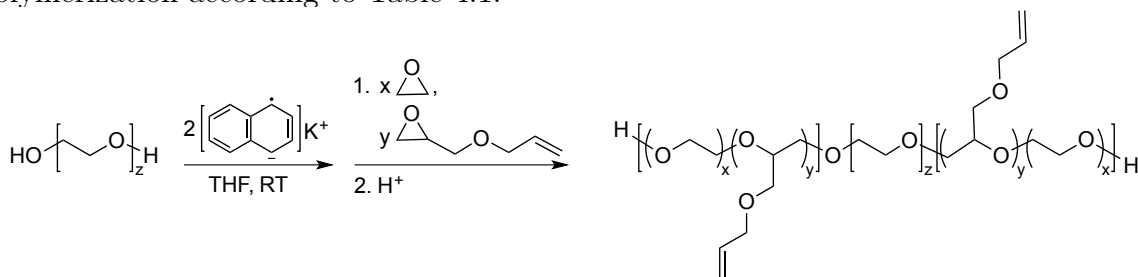
Figure 4.3 SEC traces showing the functionalization of triblock copolymer $P(\text{EO}_{98}\text{-}co\text{-AGE}_6)\text{-}b\text{-PEO}_{10\text{ kDa}}\text{-}b\text{-P}(\text{EO}_{98}\text{-}co\text{-AGE}_6)$ ($M_n = 20.0\text{ kg}\cdot\text{mol}^{-1}$; $\mathcal{D} = 1.03$) using (a) TES-catechol **5** ($\mathcal{D} = 3.18$), (b) TES-catechol **5** after passing the starting polymer through a short silica plug ($\mathcal{D} = 1.39$), and (c) with methoxy-catechol **6** after passing the starting polymer through a silica plug ($\mathcal{D} = 1.21$). Slight shift retention times result from small daily fluctuations in the instrument.

The clear improvement shown in Figure 4.3c provided compelling evidence that TES units were too labile. Despite the enhanced performance of **6**, its methyl ethers would be challenging to remove, typically requiring the use of harsh reagents like BBr_3 .^[146] It therefore became evident that different protecting groups and synthetic pathways needed to be explored. Through exchange of the TES with TBS protecting groups, the ability to use inexpensive starting materials was maintained by capitalizing upon efficient $\text{B}(\text{C}_6\text{F}_5)_3$

hydrosilation chemistry. TBS provides enhanced stability compared to TES, yet conveniently remains labile under acidic conditions. This is ideal for exposure of the catecholic moiety, as it decreases the likelihood of catechol oxidation.^[127]

4.3.4 Synthesis of Polyethers

Compared with the previous lack of methods for preparing materials with precise numbers of catechols in a polyether backbone, the mild and quantitative nature of thiol-ene chemistry for polymer functionalization, coupled with the efficient synthesis of **3**, proved ideal. A variety of random, diblock and triblock P(EO-*co*-AGE) copolymers were therefore synthesized as shown in Scheme 12. For the diblock and triblock P(EO-*co*-AGE) copolymers, copolymer blocks with varied amounts of AGE were grown from the chain end(s) of commercially available PEO homopolymers by ring-opening anionic polymerization according to Table 4.1.



Scheme 12 Representative synthesis of P(EO-*co*-AGE)-*b*-PEO-*b*-P(EO-*co*-AGE) triblock copolymers.

The use of AGE allows relative sequence control to be realized in two ways. First, restricting AGE units to certain blocks along the PEO backbone controls the general location of catechol units. The library of polymers synthesized herein includes examples in which catechols are restricted to one or both end-blocks of a polymer chain. Alternatively, starting from a random copolymer allows the catechol units to be distributed along the poly(ethylene oxide) backbone in its entirety.

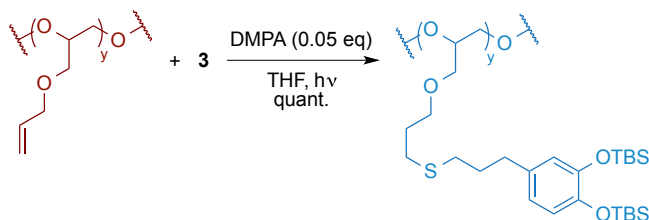
Table 4.1 PEO-PAGE copolymers synthesized and functionalized with silyl-protected catechols, **3**.

No.	Initial PEO Block		EO-AGE Copolymer				Catechol-Funct. Polymer	
	$M_n^{a,b}$	\bar{D}^a	Architecture	$M_n^{a,b}$	\bar{D}^a	AGE ^c	\bar{D}^a	Catechol ^c
1	21.7	1.03	Triblock	29.1	1.01	6	1.01	6
2	21.7	1.01	Triblock	30.1	1.04	12	1.04	12
3	21.7	1.03	Triblock	31.8	1.02	22	1.03	22
4	11.1	1.02	Triblock	20.0	1.03	12	1.05	12
5 ^d	n/a	n/a	Diblock	14.5	1.01	6	1.04	6
6 ^e	n/a	n/a	Random	17.3	1.08	28	1.11	28

^aValues determined by SEC (CHCl₃) relative to linear PEO standards, ^breported in kg·mol⁻¹, ^creported as the number of units, approximate values determined by ¹H-NMR and SEC analysis, ^ddiblock analogue was synthesized by sequential monomer addition in one pot, ^eP(EO-*co*-AGE) random copolymer.

Examining this further, previous experiments have shown the relative reactivity ratios of EO and AGE monomers in anionic polymerization to be 0.54 and 1.31, respectively.^[153] Therefore, an approximate gradient of catechol units in the polymer backbone was naturally achieved through the copolymerization of EO and AGE. Separately, the number of AGE units incorporated into the PEO backbone can be readily controlled by the initial feed ratio of AGE and EO. This allows the number of catechol units, as well as their distribution, to be precisely controlled.

4.3.5 Polymer Functionalization

**Scheme 13** Synthetic strategy for polymer functionalization with protected catechol **3**.

The strategy for the post-polymerization functionalization of the P(EO-*co*-AGE) copolymers and characterization are shown in Scheme 13 and Figure 4.4. Thiol-ene

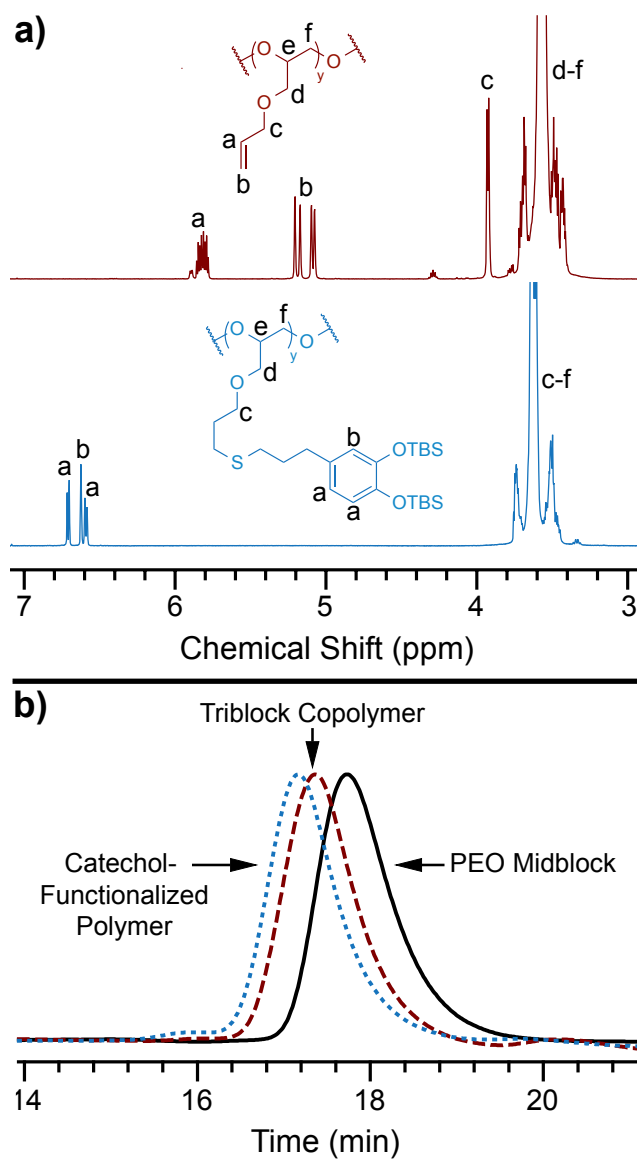


Figure 4.4 (a) $^1\text{H-NMR}$ spectra showing diagnostic peaks before (top) and after (bottom) thiol-ene coupling with **3**. (b) SEC traces of the starting PEO midblock (black solid line, $M_n = 21.7 \text{ kg}\cdot\text{mol}^{-1}$, $\mathcal{D} = 1.03$), the $\text{P}(\text{EO-co-AGE})\text{-}b\text{-PEO}\text{-}b\text{-P}(\text{EO-co-AGE})$ triblock copolymer synthesized via chain-extension (red dashed line, $M_n = 31.8 \text{ kg}\cdot\text{mol}^{-1}$, $\mathcal{D} = 1.02$), and the triblock copolymer after being functionalized with protected catechols (blue dotted line, $M_n = 45.5 \text{ kg}\cdot\text{mol}^{-1}$, $\mathcal{D} = 1.03$).

chemistry was chosen due to its mild reaction conditions, functional group tolerance, and high efficiency. The thiol-ene addition occurs via radical addition of a thiol across a carbon-carbon double bond.^[58] The reaction proceeds with quantitative yield, as evi-

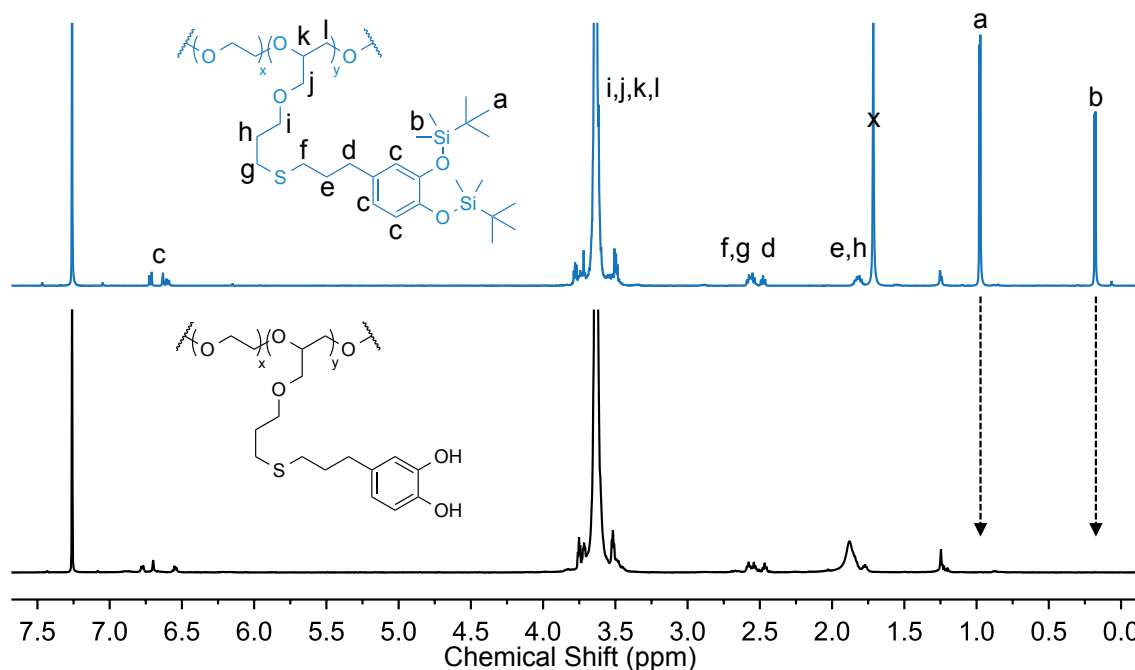


Figure 4.5 Representative $^1\text{H-NMR}$ spectra of PEO-PAGE copolymer before (top) and after (bottom) deprotection of the polyether-tethered, silyl-protected catechols. Note the disappearance of the TBS peaks (peaks a and b), demonstrating complete deprotection.

denced by complete disappearance of alkene peaks in $^1\text{H-NMR}$ (Figure 4.4a). Notably, SEC shows no appreciable increase in dispersity after functionalization (Figure 4.4b).

These results clearly demonstrate successful production of well-defined materials with controlled architecture, catechol incorporation, and catechol placement within the polyether backbone. Deprotection was then accomplished by using a modified literature procedure.^[154] In brief, the TBS groups were removed by stirring the polymer in a 1.2 M solution of HCl at 60 °C overnight. Complete disappearance of the TBS peaks in $^1\text{H-NMR}$ verifies successful deprotection (see Figure 4.5).

4.4 Conclusion

This chapter has presented a simple, high-yielding synthesis of tunable catechol-PEO systems. These efforts represent the first time catechols have been controllably dispersed throughout a PEO backbone. Additionally, the low cost of starting materials, minimal purification, and modular nature of this approach represents significant potential for the widespread use of this synthetic strategy. The precise tunability afforded by this system also facilitates systematic investigation of the effects that variables such as molecular weight, catechol incorporation, and catechol location can have on surface-anchored PEO. Finally, this chemistry provides a route to biomimetic adhesive materials that may facilitate future studies into the mechanics of mussel adhesion.

4.5 Experimental

4.5.1 Materials

All reactions were conducted in oven- or flame-dried glassware under an atmosphere of argon. Unless specified, all chemicals were purchased from Sigma-Aldrich and used as received. Tris(pentafluorophenyl)borane (>97.0%), *tert*-butyldimethylsilane (95%), and thioacetic acid (97%) were purchased from Fisher Scientific. Deuterated chloroform (CDCl_3) was obtained from Cambridge Isotope Laboratories, Inc. Allyl glycidyl ether (AGE) was purchased from TCI-America, Inc. Ethylene oxide (EO), benzyl alcohol, potassium naphthalenide, and AGE were purified as described by Lee et al.^[153] Tetrahydrofuran (THF) was obtained from a JC Meyer dry system and used immediately.

4.5.2 Instrumentation

NMR spectra were recorded on Varian VNMRs 600 MHz or Bruker Avance DMX 500 MHz spectrometers at room temperature. Unless otherwise stated, all ^1H and ^{13}C NMR spectra are reported in parts per million (ppm), and were measured relative to the signal for residual chloroform in the deuterated solvent (7.26 ppm and 77.16 ppm respectively). Thiol-ene reactions were irradiated with a UVP Black Ray UV Bench Lamp XX-15L, which emits 365 nm light at 15 W. A Micromass QTOF2 Quadrupole/Time-of-Flight Tandem mass spectrometer was used for high-resolution mass analysis using electrospray ionization (ESI). Gas chromatography (GC) was carried out on a Shimadzu GC-2014 with a Resteck column (SHRXL-5MS) and flame ionization detector (FID). Size exclusion chromatography (SEC) was performed at room temperature using chloroform with 0.25 wt% triethylamine as the mobile phase on a Waters 2695 separation module with a Waters 2414 refractive index (RI) detector and a Waters Alliance HPLC System, 2695 separation module with combined Wyatt DAWN HELEOS-II light scattering/Wyatt Optilab rEX refractive index detectors. Number average molecular weights (M_n) and weight average molecular weights (M_w) were calculated relative to linear polyethylene oxide standards or from light scattering data.

4.5.3 Methods

((4-allyl-1,2-phenylene)bis(oxy))bis(*tert*-butyldimethylsilane) (1)

To a 1000 mL 3-neck round bottom flask equipped with an addition funnel and reflux condenser was added methyl eugenol (50.4 mL, 293 mmol), anhydrous cyclohexane (250 mL, 1.2 M), and tris(pentafluorophenyl)borane (6.0 g, 11.7 mmol). The solution was allowed to stir for 15 minutes to ensure homogeneity. The addition funnel was charged with *tert*-butyldimethylsilane (99.6 mL, 601 mmol), which was added to the reaction drop-

wise over 4.5 hours. The reaction was allowed to stir at room temperature for an additional 48 hours, at which point complete conversion was observed by GC analysis. The clear, yellow reaction mixture was passed through a plug of silica gel (CH_2Cl_2 as eluent) and concentrated in vacuo to afford pure **1**.

Yield: 108.2 g clear, colorless liquid (98 %).

IR (neat): $\tilde{\nu}$ (cm^{-1}) = 2930 (w), 2858 (w), 1577 (w), 1508 (s), 1252 (s), 984 (s), 903 (s), 837 (s), 779 (s).

$^1\text{H-NMR}$ (600 MHz, CDCl_3): δ (ppm) = 6.78 (d, $J = 8.0$ Hz, 1 H), 6.69 (s, 1 H), 6.65 (d, $J = 8.1$ Hz, 1 H), 6.01–5.91 (m, 1 H), 5.10–5.02 (m, 2 H), 3.29 (d, $J = 6.6$ Hz, 2 H), 1.02 (s, 18 H), 0.22 (s, 12 H).

$^{13}\text{C-NMR}$ (150 MHz, CDCl_3): δ (ppm) = 146.75, 145.18, 137.96, 133.23, 121.64, 121.49, 121.01, 115.49, 77.16, 39.64, 26.15, 18.62, 18.61, -3.91 , -3.93 .

HR-ESI $\text{C}_{21}\text{H}_{38}\text{O}_2\text{Si}_2$: calculated 378.2410, found 378.2410.

S-(3-(3,4-bis((*tert*-butyldimethylsilyl)oxy)phenyl)propyl)ethanethioate (**2**)

To a round-bottom flask was added **1** (25.5 g, 67.3 mmol), thioacetic acid (5.2 mL, 73.8 mmol), 2,2-dimethoxy-2-phenylacetophenone (865.7 mg, 3.4 mmol) and anhydrous tetrahydrofuran (10 mL, 14.5 M). The reaction mixture was degassed by three freeze-pump-thaw cycles, backfilled with argon, and irradiated with UV light ($\lambda = 365$ nm) for three hours, or until complete conversion was observed by GC analysis. The solvent was removed in vacuo to afford **2**, which was used in the next step without further purification.

Yield: 30.4 g clear, yellow liquid (99 %).

IR (neat): $\tilde{\nu}$ (cm^{-1}) = 2929 (w), 2857 (w), 1694 (s), 1575 (w), 1509 (s), 1252 (s), 905 (s), 837 (s), 779 (s).

¹H-NMR (600 MHz, CDCl₃): δ (ppm) = 6.73 (d, J = 8.0 Hz, 1 H), 6.64 (s, 1 H), 6.60 (d, J = 8.1 Hz, 1 H), 2.86 (t, J = 7.2 Hz, 2 H), 2.56 (t, J = 7.5 Hz, 2 H), 2.32 (s, 3 H), 1.88–1.80 (m, 2 H), 0.99 (dd, J = 4.7, 1.4 Hz, 18 H), 0.19 (dd, J = 4.7, 1.4 Hz, 12 H).

¹³C-NMR (150 MHz, CDCl₃): δ (ppm) = 195.54, 146.59, 145.03, 134.23, 121.41, 121.33, 120.95, 77.16, 34.14, 31.23, 30.64, 28.50, 26.05, 18.50, 18.49, –3.98, –4.01.

HR-ESI C₂₃H₄₂O₃Si₂S: calculated 454.2393, found 454.2392.

3-(3,4-bis((*tert*-butyldimethylsilyl)oxy)phenyl)propane-1-thiol (**3**)

To a round bottom flask was added **2** (29.9 g, 67.7 mmol) and MeOH (5 mL, 13.5 M). The mixture was then sparged with argon for one hour. A degassed, saturated solution of K₂CO₃ in MeOH (10 mL) was added to the reaction via syringe. The resulting mixture was stirred at room temperature for 2.5 hours, until TLC analysis (9:1 hexanes:CH₂Cl₂ as eluent) indicated the reaction had reached completion. The reaction was quenched with a saturated aqueous solution of NH₄Cl (10 mL), diluted with deionized H₂O (50 mL), and extracted with ethyl acetate (3 × 50 mL). The combined organic extracts were dried over anhydrous MgSO₄, filtered, and concentrated under reduced pressure. The crude product was purified by silica gel chromatography (9:1 hexanes:CH₂Cl₂ as eluent) to afford **3**.

Yield: 20.9 g clear, yellow liquid (77 %).

IR (neat): $\tilde{\nu}$ (cm⁻¹) = 2929 (w), 2857 (w), 1575 (w), 1509 (s), 1252 (s), 907 (s), 838 (s), 780 (s).

¹H-NMR (600 MHz, CDCl₃): δ (ppm) = 6.74 (d, J = 8.0 Hz, 1 H), 6.65 (s, 1 H), 6.61 (d, J = 8.2 Hz, 1 H), 2.61 (t, J = 7.4 Hz, 2 H), 2.51 (q, J = 6.8 Hz, 2 H), 1.89 (p, J = 7.2 Hz, 2 H), 1.33 (t, J = 7.8 Hz, 1 H), 0.99 (dd, J = 4.0, 1.3 Hz, 18 H), 0.20 (dd, J = 4.7, 1.3 Hz, 12 H).

¹³C-NMR (150 MHz, CDCl₃): δ (ppm) = 146.67, 145.07, 134.41, 121.48, 121.39, 120.99, 35.66, 33.67, 26.11, 23.96, 18.59, 18.57, –3.90, –3.95.

HR-ESI $C_{21}H_{40}O_2Si_2S$: calculated 412.2288, found 412.2283.

4.5.4 Representative Procedure for Synthesis of Triblock Copolymers

Preparation of $P(EO_{92}\text{-}co\text{-}AGE_{11})\text{-}b\text{-}PEO_{20\text{ }kDa}\text{-}b\text{-}P(EO_{92}\text{-}co\text{-}AGE_{11})$

This procedure is based upon the synthesis of $P(EO\text{-}co\text{-}AGE)$ described by Lee et al.^[153] Polymerizations were performed in custom 5-armed, thick-walled glass reactors fitted with ACE-threads and equipped with glass-coated stir bars. The reactors were fitted with Teflon stoppers, a buret containing anhydrous tetrahydrofuran (THF), a flexible connector attached to a buret containing ethylene oxide (EO, stored on ice), and a glass column sealed with a 6 mm puresep septum and attached to a Schlenk line with a flexible connector. Reactors were assembled hot, cooled under vacuum, and subsequently purged with argon. PEO macroinitiator (30 g, 1.5 mmol) was added to the reactor via one of the arms under a positive pressure of argon. The reactor was then submitted to several cycles of evacuation followed by argon purge to remove oxygen from the system. THF was added to the reactor via buret until the PEO macroinitiator was completely dissolved. Heating to 40 °C was usually necessary for all solids to go into solution. Titration of PEO with potassium naphthalenide solution (0.3 M in THF) produced potassium alkoxide initiators at both chain ends as indicated by the persistence of a pale green color. Potassium naphthalenide was added via cannula through the 6 mm puresep septum. EO (11 g, 260 mmol) was added to the reactor in one portion by lifting the buret out of the ice and letting the contents drain into the reaction via the connector. Allyl glycidyl ether (AGE, 3.8 g, 33 mmol) was added simultaneously via gas tight syringe. The addition of monomers immediately quenched the green color and the polymerizations were carried out at room temperature for 2–3 days. Reactions were quenched with degassed methanol

and precipitated from hexanes. The polymer was purified using a plug of silica gel (10% MeOH/CH₂Cl₂ as eluent). M_n was determined by ¹H-NMR and SEC analysis. Values for D (M_w/M_n) were determined by SEC.

$$M_n = 31.8 \text{ kg}\cdot\text{mol}^{-1}; M_w/M_n = 1.02$$

¹H-NMR (600 MHz, CDCl₃): δ (ppm) = 5.87–5.93 (m), 5.82 (ddt, $J = 17.3, 10.7, 5.5$ Hz), 5.19 (broad dd, $J = 17.3, 1.7$ Hz) 5.09 (broad dd, $J = 10.3, 1.6$ Hz), 4.29 (p, $J = 6.8$ Hz), 3.92–3.93 (m), 3.41–3.72 (m), 1.49 (dd, $J = 17.3, 1.7$ Hz).

¹³C-NMR (150 MHz, CDCl₃): δ (ppm) = 145.99, 134.80, 116.80, 100.87, 78.39, 72.27, 71.23, 70.82, 70.75, 70.55, 70.15, 69.75, 61.62, 9.22.

P(EO_{101-co-AGE}₃)-*b*-PEO_{20 kDa}-*b*-P(EO_{101-co-AGE}₃)

$$M_n = 29.1 \text{ kg}\cdot\text{mol}^{-1}; M_w/M_n = 1.01$$

P(EO_{98-co-AGE}₆)-*b*-PEO_{20 kDa}-*b*-P(EO_{98-co-AGE}₆)

$$M_n = 31.1 \text{ kg}\cdot\text{mol}^{-1}; M_w/M_n = 1.04$$

P(EO_{92-co-AGE}₁₁)-*b*-PEO_{20 kDa}-*b*-P(EO_{92-co-AGE}₁₁)

$$M_n = 31.8 \text{ kg}\cdot\text{mol}^{-1}; M_w/M_n = 1.02$$

P(EO_{98-co-AGE}₆)-*b*-PEO_{10 kDa}-*b*-P(EO_{98-co-AGE}₆)

$$M_n = 20.0 \text{ kg}\cdot\text{mol}^{-1}; M_w/M_n = 1.03$$

THP-PEO_{10 kDa}-*b*-P(EO_{98-co-AGE}₆)

Synthesis of the diblock copolymer was performed in one pot by sequential monomer addition using 2-(2-hydroxyethoxy)tetrahydropyran (THP) as initiator.

$$M_n = 14.5 \text{ kg}\cdot\text{mol}^{-1}; M_w/M_n = 1.01$$

¹H-NMR (600 MHz, CDCl₃): δ (ppm) = 5.94 (dd, $J = 6.2, 1.7$ Hz, $-\text{O}-\text{CH}=\text{CH}-\text{CH}_3$), 5.91–5.81 (m, $-\text{O}-\text{CH}_2-\text{CH}=\text{CH}_2$), 5.23 (dd, $J = 17.3, 1.7$ Hz, $-\text{O}-\text{CH}_2-\text{CH}=\text{CH}_2$),

5.13 (dd, $J = 10.4, 1.6$ Hz, $-\text{O}-\text{CH}_2-\text{CH}=\text{CH}_2$), 4.60 (t, $J = 3.7$ Hz, $\text{THP}-\text{CH}-$), 4.34 (p, $J = 6.6$ Hz, $-\text{O}-\text{CH}=\text{CHCH}_3$), 3.97 (d, $J = 5.7$ Hz, $-\text{O}-\text{CH}_2-\text{CH}=\text{CH}_2$), 3.88–3.38 (broad multiplet, $-\text{CH}_2-\text{CH}-\text{O}-\text{CH}_2-\text{CH}-[\text{CH}_2-\text{O}-\text{CH}=\text{CH}-\text{CH}_3]-\text{O}-$), 1.54 (dd, $J = 6.9, 1.7$ Hz, $-\text{O}-\text{CH}=\text{CH}-\text{CH}_3$).

P(EO₃₂₀-*co*-AGE₂₈)

Synthesis of the random copolymer was performed in analogy with the synthesis of the triblocks, using benzyl alcohol as initiator.

$M_n = 17.3 \text{ kg}\cdot\text{mol}^{-1}$; $M_w/M_n = 1.08$

¹H-NMR (600 MHz, CDCl₃): δ (ppm) = 7.33 (s, 4 H, $\text{Ph}-\text{CH}_2-\text{O}-$), 5.95 (d, $J = 5.7$ Hz, $-\text{O}-\text{CH}=\text{CH}-\text{CH}_3$), 5.91–5.85 (m, $-\text{O}-\text{CH}_2-\text{CH}=\text{CH}_2$), 5.20 (dd, $J = 62.63, 13.65$ Hz, $-\text{O}-\text{CH}_2-\text{CH}=\text{CH}_2$), 4.54 (s, 2 H, $\text{Ph}-\text{CH}_2-\text{O}-$), 4.34 (m, $-\text{O}-\text{CH}=\text{CH}-\text{CH}_3$), 3.98 (d, $J = 5.2$ Hz, $-\text{O}-\text{CH}_2-\text{CH}=\text{CH}_2$), 3.77–3.45 (broad multiplet, $-\text{CH}_2-\text{CH}-\text{O}-\text{CH}_2-\text{CH}-[\text{CH}_2-\text{O}-\text{CH}=\text{CH}-\text{CH}_3]-\text{O}-$), 1.56 (d, $J = 6.9$ Hz, $-\text{O}-\text{CH}=\text{CH}-\text{CH}_3$).

4.5.5 Representative Procedure for Thiol-ene Coupling of Catechols to Copolymers

Preparation of P(EO₉₂-*co*-*f*AGE₁₁)-*b*-PEO₂₀ *kDa*-*b*-P(EO₉₂-*co*-*f*AGE₁₁)[‡]

To a round bottom flask was added P(EO₉₂-*co*-*f*AGE₁₁)-*b*-PEO₂₀ *kDa*-*b*-P(EO₉₂-*co*-*f*AGE₁₁) (2.078 g, 0.068 mmol, 1.43 mmol alkene), (**3**) (4.07 g, 9.85 mmol, 7 equiv relative to alkene), 2,2-dimethoxy-2-phenylacetophenone (19.4 mg, 0.076 mmol, 0.05 equiv relative to alkene), and anhydrous THF (10 mL). The reaction mixture was degassed by three freeze-pump-thaw cycles, backfilled with argon, and irradiated with UV light ($\lambda = 365$ nm) for four hours, or until complete disappearance of the alkene peaks as indicated

[‡]*f*AGE represents catechol-functionalized AGE after thiol-ene coupling

by $^1\text{H-NMR}$ analysis. The reaction mixture was precipitated from hexanes, filtered, and dried, yielding a white powder.

$$M_n = 45.5 \text{ kg}\cdot\text{mol}^{-1}; M_w/M_n = 1.03$$

$^1\text{H-NMR}$ (600 MHz, CDCl_3): δ (ppm) = 6.71 (d, $J = 8.0$ Hz, Ar-H), 6.63 (s, 1H), 6.60 (d, $J = 8.2$ Hz, Ar-H), 3.82–3.29 (broad m, $-\text{O}-\text{CH}_2-\text{CH}_2-\text{O}-\text{CH}-[\text{CH}_2-\text{O}-\text{CH}_2-\text{CH}_2-\text{CH}_2-\text{S}-\text{catechol}]-\text{CH}_2-\text{O}-$), 2.60–2.51 (m, $-\text{CH}_2-\text{S}-\text{CH}_2-$), 2.47 (t, $J = 7.2$ Hz, Ar- CH_2-CH_2-), 1.81 (m, $-\text{CH}_2-\text{CH}_2-\text{S}-\text{CH}_2-\text{CH}_2-$), 0.97 (d, $J = 3.3$ Hz, $-\text{Si}-\text{C}(\text{CH}_3)_3$), 0.18 (d, $J = 3.5$ Hz, $-\text{Si}(\text{CH}_3)_2$).

$\text{P}(\text{EO}_{101}\text{-co-}f\text{AGE}_3)\text{-}b\text{-PEO}_{20\text{ }kDa}\text{-}b\text{-P}(\text{EO}_{101}\text{-co-}f\text{AGE}_3)$

$$M_n = 35.2 \text{ kg}\cdot\text{mol}^{-1}; M_w/M_n = 1.01$$

$\text{P}(\text{EO}_{98}\text{-co-}f\text{AGE}_6)\text{-}b\text{-PEO}_{20\text{ }kDa}\text{-}b\text{-P}(\text{EO}_{98}\text{-co-}f\text{AGE}_6)$

$$M_n = 42.5 \text{ kg}\cdot\text{mol}^{-1}; M_w/M_n = 1.04$$

$\text{P}(\text{EO}_{92}\text{-co-}f\text{AGE}_{11})\text{-}b\text{-PEO}_{20\text{ }kDa}\text{-}b\text{-P}(\text{EO}_{92}\text{-co-}f\text{AGE}_{11})$

$$M_n = 45.5 \text{ kg}\cdot\text{mol}^{-1}; M_w/M_n = 1.03$$

$\text{P}(\text{EO}_{98}\text{-co-}f\text{AGE}_6)\text{-}b\text{-PEO}_{10\text{ }kDa}\text{-}b\text{-P}(\text{EO}_{98}\text{-co-}f\text{AGE}_6)$

$$M_n = 27.6 \text{ kg}\cdot\text{mol}^{-1}; M_w/M_n = 1.05$$

$\text{THP-PEO}_{10\text{ }kDa}\text{-}b\text{-P}(\text{EO}_{98}\text{-co-}f\text{AGE}_6)$

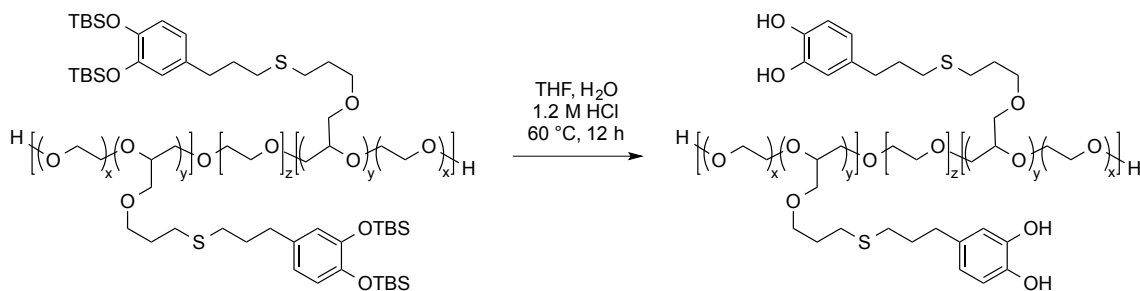
$$M_n = 18.6 \text{ kg}\cdot\text{mol}^{-1}; M_w/M_n = 1.04$$

$\text{P}(\text{EO}_{320}\text{-co-}f\text{AGE}_{28})$

$$M_n = 29.2 \text{ kg}\cdot\text{mol}^{-1}; M_w/M_n = 1.11$$

4.5.6 Representative Procedure for Deprotecting Catechol-Functionalized Polymers

Deprotection was accomplished following a modified literature procedure.^[154] To a round-bottom flask equipped with a magnetic stir bar was added 1.1 mL THF, 8.0 mL DI H₂O (yielding a solution of 12.1 % THF in H₂O), and 114.5 mg (0.004 mmol) of catechol-functionalized polymer P(EO_{101-co-f}AGE₃)-*b*-PEO_{20 kDa}-*b*-P(EO_{101-co-f}AGE₃). The mixture was stirred until the polymer was fully dissolved, then 1.01 mL of 12 M HCl was added dropwise to yield a solution of 1.2 M HCl. The solution was placed under a blanket of argon and allowed to stir for 12 hours at 60 °C. THF was removed in vacuo, and the remaining solution was extracted with CH₂Cl₂ (3 × 5 mL) using 10 wt% sodium bisulfate solution (5 mL) to expedite separation. The organic layers were combined and concentrated. Precipitation into hexanes yielded the deprotected polymer as a fluffy, white powder.



Scheme 14 Representative procedure for deprotecting catechol-functionalized polyethers.

Appendix A

External Regulation of Controlled Polymerizations

External Regulation of Controlled Polymerizations

Frank A. Leibfarth, Kaila M. Mattson, Brett P. Fors, Hazel A. Collins, and Craig J. Hawker*



catalysis · external control · functional polymers · polymerization · temporal control

Polymer chemists, through advances in controlled polymerization techniques and reliable post-functionalization methods, now have the tools to create materials of almost infinite variety and architecture. Many relevant challenges in materials science, however, require not only functional polymers but also on-demand access to the properties and performance they provide. The power of such temporal and spatial control of polymerization can be found in nature, where the production of proteins, nucleic acids, and polysaccharides helps regulate multicomponent systems and maintain homeostasis. Here we review existing strategies for temporal control of polymerizations through external stimuli including chemical reagents, applied voltage, light, and mechanical force. Recent work illustrates the considerable potential for this emerging field and provides a coherent vision and set of criteria for pursuing future strategies for regulating controlled polymerizations.

1. Introduction

The most profound developments in modern polymer chemistry have arisen from a combination of controlled polymerization techniques and precision polymer functionalization. This dual strategy has and will continue to lead to advanced materials with applications in microelectronics, biotechnology, energy, defense, and the developing world. Starting almost two decades ago with the introduction of controlled radical polymerization (CRP) methods,^[1–3] this renaissance has facilitated the rational design of polymers with predictable molecular weights and narrow polydispersities traditionally accessible only through ionic mechanisms. CRP approaches have the advantage of being tolerant towards many functional groups, amenable to a wide range of monomers, able to easily produce copolymers, and practically simple to execute. These techniques, as well as important

advances in organocatalytic ring-opening polymerization,^[4] chain-walking coordination polymerization,^[5] and ring-opening metathesis polymerization,^[6] have made it commonplace to produce well-defined polymers with control over functional group identity, placement, and polymer architecture.

Furthermore, with the ever-shrinking gap between organic and polymer chemistry,^[7] material scientists now have a number of reliable methods to post-functionalize these polymeric materials using the robust, efficient, and orthogonal “click” family of reactions.^[8]

With such powerful tools available to synthesize polymers of almost infinite variety, architecture, and functionality, what fundamental innovations can synthetic polymer chemists continue to provide that will contribute to solving the grand challenges^[9] in materials science? Nature generously provides the necessary inspiration. For example, our synthetic methods pale in comparison to the ribosome, which is able to produce flawless polymers of exceedingly high molecular weights that fold into pre-programmed secondary, tertiary, and quaternary structures. Perhaps the most impressive part of this synthetic machinery, however, is our body’s ability to provide temporal and spatial control over these polymerizations. For instance, the initiation, chain-growth, and crosslinking of actin, the cell’s most important resource for mechanical support and directed movement, is regulated by over 100 accessory proteins, providing precise control over a variety of processes including membrane permeability, cell replication, and cell motility.^[10]

Emulating the spatial and temporal control over polymerization exhibited by natural systems is a formidable challenge for polymer chemists. The potential of such

[*] F. A. Leibfarth, K. M. Mattson, Dr. B. P. Fors, Dr. H. A. Collins, Prof. Dr. C. J. Hawker
Dept. of Chemistry & Biochemistry, Materials, and Materials Research Laboratory
University of California Santa Barbara
MRL, MC 5121, Santa Barbara, CA 93106 (USA)
E-mail: hawker@mrl.ucsb.edu
Homepage: <http://hawkergroup.mrl.ucsb.edu/>



Frank Leibfarth (left) received his B.S. in chemistry and physics from the University of South Dakota in 2008. He is currently an NSF and NDSEG fellow pursuing his Ph.D. in chemistry at the University of California, Santa Barbara, under the direction of Craig J. Hawker. His dissertation work, for which he was awarded the 2012 DSM Polymer Technology Award, includes the development of functional macromolecular and supramolecular systems through advanced synthetic strategies.

Hazel A. Collins (second from left) completed her PhD on two-photon dyes for photodynamic therapy at Oxford University (UK) in 2008 under the direction of Professor Harry L. Anderson. Following her PhD studies, she led a spin-out company developing polymer membranes for fuel cells, and joined UCSB in 2012 as Assistant Director for Technology at the Dow Materials Institute. Her research interests are in developing novel materials at the interface of organic and polymer chemistry.

Craig J. Hawker, FRS (middle) received his BSc (1984) degree from Queensland, his PhD (1988) degree from Cambridge (UK), followed by a post-doctoral fellowship with Professor Jean M. J. Fréchet at Cornell from 1988 to 1990. In 2005 he moved from the IBM Almaden Research Center to the University of California, Santa Barbara where he is the Alan and Ruth Heeger Chair of Interdisciplinary Science. He is also the Director of the Materials Research Laboratory, founding Director of the Dow Materials Institute and visiting Chair Professor at King Fahd University of Petroleum and Minerals. His research activities focus on synthetic polymer chemistry and nanotechnology and have led to more than 45 patents and over 300 publications. He has received a number of awards for his work including the 2013 ACS Award in Polymer Chemistry from the American Chemical Society.

Kaila Mattson (second from right) was born and raised in Hartland, Wisconsin. She earned her B.S. in chemistry, with a minor in business, from the University of South Alabama in 2011. She is currently an NSF Graduate Research Fellow pursuing her Ph.D. in chemistry at the University of California, Santa Barbara under the direction of Professor Craig J. Hawker. Her research involves developing design principles for the synthesis of new materials, including carbon fibers and underwater adhesives.

Brett P. Fors (right) was born in Polson, Montana and carried out his undergraduate studies in chemistry at Montana State University (B.S., 2006). He went on to do his Ph.D. (2011) at the Massachusetts Institute of Technology with Professor Stephen L. Buchwald, where he worked on the development and applications of Pd catalysts for C–N cross-coupling reactions. He is currently an Elings Fellow at the University of California, Santa Barbara working in collaboration with Professor Craig J. Hawker. His research at UCSB involves the investigation of new polymerization techniques that can be effectively regulated with light.

technology is self-evident considering the myriad of high-value applications associated with (irreversible) temporal control over polymer initiation. This seemingly simple development has spawned billion-dollar industries in commodity materials such as coatings, thermosets, foams, and adhesives. Further, this technology has made its way into sophisticated materials such as photocured dental resins and complex chip manufacturing processes that employ photolithography.^[11]

The prospect of in-situ, reversible polymer initiation and termination would build on the already realized living polymerization techniques and post-functionalization methods to introduce new and innovative applications through external control of the viscosity, mechanical properties, structure, and function of macromolecules. The development of such chemistry would allow the programming of functional units in discrete locations along the polymer backbone, providing the technology necessary to tune the secondary interactions of polymer chains by precisely modifying their primary structure. Further, combining spatially and temporally controlled polymerizations with concepts such as templation and compartmentalization has the potential to create multicomponent systems where numerous functions and/or reactions can be individually addressed externally, with the ultimate goal of creating systems that are fully self-regulatory.

In order to provide a set of criteria for future work in this area and compare previous contributions, this Minireview focuses on processes which have the ability to reversibly turn polymerizations both “on” and “off” through the use of added reagents, applied voltage, light, or mechanical force (Figure 1). In an ideal system, the propagating polymer chain should switch between an active and a dormant state quickly, quantitatively, and be fully reversible under external stimulation. In addition, the active state should show the qualities of a living polymerization (minimal termination and/or chain-

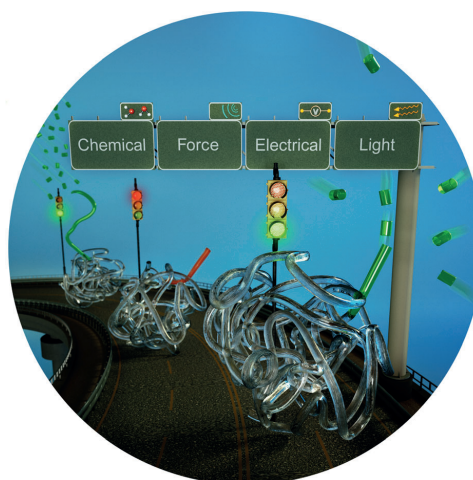


Figure 1. Temporally controlled polymerizations can be regulated by a variety of stimuli to reversibly start and stop polymerizations.

transfer, linear increase in molecular weight with conversion, and low polydispersity), switching should not compromise the polymerization rate, and the system should be tolerant to a diversity of monomers and functional groups.

Realizing the potential of spatial and temporal control of polymerization will require the expertise of many traditional chemical disciplines, including organometallic chemistry, organic synthesis, catalysis, and polymer chemistry. This Minireview is intended to emphasize the on-going work in these sometimes disparate disciplines and show the significant promise of this exciting area. Mimicking Nature's spatial and temporal control of polymerization provides dynamic control of material synthesis, opening opportunities to not only enhance properties but also create new applications for functional materials.

2. Selected External Stimuli

2.1. Allosteric Control

Biologists have long strived to understand how living systems are able to reversibly control the synthesis of biopolymers, such as polypeptides, polynucleotides, and polysaccharides. For example, production of the multi-branched polysaccharide glycogen from glucose lowers human blood glucose levels after meals, storing energy for periods of starvation. The sophisticated control system for glycogen production is essential to prevent toxicity to peripheral tissues in response to prolonged hyperglycaemia or loss of consciousness due to hypoglycaemia. It has been known for more than 50 years that insulin regulates glycogen synthase, the enzyme that progressively lengthens the glycogen polymer, but despite decades of intensive research, the molecular mechanisms remained controversial. Only recently has genetic engineering been able to show conclusively that the primary mechanism for activation of glycogen synthase is allosteric binding of glucose-6-phosphate, the production of which is stimulated by insulin.^[12]

Allosteric control of catalyst activity by the reversible binding of an effector to a location remote from the catalytically active site is one of nature's main enzyme regulation mechanisms. Synthetically, the most prominent examples of allosteric systems have been based on bimetallic catalysts where binding of the effector between the distance between two metal sites, thereby altering the rate of reaction.^[13–15] In 2010, Mirkin and co-workers reported the first example of allosteric control of a polymerization catalyst through their weak-link approach (WLA).^[16] The triple-layer architecture uses an Al^{III}-salen polymerization catalyst hinged to aromatic groups by Rh^I complexes. The “open” form (**1**) polymerizes ϵ -caprolactone, reaching complete conversion after 40 h at 90 °C with good control over molecular weight (PDI of 1.10–1.20). However, the catalyst can be almost completely deactivated in situ by the addition of two equivalents of NaBARF (BARF = tetrakis[3,5-trifluoromethylphenyl]borate) or LiB(C₆F₅)₄Et₂O, which abstracts Cl[−] from the Rh^I hinge, quantitatively converting the complex to its “closed” form (**1**²⁺) within 20 min. The “closed” complex is essentially

inactive as a polymerization catalyst due to the aromatic groups which π -stack above and below the salen catalyst, blocking access to the active site. It should be noted that the inactive state will decompose to the active form over time (ca. 7% conversion after 100 h). Furthermore, the linear dependence of the molecular weight (M_n) on percent conversion is maintained through closing and reopening (Figure 2), confirming that the activity of the catalyst is unaffected by allosteric regulation.

This work provides a critical proof-of-principle and with careful choice of the catalyst system, blocking groups, and

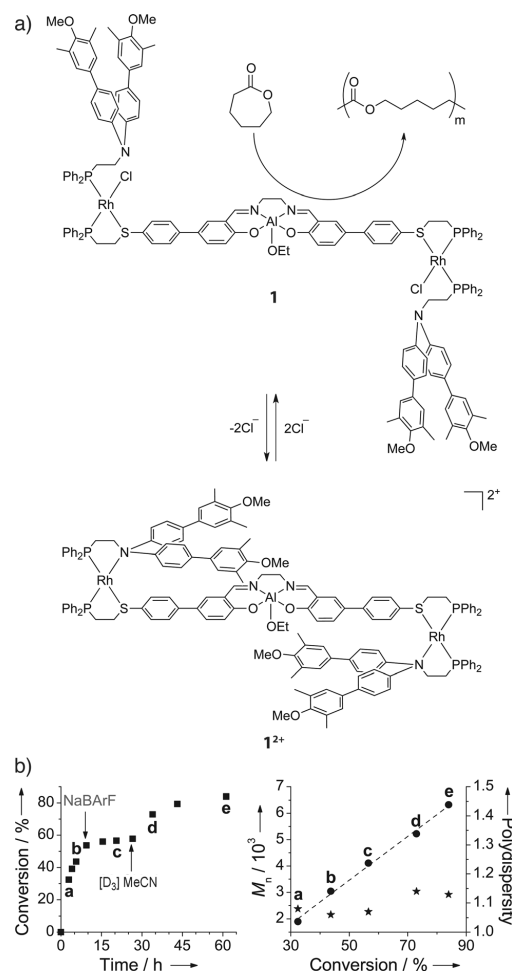


Figure 2. The triple-layer complex allosterically regulates the polymerization of ϵ -caprolactone by reversibly switching between the active (**1**) “open” and the inactive (**1**²⁺) “closed” forms. The formation of the product was monitored at various times (a–e) during the reaction using a) ¹H NMR spectroscopy and b) gel permeation chromatography (GPC) (for M_n and PDI). (Part b) adapted with permission from reference [16] and reprinted with permission from AAAS.)

allosteric effectors, the triple-layer approach could be extended to control other polymerization processes. Additionally, employing metals other than rhodium would further increase the generality of this allosteric system. Many other architectures, including supramolecular assemblies, may also be amenable to allosteric regulation and could allow polymerization of a diverse range of monomers. An even more impressive target is to utilize small molecules as allosteric effectors, mimicking natural, self-regulating allosteric systems through feedback from downstream product polymers or feedforward from upstream monomer or oligomer substrates.

2.2. Chemical Control

In addition to allosteric regulation, which relies on binding of an external effector, many reversible chemical transformations may afford temporal control over polymerization. Of these, redox-active systems were the first to be exploited, and a number of polymerization catalysts have been reported to reversibly switch between two stable oxidation states that have different catalytic efficiencies.^[17–19]

The first redox-modulated polymerization catalyst was reported by Gibson, Long and co-workers in 2006 and was based on a Ti^{IV}-salen complex where the ligand was symmetrically conjugated to two ferrocene groups (Figure 3 a).^[17] Ferrocene was selected as the redox-active switch because it is a highly reversible redox agent and its chemical and electronic properties are well understood. Though the ferrocene units are distant from the catalytic metal center, the neutral form of the complex (**2**) catalyzes the ring opening polymerization of *rac*-lactide 30 times faster than the oxidized form **2-OTf**, demonstrating that the ligand relays an electronic effect to the metal, a finding that is consistent with other Ti-salen complexes substituted with electron-withdrawing groups.^[20] Further, both **2** and **2-OTf** give a single atactic chain per metal center, and their resulting polymers have polydispersities below 1.20, indicating that propagation is well controlled.

Reversible redox control of the rate of *rac*-lactide polymerization was demonstrated by addition of two equivalents of the one electron oxidant AgOTf during polymerization, which markedly slowed monomer conversion. Subsequent addition of two equivalents of the one electron reductant Cp^{*}₂Fe returned the activity to approximately the same level as for the virgin catalyst ($k_{app} = 4.98 \times 10^{-6} \text{ s}^{-1}$, cf. $k_{app} = 4.73 \times 10^{-6} \text{ s}^{-1}$ before oxidation) (Figure 3b).^[17] Though reversible control of the polymerization rate was demonstrated with **2**, polymerization cannot be completely halted by oxidation, as both the neutral and oxidized forms of the Ti-salen complex polymerize *rac*-lactide.

In an effort to develop greater redox control of polymerization, Diaconescu and co-workers examined a series of lactide polymerization catalysts based on a new redox-active phosfen ligand, **3-M**.^[18,19] Similar to Gibson and Long's system, the phosfen ligand incorporates ferrocene, but dependent on whether yttrium,^[18] indium,^[18] or cerium^[19] is used as the catalytic center, either the ferrocene ligand or the active metal-center is oxidized upon addition of the oxidizing agent ferrocenium tetrakis(3,5-bis(trifluoromethyl)phenyl)

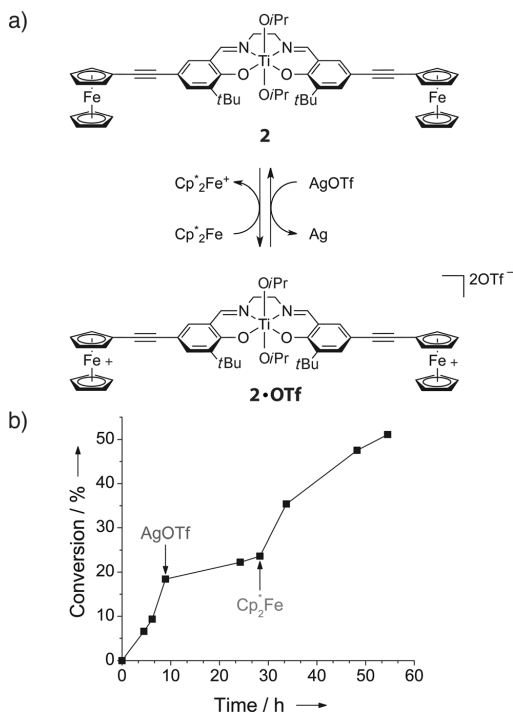


Figure 3. A plot of conversion versus time for the polymerization of *rac*-lactide with in situ redox-switching between the neutral, active form **2** and the less active, oxidized species **2-OTf**. (Adapted with permission from reference [17]. Copyright 2006 American Chemical Society.)

borate (FcBARF). Subsequent reduction by CoCp₂ returns the catalysts to their original states.

In the case of the yttrium *tert*-butoxide phosfen complex **3-Y**,^[18] reaction with one equivalent of FcBARF produces the oxidized form **3-Y-BARF** within minutes. X-ray absorption near edge structure (XANES) and Mössbauer spectroscopy supported the assignment of ferrocene as the redox-active group with the relative polymerization efficiencies of the two forms being compared at room temperature using 100 equivalents of L-lactide in THF. Whilst the neutral complex reached 74% conversion in three hours, no conversion was observed for the oxidized form. The inactivity of the oxidized form allowed polymerization to be halted in situ by addition of FcBARF. Addition of one equivalent of the reducing agent CoCp₂ was then able to revert the oxidized complex back to its neutral form within minutes. The polymerization resumed at the same rate as before oxidation with the PDI of the final polymer being below 1.06, indicating that the polymerization remained controlled through switching. Three consecutive cycles of in situ oxidation and reduction were completed (Figure 4) illustrating how the careful choice of an external oxidant and reductant can allow a controlled polymerization to be reversibly switched “off” and “on.”

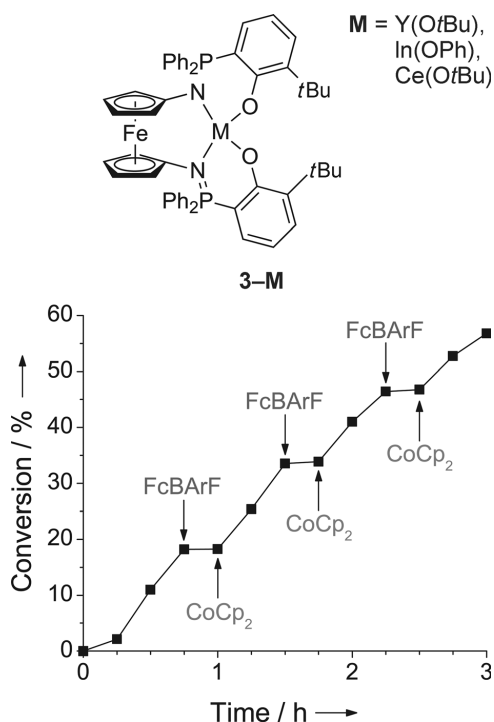


Figure 4. Redox active polymerization catalysts based on phosfen **3** [M = Y(O^tBu), In(OPh) or Ce(O^tBu)]. A plot of conversion (%) versus time for the controlled polymerization of L-lactide using **3** [M = Y(O^tBu)]. The system was redox-switched three times in situ via oxidation with FcBARF and reduction with CoCp₂. (Adapted with permission from reference [18]. Copyright 2011 American Chemical Society.)

An intriguing feature of this system is that significant changes in the polymerization behavior of the species are observed on replacement of the yttrium *tert*-butoxide with indium phenoxide in the phosfen complex.^[18] Though Mössbauer spectroscopy supports the assignment of ferrocene again being the redox-active species, both the neutral **3-In** and oxidized forms **3-In-BArF** are slow to polymerize either L-lactide or ϵ -caprolactone. However, room temperature polymerization of trimethylene carbonate demonstrated that oxidized **3-In-BArF** was the more active species, as it reached 49% conversion in 24 h as compared to 2% conversion for **3-In**. In contrast to the yttrium complex, increasing the electron withdrawing nature of the ligand by oxidizing ferrocene leads to an increase in the rate of polymerization. The opposite switching behavior of the yttrium and indium complexes demonstrates the degree of regulation that can be achieved in these chemically controlled systems with the effect of the ferrocene redox-switch being dependent on the identity of the metal.

Diaconescu and co-workers also prepared a Ce^{III}-salen species that required around eight times longer than its phosfen analogue to reach similar L-lactide conversion levels

and the PDI was marginally higher (1.34 at 93% conversion).^[19] The Ce^{IV}-salen complex produced by FcBARF oxidation was also inactive towards L-lactide polymerization, allowing reversible in situ redox-control of polymerization. Almost no loss of activity was observed before ($k_{app} = 1.96 \times 10^{-2}$) and after ($k_{app} = 1.73 \times 10^{-2}$) switching, though the PDI of the product polymer (1.73 at 90% conversion) was higher than when the oxidation state of the cerium was not changed, indicating some loss in polymerization control by redox-switching. The cerium-phosfen and -salen complexes demonstrate that, although the ligand does not participate in the direct-metal redox-switch, it remains a crucial component of the system and has a marked influence on catalytic activity.

These results demonstrate that external chemical modulation is an effective method for regulating ring-opening polymerizations in situ, and with further developments, including expanding its applicability to other polymerization mechanisms, significant opportunities exist. One of the most powerful outcomes from this work however, is the clear correlation between catalyst design and performance. The incorporation of a highly reversible redox-switch, such as ferrocene, into the ligand allows two stable oxidation states to be reversibly accessed and exploited, while the nature of the metal center also plays an important role. Developing new systems offers opportunities for effective control of polymerization depending on the appropriate choice of catalyst system, oxidant, reductant, and monomer. Future research directions include exploring lanthanides as the redox-active metal. In this case, the 4f valence shells have only a small contribution to bonding and, unlike transition metals, redox-switching has a mainly electrostatic influence on their coordination sphere.

2.3. Electrochemical Control

In terms of remote regulation, electrochemical stimulus offers a number of attractive attributes, including functional group tolerance and easily adjustable parameters for manipulating polymerization rate. Other attractive features include the orthogonality of electrochemical conditions to many common polymerization strategies, such as radical procedures, and the simple automation of electrochemical cells.

Matyjaszewski and co-workers recently reported the first electrochemically-mediated controlled radical polymerization.^[21] Their process is based on the well-developed atom transfer radical polymerization (ATRP) mechanism, which relies on the reversible oxidation of a catalytic Cu^I species to generate an alkyl radical. Subsequent reduction of the Cu^{II} species regenerates Cu^I and end-caps the growing polymer chain. Such a mechanism is ideally suited for electrochemical control,^[22] as the system can initially be charged with a catalytic amount of air stable Cu^{II}. Application of a cathodic current then reduces the catalyst to active Cu^I, which starts polymerization. Reoxidizing the complex *via* an anodic current yields the catalytically inactive Cu^{II} species and stops further polymer formation.

The resulting electrochemical process is efficient, as application of a cathodic current to a system containing

initiator, monomer, an amine-based ligand, and Cu^{II} results in almost 80% monomer conversion in only two hours.^[21] The polymerization displayed all the characteristics of a living process, including a linear relationship between M_n and conversion, a good agreement between theoretical and obtained molecular weight, and a low PDI. Further, the polymerization rate was sensitive and responsive to the applied potential. More negative potentials enhanced the polymerization rate while maintaining living polymerization characteristics. The power of electrochemically mediated ATRP (eATR) is most apparent in its temporal control, where repeated cycling of the potential from one that favors formation of Cu^{I} at the electrode, and thus polymerization, to one that favors Cu^{II} and no polymerization (Figure 5).

slow response time for deactivation of polymerization, which takes nearly 20 min for polymerization to completely stop after the potential change. Further, the current system is restricted to working in an electrochemical cell which could hinder the ability to scale-up reactions due to problems with mass transport to the working electrode and will make it difficult to provide coincident temporal and spatial control of polymerization. Given these accomplishments, eATR is a powerful system for the temporal control of polymerization that will push polymer chemists in new directions and provide novel application drivers for the synthesis of complex materials.

2.4. Photochemical Control

Of the various stimuli employed to provide in situ control over the reversible activation and deactivation of polymerizations, the inherent properties of light provide most of the necessary characteristics for an ideal system. Light is a widely available, non-invasive, and environmentally benign reagent that provides opportunities for both spatial and temporal control of polymerization. In addition to reversibly switching processes by simply turning the light "on" or "off," light further facilitates precise control over reaction kinetics by modulating the intensity of irradiation.

The well-recognized advantages of light as a stimulus are manifested in many practical and important processes, such as ultraviolet (UV) photocuring, photolithography, etc., that have resulted from photoinitiated radical and cationic polymerizations.^[24] The infrastructure and knowledge currently associated with photochemical processes also adds significantly to the potential impact of photochemical mediation of controlled polymerizations. Current approaches are, however, fundamentally limited by using light to control only the initiation step of the polymerization process. In addressing this challenge, three strategies have made significant progress toward achieving such a system, including employing light to activate the monomer,^[25,26] the polymer chain-end,^[27] or a catalyst.^[28]

The group of Manners and co-workers has reported a successful strategy for controlling anionic polymerizations based on monomer activation, where a silicon-bridged ferrocenophane monomer is the key component (Figure 6).^[25,26] Irradiation of these cyclic monomers with UV light induces an excited state, thereby selectively weakening the Fe-cyclopentadienyl (Cp) bond and allowing for displacement of a Cp ligand by a weak nucleophilic initiator (NaCp). This initiation event forms an anionic Cp chain-end that can subsequently propagate with additional excited monomers. Propagation, therefore, relies on continued photoirradiation to excite the cyclic monomers and polymerization stops when the light is turned off. Polymerization proceeds in a controlled manner and displays the characteristics of a living system, affording well-defined polymers (PDI < 1.10) with theoretical molecular weights matching experimental observations. This excellent control further allowed the synthesis of block copolymers. The dynamic control and well-defined polymerization make this system almost ideal; however, the limitation

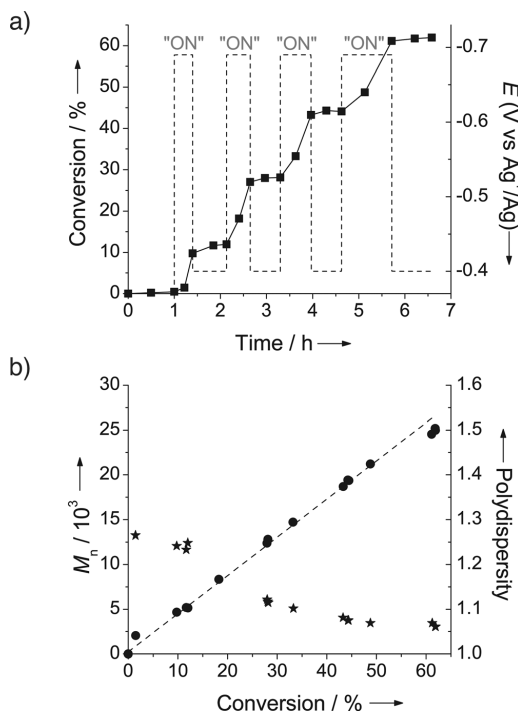


Figure 5. Temporal control of eATR demonstrated by the switching of polymerization "on" and "off" in response to applied voltage (a) while still showing the characteristics of a living polymerization (b). (Adapted with permission from reference [21] and reprinted with permission from AAAS.)

eATR fulfills many of the criteria for an ideal system for temporal control of polymerization. It switches efficiently and reversibly between an active and a dormant state, shows the qualities of a living polymerization when in its active state, and, although only the polymerization of acrylates and methacrylates has been reported,^[21,23] eATR should be broad in terms of monomer selection and functional group tolerance. Challenges for the future include improving the

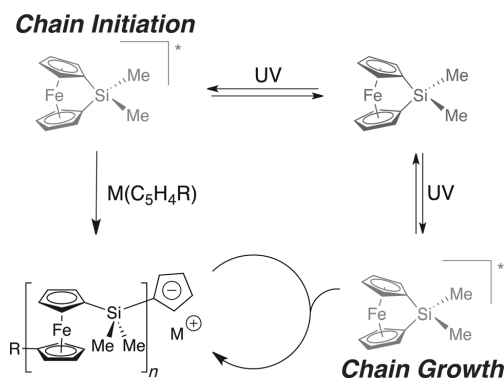


Figure 6. Monomer activation: anionic polymerization of silicon-bridged ferrocenophanes mediated by monomer excitation with UV light.

of using only specialized, strained ferrocene monomers limits the potential of this specific system. Nevertheless, this strategy of photochemical monomer activation holds great promise and clearly defines the development of other activatable monomers as a future direction.

Photoactivation of the polymer chain-end is potentially a more synthetically accessible approach, with light-sensitive alkoxyamines for nitroxide mediated radical polymerization,^[29–32] iniferter (initiator-transfer agent-terminator)^[33] or dissociation/combination (DC)^[34] reagents being developed in an effort to control radical polymerizations. Although promising, light-activated alkoxyamines have not led to a system that provides controlled polymerizations. Related to these alkoxyamine studies, preliminary work on the photolysis of organotellurium functionalized polymers also holds considerable promise, although the dynamic nature of these systems has not yet been reported.^[35,36]

Iniferter and DC polymerizations, which were pioneered by Otsu^[33] and Braun,^[34] involve homolytic cleavage of an initiator into two radical species upon exposure to UV light (Figure 7). In this system, one radical initiates polymerization and the second acts as a reversible terminating agent to give the dormant polymer. Ideally, further exposure to UV irradiation would homolytically cleave the chain-end, thus allowing continued propagation. This reversible homolysis and termination then affords a photocontrolled polymerization process. The most successful system based on this concept comes from Yang and co-workers employing a new DC reagent, 9,9'-bixanthene-9,9'-diol (BiXANDL).^[27] Upon photolysis, BiXANDL fragments into two cycloketyl xanthone radicals. These stabilized, yet reactive radicals are able to efficiently initiate polymerization as well as reversibly terminate the chain-end. Moderate control over the observed molecular weight and molecular weight distributions (PDI = 1.25–1.82) has been demonstrated for the polymerization of acrylates, methacrylates and a styrenic monomer. Further, the polymerization can be reversibly activated or deactivated by cycling exposure to UV irradiation. Although a significant advance, this system suffers from thermal instability of the

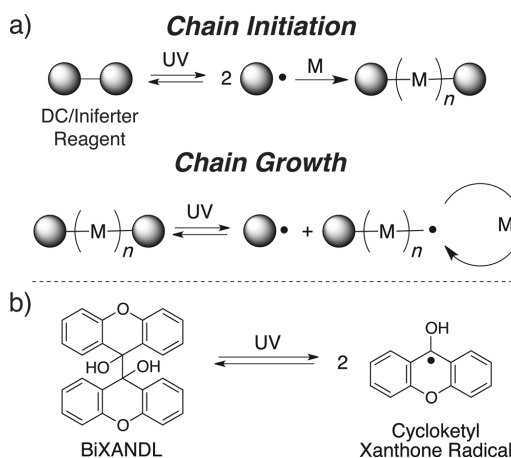


Figure 7. Chain-end activation: a) general mechanism for DC polymerization (M = monomer); b) the DC reagent BiXANDL and its light mediated fragmentation to give cycloketyl xanthone radicals.

polymer chain-end and poor control over molecular weight and PDI.

The direct photoactivation of a catalyst holds perhaps the greatest potential for regulating controlled polymerizations with light, as one only needs to control ppm levels of a catalytic species and not every monomer or every chain end. The past few years have witnessed an explosion of literature mediating small molecule organic transformations by visible light using photoredox catalysts,^[37] although the temporal control of such processes remains largely unexplored. In an innovative report employing these photoredox catalysts for photocontrolled polymerization, Hawker and co-workers have developed a living free radical polymerization of methacrylates that is efficiently controlled by visible light.^[28] The power of this process is a result of controlled polymerization under irradiation and the highly responsive, efficient, and reversible chain termination upon removal of the light (Figure 8a). Mechanistically, an Ir-based catalyst undergoes excitation with a photon to afford an Ir^{III*} species (Figure 8b). The excited catalyst is highly reducing and reacts with an alkyl bromide to give the desired alkyl radical, which initiates polymerization. The resulting Ir^{IV} can then oxidize the alkyl radical chain-end back to the dormant alkyl bromide and the entire process can be repeated with an additional photon of light. The final result is a controlled/living radical polymerization process that leads to polymers with control over molecular weight and low molecular weight distributions (PDI = 1.19–1.25). More importantly, the polymerization can be reversibly, and in a highly responsive manner, activated or deactivated by light and has been extended to produce block copolymers.

While initial work demonstrated the polymerization of only methacrylate monomers, this mechanism should be applicable to a range of monomer systems in analogy to traditional ATRP processes.^[2,38] Further, the extension of this temporal control to provide spatial control through standard

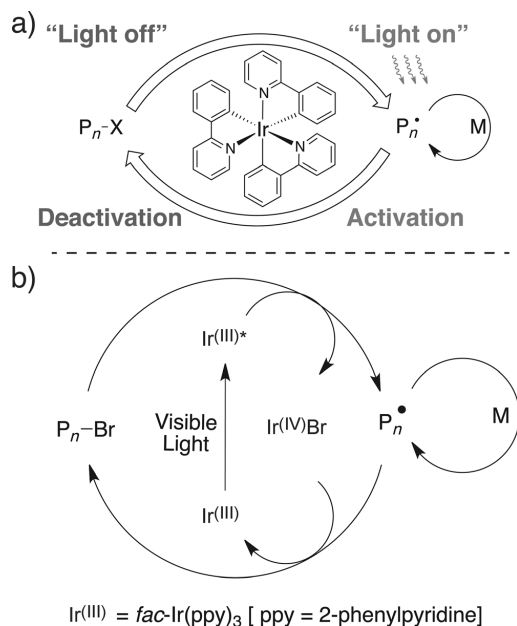


Figure 8. Catalyst activation: a) a schematic illustration of the photoredox radical polymerization concept and b) a detailed mechanism of a living radical polymerization controlled by light using a photoredox catalyst. (Adapted with permission from reference [28].)

photomasks is highly relevant and requires no major changes to this photochemically controlled, living radical process. Future challenges entail exploring the full range of polymerizable monomers and moving away from exotic metals, such as iridium, as the catalytic species and the preparation of functional macromolecules (i.e. block copolymers) with external command of final structure, architecture, and sequence.

2.5. Mechanochemical Control

In contrast to the previously described external methods for control, the application of mechanical force is a newer concept and has been proposed as a novel stimulus to affect chemical reactivity.^[39] In these processes, mechanical stresses can trigger a variety of chemistries, including bond cleavage,^[40,41] retrocycloadditions,^[42,43] and can even enable thermally inaccessible reaction pathways.^[44,45] During such “mechanochemistry”, polymer chains usually act as actuators, gathering and translating externally applied energy to the site of chemical transformation, which is often termed the mechanophore. Sonication is one of the most efficient methods to apply mechanical force in solution with strong shear-forces being created around collapsing cavitation bubbles, stretching linear polymers and accumulating significant stress midchain.^[46]

While reversible bond scission is key to mechanochemical control of polymerization, most recent work in this field has focused on enabling discrete, irreversible chemical reactions.^[39] However, these studies illustrate the potential for this approach and seminal work from Sijbesma and co-workers has demonstrated the first example of the reversible mechanochemical cleavage of metal-ligand bonds.^[47] Extending this concept to an organometallic catalyst, they subsequently demonstrated control of polymerization through the application of mechanical force.^[48] A ruthenium alkylidene complex was synthesized with axial N-heterocyclic carbene (NHC) ligands that are known to require elevated temperatures (> 80 °C) to dissociate, leading to catalytic activity (Figure 9).^[49] Both NHC ligands were substituted with long

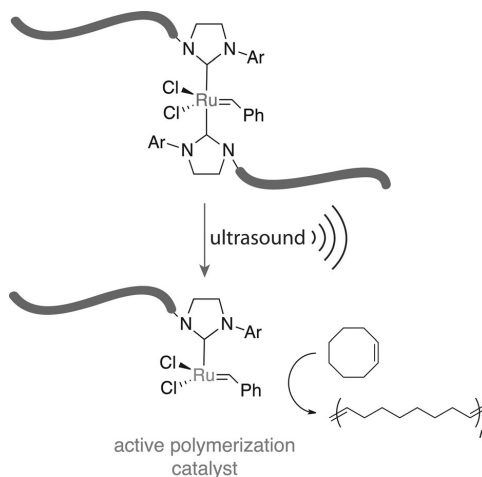


Figure 9. The mechanochemical scission of a Ru–NHC bond and the subsequent ROMP of cyclooctene.

polytetrahydrofuran chains to act as actuators, enabling mechanochemical cleavage of the Ru–NHC bond upon sonication. Significantly, GPC and NMR studies found that complete scission required sonication for 75 min (when M_n (pTHF) = 17k) and bond dissociation was irreversible. The catalyst was then used for the ring-opening polymerization of cyclooctene, reaching almost 90% conversion after sonication for two hours at low temperature (20 °C). Mechanochemical catalyst activation was confirmed by control experiments with minimal conversion being observed in the absence of sonication, or with sonication in the presence of a catalyst with butyl groups in place of the polymer actuators. Slow catalyst activation is a significant challenge for this system, leading to reduced control over molecular weight (PDI of 1.6 at 90% conversion). Further, as the latent catalyst is not regenerated after mechanochemical cleavage, interruption in sonication, therefore, causes only a pause in polymer initiation and does not reinitiate established polymer chains.

Subsequent work using a highly strained norbornene system proved the existence of the active ring opening

metathesis polymerization (ROMP) catalyst well after cessation of sonication, confirming that sonication only provides polymer initiation with catalyst decomposition being the primary mode of termination, not reformation of the latent complex.^[50] Another limitation of this system results from the mechanochemical scission of the polymers being formed from ROMP. Lastly, addition of the polymer chain to the NHC ligand negatively affects catalyst activity of the Ru catalyst, as the second order rate constant for ROMP of norbornene derivatives by the polymer-bound catalyst is 20 times lower than for the corresponding small molecule, third-generation Grubbs catalyst.^[50]

Bielawski and co-workers took a conceptually different approach to mechanochemically controlling polymerization. They utilized the dissociated ligand instead of the metal as an initiator for the polymerization of α -trifluoromethyl-2,2,2-trifluoroethyl acrylate in solution.^[51] Their system, which is based on the mechanochemical cleavage of a pyridine ligand from a palladium pincer complex, shows reversibility of ligand binding after mechanochemical cleavage. A base-mediated mechanism was therefore employed to irreversibly initiate polymerization, where the free pyridine ligand released upon sonication initiated polymerization. Once the ligand reacts with a monomer, however, it cannot rebind the metal and therefore control of chain growth is not possible.

Whilst mechanochemical control of polymerization using sonication will be limited by the rate of ligand scission and the potential for scission of covalent bonds in high molecular weight product polymers, the evaluation of different metal-ligand systems and the possibility of activating catalysts in a thermally inaccessible manner holds significant potential.^[52] A challenge for the future involves development of a system that combines the reversible ligand scission demonstrated by Bielawski with the use of a polymerization catalyst by Sijbesma. Such a mechanochemically controlled polymerization strategy would allow dynamic control of polymerization and could be applied to amplify mechanical stresses in materials and enable self-healing or diagnostic reporting of damage.

3. Outlook and Future Directions

Dynamic regulation of polymer synthesis, as evidenced by this Minireview, is a burgeoning field with potential to uncover fundamentally new chemistry with unexpected applications. To date, the most successful methods for temporally controlling polymerizations, as shown by *e*ATRP and visible light mediated polymerization, rely on switching the activity of the polymerization catalyst “on” and “off.” These approaches allow for the use of well-understood commodity monomers, polymerization mechanisms, and offer the greatest opportunities to approach an ideal system. Further, the ease and efficiency of these methodologies allow for their quick adoption in academic and industrial laboratories.

The ability to regulate catalyst activity in situ, however, is understandably underdeveloped. Synthetic chemists have traditionally focused their efforts on making catalysts with

exceedingly high activity, chemoselectivity, and enantioselectivity, without an express need to turn a reaction “off”. As modern chemistry looks more to multicomponent systems in order to solve pressing challenges in interdisciplinary areas, a number of research groups have started to look at how they can manipulate the activity and structure of catalysts to respond to applied stimuli.^[53] The following examples are not only instructive for future catalyst design, but also provide a number of unique conceptual approaches for the dynamic control of reactivity in material systems.

Drawing inspiration from both organic chemistry and natural systems, chain folding holds significant potential for temporally controlled polymerizations.^[54] An early example comes from the work of Dervan and co-workers, who designed a peptide derivative containing a crown ether-type structure that bind metal ions such as Ba^{2+} or Sr^{2+} .^[55] Upon metal binding, the peptide fragment folds into a conformation primed for DNA complexation and cleavage (Figure 10a).

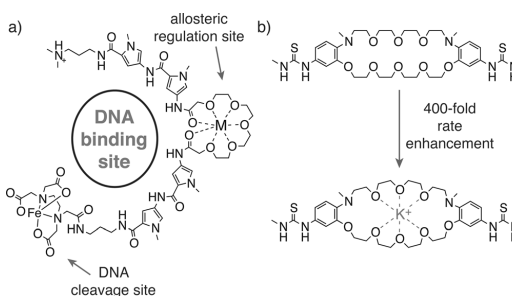


Figure 10. Examples of synthetic allosteric catalyst systems that show a large rate increase upon metal binding to crown ether-like moieties.

Employing a similar concept with a bis-thiourea based organic catalyst, Kubo and co-workers relied on K^+ binding to bring the two organocatalytic moieties into close proximity, thus achieving a 400-fold rate enhancement for phosphate diester cleavage (Figure 10b).^[56] Similar strategies can be envisaged for the external control of polymerization reactions and as described above, arguably the most successful application of allosteric catalysis in synthetic systems has been the WLA of Mirkin and co-workers.^[15,57] They have developed tweezer, sandwich, and triple-layer geometries for a number of transformations that rely on the weak binding of Lewis acidic moieties to metal centers (See section 2.1 for mechanistic details). Although all of the synthetic allosteric systems reported thus far have used metal-ligand chemistry to trigger a switch in catalyst geometry, conformation changes initiated by binding organic “signaling” molecules would be advantageous for spatially and temporally controlling polymerizations.

The potential also exists to use multiple stimuli in order to impact catalyst activity or reaction rate. Perhaps the simplest example of this strategy involves modulating the macroscopic solubility properties of a catalyst through an external stimuli (i.e. chemical oxidation, light, or pH), which in turn alters reactivity. Grubbs-type ruthenium metathesis catalysts have

served as a platform for these efforts with Plenio and Süßner pioneering this concept through the synthesis of diferrocenyl-tagged Ru catalysts (Figure 11 a).^[58] In this case, the neutral

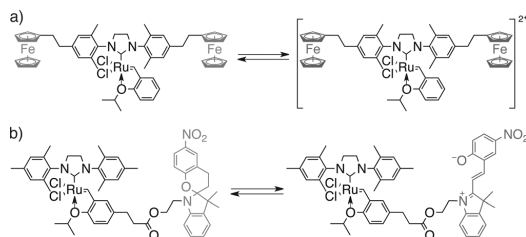


Figure 11. Solubility switches control catalysis by either oxidation of diferrocenyl units (a) or the photoswitching on spiropyran (b).

ligand is a highly active catalyst in toluene; however, addition of two equivalents of an oxidant leads to formation of cationic ferrocenyl complexes, causing the Ru catalyst to precipitate from solution, thus stopping catalysis. Addition of a reductant reformed the neutral and soluble catalyst, allowing the reaction to resume. In a complementary system, a change in solubility was externally controlled through irradiation of a spiropyran photoswitch appended to a Ru metathesis catalyst (Figure 11 b).^[59] UV light causes a ring-opening of the spiropyran to its zwitterionic form, whereas thermal relaxation of the spiropyran reforms the hydrophobic, neutral species. This solubility switch allows light to be used as a switchable phase transfer mediator, enabling temporal control of the reaction. Lastly, a number of groups have designed systems wherein pH changes affect the rate of reactivity. This concept has been employed to alter the ligand environment of a catalyst to control hydrolysis^[60] and epoxidation^[61] reactions. Further, Dunbar et al. altered the rate of ROMP through the protonation of amine containing ligands on ruthenium metathesis catalysts.^[62,63] Both solubility and pH switches hold promise as bulk property switches that can control polymerization rate, which is attractive for dynamic control of a number of large-scale systems.

Similar to the spiropyran mentioned previously, small molecule photoswitches have also provided a practical method for externally controlling a number of chemical processes. In a seminal report on catalysis, Hecht and co-workers extended the use of the azobenzene photoswitch toward reversibly modulating the activity of an organic catalyst.^[64,65] As shown in Figure 12 a, the tertiary amine organic catalyst is sterically inaccessible from substrates in its resting state. Upon irradiation with UV light, the *trans* to *cis* isomerization of azobenzene allows substrates to access the organocatalytic amine, thus catalyzing a nitroaldol (Henry) reaction. Recently, Bielawski and co-workers reported a photoswitchable NHC through the use of a diarylethene scaffold (Figure 12 b).^[66] Significantly, photoswitching modulated the electronic properties of the NHC organocatalyst, leading to a 100 fold rate increase for the more electron rich, open form of the NHC in amidation reactions.^[67] In a complementary manner, Feringa and co-workers used a light induced photoswitch not

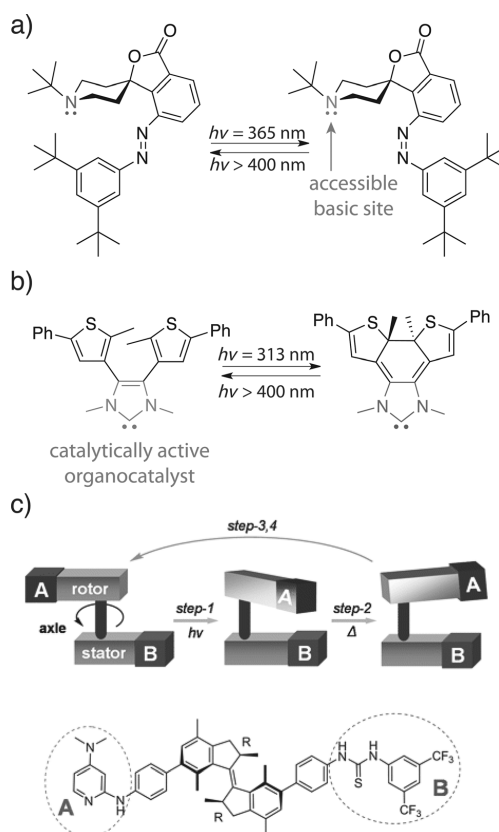


Figure 12. Light regulated catalyst systems based on photoswitches can dynamically a) regulate basicity, b) change the electronic properties of a catalyst or c) modulate the location of an intramolecular cocatalyst (Part (c) adapted from reference [68] and reprinted with permission from AAAS.)

to activate or deactivate a process, but instead to determine the stereochemical outcome of a reaction—a fascinating glimpse into the future of tacticity control for macromolecules in general (Figure 12 c).^[68] Such reversible, external control of a catalyst through photoswitching remains an under-developed concept and while Feringa and Hecht both employed photoswitches to sterically block a catalyst, other modes of regulation including competitive inhibition, reversible ligand binding, and catalyst proximity can be envisaged.^[69]

In order to realize the full potential of temporal control, again Nature provides insights into future directions. Dynamically controlling not only polymerization but also depolymerization is a fascinating concept that microtubules employ to regulate cellular processes. Further, similar to the mechanism of the ribosome, combining temporal control with the concepts of compartmentalization and multi-component systems would allow control over not only when a polymerization takes place, but could also allow segregation from other reactions and/or processes occurring simultaneous-

ly.^[70,71] Pausing a polymerization would also allow the addition and templation of a desired monomer type or monomer sequence. Unifying the spatial and temporal control of reactivity with template directed polymerizations similar to the systems of O'Reilly^[72] and Sleiman^[73] and/or with the work on sequence controlled polymerizations being pursued by Lutz^[74,75] and Sawamoto,^[76–78] will provide synergistic complex systems that move toward the grand challenges of dictating the primary structure of polymers and creating self-regulatory and “smart” processes.

4. Conclusions

The impact of controlled polymerization and orthogonal, “click” chemistry on modern polymer chemistry cannot be overstated. These advances have allowed an unprecedented level of control and functional group tolerance to be combined with the necessity to make these systems simple, user-friendly and available to non-experts in various fields. Ideas, concepts and applications for these advances have been drawn from organic chemistry, materials science, and biology, leading to a vibrant and evolving research area. It is this ability to look beyond the narrow confines of a single discipline that is one of the strengths of modern polymer chemistry and many parallels can be found in the burgeoning field of temporal and spatial regulation of controlled polymerizations. With this in mind, the significant potential provided by the development of an ideal dynamic and externally controlled polymerization process is a relevant and timely challenge for both chemists and material scientists. Success in expanding the palette of controlled polymerizations that can be regulated by external stimuli will allow the concept of “on-demand” preparation of well-defined functionalized macromolecules to be fully realized and new applications, structures, and physical properties discovered.

We would like to thank the National Science Foundation (MRSEC Program—DMR-1121053, Chemistry Program—CHE-0957492, Graduate Research Fellowships), the Department of Defense (NDSEG Fellowship), and the Dow Materials Institute for financial support.

Received: August 11, 2012

Published online: November 20, 2012

- [1] C. J. Hawker, A. W. Bosman, E. Harth, *Chem. Rev.* **2001**, *101*, 3661–3688.
- [2] K. Matyjaszewski, J. Xia, *Chem. Rev.* **2001**, *101*, 2921–2990.
- [3] G. Moad, E. Rizzardo, S. H. Thang, *Aust. J. Chem.* **2006**, *59*, 669.
- [4] N. E. Kamber, W. Jeong, R. M. Waymouth, R. C. Pratt, B. G. G. Lohmeijer, J. L. Hedrick, *Chem. Rev.* **2007**, *107*, 5813–5840.
- [5] G. J. Domski, J. M. Rose, G. W. Coates, A. D. Bolig, M. Brookhart, *Prog. Polym. Sci.* **2007**, *32*, 30–92.
- [6] a) C. W. Bielawski, R. H. Grubbs, *Prog. Polym. Sci.* **2007**, *32*, 1–29; b) K. L. Opper, K. B. Wagener, *J. Polym. Sci. Part A* **2011**, *49*, 821–831.
- [7] a) C. J. Hawker, K. L. Wooley, *Science* **2005**, *309*, 1200–1205; b) C. Boyer, M. H. Stenzel, T. P. Davis, *J. Polym. Sci. Part A* **2011**, *49*, 551–595.
- [8] a) R. K. Iha, K. L. Wooley, A. M. Nyström, D. J. Burke, M. J. Kade, C. J. Hawker, *Chem. Rev.* **2009**, *109*, 5620–5686; b) E. H. H. Wong, M. H. Stenzel, T. Junkers, C. Barner-Kowollik, *J. Polym. Sci. Part A* **2011**, *49*, 2118–2126.
- [9] C. K. Ober, S. Z. D. Cheng, P. T. Hammond, M. Muthukumar, E. Reichmanis, K. L. Wooley, T. P. Lodge, *Macromolecules* **2009**, *42*, 465–471.
- [10] T. D. Pollard, J. A. Cooper, *Science* **2009**, *326*, 1208–1212.
- [11] R. C. Jaeger, *Introduction to Microelectronic Fabrication*, Prentice Hall, Upper Saddle River, **2002**.
- [12] M. Bouskila, R. W. Hunter, A. F. M. Ibrahim, L. Delattre, M. Peggie, J. A. van Diepen, P. J. Voshol, J. Jensen, K. Sakamoto, *Cell Metab.* **2010**, *12*, 456–466.
- [13] N. C. Gianneschi, S.-H. Cho, S. T. Nguyen, C. A. Mirkin, *Angew. Chem.* **2004**, *116*, 5619–5623; *Angew. Chem. Int. Ed.* **2004**, *43*, 5503–5507.
- [14] N. C. Gianneschi, P. A. Bertin, S. T. Nguyen, C. A. Mirkin, L. N. Zakharov, A. L. Rheingold, *J. Am. Chem. Soc.* **2003**, *125*, 10508–10509.
- [15] C. G. Oliveri, P. A. Ulmann, M. J. Wiestner, C. A. Mirkin, *Acc. Chem. Res.* **2008**, *41*, 1618–1629.
- [16] H. J. Yoon, J. Kuwabara, J. H. Kim, C. A. Mirkin, *Science* **2010**, *330*, 66–69.
- [17] C. K. A. Gregson, V. C. Gibson, N. J. Long, E. L. Marshall, P. J. Oxford, A. J. P. White, *J. Am. Chem. Soc.* **2006**, *128*, 7410–7411.
- [18] E. M. Broderick, N. Guo, C. S. Vogel, C. Xu, J. Sutter, J. T. Miller, K. Meyer, P. Mehrkhodavandi, P. L. Diaconescu, *J. Am. Chem. Soc.* **2011**, *133*, 9278–9281.
- [19] E. M. Broderick, N. Guo, T. Wu, C. S. Vogel, C. Xu, J. Sutter, J. T. Miller, K. Meyer, T. Cantat, P. L. Diaconescu, *Chem. Commun.* **2011**, *47*, 9897.
- [20] C. K. A. Gregson, I. J. Blackmore, V. C. Gibson, N. J. Long, E. L. Marshall, A. J. P. White, *Dalton Trans.* **2006**, 3134.
- [21] A. J. D. Magenau, N. C. Strandwitz, A. Gennaro, K. Matyjaszewski, *Science* **2011**, *332*, 81–84.
- [22] V. Hong, A. K. Udit, R. A. Evans, M. G. Finn, *ChemBioChem* **2008**, *9*, 1481–1486.
- [23] N. Bortolamei, A. A. Isse, A. J. D. Magenau, A. Gennaro, K. Matyjaszewski, *Angew. Chem.* **2011**, *123*, 11593–11596; *Angew. Chem. Int. Ed.* **2011**, *50*, 11391–11394.
- [24] Y. Yagci, S. Jockusch, N. J. Turro, *Macromolecules* **2010**, *43*, 6245–6260.
- [25] M. Tanabe, I. Manners, *J. Am. Chem. Soc.* **2004**, *126*, 11434–11435.
- [26] M. Tanabe, G. W. M. Vandermeulen, W. Y. Chan, P. W. Cyr, L. Vanderark, D. A. Rider, I. Manners, *Nat. Mater.* **2006**, *5*, 467–470.
- [27] X. Zheng, M. Yue, P. Yang, Q. Li, W. Yang, *Polym. Chem.* **2012**, *3*, 1982.
- [28] B. P. Fors, C. J. Hawker, *Angew. Chem.* **2012**, *124*, 8980–8983; *Angew. Chem. Int. Ed.* **2012**, *51*, 8850–8853.
- [29] D.-L. Versace, Y. Guillaneuf, D. Bertin, J.-P. Fouassier, J. Lalevé, D. Gigmès, *Org. Biomol. Chem.* **2011**, *9*, 2892.
- [30] Y. Guillaneuf, D. Bertin, D. Gigmès, D.-L. Versace, J. Lalevé, J.-P. Fouassier, *Macromolecules* **2010**, *43*, 2204–2212.
- [31] E. Yoshida, *Colloid Polym. Sci.* **2010**, *288*, 73–78.
- [32] A. Goto, J. C. Scaiano, L. Maretta, *Photochem. Photobiol. Sci.* **2007**, *6*, 833.
- [33] T. Otsu, *J. Polym. Sci. Part A* **2000**, *38*, 2121–2136.
- [34] A. Bledzki, D. Braun, K. Titzschkau, *Makromol. Chem.* **1983**, *184*, 745–754.
- [35] S. Yamago, Y. Ukai, A. Matsumoto, Y. Nakamura, *J. Am. Chem. Soc.* **2009**, *131*, 2100–2101.
- [36] Y. Nakamura, T. Arima, S. Tomita, S. Yamago, *J. Am. Chem. Soc.* **2012**, *134*, 5536–5539.
- [37] J. M. R. Narayanam, C. R. J. Stephenson, *Chem. Soc. Rev.* **2011**, *40*, 102.

- [38] T. Pintauer, K. Matyjaszewski, *Chem. Soc. Rev.* **2008**, *37*, 1087.
- [39] M. M. Caruso, D. A. Davis, Q. Shen, S. A. Odom, N. R. Sottos, S. R. White, J. S. Moore, *Chem. Rev.* **2009**, *109*, 5755–5798.
- [40] M. J. Kryger, M. T. Ong, S. A. Odom, N. R. Sottos, S. R. White, T. J. Martinez, J. S. Moore, *J. Am. Chem. Soc.* **2010**, *132*, 4558–4559.
- [41] K. L. Berkowski, S. L. Potisek, C. R. Hickenboth, J. S. Moore, *Macromolecules* **2005**, *38*, 8975–8978.
- [42] K. M. Wiggins, J. A. Syrett, D. M. Haddleton, C. W. Bielawski, *J. Am. Chem. Soc.* **2011**, *133*, 7180–7189.
- [43] J. N. Brantley, K. M. Wiggins, C. W. Bielawski, *Science* **2011**, *333*, 1606–1609.
- [44] C. R. Hickenboth, J. S. Moore, S. R. White, N. R. Sottos, J. Baudry, S. R. Wilson, *Nature* **2007**, *446*, 423–427.
- [45] J. M. Lenhardt, M. T. Ong, R. Choe, C. R. Evenhuis, T. J. Martinez, S. L. Craig, *Science* **2010**, *329*, 1057–1060.
- [46] G. Cravotto, P. Cintas, *Angew. Chem.* **2007**, *119*, 5573–5575; *Angew. Chem. Int. Ed.* **2007**, *46*, 5476–5478.
- [47] J. M. J. Paulusse, R. P. Sijbesma, *Angew. Chem.* **2004**, *116*, 4560–4562; *Angew. Chem. Int. Ed.* **2004**, *43*, 4460–4462.
- [48] A. Piermattei, S. Karthikeyan, R. P. Sijbesma, *Nat. Chem.* **2009**, *1*, 133–137.
- [49] N. Ledoux, B. Allaert, A. Linden, P. Van Der Voort, F. Verpoort, *Organometallics* **2007**, *26*, 1052–1056.
- [50] R. T. M. Jakobs, R. P. Sijbesma, *Organometallics* **2012**, *31*, 2476–2481.
- [51] A. G. Tennyson, K. M. Wiggins, C. W. Bielawski, *J. Am. Chem. Soc.* **2010**, *132*, 16631–16636.
- [52] K. M. Wiggins, J. N. Brantley, C. W. Bielawski, *ACS Macro Lett.* **2012**, *1*, 623–626.
- [53] U. Lüning, *Angew. Chem.* **2012**, *124*, 8285–8287; *Angew. Chem. Int. Ed.* **2012**, *51*, 8163–8165.
- [54] M. J. Wieser, P. A. Ulmann, C. A. Mirkin, *Angew. Chem.* **2011**, *123*, 118–142; *Angew. Chem. Int. Ed.* **2011**, *50*, 114–137.
- [55] J. H. Griffin, P. B. Dervan, *J. Am. Chem. Soc.* **1987**, *109*, 6840–6842.
- [56] T. Tozawa, S. Tokita, Y. Kubo, *Tetrahedron Lett.* **2002**, *43*, 3455–3457.
- [57] N. C. Gianneschi, M. S. Masar, C. A. Mirkin, *Acc. Chem. Res.* **2005**, *38*, 825–837.
- [58] M. Süßner, H. Plenio, *Angew. Chem.* **2005**, *117*, 7045–7048; *Angew. Chem. Int. Ed.* **2005**, *44*, 6885–6888.
- [59] G. Liu, J. Wang, *Angew. Chem.* **2010**, *122*, 4527–4531; *Angew. Chem. Int. Ed.* **2010**, *49*, 4425–4429.
- [60] S. Oishi, J. Yoshimoto, S. Saito, *J. Am. Chem. Soc.* **2009**, *131*, 8748–8749.
- [61] S. Zhong, Z. Fu, Y. Tan, Q. Xie, F. Xie, X. Zhou, Z. Ye, G. Peng, D. Yin, *Adv. Synth. Catal.* **2008**, *350*, 802–806.
- [62] M. A. Dunbar, S. L. Balof, L. J. LaBeaud, B. Yu, A. B. Lowe, E. J. Valente, H.-J. R. Schanz, *Chem. Eur. J.* **2009**, *15*, 12435–12446.
- [63] M. A. Dunbar, S. L. Balof, A. N. Roberts, E. J. Valente, H.-J. Schanz, *Organometallics* **2011**, *30*, 199–203.
- [64] M. V. Peters, R. S. Stoll, A. Kuhn, S. Hecht, *Angew. Chem.* **2008**, *120*, 6056–6060; *Angew. Chem. Int. Ed.* **2008**, *47*, 5968–5972.
- [65] R. S. Stoll, M. V. Peters, A. Kuhn, S. Heiles, R. Goddard, M. Bühl, C. M. Thiele, S. Hecht, *J. Am. Chem. Soc.* **2009**, *131*, 357–367.
- [66] B. M. Neilson, V. M. Lynch, C. W. Bielawski, *Angew. Chem.* **2011**, *123*, 10506–10510; *Angew. Chem. Int. Ed.* **2011**, *50*, 10322–10326.
- [67] B. M. Neilson, C. W. Bielawski, *J. Am. Chem. Soc.* **2012**, *134*, 12693–12699.
- [68] J. Wang, B. L. Feringa, *Science* **2011**, *331*, 1429–1432.
- [69] R. S. Stoll, S. Hecht, *Angew. Chem.* **2010**, *122*, 5176–5200; *Angew. Chem. Int. Ed.* **2010**, *49*, 5054–5075.
- [70] B. Helms, S. J. Guillaudeu, Y. Xie, M. McMurdo, C. J. Hawker, J. M. J. Fréchet, *Angew. Chem.* **2005**, *117*, 6542–6545; *Angew. Chem. Int. Ed.* **2005**, *44*, 6384–6387.
- [71] S. Hecht, J. M. J. Fréchet, *Angew. Chem.* **2001**, *113*, 76–94; *Angew. Chem. Int. Ed.* **2001**, *40*, 74–91.
- [72] R. McHale, J. P. Patterson, P. B. Zetterlund, R. K. O'Reilly, *Nat. Chem.* **2012**, *4*, 491–497.
- [73] P. K. Lo, H. F. Sleiman, *J. Am. Chem. Soc.* **2009**, *131*, 4182–4183.
- [74] N. Badi, J.-F. Lutz, *Chem. Soc. Rev.* **2009**, *38*, 3383.
- [75] S. Pfeifer, J.-F. Lutz, *J. Am. Chem. Soc.* **2007**, *129*, 9542–9543.
- [76] S. Ida, T. Terashima, M. Ouchi, M. Sawamoto, *J. Am. Chem. Soc.* **2009**, *131*, 10808–10809.
- [77] S. Ida, M. Ouchi, M. Sawamoto, *J. Am. Chem. Soc.* **2010**, *132*, 14748–14750.
- [78] Y. Hibi, M. Ouchi, M. Sawamoto, *Angew. Chem.* **2011**, *123*, 7572–7575; *Angew. Chem. Int. Ed.* **2011**, *50*, 7434–7437.

Appendix B

Revisiting Thiol-yne Chemistry: Selective and Efficient Monoaddition for Block and Graft Copolymer Formation

Reproduced with permission: J. K. Sprafke, J. M. Spruell, K. M. Mattson, D. Montarnal, A. J. McGrath, R. Pöttsch, D. Miyajima, J. Hu, A. A. Latimer, B. I. Voit, T. Aida, C. J. Hawker, *J. Polym. Sci., Part A: Polym. Chem.* **2015**, *53*, 319–326. © 2014 Wiley Periodicals, Inc. CCC License Number 3932121363220.

Revisiting Thiol-yne Chemistry: Selective and Efficient Monoaddition for Block and Graft Copolymer Formation

This manuscript is dedicated to Prof. Jean Fréchet on the occasion of his 70th birthday and to his extraordinary contributions to polymer science.

Johannes K. Sprafke,¹ Jason M. Spruell,¹ Kaila M. Mattson,^{1,2} Damien Montarnal,¹ Alaina J. McGrath,¹ Robert Pötzsch,^{1,3} Daigo Miyajima,^{1,4} Jerry Hu,¹ Allegra A. Latimer,^{1,2} Brigitte I. Voit,³ Takuzo Aida,⁴ Craig J. Hawker^{1,2,5}

¹Materials Research Laboratory, University of California, Santa Barbara, California 93106

²Department of Chemistry and Biochemistry, University of California, Santa Barbara, California 93106

³Leibniz Institute of Polymer Research Dresden, Hohe Strasse 6, 01069 Dresden, Germany

⁴Department of Chemistry and Biotechnology, School of Engineering, The University of Tokyo, 7-3-1 Hongo, Bunkyo-ku, Tokyo 113-8656, Japan

⁵Department of Materials, University of California, Santa Barbara, California 93106

Correspondence to: C. J. Hawker (E-mail: hawker@mrl.ucsb.edu)

Received 6 June 2014; accepted 29 July 2014; published online 18 August 2014

DOI: 10.1002/pola.27345

ABSTRACT: The untapped potential of radical thiol-yne monoaddition chemistry is exploited to overcome the known limitations of thiol-ene chemistry in polymer coupling and block copolymer formation. By careful choice of alkyne, the reaction can selectively lead to the mono-addition product with efficiencies surpassing those achieved by traditional thiol-ene chemistry. This improvement is illustrated by the nearly quantitative

synthesis of a variety of diblock and graft copolymers. © 2014 Wiley Periodicals, Inc. *J. Polym. Sci., Part A: Polym. Chem.* **2015**, *53*, 319–326

KEYWORDS: block copolymers; click chemistry; functionalization of polymers; synthesis; thiol-yne

INTRODUCTION Block copolymers and related advanced macromolecular architectures have played a pivotal role in the development of nanostructured materials, enabling transformative technologies ranging from thermoplastic elastomers to drug delivery vehicles.¹ Polymer–polymer coupling provides an efficient synthetic route to a wide variety of block copolymers, particularly when it is challenging to find sequential polymerization conditions compatible with various monomer families. An additional benefit from a polymer-coupling strategy is the ability to start from stable, well-defined starting polymers leading to the reproducible synthesis of block copolymers with predetermined molecular weights (Scheme 1).² Synthetically, polymer coupling reactions are among the most challenging chemical transformations and are limited by low end group concentration, steric effects and decreased reactivity.

In recent years, the potential of polymer–polymer coupling reactions for the preparation of block copolymers have been

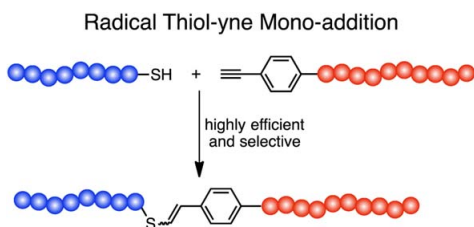
illustrated by “click” strategies, a set of highly efficient and orthogonal chemistries that have been widely used in the synthesis of small molecules and the functionalization of polymers.³ The additional challenges inherent in the coupling of two polymer chain ends have been highlighted by Barner-Kowollik et al.⁴ who proposed further requirements, including equimolar stoichiometries, simplified purification, high yields and fast timescales. One of the most widely used reactions in the context of click chemistry is the radical hydrothiolation of alkenes, referred to as thiol-ene chemistry, which has been used in the synthesis of polymer networks,⁵ functional surfaces,⁶ and dendrimers.^{7,8} Advantages of this reaction over other methodologies include facile synthetic access to both alkenes and thiols as well as spatiotemporal control that can be achieved by using a radical photoinitiator. Efficient polymer–polymer coupling, which can be regarded as a litmus test for any “click” reaction, has, despite significant efforts, thus far been elusive by means of thiol-ene chemistry with reported coupling efficiencies reaching only 25%.⁹

Johannes K. Sprafke and Jason M. Spruell contributed equally to this work.

Additional Supporting Information may be found in the online version of this article.

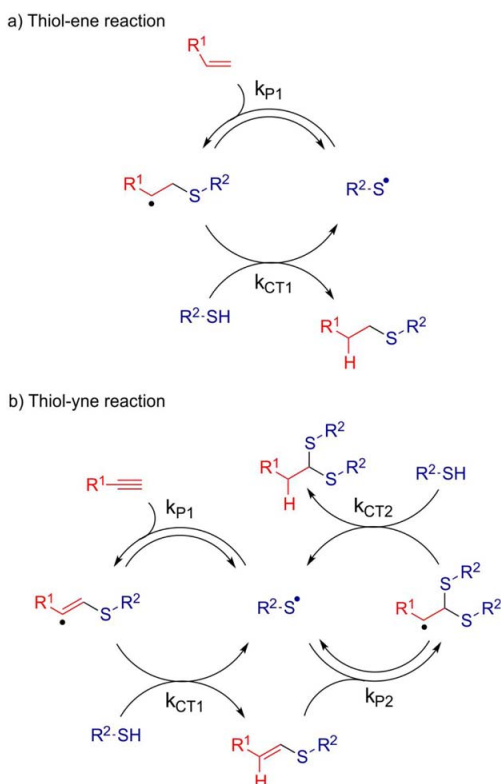
© 2014 Wiley Periodicals, Inc.





SCHEME 1 Graphical representation of thiol-yne monoaddition as a "Click" reaction for block copolymer formation.

The factors that determine the efficiency of the radical thiol-ene reaction are well understood, as is the reaction mechanism [Scheme 2(a)].^{8(b),10} In short, a radical initiator activated by either heat or light converts a thiol into a thiyl radical that then adds to the alkene, generating a sp^3 carbon-centered radical (propagation step). This radical then abstracts a hydrogen atom from another thiol to form the thioether product and regenerates a thiyl radical that propagates a further cycle (chain transfer step). Electron-rich alkenes have the highest radical addition rates, while the rate of hydrogen abstraction is limited by the stability of the



SCHEME 2 Mechanism of (a) the thiol-ene reaction and (b) the thiol-yne reaction.

carbon centered radical. Indeed, thiol-ene reactions of styrene or methacrylates involving highly stabilized radicals have much lower hydrogen abstraction rates, resulting in a variety of side reactions, particularly homopolymerization, that lower the efficiency of the coupling reaction.^{8(b)}

In order to improve the efficiency of reactions involving readily available thiol chain ends for block copolymer synthesis, we turned our attention to radical intermediates that are less stable than the sp^3 -centered radicals formed from the commonly used alkenes in thiol-ene chemistry. Vinyl radicals are intermediates in the thiol-yne reaction and are known to be significantly less stable than alkyl radicals. This suggests that thiol-yne monoaddition may be a more efficient alternative to the classic thiol-ene reaction.

While the thiol-yne reaction has recently gained popularity for its ability to cleanly form bis-adducts without significant monoadduct accumulation,¹¹ initial studies nearly a century ago demonstrated that for select substrates, such as phenylacetylene derivatives, quantitative monoaddition could be achieved.¹² This selectivity can be explained by the generally accepted mechanism for the thiol-yne reaction that follows the identical propagation and chain transfer steps as the thiol-ene reaction [Scheme 2(b)].^{11(a)} The first addition of the thiol to the alkyne forms a vinyl sulfide intermediate that can then react with another thiol to form the bis-adduct. In both reactions, the addition of the thiyl radical is reversible, whereas the hydrogen abstraction is irreversible. Therefore, the selectivity for mono- or bis-addition is solely determined by the ratio of the two hydrogen abstraction steps, k_{CT1} and k_{CT2} , which in turn depends on the relative stability of the carbon-centered radical intermediates. In the case of the thiol-yne reaction with phenylacetylene, the stabilized benzyl radical formed in the second addition step results in a significantly lower k_{CT2} when compared to k_{CT1} , and the initial vinyl radical. A direct consequence of this is the high selectivity for monoaddition when 1 equiv of thiol is used in conjugation with phenylacetylene derivatives, which as noted above is in direct contrast to the bis-additions typically observed for thiol-yne reactions.

EXPERIMENTAL

Additional examples can be found in the Supporting Information.

General Information

Unless otherwise noted, all commercially obtained solvents and reagents were used without further purification. Poly(dimethylsiloxane-*co*-[(mercaptopropyl)methylsiloxane]) (PDMS-*co*-PMMS_{8k}) **9** was purchased from Gelest. Methyl 4-ethynylbenzoate was purchased from Sigma-Aldrich. Polyethylene oxide (PEO) samples PEO_{1k} **3**, PEO_{2k} **4**, and PEO_{5k} **5** were synthesized according to a published procedure.¹³ NMR spectra were collected on a Varian VNMRs 600 MHz SB, Bruker Avance DMX 500 MHz SB, or a Varian Unity Inova 400-MHz spectrometer. All diffusion measurements were

carried out on a Bruker 300-MHz super-wide bore NMR spectrometer. Chemical shifts are reported in parts per million (ppm) and referenced to the residual solvent signal. Matrix-assisted laser desorption/ionization time-of-flight mass spectrometry (MALDI-TOF MS) data were collected on a Bruker Microflex LRT, with a 60-Hz nitrogen laser (337 nm). Micromass QTOF2 Quadrupole/time-of-flight tandem mass spectrometer was used for high-resolution mass analysis using electrospray ionization (ESI). Photoluminescence spectra were recorded on a Cary Eclipse fluorescence spectrophotometer and UV-vis absorption spectra on a Shimadzu UV3600 UV-NIR spectrometer. Gel permeation chromatography (GPC) analysis was performed on a Waters Alliance HPLC system equipped with two 300×7.5 mm Agilent PLGEL 5 mm MIXED-D columns, a Waters 2410 differential refractometer (refractive index, RI), and a Waters 2998 photodiode array detector. Thiol-yne reactions were irradiated using a UVP Black Ray UV bench lamp XX-15L, which emits 365-nm light at 15 W. Reactions under microwave irradiation were carried out in a Biotage microwave reactor.

Representative Synthesis of Hydroxyl-Terminated Polystyrene: Preparation of PS-OH_{6k}

Styrene polymerization with *s*-BuLi as initiator was performed in dry cyclohexane under a purified argon atmosphere. About 1.4 M *s*-BuLi (6.4 mL, 9.0 mol) was added to 500 mL cyclohexane at room temperature followed by the addition of purified styrene (50 mL, 0.43 mol). After stirring for 10 min, the reaction mixture was heated to 45 °C and stirred overnight (ca. 12 h). Before the termination of the reaction, an excess amount of ethylene oxide (3.0 g) was added to the resulting reaction solution in order to end-cap the polystyrene (PS). After stirring for 10 min, the polymerization was quenched by the addition of an excess amount of MeOH (10 mL). The resultant PS was purified by precipitation into MeOH from CH₂Cl₂.

¹H NMR (500 MHz, CDCl₃): δ 7.31–6.32 (br, 277H, CH_{Ar}), 3.31 (s, 2H, CH₂OH), 2.53–0.87 (br, 210H, CH₂, CHAr), 0.78–0.60 (br, 6H, CH₃); M_n (¹H NMR) = 5770 g·mol⁻¹; GPC (CHCl₃, PS standard): M_n = 5900 g·mol⁻¹, polydispersity index (PDI) (M_w/M_n) = 1.05; MALDI-TOF MS: M_n = 5930 g·mol⁻¹.

Representative Synthesis of Phenylacetylene End-Functionalized PS from Hydroxyl-Terminated Precursor: Preparation of PS_{6k}-Cl_{1k} (1)

PS-OH_{6k} (2.7 g, 0.45 mmol), 4-ethylbenzoic acid (0.55 g, 3.8 mmol), 4-dimethylaminopyridine (99 mg, 0.81 mmol), and 4-(dimethylamino)pyridinium *p*-toluenesulfonate (0.24 g, 0.81 mmol) were placed in a dry flask under argon atmosphere and dissolved in dry CH₂Cl₂ (30 mL). Dicyclohexylcarbodiimide (0.78 g, 3.8 mmol) was added and the reaction stirred under argon at room temperature for 24 h. The reaction mixture was then filtered and the solvent removed. The crude product was passed through a short plug of silica (CH₂Cl₂)

to obtain the pure PS_{6k}-Cl_{1k} (2.5 g, 0.42 mmol, 93%) as a colorless solid.

¹H NMR (600 MHz, CDCl₃): δ 7.74–7.72 (br, 2H, CH_{Ar}), 7.52–7.49 (br, 2H, CH_{Ar}), 7.33–6.31 (br, 282H, CH_{Ar}), 4.15–3.87 (br, 2H, CH₂O₂C), 3.23 (s, 1H, CCH), 2.57–0.84 (br, 182H, CH₂, CHAr), 0.80–0.57 (br, 6H, CH₃); M_n (¹H NMR) = 6070 g·mol⁻¹; GPC (CHCl₃, PS standard): M_n = 6000 g·mol⁻¹, PDI (M_w/M_n) = 1.08; MALDI-TOF MS: M_n = 6060 g·mol⁻¹.

Preparation of Hydroxyl-Terminated Polycaprolactone (PCL): PCL-OH_{11k}

In a flame-dried sealed tube, dry ϵ -caprolactone (4.0 g, 35 mmol, 3.7 mL) (distilled from CaH₂) and benzyl alcohol (14 mg, 0.13 mmol, 13 mL) were dissolved in dry toluene (9 mL) under argon and the mixture was heated to 110 °C. Freshly distilled Sn(Oct)₂ (100 mg, 0.25 mmol, 63 mL) was added and the reaction mixture stirred for 2 h at 110 °C. The product PCL-OH_{11k} (2.7 g) was obtained as a colorless solid from precipitation into hexanes.

¹H NMR (600 MHz, CDCl₃): δ 7.36–7.31 (br, 5H, CH_{Ar}), 5.11 (s, 2H, ArCH₂OR), 4.05 (t, J = 6.7 Hz, 182 H, CH₂OCO), 3.64 (t, J = 6.5 Hz, 2H, CH₂OH), 2.30 (t, J = 7.5 Hz, 185H, O₂CCH₂), 1.67–1.61 (m, 397H, CH₂), 1.41–1.35 (m, 185H, CH₂); M_n (¹H NMR) = 10,700 g·mol⁻¹; GPC (CHCl₃, PS standard): M_n = 20,200 g·mol⁻¹, PDI (M_w/M_n) = 1.15.

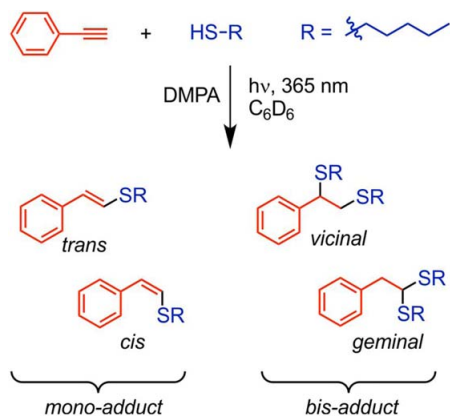
Synthesis of Phenylacetylene End-Functionalized PCL from Hydroxyl-Terminated Precursor: Preparation of PCL_{11k}-Cl_{1k} (2)

PCL-OH_{11k} (0.75 g, 70 mmol), 4-ethylbenzoic acid (52 mg, 0.35 mmol), and 4-(dimethylamino)pyridinium *p*-toluenesulfonate (21 mg, 70 mmol) were placed in a dry flask under argon atmosphere and dissolved in dry CH₂Cl₂ (8 mL). Dicyclohexylcarbodiimide (73 mg, 0.35 mmol) was added and the reaction stirred under argon at room temperature for 24 h. Then, the reaction mixture was filtered and the solvent removed. The crude product was passed through a short plug of silica (CH₂Cl₂) and then purified using a short gravimetric SEC column (toluene). The product PCL_{11k}-Cl_{1k} (2) was obtained by precipitation from CH₂Cl₂ into hexanes as a colorless powder (690 mg, 64 mmol, 92%).

¹H NMR (600 MHz, CDCl₃): δ 7.98 (d, J = 8.2 Hz, 2H, CH_{Ar}), 7.54 (d, J = 7.9 Hz, 2H, CH_{Ar}), 7.38–7.31 (br, 5H, CH_{Ar}), 5.11 (s, 2H, ArCH₂OR), 4.32 (t, J = 6.5 Hz, 2H, CH₂OCOAr), 4.06 (t, J = 6.7 Hz, 187 H, CH₂OCO), 3.23 (s, 1H, CCH), 2.30 (t, J = 7.5 Hz, 189H, O₂CCH₂), 1.68–1.62 (m, 410H, CH₂), 1.41–1.36 (m, 190H, CH₂); M_n (¹H NMR) = 11,400 g·mol⁻¹; GPC (CHCl₃, PS standard): M_n = 21,800 g·mol⁻¹, PDI (M_w/M_n) = 1.12.

Representative Synthesis of Chlorine-Terminated Polysiloxane: Preparation of PDMS-Cl_{1k}

About 20 g of hexamethylcyclotrisiloxane (D3) was dried with 500 mg of NaH in a Schlenk tube over night at 80 °C. The pure D3 monomer was distilled bulb to bulb to a three-neck round bottom flask cooled in liquid nitrogen bath. The net weight of pure D3 monomer was 13.8 g. About 200 mL of



SCHEME 3 Product distribution of the thiol-yne reaction between phenylacetylene and 1-hexanethiol.

tetrahydrofuran (THF) was added into the flask. 10 mL of 1.4 M *s*-BuLi was added into the solution at room temperature. After 2 h, 4.5 mL of chloro(3-chloropropyl)dimethylsilane was added to quench the reaction. About 10 h later, the mixture was precipitated in 500 mL of MeOH/H₂O twice. ¹H NMR (400 MHz, CDCl₃): δ 3.51 (t, *J* = 7.0 Hz, 2H, CH₂CH₂Cl), 1.84–1.76 (m, 2H, CH₂CH₂Cl), 1.61–1.51 (m, 1H, CH₂CH₃), 1.19–1.09 (m, 1H, CH₂CH₃), 0.96–0.90 (2 x t, 6H, CH₃), 0.68–0.61 (m, 2H, SiCH₂), 0.58–0.49 (m, 1H, CH₃CH), 0.16–0.03 (m, 78H, Si(O)(CH₃)(CH₃)); *M_n* (¹H NMR) = 1160 g·mol⁻¹; GPC (CHCl₃, PS standard): *M_n* = 1100 g·mol⁻¹, PDI (*M_w*/*M_n*) = 1.27.

Synthesis of Thiol-Terminated Polysiloxane from Chlorine-Terminated Precursor: Preparation of PDMS_{1k} (6)

Polydimethylsiloxane (PDMS)-Cl_{1k} (1.00 g, 862 mmol) and potassium thioacetate (520 mg, 4.55 mmol) were dissolved in a mixture of *N,N*-dimethylformamide (2.5 mL) and dimethoxyethane (2.5 mL) and heated at 110 °C for 2 h in a microwave reactor. To the reaction, mixture were added CH₂Cl₂ and water. The phases were separated and the organic phase washed twice with water and once with brine. The crude product was dried under high vacuum and directly used for the following deprotection. The crude product (700 mg) was dissolved in THF (3 mL) under argon atmosphere and cooled to 0 °C. To the solution was added hydrazine (35% in H₂O, 0.29 mL, 8.18 mmol) and then stirred at room temperature for 30 min, followed by stirring at 35 °C for 2 h. After the addition of glacial acetic acid (1 mL) and water (10 mL), the organic phase was washed twice with water and then dried over sodium sulfate. After removal of the solvent, the pure product (600 mg) was obtained as a colorless oil.

¹H NMR (600 MHz, CDCl₃): δ 2.53 (dt, *J* = 7.5 Hz, 2H, CH₂CH₂SH), 1.67–1.62 (m, 2H, CH₂CH₂SH), 1.60–1.53 (m, 1H, CH₂CH₃), 1.32 (t, *J* = 7.9 Hz, 1H, CH₂SH), 1.18–1.11 (m, 1H, CH₂CH₃), 0.95–0.91 (2 x t, 6H, CH₃), 0.66–0.62 (m, 2H, SiCH₂), 0.57–0.51 (m, 1H, CH₃CH), 0.13–0.01 (m, 85H,

TABLE 1 Product Distribution of the Thiol-yne Reaction Between Phenylacetylene and 1-Hexanethiol

Alkyne Conc. (mM)	Alkyne:Thiol (Feed)	Mono-Adduct (%)	<i>Cis/trans</i> Ratio	Bis-Adduct (%)
5	1:1	100	72/28	0
50	1:1	100	40/60	0
500	1:1	100	19/81	0
500	1:1.25	97	16/84	3
500	1:1.5	94	15/85	6
500	1:2	86	16/84	14
500	1:5	36	14/86	64
500	1:10	5	20/80	95

Si(O)(CH₃)(CH₃)); *M_n* (¹H NMR) = 1240 g·mol⁻¹; GPC (CHCl₃, PS standard): *M_n* = 1300 g·mol⁻¹, PDI (*M_w*/*M_n*) = 1.30.

Synthesis of Poly[styrene-co-(4-ethynyl styrene)] (PS-co-PES_{20k} 8)

Styrene (1.10 mL, 8.91 mmol), 4-(3'-trimethylsilylpropargyloxy)styrene¹⁴ (0.309 g, 1.54 mmol), and azobisisobutyronitrile (0.012 g, 0.071 mmol) were diluted in benzene (8 mL) in a Schlenk tube. The solution was deoxygenated by freezing in liquid nitrogen, evacuating the flask, and then thawing at room temperature. This process was repeated four times, upon which the vessel was placed in an oil bath heated to 70 °C for 14 h. The reaction was terminated by exposing to air, concentrating the solution *in vacuo*, then precipitating twice into MeOH (100 mL) affording a white powder (0.325 g, conversion = 25%). This solid was dissolved in THF (3 mL) at room temperature, after which a solution of tetra-*n*-butylammonium fluoride (TBAF, 3.0 mL of 1.0 M in THF) was added dropwise. The reaction mixture was stirred for 12 h, concentrated *in vacuo*, and precipitated twice into MeOH (100 mL) affording **8** as a white powder (0.301 g); *M_n* = 20,400 g·mol⁻¹, PDI (*M_w*/*M_n*) = 1.65.

¹H NMR (600 MHz, CDCl₃): δ 7.33–6.18 (br, 21H, CH_{Ar}), 3.04 (s, 1H, CH_{acet}), 2.27–0.86 (br, 15H, CH₂, CH_{Ar}). Styrene:alkyne ratio = 77:23.

Synthesis of Silyl-Protected Catechol Derivative CatSH (19)

To a round bottom flask were added ((4-allyl-1,2-phenylene)-bis(oxy))bis(triethylsilane)¹⁵ (10.9 g, 28.9 mmol), ethane dithiol (19.4 mL, 231 mmol) and 2,2-dimethoxy-2-phenylacetophenone (148 mg, 0.58 mmol) and sparged with argon for 30 min. The reaction was irradiated with UV light for 1 h and checked by gas chromatograph (GC) to ensure complete consumption of alkene. The excess ethane dithiol was removed by vacuum distillation and the resulting mixture was passed through a column using 25% CH₂Cl₂/hexanes as the eluent to remove residual impurities to afford (CatSH **19**) (11.6 g, 85%) as a colorless oil.

¹H NMR (500 MHz, CDCl₃): δ 6.72 (d, *J* = 8.0 Hz, 1H), 6.63 (d, *J* = 2.0 Hz, 1H), 6.59 (dd, *J* = 8.0, 2.0 Hz, 1H), 2.79–2.64

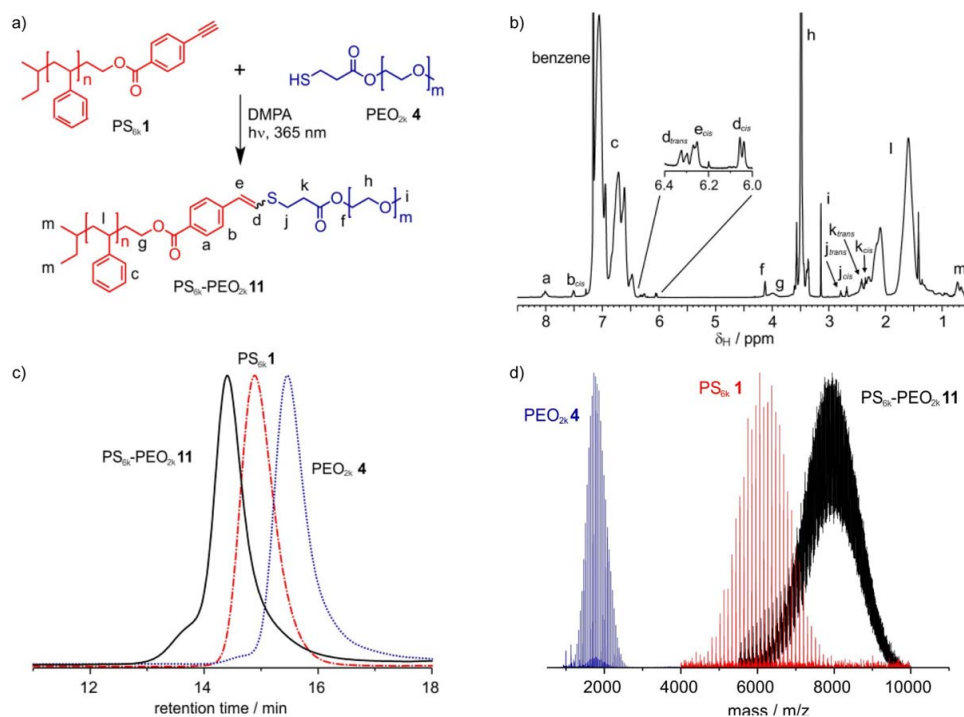


FIGURE 1 Thiol-yne monoaddition of PS_{6k} **1** and PEO_{2k} **4**. (a) Reaction scheme, (b) ^1H NMR spectrum of diblock PS_{6k} -*b*- PEO_{2k} **11** (C_6D_6 , 298 K, 600 MHz) (c) GPC traces of PEO_{2k} **4** (blue dotted line), PS_{6k} **1** (red dashed-dotted line), and PS_{6k} -*b*- PEO_{2k} **11** (black line) (d) Overlay of the MALDI-TOF mass spectra of PS_{6k} -*b*- PEO_{2k} **11** (black), PS_{6k} **1** (red), and PEO_{2k} **4** (blue) allowing determination of the exact molecular weights M_n (PEO_{2k} **4**) = 1750 $\text{g}\cdot\text{mol}^{-1}$, M_n (PS_{6k} **1**) = 6060 $\text{g}\cdot\text{mol}^{-1}$ and M_n (PS_{6k} -*b*- PEO_{2k} **11**) = 7810 $\text{g}\cdot\text{mol}^{-1}$. The mass of the diblock corresponds to the sum of the two homopolymers.

(m, 4H), 2.59 (t, $J = 7.4$ Hz, 2H), 2.50 (t, $J = 7.4$ Hz, 2H), 1.85 (p, $J = 7.4$ Hz, 2H), 1.71 (t, $J = 7.8$ Hz, 1H), 0.98 (td, $J = 7.9$, 2.6 Hz, 18 H), 0.79 (qd, $J = 7.9$, 2.7 Hz, 12H); ^{13}C NMR (500 MHz, CDCl_3): δ 146.7, 145.1, 134.5, 121.4, 120.9, 120.4, 36.3, 34.1, 31.4, 24.9, 6.8, 5.3; high-resolution mass spectrometry (ESI-/TOF) calculated $(M + \text{Na})^+$ 495.2219, observed $(M + \text{Na})^+$ 495.2204.

General Procedure for Thiol-yne Coupling Reactions

The phenylacetylene-functionalized polymer (25 mM), thiol (27.5 mM), and photoinitiator 2,2-dimethoxy-2-phenylacetophenone (DMPA) (0.2 equiv per thiol) were dissolved in benzene. The reaction mixture was purged with argon and irradiated with UV light (365 nm, 15 W) until the reaction was complete, as indicated by ^1H NMR, and the product could be isolated.

RESULTS AND DISCUSSION

Small Molecule Model Studies

To demonstrate the potential of this modified thiol-yne reaction for polymer-polymer coupling and functionalization, a series of model reactions between phenylacetylene and 1-

hexanethiol with 5 mol % DMPA as the photoinitiator were investigated.^{12(f)} The reactions were carried out in d_6 -benzene and followed by ^1H NMR spectroscopy, which allowed complete identification and quantification of the products (Scheme 3 and Table 1). After 1 h of irradiation, complete and selective conversion to the vinyl sulfide monoadduct (mixture of *cis* and *trans* products) was observed under various starting concentrations (5–500 mM). It should be noted that no evidence of the 1,1-disubstituted vinyl sulfide monoadduct was observed under any conditions.¹⁶

This high efficiency, particularly at low concentrations, demonstrates the potential of this reaction for polymer coupling given the molecular weight dilution of the chain ends even for low molecular weight polymers. The strong preference for monoaddition is further emphasized by the formation of only 14% bis-adduct when 2 equiv of thiol are used under the highest concentration conditions. Surprisingly, to push the bis-addition reaction to near completion, 10 equiv of thiol were required. Encouraged by the selectivity and efficiency of the model reactions, we then applied the reaction to polymer-polymer coupling.

TABLE 2 GPC Data of Starting Homopolymers and Coupling Products

No.	Homopolymer	M_n (kDa) ^a	PDI ^a
1	PS _{6k} (alkyne)	6.0	1.08
2	PCL _{11k} (alkyne)	21.8	1.12
3	PEO _{1k} (thiol)	1.9	1.10
4	PEO _{2k} (thiol)	4.0	1.10
5	PEO _{5k} (thiol)	11.0	1.06
6	PDMS _{1k} (thiol)	1.3	1.30
7	PDMS _{3k} (thiol)	3.3	1.16
8	PS- <i>co</i> -PES _{20k} (alkyne)	20.4	1.65
9	PDMS- <i>co</i> -PMMS _{8k} (thiol)	8.1 ^b	1.81
No.	Coupling Product	M_n (kDa) ^a	PDI ^a
10	PS _{6k} - <i>b</i> -PEO _{1k}	9.1	1.10
11	PS _{6k} - <i>b</i> -PEO _{2k}	10.1	1.11
12	PS _{6k} - <i>b</i> -PEO _{5k}	16.4	1.14
13	PS _{6k} - <i>b</i> -PDMS _{1k}	8.7	1.10
14	PS _{6k} - <i>b</i> -PDMS _{3k}	10.4	1.08
15	PCL _{11k} - <i>b</i> -PEO _{5k}	30.4	1.22
16	PS _{20k} - <i>g</i> -Catechol	83.9	2.12
17	PS _{20k} - <i>g</i> -Octyl	28.1	2.20
18	PDMS _{8k} - <i>g</i> -PS _{6k}	82.0 ^c	1.57

All values determined by GPC (CHCl₃) using:

^a PS standards.

^b PDMS standards.

^c MALS detector.

Structural Evidence for Diblock Formation

To demonstrate the applicability of this modified thiol-yne reaction for block copolymer formation, coupling of phenylacetylene end-functionalized PS PS_{6k} **1** and thiol-terminated PEO_{2k} **4** to form the PS_{6k}-*b*-PEO_{2k} diblock copolymer **11** was investigated (Fig. 1). The starting polymers were synthesized by postpolymerization modification of hydroxyl-terminated precursors that were either commercially available (PEO_{2k} **4**) or synthesized by anionic polymerization (PS_{6k} **1**). After optimizing the reaction conditions for polymer coupling (25 mM reactant concentration, 2 h irradiation, 20 mol % DMPA), a range of analytical techniques were used to confirm the high efficiency of diblock copolymer formation. For example, GPC analysis revealed a reduction in retention time for the product obtained from the coupling reaction when compared to both starting polymers with a low PDI being maintained [Fig. 1(c)]. In a similar fashion, the ¹H NMR spectrum of **11** shows the expected disappearance of the resonance for the terminal alkyne group of the starting PS_{6k} **1** with peaks corresponding to the linker group derived from the end functionalities of **1** and **4** (peaks a, b, j, k) being shifted compared to the starting polymers (Supporting Information Fig. S2). Direct evidence for formation of the vinyl sulfide group comes from the appearance of doublets "e" and "d" for both the *cis* and the *trans* vinylic protons, between 6.0 and 6.5 ppm [Fig. 1(b)]. These and all other peaks were assigned unambiguously using a

model compound with the help of correlation spectroscopy and nuclear Overhauser effect spectroscopy two-dimensional NMR techniques (see Supporting Information). Further evidence for formation of diblock PS_{6k}-*b*-PEO_{2k} **11** comes from both matrix-assisted laser desorption/ionization [Fig. 1(d)] and diffusion-ordered spectroscopy (DOSY) which showed an array of peaks corresponding to a single diffusing species (Supporting Information Fig. S3).

Confirmation of High Coupling Efficiency

While the above studies provide structural evidence for diblock formation, it is critical to quantify the coupling efficiency. Initial evidence for the high efficiency of the reaction comes from integration of the ¹H NMR signals of the vinyl sulfide protons in the crude reaction mixture. Based on the PS chain end as calibration, the sum of the integrals of the *cis* and *trans* signals of vinyl proton "d" is close to the expected value of 1.0 (Supporting Information Fig. S2). Further support for the efficiency of the coupling process comes from comparison of the analytical data of the crude material with that of the purified product. Precipitation of the crude material into methanol would be expected to remove any unreacted PEO_{2k} **4** and possible disulfide byproduct. Significantly, the GPC trace remained essentially unchanged after purification with integration of the PS versus the PEO backbone signals in the ¹H NMR spectrum matching the ratio expected for PS_{6k}-*b*-PEO_{2k} **11** (Supporting Information Fig. S5). This absence of change in the NMR and GPC data strongly suggests the minimal presence of unreacted PEO homopolymer/byproducts and confirms the high efficiency of the coupling reaction under a variety of conditions.

The unique absorption feature of the vinyl sulfide linkage (strong absorption at 320 nm, extending to 370 nm, Supporting Information Fig. S6) also provides a useful means of selectively detecting vinyl sulfide containing species in the presence of potential impurities, such as the starting PEO and PS homopolymers, which do not absorb in this region. When overlaid, the GPC trace obtained at 330 nm is in good agreement with the chromatogram obtained from the RI detector. However, a small shoulder at shorter retention times is present in the RI trace that is absent in the 330 nm absorption. This shoulder indicates the presence of a small amount of higher molecular weight polymers that may arise from bis-adduct formation or be products from radical recombination processes. These impurities can be removed by column chromatography and are minor (<5%) (Supporting Information Fig. S5).

Utilizing Thiol-yne Monoaddition to Prepare Complex Polymer Architectures

Diverse Diblock Copolymers

The generality and utility of thiol-yne monoaddition for polymer coupling was demonstrated by the successful synthesis of a variety of diblock copolymers from both higher molecular weight starting materials and alternate backbones (Table 2). In addition to thiol-terminated PEO_{1k} **3** and PEO_{5k} **5**, two PDMS derivatives PDMS_{1k} **6** and PDMS_{3k} **7** were synthesized

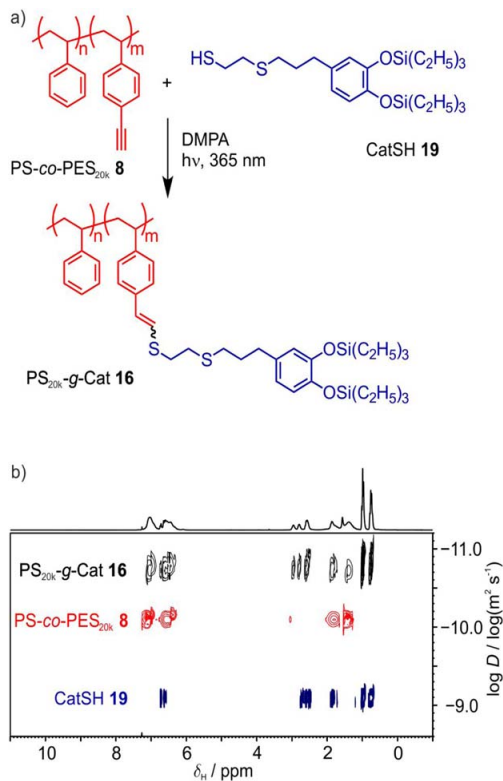


FIGURE 2 Grafting of CatSH **19** onto PS-co-PES_{20k} **8**. (a) Reaction scheme, $m = 0.23$, $n = 0.77$, (b) overlaid DOSY plots from independent diffusion measurements of CatSH **19** (blue), PS-co-PES_{20k} **8** (red), and PS_{20k}-g-Cat **16** (black) in CDCl₃ at 298 K.

by anionic polymerization followed by end group conversion into the desired thiol. Significantly, all of these polymers gave excellent coupling efficiencies with PS_{6k} **1** (see Supporting Information). The successful coupling of phenylacetylene-terminated polycaprolactone PCL_{11k} **2** with PEO_{5k} **5** further extends the range of the coupling methodology to alternate diblock copolymers and increased molecular weights with high coupling efficiency.

Functionalization of Polyfunctional Backbones

The utility of selective radical thiol-yne monoaddition for the preparation of complex macromolecular architectures was further examined by grafting small molecules or polymer chains to a polyfunctional backbone. It should be noted that grafting reactions can be even more challenging than diblock formation due to steric crowding along the backbone and the likelihood of radical-radical coupling between the multifunctional backbones.¹⁷

As a further demonstration of the efficiency of thiol-yne monoaddition for the preparation of complex macromolecu-

lar architectures, a variety of graft copolymers were prepared. Copolymerization of styrene with silyl-protected 4-ethynyl styrene followed by TBAF deprotection, afforded the random copolymer poly[styrene-co-(4-ethynyl styrene)] PS-co-PES_{20k} **8** with 23% backbone incorporation of phenylacetylene groups. This polymer was successfully functionalized with both 1-octanethiol **20** and the more complex catechol derivative CatSH **19** (Fig. 2) that has been shown to provide polymers with strong adhesion under a variety of environments.¹⁸

Formation of Grafted Copolymers

The grafting process maintains its high degree of fidelity if the backbone functionalities are thiols rather than phenylacetylene groups and even tolerates the grafting of polymer chains. This is exemplified by the grafting of PS_{6k} **1** onto the commercially available, PDMS-based copolymer, PDMS-co-PMMS_{6k} **9**, where 13% of the repeat units bear a mercaptopropyl side chain (Fig. 3). GPC of the crude product shows a dramatic increase in molecular weight after 2 h of irradiation [Fig. 3(b) and Supporting Information Fig. S32]. The M_n of the graft polymer was found to be 82 kg·mol⁻¹, which correlates with efficient grafting and the near-quantitative nature of this process is supported by the complete conversion of end-functional group resonances as determined by ¹H NMR spectroscopy (Supporting Information Fig. S31).

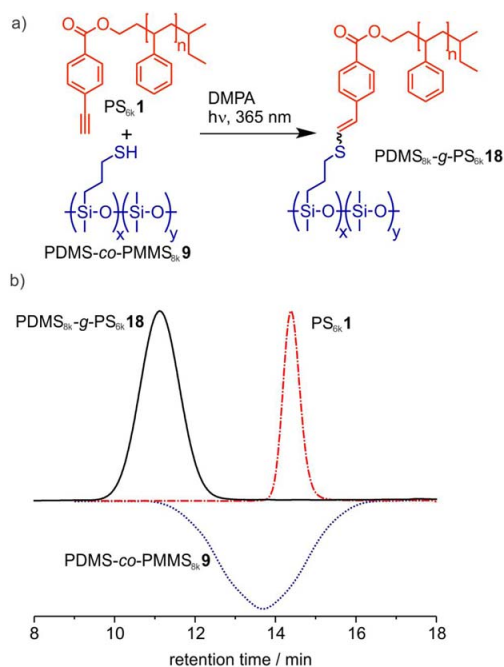


FIGURE 3 Grafting of PS_{6k} **1** onto PDMS-co-PMMS_{6k} **9**. (a) Reaction scheme, (b) GPC (CHCl₃) traces of PDMS-co-PMMS_{6k} **9** (blue dotted line), PS_{6k} **1** (red dashed-dotted line), and PDMS_{6k}-g-PS_{6k} **18** after purification by precipitation (black line).

CONCLUSIONS

In summary, we have identified selective thiol-yne monoaddition to phenylacetylene derivatives as a powerful synthetic tool for the construction of macromolecular architectures, as demonstrated by the efficient synthesis of both diblock and graft copolymers. Advantages of this new approach include facile synthesis of starting materials, equimolar stoichiometries of building blocks, high overall yields and efficient coupling. The high functional group tolerance of thiol-yne chemistry makes this methodology applicable to the synthesis of a wide range of functionalized polymers. In a wider context, the use of phenylacetylene derivatives also represents a critical improvement over vinyl substrates traditionally used in the radical thiol-ene reaction and offers wide application in many areas of materials chemistry.

ACKNOWLEDGMENTS

We thank Eric D. Pressly for helpful discussions. This work was supported by the NSF MRSEC and RISE Programs under award no. DMR-1121053 (J. K. Sprafke, D. Montarnal, R. Pötzsch, D. Miyajima, J. Hu, A. J. McGrath, K. M. Mattson, A. A. Latimer, and C. J. Hawker). Partial support by the National Institutes of Health as a Program of Excellence in Nanotechnology (HHSN268201000046C) (A. J. McGrath, A. A. Latimer, and C. J. Hawker) is also gratefully acknowledged. J. M. Spruell thanks the California NanoSystems Institute for an Elings Prize Fellowship. R. Pötzsch thanks the Studienstiftung des deutschen Volkes for a PhD scholarship and Förderverein des Leibniz-Instituts für Polymerforschung for a travel support. K. M. Mattson thanks the NSF Graduate Research Fellowship and ConvEne IGERT Program (NSF-DGE 0801627) for funding. The MRL Shared Experimental Facilities are supported by the MRSEC Program of the National Science Foundation under award NSF DMR-1121053; a member of the NSF-funded Materials Research Facilities Network.

REFERENCES AND NOTES

- 1 F. S. Bates, G. H. Fredrickson, *Phys. Today* **1999**, *52*, 32–39.
- 2 (a) J. A. Opsteen, J. C. M. van Hest, *Chem. Commun.* **2005**, 57–62; (b) A. J. Inglis, S. Sinnwell, M. H. Stenzel, C. Barner-Kowollik, *Angew. Chem. Int. Ed.* **2009**, *48*, 2411–2418; (c) E. D. Pressly, R. J. Amir, C. J. Hawker, *J. Polym. Sci. Part A: Polym. Chem.* **2011**, *49*, 814–819; (d) C. F. Hansell, P. Espeel, M. M. Stamenovic, I. A. Barker, A. P. Dove, Du F. E. Prez, R. K. O'Reilly, *J. Am. Chem. Soc.* **2011**, *133*, 13828–13833; (e) M. A. Tasdelen, G. Yilmaz, B. Iskin, Y. Yagci, *Macromolecules* **2012**, *45*, 56–61; (f) K. K. Oehlenschlaeger, J. O. Mueller, N. B. Heine, M. Glassner, M. K. Guimard, G. Delaittre, F. G. Schmidt, C. Barner-Kowollik, *Angew. Chem. Int. Ed.* **2013**, *52*, 762–768; (g) V. X. Truong, A. P. Dove, *Angew. Chem. Int. Ed.* **2013**, *52*, 4132. (h) C. J. Hawker, V. V. Fokin, M. G. Finn, K. B. Sharpless, *Aust. J. Chem.* **2007**, *60*, 381–383.
- 3 (a) H. C. Kolb, M. G. Finn, K. B. Sharpless, *Angew. Chem. Int. Ed.* **2001**, *40*, 2004–2009; (b) R. K. Iha, K. L. Wooley, A. M. Nyström, D. J. Burke, M. J. Kade, C. J. Hawker, *Chem. Rev.* **2009**, *109*, 5620–5686; (c) Kempe, K.; A. Krieg, C. R. Becer, U. S. Schubert, *Chem. Soc. Rev.* **2012**, *41*, 176–198; (d) A. S. Goldmann, M. Glassner, A. J. Inglis, C. Barner-Kowollik, *Macromol. Rapid Commun.* **2013**, *34*, 810–815; (e) R. K. O'Reilly, M. J. Joralemon, C. J. Hawker, K. L. Wooley, *Chem. Eur. J.* **2006**, *12*, 6776–6786; (f) J. N. Hunt, K. E. Feldman, N. A. Lynd, J. Deek, L. M. Campos, J. M. Spruell, B. M. Hernandez, E. J. Kramer, C. J. Hawker, *Adv. Mater.* **2011**, *23*, 2327–2332; (g) M. A. Cole, C. N. Bowman, *J. Polym. Sci. Part A: Polym. Chem.* **2013**, *51*, 1749–1757.
- 4 C. Barner-Kowollik, Du F. E. Prez, P. Espeel, C. J. Hawker, T. Junkers, H. Schlaad, Van W. Camp, *Angew. Chem. Int. Ed.* **2011**, *50*, 60–62.
- 5 (a) N. B. Cramer, J. P. Scott, C. N. Bowman, *Macromolecules* **2002**, *35*, 5361–5366; (b) H. W. Ooi, K. S. Jack, A. K. Whittaker, H. Peng, *J. Polym. Sci. Part A: Polym. Chem.* **2013**, *51*, 4626–4636.
- 6 (a) N. Gupta, B. F. Lin, L. M. Campos, M. D. Dimitriou, S. T. Hikita, N. D. Treat, M. V. Tirrell, D. O. Clegg, E. J. Kramer, C. J. Hawker, *Nat. Chem.* **2010**, *2*, 138–145; (b) L. M. Campos, I. Meinel, R. G. Guino, M. Schierhorn, N. Gupta, G. D. Stucky, C. J. Hawker, *Adv. Mater.* **2008**, *20*, 3728–3734.
- 7 K. L. Killops, L. M. Campos, C. J. Hawker, *J. Am. Chem. Soc.* **2008**, *130*, 5062–5064.
- 8 (a) C. E. Hoyle, A. B. Lowe, C. N. Bowman, *Chem. Soc. Rev.* **2010**, *39*, 1355–1341; (b) C. E. Hoyle, C. N. Bowman, *Angew. Chem. Int. Ed.* **2010**, *49*, 1540–1546; (c) M. J. Kade, D. J. Burke, C. J. Hawker, *J. Polym. Sci. Part A: Polym. Chem.* **2010**, *48*, 743–750.
- 9 (a) S. P. S. Koo, M. M. Stamenovic, R. A. Prasath, A. J. Inglis, Du F. E. Prez, C. Barner-Kowollik, Van W. Camp, T. Junkers, *J. Polym. Sci. Part A: Polym. Chem.* **2010**, *48*, 1699–1707; (b) P. Derboven, D. R. D'hooge, M. M. Stamenovic, P. Espeel, G. B. Marin, Du F. E. Prez, M. F. Reyniers, *Macromolecules* **2013**, *46*, 1732–1737.
- 10 B. H. Northrop, R. N. Coffey, *J. Am. Chem. Soc.* **2012**, *134*, 13804–13811.
- 11 (a) A. B. Lowe, C. E. Hoyle, C. N. Bowman, *J. Mater. Chem.* **2010**, *20*, 4745–4751; (b) D. Konkolewicz, A. Gray-Weale, S. Perrier, *J. Am. Chem. Soc.* **2009**, *121*, 18075–18080; (c) O. Türlünc, M. A. R. Meier, *J. Polym. Sci. Part A: Polym. Chem.* **2012**, *50*, 1689–1695; (d) Y. Shen, Y. Ma, Z. Li, *J. Polym. Sci. Part A: Polym. Chem.* **2013**, *51*, 708–715; (e) N. Ren, X. Huang, X. Huang, Y. Qian, C. Wang, Z. Xu, *J. Polym. Sci. Part A: Polym. Chem.* **2012**, *50*, 3149–3157.
- 12 (a) S. Ruhemann, H. E. Stapelton, *J. Chem. Soc. Trans.* **1900**, *77*, 1179–1185; (b) S. Ruhemann, *J. Chem. Soc. Trans.* **1905**, *87*, 461–468; (c) E. P. Kohler, H. Potter, *J. Am. Chem. Soc.* **1935**, *57*, 1316–1318; (d) A. A. Oswald, K. Griesbaum, B. E. Hudson, J. M. Bregman, *J. Am. Chem. Soc.* **1964**, *86*, 2877–2881; (e) K. Griesbaum, *Angew. Chem. Int. Ed. Engl.* **1970**, *9*, 273–276; (f) R. Pötzsch, H. Komber, B. C. Stahl, C. J. Hawker, B. I. Voit, *Macromol. Rapid Commun.* **2013**, *34*, 1172–1178; (g) R. Pötzsch, B. C. Stahl, H. Komber, C. J. Hawker, B. I. Voit, *Polym. Chem.* **2014**, *5*, 2911–2921.
- 13 P. Lundberg, M. V. Walter, M. I. Montanez, D. Hult, A. Hult, A. Nyström, M. Malkoch, *Polym. Chem.* **2011**, *2*, 394–398.
- 14 S. Fleischmann, H. Komber, B. Voit, *Macromolecules* **2008**, *41*, 5255–5260.
- 15 J. Heo, T. Kang, S. G. Jang, D. S. Hwang, J. M. Spruell, K. L. Killops, J. H. Waite, C. J. Hawker, *J. Am. Chem. Soc.* **2012**, *134*, 20139–20145.
- 16 The dramatic change in the cis/trans ratios of the sulfide monoadducts may be explained by formation of the thermodynamic product (trans) at high reactant and initiator concentrations and the kinetic product (cis) at lower concentrations, as observed for Ynamides: B. Banerjee, D. N. Litvinov, J. Kang, J. D. Bettale, S. L. Castle, *Org. Lett.* **2010**, *12*, 2650–2652.
- 17 H. Gao, K. Matyjaszewski, *J. Am. Chem. Soc.* **2007**, *129*, 6633–6639.
- 18 F. A. Leibfarth, C. J. Hawker, *J. Polym. Sci. Part A: Polym. Chem.*, **2013**, *51*, 3769–3782.

Appendix C

A Highly Reducing Metal-Free Photoredox Catalyst: Design and Application in Radical Dehalogenations

Reproduced from: E. H. Discekici, N. J. Treat, S. O. Poelma, K. M. Mattson, Z. H. Hudson, Y. Luo, C. J. Hawker, J. Read de Alaniz, *Chem. Commun.* **2015**, *51*, 11705–11708 with permission from The Royal Society of Chemistry.



Cite this: *Chem. Commun.*, 2015, 51, 11705

Received 6th June 2015,
Accepted 18th June 2015

DOI: 10.1039/c5cc04677g

www.rsc.org/chemcomm

A highly reducing metal-free photoredox catalyst: design and application in radical dehalogenations[†]

Emre H. Discekici,^{‡a} Nicolas J. Treat,^{‡b} Saemi O. Poelma,^a Kaila M. Mattson,^a Zachary M. Hudson,^b Yingdong Luo,^a Craig J. Hawker^{*ab} and Javier Read de Alaniz^{*a}

Here we report the use of 10-phenylphenothiazine (PTH) as an inexpensive, highly reducing metal-free photocatalyst for the reduction of carbon–halogen bonds via the trapping of carbon-centered radical intermediates with a mild hydrogen atom donor. Dehalogenations were carried out on various substrates with excellent yields at room temperature in the presence of air.

In recent years, photoredox chemistry has enabled the development of a wide variety of synthetic transformations.¹ These methods are based on photocatalysts which, upon absorption of light, enter either a highly reducing or oxidizing excited state capable of facilitating redox-based transformations. In particular, the reduction of activated carbon–halide (C–X) bonds has generated wide interest, largely because of the broad synthetic utility of resulting carbon-centered radical intermediates.^{1–10} One example includes subsequent trapping of these intermediates with a mild H-atom source to achieve radical dehalogenations.^{3,5,6,9} In this case, the power of using a photoredox approach is that it offers a more efficient and safer alternative to traditional dehalogenation protocols involving metal–halogen exchange,^{11,12} stoichiometric tin hydride,¹³ and various other highly toxic reagents.^{14–16} However, despite the notable advantages of photoredox catalysis,¹ a number of major challenges still exist. This includes the use of catalysts based on rare-earth transition metals such as Ru and Ir, which have inherent limitations due to the cost of the catalyst itself (~\$1 mg⁻¹ for Ir(ppy)₃),¹⁷ as well as the expense associated with the removal of trace metals from the desired products – critical for applications from pharmaceuticals to micro-electronics. In addition, although an assortment of activated carbon–halogen bonds have been accessed using these catalysts,¹ higher energy unactivated halides are a significantly more challenging task, with only unactivated

iodides being explored to date.^{5,18} To this end, a more affordable gold-based photocatalyst has been developed,¹⁰ and although offering broader substrate scope, the disadvantages of metal-based systems remain. In addressing this, the use of an organic perylene diimide (PDI)-based photocatalyst was recently reported, and while providing a metal-free alternative, it requires elevated temperatures and has a scope limited to activated aryl-halides.⁸ In this context, we envisioned the development of a highly reducing, inexpensive, metal-free photocatalyst that could offer access to a wide range of carbon–halogen substrates under markedly mild conditions (Fig. 1).

Our groups previously employed 10-phenylphenothiazine (PTH) as a metal-free catalyst for photomediated atom transfer radical polymerizations (ATRP).¹⁹ In this system, PTH acts as a photoreductant in a similar manner to Ir(ppy)₃ with a reduction potential ($E_{1/2}^* = -2.1$ V vs. SCE) significantly higher than Ir(ppy)₃ ($E_{1/2}^* = -1.7$ V vs. SCE). Based on our interest in metal-free ATRP, we envisioned that the same radical based processes enabled by PTH could also be used to access a variety of carbon-centered radical intermediates that could be used for subsequent synthetic transformations, such as the reduction of carbon–halogen bonds. Highlighted by the use of mild reagents and a readily accessible light source, coupled with its high degree of oxygen tolerance, we believe this novel metal-free system will serve as a platform for expanding the synthetic utility of photoredox chemistry.

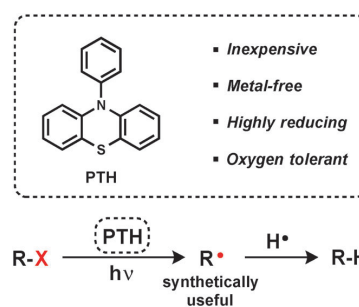


Fig. 1 Properties and application of 10-phenylphenothiazine (PTH).

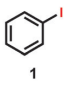
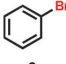
^a Department of Chemistry and Biochemistry, University of California, Santa Barbara, California, 93106, USA. E-mail: javier@chem.ucsb.edu

^b Materials Department, Materials Research Laboratory, University of California, Santa Barbara, California, 93106, USA

[†] Electronic supplementary information (ESI) available. See DOI: 10.1039/c5cc04677g

[‡] These authors contributed equally to this work.

Table 1 Comparison of reduction capabilities of Ir(ppy)₃, PDI with PTH for the reduction of iodo- and bromobenzene^a

Ph-X Substrate	Photocatalyst hv. conditions		Ph-H Yield
	Time	Photocatalyst	
 1	1 h	PTH	98 %
		Ir(ppy) ₃	23 %
		PDI	0 %
 2	72 h	PTH	85 %
		Ir(ppy) ₃	0 %
		PDI	0 %

^a Reaction conditions using PTH and Ir(ppy)₃: iodo- or bromobenzene (1 equiv.), PTH (5 mol%) or Ir(ppy)₃ (1 mol%),⁵ formic acid (5 equiv.) and tributylamine (5 equiv.), acetonitrile (0.08 M of substrate) at RT with irradiation by 380 nm LEDs (1.8 μW cm⁻²). ¹H NMR yield determined using 1,3,5-trimethoxybenzene or 1,2,4,5-tetramethylbenzene as internal standard. Reaction conditions using PDI: iodo- or bromobenzene (1 equiv.), PDI (5 mol%), triethylamine (8 equiv.), dimethylformamide (0.02 M of substrate) at 40 °C with irradiation from 465 nm LEDs (5 μW cm⁻²). ¹H NMR yield determined using 1,2,4,5-tetramethylbenzene as internal standard.

The initial test system chosen for investigation was the reduction of iodobenzene, employing PTH as the photocatalyst. After optimization (Tables S1–S3, ESI[†]), quantitative reduction of iodobenzene (**1**) to benzene (98% yield) could be achieved in 1 h under 380 nm LED irradiation (Table 1) in the presence of 5 mol% PTH and 5 equivalents each of tributylamine and formic acid. It is worth noting that although we utilize higher catalyst loadings than traditional metal-based photoredox systems such as Ir(ppy)₃, calculations based on a cost per reaction basis illustrate that 5 mol% PTH is still over an order of magnitude cheaper than using 0.01 mol% of rare-earth derived Ir(ppy)₃ (see ESI[†]). Significantly, the reaction was compatible with a range of solvents as well as amine sources leading to similar yields and reaction rates. Notably, quantitative reduction could also be achieved with catalyst loadings as low as 0.5 mol%, albeit at a slower reaction rate. Full conversion of iodobenzene was also observed using visible light sources, such as 25 W CFLs and blue LEDs (Table S1 and S3, ESI[†]). This demonstrates the inherent flexibility of PTH as a photoredox catalyst platform, which was further enhanced by the use of a commercially available N-Me phenothiazine derivative for the successful reduction of iodobenzene (see ESI[†]).

To validate PTH as an organic photoredox catalyst, a series of control experiments in the absence of light, catalyst, or amine were conducted. In each case, no reaction was observed (Table S2, ESI[†]). We next sought to compare the performance of PTH with widely used photoredox systems such as Ir(ppy)₃, as well as the metal-free PDI based system, and in both cases we observed higher reactivity.²⁰ For example, only 23% yield was obtained after 1 h for the reduction of iodobenzene using Ir(ppy)₃ when compared to the quantitative reduction observed for PTH (Table 1).²¹ It is worth noting that the 380 nm LED light source matches the excitation maximum of Ir(ppy)₃ (378 nm),¹ while the absorption spectrum of PTH has only

a small shoulder at this wavelength (Fig. S2, ESI[†]). However, this does not appear to hinder reactivity. Similarly, comparison of the perylene diimide-based photocatalyst also showed no reduction of iodobenzene after 1 h.

This increased performance encouraged the examination of PTH as a photocatalyst for the reduction of more challenging unactivated brominated substrates, which to date has not been accessible using a metal-free photoredox system. Significantly, bromobenzene was successfully reduced in 85% yield after 72 h (by comparison, no reaction was observed after 72 h using Ir(ppy)₃ or PDI). These results nicely demonstrate that the higher-energy excited state reduction potential of PTH is necessary to activate more challenging C–Br bonds ($E^{\text{red}} = -2.05$ to -2.57).^{22,23}

With a general protocol in place, we next set out to demonstrate the broad applicability of PTH as a photoredox catalyst for a library of aryl iodides and bromides including unactivated, or even deactivated derivatives (Table 2). Excellent activity was observed with compounds containing electron-rich substituents such as **3**, **4**, and **5** being dehalogenated in high yields. Additionally, achieving high fidelity reduction of substrates **4**, **6**, and **7** exemplifies the mildness of our protocol and its tolerance across many different functional groups including acids, phenolic alcohols, and amines. A range of more challenging aryl bromides (**8–18**) were then examined, with near quantitative conversion to the dehalogenated product being observed for substrates **8–11**. Extension to more synthetically interesting heterocyclic aryl bromides was also observed with excellent yields being obtained for brominated pyridine (**13**), benzothiazole (**14**), and thiophene systems (**15–16**). Particularly noteworthy was the application of PTH for the reduction of primary aryl bromides (**17–18**), and even electron-rich aryl bromides like 4-bromophenol (**12**) could be reduced in good yield. The use of one set of conditions for the reduction of both unactivated alkyl and aryl bromides further demonstrates the synthetic versatility of PTH-based organic photoredox catalysts.

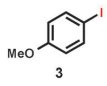
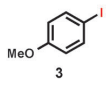
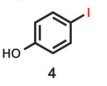
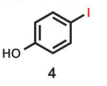
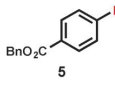
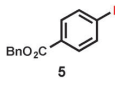
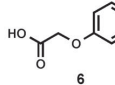
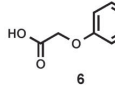
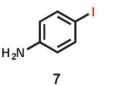
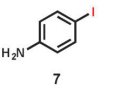
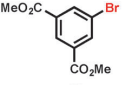
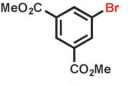
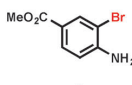
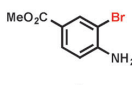
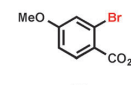
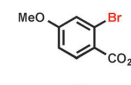
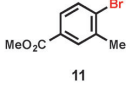
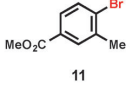
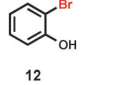
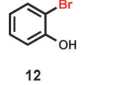
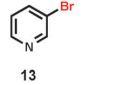
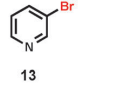
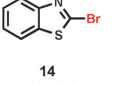
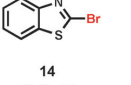
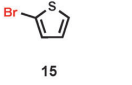
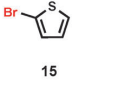
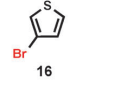
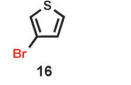
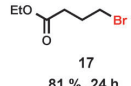
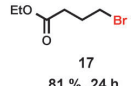
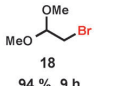
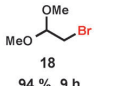
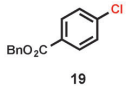
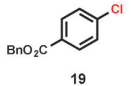
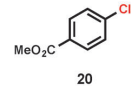
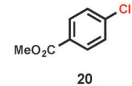
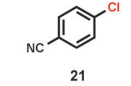
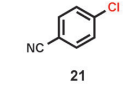
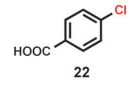
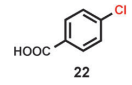
Encouraged by the successful reduction of a wide range of C–Br bonds, we next explored the reduction of activated aryl chlorides. After 24 h of irradiation time in the presence of PTH, benzyl 4-chlorobenzoate was successfully reduced, with the desired product being isolated in 83% yield. A variety of other activated aryl chlorides were subsequently examined with methyl benzoate, benzonitrile, and benzoic acid derivatives undergoing dechlorination in good yields (**20–22**).

With a broad substrate scope and the potential of this metal-free photoredox system established, the physical aspects of PTH were studied in more detail, in particular the high excited state reduction potential, given by:

$$E_{1/2}^* = E_{1/2}^{\text{ox}} - hc/\lambda_{\text{max}}$$

where $E_{1/2}^*$ is the excited state reduction potential, $E_{1/2}^{\text{ox}}$ is the ground state oxidation potential, h is Planck's constant, c is the speed of light and λ_{max} is the photoluminescence maximum.²⁴ While the ground state oxidation potential of PTH ($E_{1/2}^{\text{ox}} = 0.68$ vs. SCE)¹⁹ is only slightly lower than that of Ir(ppy)₃ ($E_{1/2}^{\text{ox}} = 0.77$ vs. SCE), the photoluminescence maximum of PTH ($\lambda_{\text{max}} = 445$ nm, Fig. S3, ESI[†]) is significantly lower (Ir(ppy)₃ $\lambda_{\text{max}} = 500$ nm).¹ In contrast to the triplet emission of Ir(ppy)₃, the higher-energy

Table 2 Substrate scope of reductive dehalogenations of iodides, bromides, and chlorides using PTH^a

R-X	5 mol % PTH NBu ₃ , HCOOH 380 nm light MeCN, rt	R-H
Aryl Iodides		
		
92 %, 5 h (89 %, 24 h)		
		
90 %, 24 h (88 %, 24 h)		
		
95 %, 1.5 h ^b		
		
100 %, 22 h		
		
50 %, 24 h (46 %, 24 h)		
Aryl/Alkyl Bromides		
		
94 %, 24 h ^b		
		
100 %, 49 h		
		
100 %, 48 h (81 %, 48 h)		
		
94 %, 48 h		
		
23 %, 72 h		
		
88 %, 24 h (94 %, 48 h)		
		
89 %, 9 h		
		
92 %, 48 h		
		
91 %, 72 h		
		
81 %, 24 h		
		
94 %, 9 h		
Aryl Chlorides		
		
83 %, 24 h ^b		
		
94 %, 72 h		
		
94 %, 72 h (68 %, 72 h)		
		
62 %, 72 h		

^a Reaction conditions: substrate (1 equiv.), PTH (5 mol%), formic acid (5 equiv.), tributylamine (5 equiv.), acetonitrile (0.08 M of substrate) at RT with irradiation by 380 nm LEDs. ¹H NMR yield determined using 1,3,5-trimethoxybenzene or 1,2,4,5-tetramethylbenzene as internal standard. Yields and times in parentheses were run in the presence of air. ^b Isolated yields run on 0.2 mmol scale.

emission from PTH is the result of fluorescence from the singlet state, with an observed lifetime of < 3 ns (see ESI[†]). To confirm,

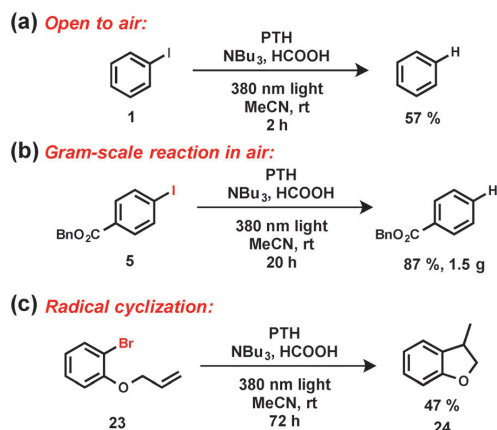
we measured the energy of the triplet excited state of PTH at 77 K, and under these conditions it more closely resembled the energy of Ir(ppy)₃ ($\lambda_{\text{max}} = 510 \text{ nm}$). This implies that the increased excited state energy of the singlet is the primary origin of PTH's ability to access higher energy bonds.

To probe whether the singlet excited state of PTH could be responsible for the catalysis in this system, the reduction of iodobenzene was performed open to air, with oxygen acting as a potent triplet quencher.⁷ Under these conditions, where triplet pathways should be inhibited, a 57% yield was observed after 2 h, suggesting that the singlet state may be the primary mode of catalysis. Further, the reaction proceeded to 90% yield within 15 h with only a moderate decrease in reaction rate being observed. Encouraged by these results, we further examined the oxygen tolerance of PTH with a range of substrates from each aryl halide class. Significantly, a variety of aryl iodides (3–4, 7), bromides (10, 13), and chlorides (21) could be successfully dehalogenated in moderate to good yields (Table 2), confirming the oxygen tolerance of PTH with yields being similar in all cases to those obtained for carefully deoxygenated solutions, suggesting new opportunities previously unavailable with traditional photocatalysis.

After observing reactivity in the presence of air, this phenomenon was further probed by the use of a PTH-based catalyst functionalized with a triplet-sensitizing moiety (Fig. S3, ESI[†]). In this case, conjugation with benzophenone, a well-known triplet sensitizer, was expected to greatly increase the rate of intersystem crossing leading to an exclusive, triplet state excited catalyst, PTH-BP. Photoluminescence spectra were obtained both at room temperature and 77 K with luminescence observed only at 77 K, indicating that fluorescence from the singlet state had been completely deactivated (Fig. S6 and S7, ESI[†]). Moreover, the use of PTH-BP for the reduction of iodobenzene under our optimized conditions resulted in no reaction, suggesting that the singlet state is necessary for catalysis.²⁵

To illustrate the scalability and practical nature of PTH as an organic photoredox catalyst, we then conducted a multigram-scale reaction in the presence of air (Scheme 1). We envisioned a very rudimentary experimental set-up with no precautions taken to ensure an air or moisture-free environment. Using a 125 mL Erlenmeyer flask, we scaled up our general conditions by 7000% using benzyl 4-iodobenzoate as our substrate, and observed 98% conversion by ¹H NMR after 20 h. The reaction was purified by column chromatography to yield the desired product in 87% yield (1.5 g), demonstrating both the scalability and robustness of our protocol. Further, during the course of purification, we were also able to isolate the PTH catalyst used in the reaction. This catalyst sample was then re-used in the reduction of 5, and quantitative conversion to the desired product was observed after 1.5 h, again highlighting the simplicity and inherent robustness of PTH.

Additionally, mechanistic experiments were conducted providing strong evidence of an oxidative-quenching cycle with deuterium studies supporting the primary source of hydrogen atoms being the tributylamine (for in-depth discussion see ESI[†] and Scheme S1). Furthermore, evidence of a radical-based mechanism was obtained *via* a successful radical cyclization of substrate 23 (Scheme 1b). The desired product 24 was obtained in 47% yield, providing strong



Scheme 1 (a) Reaction in the presence of air (triplet quencher) proceeds. (b) Preparative scale reaction conducted without degassing demonstrates modularity and scalability. (c) Cyclization suggests radical mechanism.

support for the reaction proceeding *via* a radical process, as well as preliminary evidence illustrating that generated radical intermediates can be used for carbon–carbon bond forming reactions.

In conclusion, we have developed a highly reducing, organic photocatalytic platform with broad applicability for the generation of carbon-centered radical intermediates on route to efficient dehalogenations of aryl and alkyl iodides, bromide and chlorides. In addition to offering an inexpensive, metal-free alternative to current halide reductions, this approach is highlighted by a robust and facile nature with high yields being obtained even in the presence of air. Moreover, in contrast to classic photoredox systems, preliminary evidence suggests that PTH is primarily operating through the singlet state. Further investigations regarding the mechanism, the tunability of the catalyst, and its potential to open doors for new organic bond forming transformations are currently in progress.

We thank the MRSEC program of the National Science Foundation (DMR 1121053, C.J.H., J.R.A.) and The Dow Chemical Company through the Dow Materials Institute at UCSB (N.J.T., E.H.D., K.M.M., S.O.P., Y.L., C.J.H., J.R.A.) for financial support. N.J.T., E.H.D., and K.M.M. thank the NSF Graduate Research Fellowship for funding and Z.M.H. acknowledges the California

NanoSystems Institute for an Elings Prize Fellowship in Experimental Science.

Notes and references

- (a) C. K. Prier, D. A. Rankic and D. W. C. MacMillan, *Chem. Rev.*, 2013, **113**, 5322–5363; (b) D. M. Schultz and T. P. Yoon, *Science*, 2014, **343**, 1239176; (c) J. M. R. Narayanam and C. R. J. Stephenson, *Chem. Soc. Rev.*, 2010, **40**, 102; (d) D. A. Nicewicz and T. M. Nguyen, *ACS Catal.*, 2014, **4**, 355–360.
- D. A. Nicewicz and D. W. C. Macmillan, *Science*, 2008, **322**, 77–80.
- J. M. R. Narayanam, J. W. Tucker and C. R. J. Stephenson, *J. Am. Chem. Soc.*, 2009, **131**, 8756–8757.
- S. Fukuzumi, K. Hironaka and T. Tanaka, *J. Am. Chem. Soc.*, 1983, **105**, 4722–4727.
- J. D. Nguyen, E. M. D'Amato, J. M. R. Narayanam and C. R. J. Stephenson, *Nat. Chem.*, 2012, **4**, 854–859.
- C. D. McTiernan, S. P. Pitre, H. Ismaili and J. C. Scaiano, *Adv. Synth. Catal.*, 2014, **356**, 2819–2824.
- C. D. McTiernan, S. P. Pitre and J. C. Scaiano, *ACS Catal.*, 2014, **4**, 4034–4039.
- I. Ghosh, T. Ghosh, J. I. Bardagi and B. Konig, *Science*, 2014, **346**, 725–728.
- S. M. Senaweera, A. Singh and J. D. Weaver, *J. Am. Chem. Soc.*, 2014, **136**, 3002–3005.
- G. Revol, T. McCallum, M. Morin, F. Gagosz and L. Barriault, *Angew. Chem., Int. Ed.*, 2013, **52**, 13342–13345.
- P. Knochel, W. Dohle, N. Gommermann, F. F. Kneisel, F. Kopp, T. Korn, I. Sapountzis and V. A. Vu, *Angew. Chem., Int. Ed.*, 2003, **42**, 4302–4320.
- W. F. Bailey and J. J. Patricia, *J. Organomet. Chem.*, 1988, **352**, 1–46.
- W. P. Neumann, *Synthesis*, 1987, 665–683.
- A. Krief and A.-M. Laval, *Chem. Rev.*, 1999, **99**, 745–778.
- K. Miura, Y. Ichinose, K. Nozaki, K. Fugami, K. Oshima and K. Utimoto, *Bull. Chem. Soc. Jpn.*, 1989, **62**, 143–147.
- M. R. Medeiros, L. N. Schacherer, D. A. Spiegel and J. L. Wood, *Org. Lett.*, 2007, **9**, 4427–4429.
- Based on Sigma-Aldrich price on January 21, 2015.
- H. Kim and C. Lee, *Angew. Chem., Int. Ed.*, 2012, **51**, 12303–12306.
- N. J. Treat, H. Sprafke, J. W. Kramer, P. G. Clark, B. E. Barton, J. Read de Alaniz, B. P. Fors and C. J. Hawker, *J. Am. Chem. Soc.*, 2014, **136**, 16096–16101.
- To eliminate any question of difference in catalyst loading causing the increased performance, 5 mol% Ir(ppy)₃ was also tested and gave a slightly lower yield after 1 h (19%).
- J.-B. Xia, C. Zhu and C. Chen, *Chem. Commun.*, 2014, **50**, 11701–11704.
- A. J. Fry and R. L. Krieger, *J. Org. Chem.*, 1976, **41**, 54–57.
- S. Rondinini, P. R. Mussini, P. Muttini and G. Sello, *Electrochim. Acta*, 2001, **46**, 3245–3258.
- J. W. Tucker and C. R. J. Stephenson, *J. Org. Chem.*, 2012, **77**, 1617–1622.
- Although these results in the presence of oxygen support singlet catalysis, a combination of both singlet and triplet states operating under our oxygen free conditions cannot be completely ruled out at this time.

Appendix D

Simple Benchtop Approach to Polymer Brush Nanostructures Using Visible-Light-Mediated Metal-Free Atom Transfer Radical Polymerization

Reprinted with permission from E. H. Discekici, C. W. Pester, N. J. Treat, J. Lawrence, K. M. Mattson, B. Narupai, E. P. Toumayan, Y. Luo, A. J. McGrath, P. G. Clark, J. Read de Alaniz, C. J. Hawker *ACS Macro Lett.* **2016**, *5*, 258–262. © 2016 American Chemical Society.

Simple Benchtop Approach to Polymer Brush Nanostructures Using Visible-Light-Mediated Metal-Free Atom Transfer Radical Polymerization

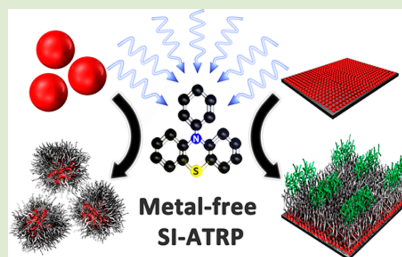
Emre H. Discekici,^{†,‡} Christian W. Pester,[‡] Nicolas J. Treat,^{‡,§} Jimmy Lawrence,[‡] Kaila M. Mattson,^{†,‡} Benjaporn Narupai,^{†,‡} Edward P. Toumayan,^{‡,⊥} Yingdong Luo,^{†,‡} Alaina J. McGrath,[‡] Paul G. Clark,^{||} Javier Read de Alaniz,^{*,†,‡} and Craig J. Hawker^{*,†,‡,§}

[†]Department of Chemistry and Biochemistry, [‡]Materials Research Laboratory, [§]Materials Department, and [⊥]Department of Chemical Engineering, University of California, Santa Barbara, California 93106, United States

^{||}The Dow Chemical Company, Midland, Michigan 48674, United States

Supporting Information

ABSTRACT: The development of an operationally simple, metal-free surface-initiated atom transfer radical polymerization (SI-ATRP) based on visible-light mediation is reported. The facile nature of this process enables the fabrication of well-defined polymer brushes from flat and curved surfaces using a “benchtop” setup that can be easily scaled to four-inch wafers. This circumvents the requirement of stringent air-free environments (i.e., glovebox), and mediation by visible light allows for spatial control on the micron scale, with complex three-dimensional patterns achieved in a single step. This robust approach leads to unprecedented access to brush architectures for nonexperts.



Surface-initiated polymerizations are a powerful and widely utilized approach to the preparation of robust and functional polymer surfaces.¹ Significant advances in this area have been enabled by the development of controlled radical polymerization strategies, including nitroxide-mediated polymerization (NMP),² reversible addition–fragmentation chain transfer polymerization (RAFT),³ and atom transfer radical polymerization (ATRP).⁴ These methods allow a wide variety of brush structures with controllable thickness and composition, including block copolymer structures, to be prepared.⁵ Access to these diverse architectures has led to numerous applications in areas such as antifouling coatings,^{6–8} drug delivery,⁷ stimuli-responsive materials,⁹ and nanoporous membranes.¹⁰

Until recently, the fabrication of patterned polymer brushes has required advanced techniques such as electron-beam lithography,^{11,12} interference lithography,¹³ and microcontact printing^{14–16} to spatially localize initiating species. Recently, methods such as surface-initiated electrochemical ATRP (eATRP)^{17–20} have been reported by several groups as versatile alternatives to traditional surface patterning procedures. While these techniques offer notable improvements in the field, they also pose certain challenges, including delayed response time for complete deactivation, requirement for copper-based catalysts, and the lack of easy access to arbitrarily patterned surfaces.²¹

In addressing these challenges, our group reported a light-mediated ATRP process using an Ir-based photoredox catalyst^{22–24} to spatially and temporally control polymer

brush synthesis from uniformly functionalized initiating layers.²⁵ The key to the success of this method is the use of light as a mild, noninvasive stimulus for selective polymer growth, allowing access to three-dimensional nanostructures in a single step. While this process provides a significant advancement in patterned polymer brush fabrication, the need for a metal catalyst remains problematic for a number of applications in areas such as microelectronics and bioinspired materials.^{26,27} Heavy metal-based marine antifouling coatings serve as a prime example, as bioaccumulation of released metal ions in the environment is known to harm wildlife.^{28,29} As a result, significant effort has been exerted to develop systems with decreased catalyst loadings^{30–32} as well as improved postprocess purification of trace metals.^{33–35} Additionally, the very high cost of Ir(ppy)₃ (\$1080/g) coupled with rigorous deoxygenation procedures (multiple freeze–pump–thaw steps) make implementation on a large scale impractical and therefore greatly hinder their development and application.³⁶

Drawing inspiration from recent developments in photocontrolled living radical polymerizations,³⁷ such as phenothiazine-based metal-free ATRP,³⁸ and its observed oxygen tolerance in small molecule dehalogenations,³⁹ we sought to develop a metal-free, benchtop system for the preparation of surface-tethered polymer brushes (Figure 1). This straightfor-

Received: January 4, 2016

Accepted: January 29, 2016

Published: February 2, 2016

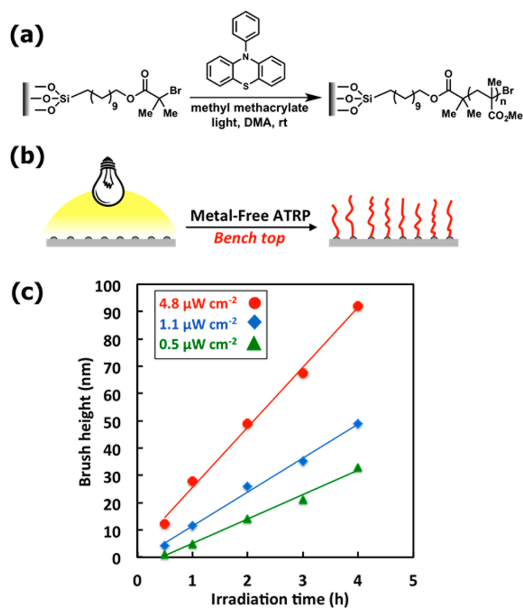


Figure 1. (a) Chemical scheme and conditions for metal-free ATRP using α -bromoisobutyrate-based initiator-functionalized silicon substrates. (b) Illustration of surface-initiated, metal-free ATRP (c) Plot of brush height as a function of irradiation time using varied light intensities in the benchtop chamber.

ward procedure involves the use of a modified Petri dish with a covering glass slide, allowing for top-down irradiation of surfaces (see SI, Figure S2). Well-defined single-layer patterns, gradient structures, and block copolymer architectures are readily available using traditional binary and/or grayscale photomasks. The use of irradiation from commercially available light sources, including compact fluorescent lamps (CFLs) and even natural sunlight, further simplifies this process.

To understand the potential of this method, kinetic experiments were conducted to track the relationship between brush height and irradiation time. Using silicon substrates uniformly functionalized with α -bromoisobutyrate-based initiators (Figure 1a), a series of polymerizations to prepare poly(methyl methacrylate) (PMMA) brushes were performed using irradiation with visible light ($\lambda = 405$ nm) at a range of intensities for varied lengths of time (Figure 1c). After thorough washing, thicknesses were measured using optical reflectometry, and a linear relationship between brush height and irradiation time was observed for each of the intensities investigated. As a control, an analogous series of experiments using 1.1 $\mu\text{W/cm}^2$ intensity light were performed in an inert glovebox environment, yielding comparable results to the benchtop system (see SI, Figure S4).

After observing a linear increase in brush height, the ability of phenothiazine-mediated SI-ATRP to grow diblock copolymers was explored. Thus, a uniform PMMA brush was first prepared under optimized conditions and measured to be 30 nm. Following this, a diblock copolymer was synthesized via chain extension with 2,2,2-trifluoroethyl methacrylate (TFEMA) (Figure 2). Optical reflectometry measurements indicated an increase in overall brush thickness of approximately 26 nm, suggesting retention of active chain ends. Moreover, character-

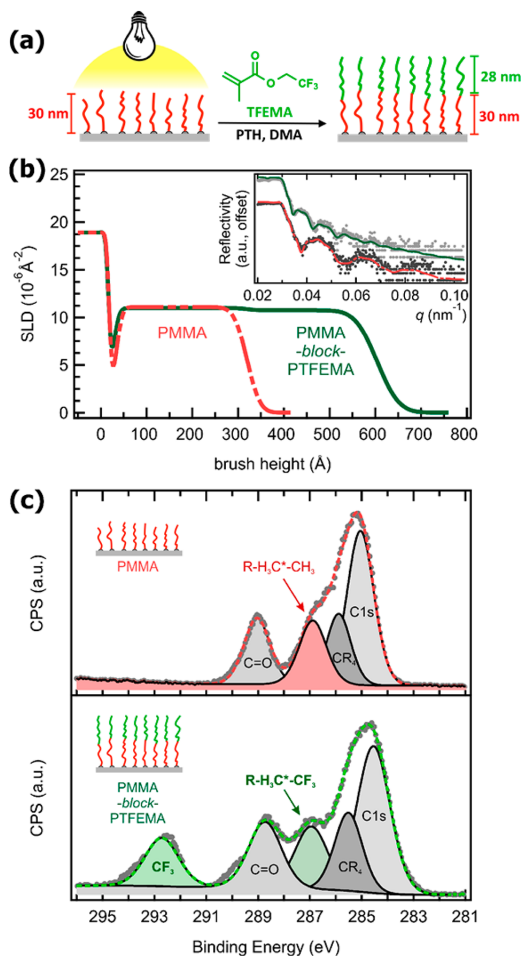


Figure 2. (a) Metal-free SI-ATRP preparation of uniform diblock copolymers via chain extension of PMMA, with brush heights measured by optical reflectometry. (b) X-ray reflectivity (XRR) data illustrate an increase in film thickness from the initial block. Raw data and fitting are shown in the inset. (c) X-ray photoelectron spectroscopy (XPS) plots show the emergence of characteristic signals of covalently bound fluorine found in the PTFEMA block.

ization by X-ray reflectivity (XRR) revealed a collapse of refractive fringes (Figure 2b, inset) corresponding to thicknesses that match those obtained by optical reflectometry. Scattering length densities (Figure 2b) were fitted via a three- and four-layer model for the PMMA homopolymer and diblock copolymer brushes, respectively, further confirming the increase in brush thickness after block copolymer formation. Additional characterization by X-ray photoelectron spectroscopy (XPS) reaffirmed diblock copolymer composition, with the emergence of a fluorine–CF₃ peak at 292.72 eV (Figure 2c). These results suggest that chain extension is achievable when performing benchtop ATRP with *N*-phenyl phenothiazine as the catalyst.

A profound advantage of light-mediated surface polymerization is the ability to exert direct spatial control over brush growth using readily available photomasks with arbitrary patterns.⁴⁰ Using the benchtop setup, a binary photomask

containing discrete line features with spacings down to $2\ \mu\text{m}$ (Figure 3b), as well as various polygonal structures down to $1\ \mu\text{m}$

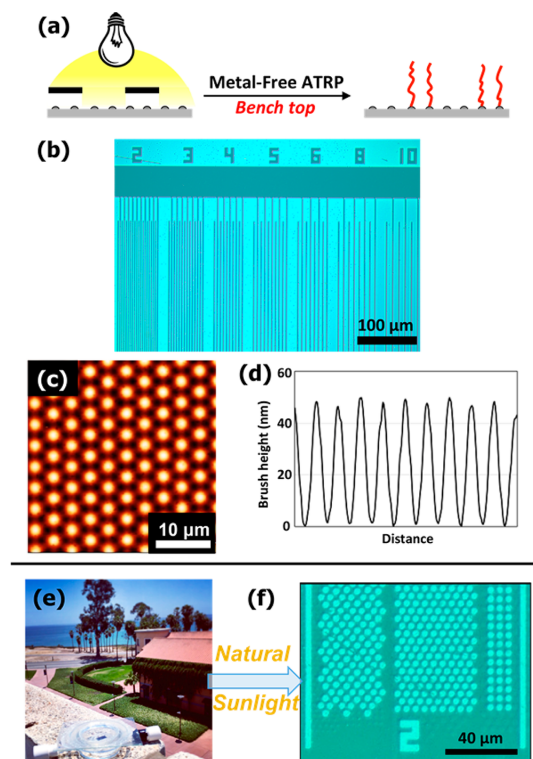


Figure 3. (a) Binary photomasks enable one-step patterning. (b) Optical micrograph of micron-scale line features ($2\text{--}10\ \mu\text{m}$). (c) AFM image of $1\ \mu\text{m}$ features and (d) corresponding AFM height profile. (e) Polymerization using sunlight and (f) optical micrograph of patterned $2\ \mu\text{m}$ features (see SI for setup).

μm , was placed over a silicon substrate and irradiated using optimized conditions. After 3 h, well-defined patterning was observed by optical microscopy. Characterization by AFM revealed highly uniform patterning for $1\ \mu\text{m}$ features (Figure 3c and d). Experiments were then conducted using a grayscale photomask to demonstrate the facile production of complex gradient structures (see SI, Figure S6). A well-defined gradient was observed, exemplifying the ability of metal-free SI-ATRP to prepare arbitrary patterns on surfaces.

In order to further highlight the capabilities of the benchtop setup, a polymerization was then conducted under natural sunlight. With no additional precautions, the reaction was performed by placing the apparatus in direct sunlight for 4 h, and after thorough washing, well-defined patterns were observed (Figure 3e and f). This offers a significant advantage over previous light-mediated systems, which were limited to the glovebox, and further demonstrates the modularity and ease of phenothiazine-mediated, metal-free SI-ATRP.

As an additional example of modularity, we investigated the application of this methodology to a larger-scale surface (i.e., four-inch diameter silicon wafer). This use is of particular interest as there are few reports of using SI-ATRP for polymer brush synthesis on large-scale wafers.⁴¹ When reported, these

methods do not allow for well-defined spatial control. Using the benchtop chamber, an initiator-functionalized four-inch wafer was patterned using a binary photomask with irradiation from a commercially available compact fluorescent lamp (see SI, Figure S9). Arbitrary micron-scale patterns, as well as millimeter-scale patterns were all obtained in a single step (Figure 4), reaffirming the potential of metal-free SI-ATRP for large-scale wafer applications.

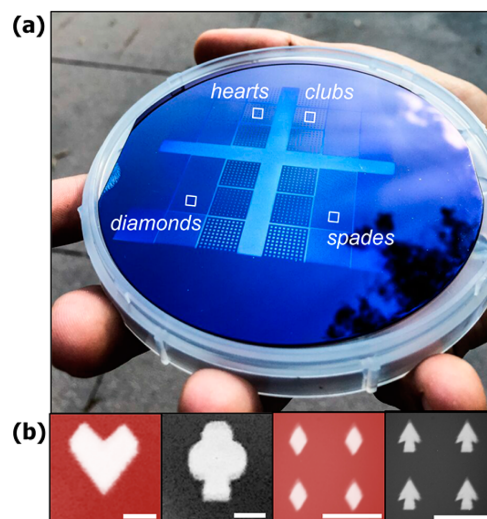


Figure 4. (a) Photograph of large area patterning in a single step of a four-inch wafer using a binary photomask. (b) Optical micrographs of patterned arbitrary features. Scale bars are $200\ \mu\text{m}$.

For patterning diblock copolymer architectures, the ability to achieve selective initiation from existing homopolymer brushes is particularly powerful as it enables the fabrication of diverse, spatially defined structures. Much like the experiments used to obtain uniform diblocks, analogous experiments were conducted using a binary photomask containing various micron-scale features. First, a uniform homopolymer layer of 38 nm was prepared using 2-(methylthio)ethyl methacrylate (MTEMA) as the monomer. After washing, a subsequent chain extension experiment was conducted using TFEMA with irradiation through a binary photomask to achieve high-fidelity PMTEMA-*b*-PTFEMA diblock copolymer patterns (Figure 5). In addition to characterization by optical microscopy, dynamic secondary ion mass spectrometry (SIMS) was implemented to chemically map the patterned brush surface. Indeed when the ^{19}F signal was scanned, a micron-scale pattern of the PTFEMA layer can be clearly observed. Moreover, an inverse pattern is obtained when scanning for the ^{32}S signal found in the starting PMTEMA brush (^{19}F -containing layer masks the underlying ^{32}S signal). As a ^{12}C reference scan of the entire brush region shows a continuous brush layer, the patterning must be due to the presence of domains of fluorinated blocks on an underlying brush layer as depicted graphically in Figure 5a (see also SI, Figure S10). Furthermore, analogous SIMS results were obtained for patterned PMMA-*b*-PTFEMA copolymer brushes (see SI, Figure S11), demonstrating that efficient patterning occurs for a number of polymer systems. These data thoroughly

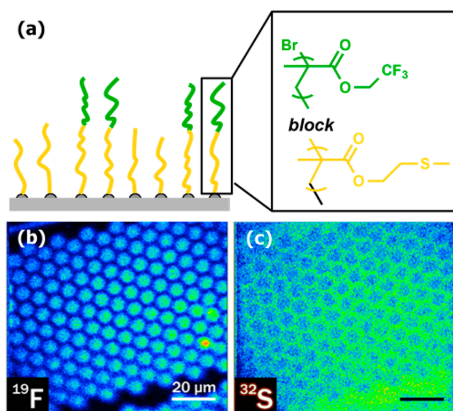


Figure 5. (a) Schematic of PMTEMA-*b*-PTFEMA patterned surfaces. (b) Dynamic secondary ion mass spectroscopy (SIMS) image of patterned fluorine signal from PTFEMA. (c) SIMS image of patterned sulfur signal from PMTEMA.

support the ability to achieve high fidelity spatially controlled reinitiation of chain ends with metal-free SI-ATRP.

Encouraged by the results obtained on silicon wafers, it was next sought to extend metal-free SI-ATRP to curved surfaces, such as silica nanoparticles. The field of surface modification of nanoparticles with polymer brushes has seen growing interest due to the resulting properties of well-defined core-shell architectures, with applications in optics, magnetics, electronics, and drug delivery.^{7,42} We envisioned potentially furthering the scope of these applications by taking advantage of a metal-free approach to these materials, as well as offering a system that would not require tedious purification steps.

To illustrate the versatility of this approach and the ability to grow brushes from particle surfaces in solution, commercially available silica nanoparticles were functionalized with α -bromoisobutyrate-based ATRP initiators. The nanoparticles were subsequently subjected to light-mediated, solution-based conditions in the presence of *N*-phenyl phenothiazine as catalyst (see SI). After 4 h of irradiation, the particles were purified via rigorous washing and centrifugation steps. Next, attenuated total reflectance-Fourier transform infrared (ATR-FTIR) spectroscopy was used to analyze and compare the PMMA-functionalized particles to the bare and initiator bound particles. The results for the SiO₂-PMMA nanoparticles showed the emergence of a peak at 1725 cm⁻¹, representative of carbonyl groups present in the PMMA backbone (Figure 6a). Moreover, transmission electron microscopy (TEM) was used to image the dried SiO₂ nanoparticles, and a clear PMMA shell was observed (Figure 6c,d), the thickness of which correlates with the mass loss obtained by TGA (see SI). Thermogravimetric analysis (TGA) of the polymer-grafted nanoparticles compared to the bare and initiator-functionalized nanoparticles clearly showed a greater weight loss for the PMMA-functionalized nanoparticles (see SI, Figure S12). Subsequent analysis of cleaved polymers by ¹H NMR and gel permeation chromatography (GPC) also further supported the presence of PMMA (see SI, Figure S13). These results are promising preliminary evidence showing the versatility of visible-light-mediated SI-ATRP for the synthesis of polymer brushes across a wide range of surfaces and reaction conditions.

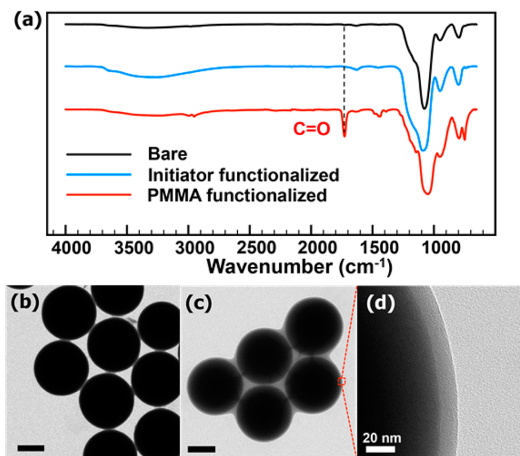


Figure 6. (a) ATR-FTIR showing the emergence of the carbonyl signal at 1725 cm⁻¹ for PMMA-functionalized SiO₂ nanoparticles versus bare and initiator-functionalized particles. (b) TEM of bare SiO₂ nanoparticles. (c) TEM image of PMMA-functionalized core-shell SiO₂ nanoparticles. (d) Magnification of PMMA-functionalized SiO₂ nanoparticles (scale bars are 200 nm unless otherwise noted).

In conclusion, a robust and versatile benchtop method for the fabrication of surface-tethered polymer brushes using light-mediated, metal-free ATRP on both wafers and nanoparticles has been demonstrated. Utilizing an inexpensive organic phenothiazine-based photocatalyst in combination with a simplified benchtop reaction chamber and readily available visible-light sources, spatially controlled brush growth was demonstrated, even on large 4 in. wafer surfaces. Investigation of monomer scope and extension of synthetic versatility of this system for the preparation of increasingly complex functional materials on a wide array of surfaces are currently underway.

■ ASSOCIATED CONTENT

Supporting Information

The Supporting Information is available free of charge on the ACS Publications website at DOI: 10.1021/acsmacrolett.6b00004.

General reagent information, general analytical information, light sources, synthesis of 10-phenylphenothiazine, synthesis of uniformly functionalized alkyl bromide silicon surfaces, attachment of alkyl bromide initiator to surface, catalyst loading experiments, irradiation time vs brush height experiments, irradiation time vs brush height experiments, and additional experimental details (PDF)

■ AUTHOR INFORMATION

Corresponding Authors

*E-mail: hawker@mrl.ucsb.edu.

*E-mail: javier@chem.ucsb.edu.

Notes

The authors declare no competing financial interest.

■ ACKNOWLEDGMENTS

We thank the MRSEC program of the National Science Foundation (DMR 1121053, C.J.H., J.R.A.) and The Dow

Chemical Company through the Dow Materials Institute at UCSB (E.H.D., N.J.T., C.W.P., B.N., K.M.M., E.T., J.L., Y.L., A.J.M., C.J.H., J.R.A.) for financial support. E.H.D., N.J.T. and K.M.M. thank the NSF Graduate Research Fellowship, and C.W.P. acknowledges the Alexander von Humboldt Foundation for financial support. K.M.M., B.N., and C.J.H. also acknowledge the PREM program of the National Science Foundation (DMR-1205194) for support. We sincerely thank Richard Bock for the fabrication of the benchtop chamber, David Bothman and Lee Sawyer for photomask fabrication, Thomas Mates for SIMS imaging, and Amanda Strom and Rachel Behrens for help with polymer characterization.

REFERENCES

- (1) Barbey, R.; Lavanant, L.; Paripovic, D.; Schüwer, N.; Sugnaux, C.; Tugulu, S.; Klok, H.-A. *Chem. Rev.* **2009**, *109*, 5437–5527.
- (2) (a) Husseman, M.; Malmström, E. E.; McNamara, M.; Mate, M.; Mecerreyes, D.; Benoit, D. G.; Hedrick, J. L.; Mansky, P.; Huang, E.; Russell, T. P.; Hawker, C. J. *Macromolecules* **1999**, *32*, 1424–1431. (b) Devonport, W.; Michalak, L.; Malmstrom, E.; Mate, M.; Kurdi, B.; Hawker, C. J.; Barclay, G. G.; Sinta, R. *Macromolecules* **1997**, *30*, 1929–1934.
- (3) Baum, M.; Brittain, W. J. *Macromolecules* **2002**, *35*, 610–615.
- (4) Pyun, J.; Jia, S.; Kowalewski, T.; Patterson, G. D.; Matyjaszewski, K. *Macromolecules* **2003**, *36*, 5094–5104.
- (5) Matyjaszewski, K.; Miller, P. J.; Shukla, N.; Immaraporn, B.; Gelman, A.; Luokala, B. B.; Siclovan, T. M.; Kickelbick, G.; Vallant, T.; Hoffmann, H.; Pakula, T. *Macromolecules* **1999**, *32*, 8716–8724.
- (6) Dalsin, J. L.; Hu, B.-H.; Lee, B. P.; Messersmith, P. B. *J. Am. Chem. Soc.* **2003**, *125*, 4253–4258.
- (7) Krishnamoorthy, M.; Hakobyan, S.; Ramstedt, M.; Gautrot, J. E. *Chem. Rev.* **2014**, *114*, 10976–11026.
- (8) Sun, G.; Cho, S.; Yang, F.; He, X.; Pavia-Sanders, A.; Clark, C.; Raymond, J. E.; Verkhoturov, S. V.; Schweikert, E. A.; Thackeray, J. W.; Trefonas, P.; Wooley, K. L. *J. Polym. Sci., Part A: Polym. Chem.* **2015**, *53*, 193–199.
- (9) Stuart, M. A. C.; Huck, W. T. S.; Genzer, J.; Müller, M.; Ober, C.; Stamm, M.; Sukhorukov, G. B.; Szleifer, I.; Tsukruk, V. V.; Urban, M.; Winnik, F.; Zauscher, S.; Luzinov, I.; Minko, S. *Nat. Mater.* **2010**, *9*, 101–113.
- (10) Sun, L.; Baker, G. L.; Bruening, M. L. *Macromolecules* **2005**, *38*, 2307–2314.
- (11) Ballav, N.; Schilp, S.; Zharnikov, M. *Angew. Chem., Int. Ed.* **2008**, *47*, 1421–1424.
- (12) Khan, M. N.; Tjong, V.; Chilkoti, A.; Zharnikov, M. *Angew. Chem., Int. Ed.* **2012**, *51*, 10303–10306.
- (13) Schuh, C.; Santer, S.; Prucker, O.; Ruhe, J. R. *Adv. Mater.* **2009**, *21*, 4706–4710.
- (14) Zhou, F.; Zheng, Z.; Yu, B.; Liu, W.; Huck, W. T. S. *J. Am. Chem. Soc.* **2006**, *128*, 16253–16258.
- (15) Azzaroni, O.; Moya, S. E.; Brown, A. A.; Zheng, Z.; Donath, E.; Huck, W. T. S. *Adv. Funct. Mater.* **2006**, *16*, 1037–1042.
- (16) Li, B.; Yu, B.; Ye, Q.; Zhou, F. *Acc. Chem. Res.* **2015**, *48*, 229–237.
- (17) Li, B.; Yu, B.; Huck, W. T. S.; Zhou, F.; Liu, W. *Angew. Chem., Int. Ed.* **2012**, *51*, 5092–5095.
- (18) Shida, N.; Koizumi, Y.; Nishiyama, H.; Tomita, I.; Inagi, S. *Angew. Chem., Int. Ed.* **2015**, *54*, 3922–3926.
- (19) Yan, J.; Li, B.; Yu, B.; Huck, W. T. S.; Liu, W.; Zhou, F. *Angew. Chem., Int. Ed.* **2013**, *52*, 9125–9129.
- (20) Li, B.; Yu, B.; Huck, W. T. S.; Liu, F. W.; Zhou, F. *J. Am. Chem. Soc.* **2013**, *135*, 1708–1710.
- (21) (a) Leibfarth, F. A.; Mattson, K. M.; Fors, B. P.; Collins, H. A.; Hawker, C. J. *Angew. Chem., Int. Ed.* **2013**, *52*, 199–210. (b) Hadadpour, M.; Ragogna, P. J. *J. Polym. Sci., Part A: Polym. Chem.* **2015**, *53*, 2747–2754.
- (22) (a) Fors, B. P.; Hawker, C. J. *Angew. Chem., Int. Ed.* **2012**, *51*, 8850–8853. (b) Treat, N. J.; Fors, B. P.; Kramer, J. W.; Christianson, M.; Chiu, C.-Y.; Alaniz, J. R. de; Hawker, C. J. *ACS Macro Lett.* **2014**, *3*, 580–584.
- (23) Yamago, S.; Nakamura, Y. *Polymer* **2013**, *54*, 981–994.
- (24) Pester, C. W.; Poelma, J. E.; Narupai, B.; Patel, S. N.; Su, G. M.; Mates, T. E.; Luo, Y.; Ober, C. K.; Hawker, C. J.; Kramer, E. J. *J. Polym. Sci., Part A: Polym. Chem.* **2016**, *54*, 253–262.
- (25) Poelma, J. E.; Fors, B. P.; Meyers, G. F.; Kramer, J. W.; Hawker, C. J. *Angew. Chem., Int. Ed.* **2013**, *52*, 6844–6848.
- (26) Ouchi, M.; Terashima, T.; Sawamoto, M. *Chem. Rev.* **2009**, *109*, 4963–5050.
- (27) Matyjaszewski, K.; Tsarevsky, N. V. *J. Am. Chem. Soc.* **2014**, *136*, 6513–6533.
- (28) Yang, W. J.; Neoh, K.-G.; Kang, E.-T.; Teo, S. L.-M.; Rittschof, D. *Prog. Polym. Sci.* **2014**, *39*, 1017–1042.
- (29) Chambers, L. D.; Stokes, K. R.; Walsh, F. C.; Wood, R. J. K. *Surf. Coat. Technol.* **2006**, *201*, 3642–3652.
- (30) Kwak, Y.; Magenau, A. J. D.; Matyjaszewski, K. *Macromolecules* **2011**, *44*, 811–819.
- (31) Gnanou, Y.; Hizal, G. *J. Polym. Sci., Part A: Polym. Chem.* **2004**, *42*, 351–359.
- (32) Magenau, A. J. D.; Strandwitz, N. C.; Gennaro, A.; Matyjaszewski, K. *Science* **2011**, *332*, 81–84.
- (33) Shen, Y.; Zhu, S. *Macromolecules* **2001**, *34*, 8603–8609.
- (34) Munirasu, S.; Aggarwal, R.; Baskaran, D. *Chem. Commun.* **2009**, *30*, 4518–3.
- (35) Matyjaszewski, K.; Pintauer, T.; Gaynor, S. *Macromolecules* **2000**, *33*, 1476–1478.
- (36) Azzaroni, O. *J. Polym. Sci., Part A: Polym. Chem.* **2012**, *50*, 3225–3258.
- (37) Ohtsuki, A.; Lei, L.; Tanishima, M.; Goto, A.; Kaji, H. *J. Am. Chem. Soc.* **2015**, *137*, 5610–5617.
- (38) (a) Treat, N. J.; Sprafke, H.; Kramer, J. W.; Clark, P. G.; Barton, B. E.; Read de Alaniz, J.; Fors, B. P.; Hawker, C. J. *J. Am. Chem. Soc.* **2014**, *136*, 16096–16101. (b) Pan, X.; Lamson, M.; Yan, J.; Matyjaszewski, K. *ACS Macro Lett.* **2015**, *4*, 192–196.
- (39) Discekici, E. H.; Treat, N. J.; Poelma, S. O.; Mattson, K. M.; Hudson, Z. M.; Luo, Y.; Hawker, C. J.; de Alaniz, J. R. *Chem. Commun.* **2015**, *51*, 11705.
- (40) Chen, T.; Amin, I.; Jordan, R. *Chem. Soc. Rev.* **2012**, *41*, 3280.
- (41) Zhang, T.; Du, T.; Kalbakova, J.; Schubel, R.; Rodrigues, R. D.; Chen, T.; Zahn, D.; Jordan, R. *Polym. Chem.* **2015**, *6*, 8176–8183.
- (42) Wu, L.; Glebe, U.; Böker, A. *Polym. Chem.* **2015**, *6*, 5143–5184.

Appendix E

Chemoselective Radical

Dehalogenation and C–C Bond

Formation on Aryl Halide Substrates

Using Organic Photoredox Catalysts

Reprinted with permission from S. O. Poelma, G. L. Burnett, E. H. Discekici, K. M. Mattson, N. J. Treat, Y. Luo, Z. H. Hudson, S. L. Shankel, P. G. Clark, J. W. Kramer, C. J. Hawker, J. Read de Alaniz, *J. Org. Chem.* **2016**, *81*, 7155–7160. © 2016 American Chemical Society.

Chemoselective Radical Dehalogenation and C–C Bond Formation on Aryl Halide Substrates Using Organic Photoredox Catalysts

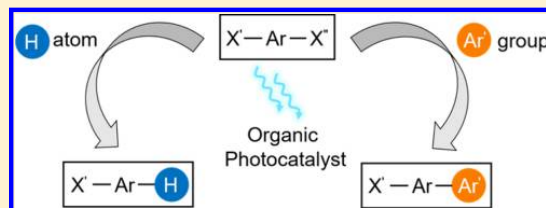
Saemi O. Poelma,[†] G. Leslie Burnett,[†] Emre H. Discekici,[†] Kaila M. Mattson,[†] Nicolas J. Treat,[‡] Yingdong Luo,[†] Zachary M. Hudson,[‡] Shelby L. Shankel,[†] Paul G. Clark,[§] John W. Kramer,[§] Craig J. Hawker,^{*,†,‡} and Javier Read de Alaniz^{*,†}

[†]Department of Chemistry and Biochemistry and [‡]Materials Department, Materials Research Laboratory, University of California, Santa Barbara, California 93106, United States

[§]The Dow Chemical Company, Midland, Michigan 48674, United States

Supporting Information

ABSTRACT: Despite the number of methods available for dehalogenation and carbon–carbon bond formation using aryl halides, strategies that provide chemoselectivity for systems bearing multiple carbon–halogen bonds are still needed. Herein, we report the ability to tune the reduction potential of metal-free phenothiazine-based photoredox catalysts and demonstrate the application of these catalysts for chemoselective carbon–halogen bond activation to achieve C–C cross-coupling reactions as well as reductive dehalogenations. This procedure works both for conjugated polyhalides as well as unconjugated substrates. We further illustrate the usefulness of this protocol by intramolecular cyclization of a pyrrole substrate, an advanced building block for a family of natural products known to exhibit biological activity.



INTRODUCTION

Reductive dehalogenation and carbon–carbon (C–C) cross-coupling reactions with aryl halides are widely utilized in the synthetic organic community as they facilitate the construction of a range of valuable products. Standard methods in this field utilize metal catalysts, which present certain inherent limitations such as high cost or toxicity (e.g., catalytic Pd, Ni, and Rh or stoichiometric Bu_3SnH and SmI_2), as well as harsh and toxic reaction conditions (e.g., pressurized H_2 , N_2H_4 , and HSiR_3 as reductants).^{1–3} For these challenges to be addressed, recent developments employing mild, photochemical-based procedures have been reported with many photocatalysts being rare earth metal based.^{4,5} To avoid the use of expensive metal catalysts, there has been a concerted effort toward implementing organic photocatalysts, including perylene diimide (PDI)⁶ and eosin Y.⁷

These photoredox-based reductions proceed via a carbon-centered radical intermediate that is subsequently trapped using a H atom source or, in many cases, a radical trapping species to form C–C bonds.⁸ This includes aryl–aryl bond formations as well as radical cyclizations and atom transfer radical additions.^{6,9–12} Such a versatile transformation warrants the development of photocatalytic systems that can chemoselectively activate carbon–halogen bonds (C–X), giving potential for taking a single synthetic derivative bearing multiple C–X bonds and synthesizing a large library of complex targets. Currently, there are very few reports demonstrating the concept of chemoselective dehalogenations,

and these are limited to metal-based nonphotocatalyzed systems.^{13–16}

Our group recently reported the use of 10-phenylphenothiazine (PTH, **1**) for photomediated, controlled radical polymerizations and radical dehalogenation of aryl and alkyl halides (Figure 1).^{17–19} PTH was found to be a highly reducing organic photocatalyst ($E_{1/2}^* = -2.1$ V vs SCE) with the ability to access a variety of unactivated carbon–halogen bonds that were inaccessible with previous metal-free systems.¹⁹ This

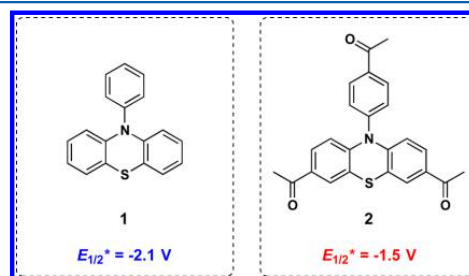


Figure 1. Structure and reduction potential of PTH (**1**) and tris-acetyl-PTH (**2**).

Special Issue: Photocatalysis

Received: May 3, 2016

Published: June 8, 2016

initial work demonstrated that catalyst **1** can be used for dehalogenations, is tolerant of oxygen, and can be synthesized in a single step from commercially available materials. Herein, we apply this metal-free photoredox strategy to the chemoselective activation of aryl groups bearing multiple carbon–halogen bonds through catalyst design, specifically tuning the reduction potential of the PTH scaffold. This approach can be applied to selective dehalogenation as well as selective C–C bond formation (Figure 2).

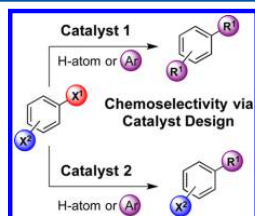


Figure 2. Representative scheme of (a) chemoselective dehalogenation and (b) chemoselective C–C bond formation on a polyhalogenated substrate using an organic photoredox catalyst (X = halides, Ar = aryl group, R = H atom or aryl group).

RESULTS AND DISCUSSION

In developing a catalyst to enable chemoselective reactivity, we hypothesized that incorporating electronically deficient groups on the PTH scaffold could lower the excited state reduction potential of catalyst **1**. Thus, a tris-acetyl-PTH catalyst (**2**) substituted with electron-withdrawing groups on each aryl ring para to the nitrogen was synthesized by subjecting **1** to a Friedel–Crafts acylation with AlCl_3 in acetic anhydride. This slight structural modification was found to have a significant influence on the excited state reduction potential ($E_{1/2}^* = -1.5$ V vs SCE, see Figure 1) as compared to the originally employed photocatalyst. Furthermore, although visible light was not employed in this study, catalyst **2** was found to absorb well into the visible regime, giving the opportunity to use more mild sources of irradiation while still reducing unactivated substrates.

After observing such a large difference in catalyst reduction potential, we next sought to understand whether or not these

values translated into actual changes in reactivity. Thus, a representative aryl iodide (**S1**), bromide (**3**), and chloride (**5**) were chosen as test candidates for dehalogenations using our previously optimized conditions, and reaction progress was monitored using ^1H NMR.¹⁹ First, iodobenzene was combined with tributylamine, formic acid, and catalyst **1**, and within 1 h, near complete conversion of the starting material to the dehalogenated product was observed (see Figure S1). In contrast, when catalyst **2** was used under the same reaction conditions, little to no reaction was observed after 1 h. However, at 72 h, both catalysts quantitatively reduced the substrate, which was an encouraging initial result as it suggested differing rates of reactivity. Next, 3-bromopyridine (**3**) was examined, and a similar behavior occurred with the rate of debromination using **1** being significantly faster (4 h, 78%) than when **2** was used (4 h, 14%) (Figure 3a). Again, quantitative conversion of the substrate to the desired product could be achieved using both catalysts with prolonged reaction times (see Figure S2). Next, a more challenging substrate bearing a C–Cl bond with an activating ester group was examined (Figure 3b). In this case, **1** led to quantitative dechlorination within 24 h, but the use of **2** was noticeably slower, reaching only 6% yield within the same time frame and still exhibiting low conversion after 72 h (21%) (see Figure S2). Importantly, these results are within expectations for the relative reduction potentials of the catalysts, as iodides and bromides are known to have lower reduction potentials than chlorides.²⁰ Encouraged by these results, it was hypothesized that these different reaction rates would lead to selective dehalogenation on substrates with multiple carbon–halogen bonds.

To test chemoselective dehalogenation mediated by **2**, we first examined benzene derivative **7**, which is substituted with four different halogens: iodide, bromide, chloride, and fluoride. The optimized reaction conditions for reductive dehalogenation from the previously reported study were used.¹⁹ After 5 h of irradiation in the presence of **2**, selective deiodination led to **8**, which was obtained in 96% yield with only 4% of deiodinated and debrominated product **9** being formed (Figure 4a). In contrast, when catalyst **1** was used, no selectivity for the formation of **8** and **9** was observed (41 and 59% yield, respectively) within the same 5 h time frame. However, after 48 h, the use of **1** as photocatalyst afforded **9** in 90% yield,

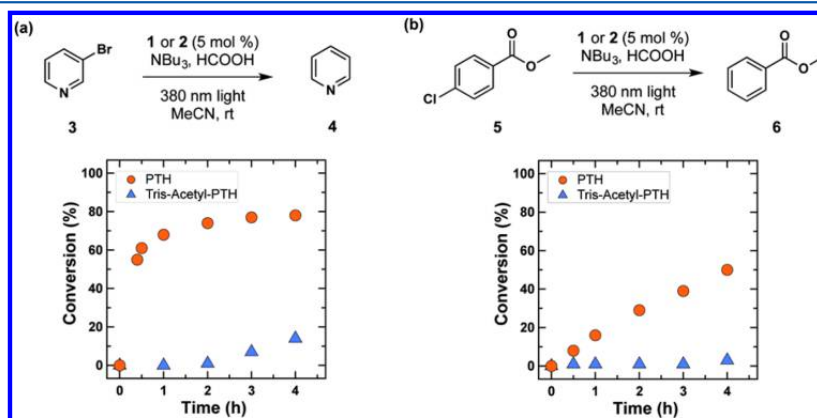


Figure 3. Rate of dehalogenation of (a) 3-bromopyridine (**3**) and (b) methyl 4-chlorobenzoate (**5**) mediated by **1** and **2** for the first 4 h of reaction. ^1H NMR yield determined using 1,2,4,5-tetramethylbenzene as an internal standard.

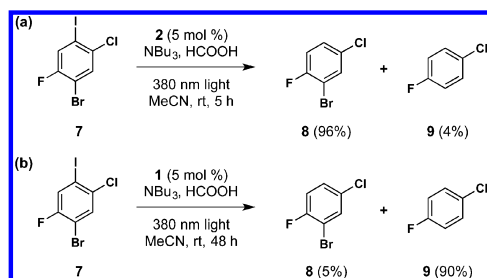


Figure 4. Chemoselective dehalogenation of **7** to its deiodinated product **8** and deiodinated and debrominated product **9** with catalysts **1** and **2**. ^1H NMR yield determined using 1,2,4,5-tetramethylbenzene as an internal standard.

demonstrating significant selectivity toward C–I and C–Br bonds over C–Cl and C–F bonds (Figure 4b). Indeed, this initial study using a conjugated multihalogenated substrate gave evidence that different bonds could be selectively activated by catalyst design.

We next examined the reduction of 2-bromo-6-iodobenzonitrile (**10**) and envisioned that inclusion of the electron-withdrawing nitrile functionality would further activate the iodide and bromide, which would help elucidate the tolerance of the iodide selectivity for catalyst **2**. As anticipated, utilizing **2** as a photocatalyst led to deiodinated product **11** in 97% yield with only 3% of **12** after 24 h (Figure 5a). When more reducing

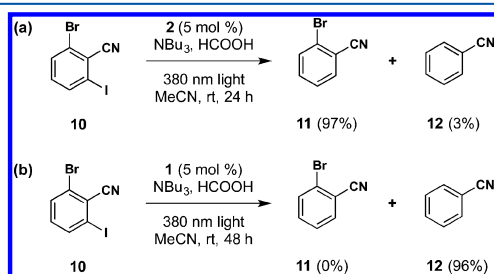


Figure 5. Chemoselective dehalogenation of **10** to its deiodinated product **11** and deiodinated and debrominated product **12** with catalysts **1** and **2**. ^1H NMR yield determined using 1,2,4,5-tetramethylbenzene as an internal standard.

photocatalyst **1** was used, fully reduced product **12** was afforded in 83% yield after 24 h and eventually increased to 96% yield after 48 h (Figure 5b). These experiments further highlight that tuning the reduction potential of the PTH scaffold provides a strategy for chemoselective dehalogenation.

To further investigate the potential of this approach, we prepared a substrate bearing activated C–I and C–Br bonds on separate rings with a carbon spacer. In contrast to the previous substrate (**10**), we envisioned that this newly prepared bis-ester

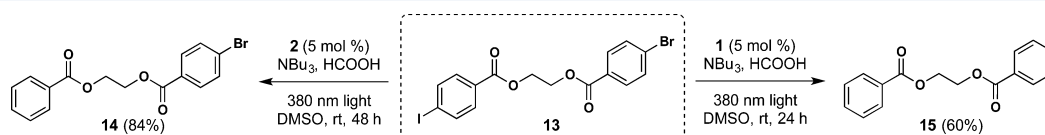


Figure 6. Selective dehalogenation of **13** with catalysts **1** and **2**.

(**13**) would allow for examination of the reduction of the C–I bond without affecting the electronics of the other ring containing the C–Br bond (Figure 6). It was found that with **2**, deiodinated product **14** could be isolated in 84% yield after 48 h. With the use of **1**, both the iodide and bromide could be reduced to give **15** in 60% isolated yield in only 24 h.

Having demonstrated successful chemoselective dehalogenation on substrates with multiple C–X bonds with this methodology, we turned our attention to C–C bond forming reactions. Inspired by the work of König and co-workers,⁶ we examined the C–C cross coupling of 4-bromobenzonitrile (**16**) with pyrrole in DMSO and found that desired product **17** could be isolated in 56% yield (Figure 7a). The key component in

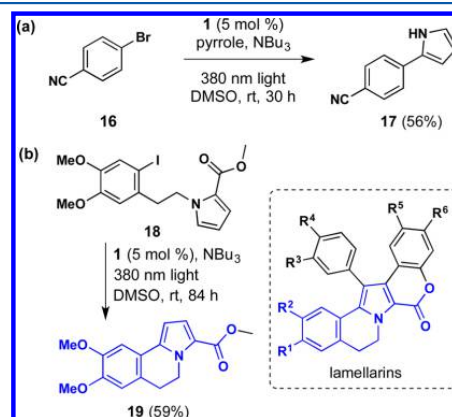


Figure 7. C–C bond forming reactions of (a) **16** with pyrrole and (b) intramolecular cyclization of **18** toward the core of the lamellarins.

C–C bond formation was the use of a large excess of pyrrole to out-compete the H atom abstraction from tributylamine and facilitate trapping of the aryl radical. In addition, using a highly polar solvent, DMSO, significantly aided the C–C bond formation, presumably due to its ability to solvate the charged radical pairs of the catalyst and the substrate.²¹

Following intermolecular aryl–aryl cross coupling with pyrrole derivatives mediated by **1**, we explored the utility of the PTH-based photoredox system for intramolecular cyclization. In particular, we examined a system based on the lamellarins, which are polyaromatic marine alkaloids containing condensed pentacyclic skeletons and are known to show biological activity toward tumor cells (Figure 7b).^{22,23} First, an electron-rich aryl iodide with a tethered pyrrole methyl ester (**18**) was prepared according to a literature procedure.²⁴ Using the same reaction conditions as for the coupling of 4-bromobenzonitrile, only excluding the trapping agent, the lamellarin core (**19**) was isolated in 59% yield.

Having successfully demonstrated C–C bond formation with PTH photocatalyst **2**, we sought to conduct C–C cross

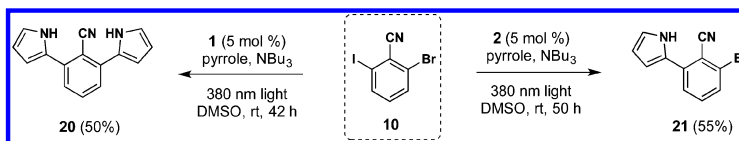


Figure 8. Selective C–C cross coupling reactions of a conjugated polyhalide with pyrrole.

coupling reactions in a chemoselective manner. A substrate bearing C–I and C–Br bonds with an activating nitrile group (**10**) was chosen as the model compound and subjected to the same reaction conditions with an excess amount of pyrrole in the presence of catalyst **1** or **2** (Figure 8). In the reaction with **1**, disubstituted pyrrole **20** was obtained in 50% yield after 42 h. Of particular note, when **2** was used as the photocatalyst, only the C–I bond was activated, leading to the formation of monosubstituted pyrrole **21** in 55% yield. This result demonstrated that selective bond formation was achieved by the preferential reduction of the more highly accessible C–I bond over the corresponding C–Br bond, producing an aryl radical, which in turn was trapped by pyrrole.

In conclusion, we have developed a new metal-free photoredox catalyst based on the PTH scaffold to perform mild and efficient chemoselective dehalogenation and C–C bond forming reactions. We observed that the less reducing catalyst, tris-acetyl-PTH (**2**), can selectively activate C–I bonds, whereas the more reducing PTH catalyst (**1**) can activate both C–I and C–Br bonds. We believe that this protocol will provide a simple, mild, and efficient method for chemoselective dehalogenation and C–C coupling reactions. Further investigation exploring a range of substrates to further elucidate the scope of this methodology is currently underway.

EXPERIMENTAL SECTION

General Methods. Unless stated otherwise, reactions were conducted in flame-dried glassware under an atmosphere of argon using reagent-grade solvents. All commercially obtained reagents were used as received. Reactions were performed at room temperature (rt, approximately 23 °C) unless stated otherwise. LED strips (380 nm) were purchased from Elemental LED (see www.elementaled.com). Reactions were placed next to the 380 nm source under vigorous stirring while cooling with compressed air. The light intensity was measured to be 1.8 $\mu\text{W}/\text{cm}^2$. Thin-layer chromatography (TLC) was conducted with Merck silica gel 60 F254 precoated plates (0.25 mm) and visualized by exposure to UV light (254 nm) or stained with anisaldehyde or potassium permanganate. Flash column chromatography was performed using normal-phase silica gel (60 Å, 230–240 mesh, Merck KGA). ^1H NMR spectra were recorded at 400, 500, or 600 MHz and are reported relative to deuterated solvent signals (7.26 ppm). Data for ^1H NMR spectra are reported as follows: chemical shift (δ ppm), multiplicity, coupling constant (Hz), and integration. For quantitative ^1H NMR to monitor yields, a 15 s relaxation delay parameter was used with 1,2,4,5-tetramethylbenzene as the internal standard. ^{13}C NMR spectra were recorded at 100 or 125 MHz and are reported relative to deuterated solvent signals (77.16 ppm). Data for ^{13}C NMR spectra are reported as follows: shift (δ ppm). High-resolution mass spectra (HRMS) were obtained using a TOF mass spectrometer, and infrared (IR) spectra were obtained using a Fourier transform infrared spectrometer with an ATR accessory.

1,1'-(10-(4-Acetylphenyl)-10H-phenothiazine-3,7-diyl)bis(ethan-1-one) (2**).** To a 100 mL round-bottom flask with stir bar were added CS_2 (4.4 mL) and AlCl_3 (871 mg, 6.5 mmol, 5.9 equiv). The mixture was cooled to 0 °C, and a mixture of acetic anhydride (0.51 mL, 5.4 mmol, 4.9 equiv) and phenyl phenothiazine (300 mg, 1.1 mmol, 1 equiv) in CS_2 (2.7 mL) was slowly added dropwise via dropping funnel, resulting in the immediate appearance of a dark purple color.

The reaction was allowed to warm slowly to room temperature, stirred for 19 h, and poured over ice water (30 mL), resulting in the immediate appearance of a yellow color. HCl (3 M, 7 mL) was then added dropwise with stirring. The mixture was washed with toluene (3 \times 50 mL), and the combined organic layers were washed successively with deionized water, sat. aq NaHCO_3 , deionized water, and brine. The organic layer was dried over MgSO_4 , filtered, and concentrated to a yellow solid, which was purified by column chromatography with toluene/EtOAc (17:3) to afford **2** (289 mg, 66% yield). Mp 231–233 °C; ^1H NMR (500 MHz, CDCl_3) δ 8.27–8.22 (m, 2H), 7.58 (d, J = 2.0 Hz, 2H), 7.51–7.47 (m, 2H), 7.41 (dd, J = 8.7, 2.1 Hz, 2H), 6.09 (d, J = 8.6 Hz, 2H), 2.71 (s, 3H), 2.47 (s, 6H); ^{13}C NMR (125 MHz, CDCl_3) δ 196.9, 195.7, 146.2, 144.0, 137.7, 132.8, 131.5, 130.9, 128.2, 127.2, 119.9, 115.7, 26.9, 26.3; IR (ATR) 3104, 3056, 2993, 2922, 1664, 1568, 1475, 1237, 961, 822 cm^{-1} ; HRMS (EI) m/z [M] $^+$ calcd for $\text{C}_{24}\text{H}_{19}\text{NO}_3$ 401.1086, found 401.1083.

2-Hydroxyethyl 4-Iodobenzoate (S2**).** To a solution of ethylene glycol (2.0 mL, 35.863 mmol, 2.0 equiv), triethylamine (1.0 mL, 7.175 mmol, 2.0 equiv), and DMAP (0.0239 g, 0.196 mmol, 0.05 equiv) in CH_2Cl_2 (36 mL) at 0 °C was added 4-iodobenzoyl chloride (0.9795 g, 3.676 mmol, 1.0 equiv). The solution was warmed to room temperature and stirred for 12 h. The reaction was then quenched with an ammonium chloride solution (1 M, 20 mL). The aqueous layer was extracted with CH_2Cl_2 (3 \times 20 mL), and the combined organic layers were dried over MgSO_4 , filtered, and then concentrated in vacuo. The residue was purified by column chromatography with hexanes/EtOAc (gradient from 4:1 to 1:1) as the eluant to afford **S2** (0.83 g, 78%) as a colorless solid. Mp 84–86 °C; ^1H NMR (400 MHz, CDCl_3) δ 7.77 (dd, J = 20.0, 8.0 Hz, 4H), 4.46–4.42 (m, 2H), 3.96–3.92 (m, 2H), 2.21 (s, 1H); ^{13}C NMR (100 MHz, CDCl_3) δ 166.6, 137.9, 131.2, 129.4, 101.2, 66.9, 61.4; IR (ATR) 3497, 2958, 2916, 2873, 1695, 1584, 1378, 1274, 1083 cm^{-1} ; HRMS (EI) m/z [M] $^+$ calcd for $\text{C}_9\text{H}_9\text{IO}_3$ 291.9596, found 291.9594.

2-((4-Bromobenzoyloxy)ethyl 4-Iodobenzoate (13**)).** To a solution of **S2** (0.8323 g, 2.850 mmol, 1.0 equiv), triethylamine (0.900 mL, 6.457 mmol, 2.3 equiv), and DMAP (10.0 mg, 0.082 mmol, 0.03 equiv) in CH_2Cl_2 (12 mL) at 0 °C was added 4-bromobenzoyl chloride (1.110 g, 5.058 mmol, 1.8 equiv). The solution was warmed to room temperature and stirred for 12 h. The reaction was then quenched with an ammonium chloride solution (1M, 30 mL). The aqueous layer was extracted with CH_2Cl_2 (3 \times 20 mL) and the combined organic layers were dried over MgSO_4 , filtered, and then concentrated in vacuo. The residue was purified by column chromatography with toluene/EtOAc (gradient from 100:0 to 99:1) as the eluant to afford **13** (1.35 g, 99%) as a colorless solid. Mp 142–144 °C; ^1H NMR (400 MHz, CDCl_3) δ 7.90 (d, J = 8.5 Hz, 2H), 7.80 (d, J = 8.5 Hz, 2H), 7.74 (d, J = 8.5 Hz, 2H), 7.58 (d, J = 8.5 Hz, 2H), 4.65 (s, 4H); ^{13}C NMR (100 MHz, CDCl_3) δ 166.0, 165.8, 138.0, 132.0, 131.3, 131.2, 129.3, 128.7, 128.5, 101.3, 63.0; IR (ATR) 3083, 3033, 2960, 1709, 1583, 1258, 1101, 1010 cm^{-1} ; HRMS (EI) m/z [M] $^+$ calcd for $\text{C}_{16}\text{H}_{12}\text{BrIO}_4$ 473.8964, found 473.8968.

2-(Benzoyloxy)ethyl 4-Bromobenzoate (14**).** A vial equipped with a magnetic stir bar and fitted with a Teflon screw cap septum was charged with **13** (47.5 mg, 0.100 mmol, 1.0 equiv), tris-acetyl-PTH (2.0 mg, 0.095 mmol, 0.05 equiv), formic acid (19 μL , 0.504 mmol, 5.0 equiv), tributylamine (120 μL , 0.504 mmol, 5.0 equiv), and DMSO (1 mL). The reaction mixture was sparged for 15 min with argon and then vigorously stirred in front of 380 nm LEDs while cooling with compressed air to maintain ambient temperature. After 48 h, the reaction mixture was diluted with EtOAc (10 mL) and quenched with H_2O (30 mL). After the layers were separated, the aqueous layer was

extracted with EtOAc (3 × 20 mL), and the combined organic layers were dried over MgSO₄, filtered, and concentrated in vacuo. The residue was purified by column chromatography with hexanes/EtOAc (gradient from 99:1 to 7:1) as the eluant to afford **14** (29.2 mg, 84%) as a colorless solid. Mp 41–44 °C; ¹H NMR (500 MHz, CDCl₃) δ 8.05 (d, *J* = 6.9 Hz, 2H), 7.91 (d, *J* = 8.6 Hz, 2H), 7.61–7.53 (m, 3H), 7.44 (t, *J* = 7.8 Hz, 2H), 4.66 (s, 4H); ¹³C NMR (100 MHz, CDCl₃) δ 166.5, 165.8, 133.3, 131.9, 131.3, 129.8, 128.8, 128.6, 128.54, 128.46, 63.1, 62.7; IR (ATR) 3064, 2955, 2920, 1717, 1590, 1451, 1398, 1259, 1096 cm⁻¹; HRMS (EI) *m/z* [M]⁺ calcd for C₁₆H₁₃BrO₄ 347.9997, found 347.9990.

Ethane-1,2-diyl Dibenzoate (15). A vial equipped with a magnetic stir bar and fitted with a Teflon screw cap septum was charged with **13** (49.9 mg, 0.100 mmol, 1.0 equiv), PTH (1.4 mg, 0.005 mmol, 0.05 equiv), formic acid (19 μL, 0.504 mmol, 5.0 equiv), tributylamine (120 μL, 0.504 mmol, 5.0 equiv), and DMSO (1 mL). The reaction mixture was sparged for 15 min with argon and then vigorously stirred in front of 380 nm LEDs while cooling with compressed air to maintain ambient temperature. After 48 h, the reaction mixture was diluted with EtOAc (10 mL) and quenched with H₂O (30 mL). After the layers were separated, the aqueous layer was extracted with EtOAc (3 × 20 mL), and the combined organic layers were dried over MgSO₄, filtered, and concentrated in vacuo. The residue was purified by column chromatography with hexanes/EtOAc (gradient from 99:1 to 7:1) as the eluant to afford **15** (16.2 mg, 60%) as a colorless solid.²⁵ Mp 64–66 °C; ¹H NMR (400 MHz, CDCl₃) δ 8.07 (d, *J* = 7.4 Hz, 4H), 7.57 (t, *J* = 7.5 Hz, 2H), 7.44 (t, *J* = 7.6 Hz, 4H), 4.67 (s, 4H); ¹³C NMR (100 MHz, CDCl₃) δ 166.5, 133.3, 129.9, 129.8, 128.6, 62.9; IR (ATR) 3064, 2959, 2914, 1710, 1602, 1451, 1265, 1113 cm⁻¹; HRMS (EI) *m/z* [M]⁺ calcd for C₁₆H₁₄O₄ 270.0892, found 270.0889.

4-(1H-Pyrrol-2-yl)benzonitrile (17). To a 1 dram vial was added a solution of **16** (18.2 mg, 0.100 mmol, 1.0 equiv), pyrrole (0.35 mL, 5.00 mmol, 50.0 equiv), **1** (1.4 mg, 0.005 mmol, 0.05 equiv), and tributylamine (0.12 mL, 0.500 mmol, 5.0 equiv) in DMSO (1.0 mL). The solution was purged with argon for 10 min. The vial was placed next to the 380 nm light under vigorous stirring while cooling with compressed air for 24 h. The reaction was then quenched by adding DI water, and the crude product was extracted with EtOAc (3 × 30 mL). The combined organic layers were washed with brine, dried over MgSO₄, and filtered. The solvent was removed in vacuo, and the product was purified by column chromatography using hexane/EtOAc (99:1 to 70:30) to afford **17** (9.4 mg, 56% yield) as yellowish crystals.²⁶ Mp 102–104 °C; ¹H NMR (400 MHz, CDCl₃) δ 8.62 (s, 1H), 7.63 (d, *J* = 8.4 Hz, 2H), 7.54 (d, *J* = 8.5 Hz, 2H), 6.95 (s, 1H), 6.67 (s, 1H), 6.35 (q, *J* = 2.7 Hz, 1H); ¹³C NMR (100 MHz, CDCl₃) δ 136.8, 132.9, 130.2, 123.8, 121.1, 119.3, 111.1, 108.9; IR (ATR) 3358, 3103, 3058, 2996, 2923, 2852, 2223, 1606, 1502, 1453, 1418, 1180, 1116, 839 cm⁻¹; HRMS (EI) *m/z* [M]⁺ calcd for C₁₁H₈N₂ 168.0687, found 168.0682.

Methyl 1-(2-Iodo-4,5-dimethoxyphenethyl)-1H-pyrrole-2-carboxylate (18). Methyl 2-pyrrolicarboxylate (216 mg, 1.7 mmol, 1.0 equiv) and NaH (60% dispersion, 74 mg, 1.85 mmol, 1.1 equiv) were stirred in dry DMF (3.4 mL) in an ice-bath for 30 min. A solution of 2-iodo-4,5-dimethoxyphenethyl 4-methylbenzenesulfonate²⁷ (957 mg, 2.1 mmol, 1.2 equiv) in dry DMF (4.3 mL) was added, and the mixture was stirred for 20 h at room temperature. The DMF was then evaporated under reduced pressure, and Et₂O was added. The organic solution was washed with 1 M HCl, saturated NaHCO₃, and brine, dried, and concentrated. The residue was purified by column chromatography with hexanes/EtOAc (gradient from 95:5 to 90:10) to afford **18** (485 mg, 68%) as a white solid. Mp 69–71 °C; ¹H NMR (600 MHz, CDCl₃) δ 7.20 (s, 1H), 6.95 (dd, *J* = 3.9, 1.8 Hz, 1H), 6.56 (t, *J* = 2.2 Hz, 1H), 6.36 (s, 1H), 6.02 (dd, *J* = 4.0, 2.5 Hz, 1H), 4.47 (t, *J* = 6.9 Hz, 2H), 3.84 (s, 3H), 3.83 (s, 3H), 3.71 (s, 3H), 3.11 (t, *J* = 6.9 Hz, 2H); ¹³C NMR (100 MHz, CDCl₃) δ 161.6, 149.2, 148.3, 133.5, 129.5, 121.4, 121.3, 118.6, 112.9, 107.9, 88.0, 56.2, 55.9, 51.2, 49.3, 42.2; IR (ATR) 3101, 2950, 2836, 1698, 1507, 1437, 1330, 1239, 1211, 1107 cm⁻¹; HRMS (EI) *m/z* [M]⁺ calcd for C₁₆H₁₈INO₄ 415.0281, found 415.0285.

Methyl 8,9-Dimethoxy-5,6-dihydropyrrolo[2,1-*a*]isoquinoline-3-carboxylate (19). To a 2 dram vial was added a solution of **18** (400 mg, 0.96 mmol, 1.0 equiv), **1** (13.3 mg, 0.05 mmol, 0.05 equiv), and tributylamine (1.1 mL, 4.8 mmol, 5.0 equiv) in DMSO (4.8 mL). The solution was purged with argon for 10 min. The vial was placed next to the 380 nm light under vigorous stirring while cooling with compressed air for 84 h. The reaction was then quenched by adding DI water, and the crude product was extracted with EtOAc (3 × 30 mL). The combined organic layers were washed with brine and DI water, dried over Na₂SO₄, and filtered. The solvent was removed in vacuo, and the product was purified by column chromatography using hexane/EtOAc (gradient from 100:0 to 70:30) to afford **19** (163 mg, 59% yield) as off-white crystals. Mp 86–89 °C; ¹H NMR (400 MHz, CDCl₃) δ 7.05 (s, 1H), 7.00 (d, *J* = 4.1 Hz, 1H), 6.73 (s, 1H), 6.42 (d, *J* = 4.1 Hz, 1H), 4.60 (t, *J* = 6.8 Hz, 2H), 3.92 (s, 3H), 3.90 (s, 3H), 3.83 (s, 3H), 3.01 (t, *J* = 6.8 Hz, 2H); ¹³C NMR (100 MHz, CDCl₃) δ 161.9, 148.8, 148.3, 136.5, 124.7, 121.4, 121.1, 118.5, 111.0, 106.9, 103.5, 56.2, 56.1, 51.2, 42.4, 28.7; IR (ATR) 3000, 2954, 2933, 2850, 1694, 1611, 1429, 1243, 1130, 1007, 856, 759 cm⁻¹; HRMS (EI) *m/z* [M]⁺ calcd for C₁₆H₁₇NO₄ 287.1158, found 287.1160.

2,6-Di(1H-pyrrol-2-yl)benzonitrile (20). To a 2 dram vial was added a solution of **10** (154 mg, 0.500 mmol, 1.0 equiv), pyrrole (1.75 mL, 25.0 mmol, 50.0 equiv), **1** (6.9 mg, 0.025 mmol, 0.05 equiv), and tributylamine (0.60 mL, 2.5 mmol, 5.0 equiv) in DMSO (2.5 mL). The solution was purged with argon for 10 min. The vial was placed next to the 380 nm light under vigorous stirring while cooling with compressed air for 50 h. The reaction was then quenched by adding DI water, and the crude product was extracted with EtOAc (3 × 30 mL). The combined organic layers were washed with brine and DI water, dried over Na₂SO₄, and filtered. The solvent was removed in vacuo, and the product was purified by column chromatography using hexane/EtOAc (gradient from 9:1 to 2:1) to afford **20** (59.0 mg, 50% yield) as an off-white solid. Mp 190–193 °C; ¹H NMR (500 MHz, CDCl₃) δ 9.16 (s, 2H), 7.52 (dd, *J* = 8.6, 7.1 Hz, 1H), 7.44 (d, *J* = 0.5 Hz, 1H), 7.42 (d, *J* = 0.9 Hz, 1H), 6.99 (td, *J* = 2.8, 1.5 Hz, 2H), 6.81 (ddd, *J* = 3.7, 2.7, 1.5 Hz, 2H), 6.36 (dt, *J* = 3.7, 2.6 Hz, 2H); ¹³C NMR (100 MHz, CDCl₃) δ 137.6, 133.2, 128.4, 124.9, 121.2, 120.9, 111.0, 110.4, 101.5; IR (ATR) 3406, 3362, 3121, 2957, 2924, 2853, 2212, 1579, 1468, 1416, 1113, 1088, 1036, 798, 739 cm⁻¹; HRMS (EI) *m/z* [M - H]⁺ calcd for C₁₃H₁₀N₂ 232.0875, found 232.0868.

2-Bromo-6-(1H-pyrrol-2-yl)benzonitrile (21). To a 2 dram vial was added a solution of **10** (154 mg, 0.500 mmol, 1.0 equiv), pyrrole (1.75 mL, 25.0 mmol, 50.0 equiv), **2** (10.0 mg, 0.025 mmol, 0.05 equiv), and tributylamine (0.60 mL, 2.5 mmol, 5.0 equiv) in DMSO (2.5 mL). The solution was purged with argon for 10 min. The vial was placed next to the 380 nm light under vigorous stirring while cooling with compressed air for 50 h. The reaction was then quenched by adding DI water, and the crude product was extracted with EtOAc (3 × 30 mL). The combined organic layers were washed with brine and DI water, dried over Na₂SO₄, and filtered. The solvent was removed in vacuo, and the product was purified by column chromatography using hexane/EtOAc (gradient from 9:1 to 2:1) to afford **21** (67.1 mg, 55% yield) as an off-white solid. Mp 131–133 °C; ¹H NMR (400 MHz, CDCl₃) δ 9.29 (s, 1H), 7.59 (d, *J* = 8.1 Hz, 1H), 7.48 (d, *J* = 7.9 Hz, 1H), 7.39 (t, *J* = 8.0 Hz, 1H), 7.00 (s, 1H), 6.83 (s, 1H), 6.40–6.31 (m, 1H); ¹³C NMR (100 MHz, CDCl₃) δ 138.4, 133.8, 129.9, 127.32, 127.26, 125.6, 121.7, 118.7, 111.6, 110.7, 109.2; IR (ATR) 3388, 3072, 2918, 2852, 2226, 1586, 1558, 1543, 1460, 1125, 1042, 730 cm⁻¹; HRMS (EI) *m/z* [M]⁺ calcd for C₁₁H₈N₂Br 245.9793, found 245.9798.

■ ASSOCIATED CONTENT

● Supporting Information

The Supporting Information is available free of charge on the ACS Publications website at DOI: 10.1021/acs.joc.6b01034.

NMR conversions for **S1**, **3**, and **5** and proposed mechanism for dehalogenation, and NMR spectra of isolated products **2**, **S2**, **13–15**, and **17–21** (PDF)

■ AUTHOR INFORMATION

Corresponding Authors

*E-mail: hawker@mrl.ucsb.edu.*E-mail: javier@chem.ucsb.edu.

Notes

The authors declare no competing financial interest.

■ ACKNOWLEDGMENTS

We thank the MRSEC program of the National Science Foundation (DMR 1121053) and The Dow Chemical Company through the Dow Materials Institute at UCSB for financial support. NMR instrumentation was supported by the NIH Shared Instrumentation Grant (SIG) 1S10OD012077-01A1.

■ REFERENCES

- (1) Chen, X.; Engle, K. M.; Wang, D.-H.; Yu, J.-Q. *Angew. Chem., Int. Ed.* **2009**, *48*, 5094–5115.
- (2) Chen, J.; Zhang, Y.; Yang, L.; Zhang, X.; Liu, J.; Li, L.; Zhang, H. *Tetrahedron* **2007**, *63*, 4266–4270.
- (3) Alonso, F.; Beletskaya, I. P.; Yus, M. *Chem. Rev.* **2002**, *102*, 4009–4092.
- (4) Narayanam, J. M. R.; Stephenson, C. R. J. *Chem. Soc. Rev.* **2011**, *40*, 102–113.
- (5) Senaweera, S.; Weaver, J. D. *J. Am. Chem. Soc.* **2016**, *138*, 2520–2523.
- (6) Ghosh, I.; Ghosh, T.; Bardagi, J. I.; König, B. *Science* **2014**, *346*, 725–728.
- (7) Meyer, A. U.; Slanina, T.; Yao, C.-J.; König, B. *ACS Catal.* **2016**, *6*, 369–375.
- (8) Prier, C. K.; Rankic, D. A.; MacMillan, D. W. C. *Chem. Rev.* **2013**, *113*, 5322–5363.
- (9) Nguyen, J. D.; Tucker, J. W.; Konieczynska, M. D.; Stephenson, C. R. J. *J. Am. Chem. Soc.* **2011**, *133*, 4160–4163.
- (10) Wallentin, C.-J.; Nguyen, J. D.; Finkbeiner, P.; Stephenson, C. R. J. *J. Am. Chem. Soc.* **2012**, *134*, 8875–8884.
- (11) Tucker, J. W.; Nguyen, J. D.; Narayanam, J. M. R.; Krabbe, S. W.; Stephenson, C. R. J. *Chem. Commun.* **2010**, *46*, 4985–4987.
- (12) Nguyen, J. D.; D'Amato, E. M.; Narayanam, J. M. R.; Stephenson, C. R. J. *Nat. Chem.* **2012**, *4*, 854–859.
- (13) Czaplik, W. M.; Grube, S.; Mayer, M.; Jacobi von Wangelin, A. *Chem. Commun.* **2010**, *46*, 6350–6352.
- (14) Chelucci, G.; Figus, S. *J. Mol. Catal. A: Chem.* **2014**, *393*, 191–209.
- (15) Arendt, K. M.; Doyle, A. G. *Angew. Chem., Int. Ed.* **2015**, *54*, 9876–9880.
- (16) While this manuscript was in review, a chemoselective C–C bond forming transformation mediated by an organic photocatalyst system was reported: Ghosh, I.; König, B. *Angew. Chem., Int. Ed.* **2016**, DOI: 10.1002/anie.201602349.
- (17) Treat, N. J.; Sprafke, H.; Kramer, J. W.; Clark, P. G.; Barton, B. E.; Read de Alaniz, J.; Fors, B. P.; Hawker, C. J. *J. Am. Chem. Soc.* **2014**, *136*, 16096–16101.
- (18) Discekici, E. H.; Pester, C. W.; Treat, N. J.; Lawrence, J.; Mattson, K. M.; Narupai, B.; Toumayan, E. P.; Luo, Y.; McGrath, A. J.; Clark, P. G.; Read de Alaniz, J.; Hawker, C. J. *ACS Macro Lett.* **2016**, *5*, 258–262.
- (19) Discekici, E. H.; Treat, N. J.; Poelma, S. O.; Mattson, K. M.; Hudson, Z. M.; Luo, Y.; Hawker, C. J.; Read de Alaniz, J. *Chem. Commun.* **2015**, *51*, 11705–11708.
- (20) Andrieux, C. P.; Blocman, C.; Dumas-Bouchiat, J.-M.; Saveant, J.-M. *J. Am. Chem. Soc.* **1979**, *101*, 3431–3441.
- (21) Lewis, F. D. *Acc. Chem. Res.* **1986**, *19*, 401–405.
- (22) Andersen, R. J.; Faulkner, D. J.; He, C.-H.; Van Duyne, G. D.; Clardy, J. *J. Am. Chem. Soc.* **1985**, *107*, 5492–5495.
- (23) Lindquist, N.; Fenical, W.; Van Duyne, G. D.; Clardy, J. *J. Org. Chem.* **1988**, *53*, 4570–4574.
- (24) Pla, D.; Marchal, A.; Olsen, C. A.; Albericio, F.; Álvarez, M. J. *Org. Chem.* **2005**, *70*, 8231–8234.
- (25) Ren, W.; Emi, A.; Yamane, M. *Synthesis* **2011**, 2303–2309.
- (26) Du, W.; Zhao, M.-N.; Ren, Z.-H.; Wang, Y.-Y.; Guan, Z.-H. *Chem. Commun.* **2014**, *50*, 7437–7439.
- (27) Ruiz, J.; Ardeo, A.; Ignacio, R.; Sotomayor, N.; Lete, E. *Tetrahedron* **2005**, *61*, 3311–3324.

Appendix F

Engineering Surfaces Through Sequential Stop-Flow Photopatterning

Reprinted with permission from C.W. Pester, B. Narupai, K.M. Mattson, D.P. Bothman, D. Klinger, K.W. Lee, E.H. Discekici, C.J. Hawker *Adv. Mater.* **2016**, *in press*, © 2016 WILEY-VCH Verlag GmbH & Co. KGaA, Weinheim. CCC License Number 3946620818303.

Engineering Surfaces through Sequential Stop-Flow Photopatterning

Christian W. Pester,* Benjaporn Narupai, Kaila M. Mattson, David P. Bothman, Daniel Klinger, Kenneth W. Lee, Emre H. Discekici, and Craig J. Hawker*

Dedicated to Prof. Edward J. Kramer

Polymer films are scientifically and industrially relevant for a broad collection of applications, ranging from marine paints^[1] and biomedical devices^[2] to flame-retardant coatings.^[3] Their fabrication typically involves physisorption-based techniques,^[4] such as spray-, dip- or spin-coating, which modify surface properties uniformly. While effective, these physisorption strategies do not provide the ability to pattern films, inherently limiting polymer coatings to a single functionality or physical property.

To address this limitation, the covalent attachment of polymers has emerged as a viable strategy for the preparation of multifunctional surfaces, either by grafting polymers to, or growing them from a surface via surface-initiated controlled radical polymerization (SI-CRP).^[5,6] Here, external regulation of SI-CRP,^[6–10] e.g., via light, plays a crucial role in controlling the distribution of surface functional groups.^[11–13] Such topographically and/or chemically patterned polymer brushes are valuable for a plethora of interdisciplinary applications.^[14–20] For example, they allow fabrication of “intelligent” substrates which selectively adapt to their environment on the microscale or nanoscale^[21] through spatial control of wetting,^[22] mechanical,^[23–25]

biological,^[26–28] or electronic^[29] properties. A series of recent reviews highlight both the capabilities and drawbacks of current 2D and 3D polymer brush patterning techniques.^[14–20]

Polymer brushes can be patterned via either “bottom-up”^[13,30–34] or “top-down”^[35,36] strategies. Soft lithography^[37–39] is a prominent example for a contact-based bottom-up approach: elastomeric stamps are used to print patterns of polymerization initiators, which can subsequently be amplified via SI-CRP. In contrast, top-down strategies, e.g., e-beam lithography, locally remove either surface-anchored initiators (prior to SI-CRP), or previously grown polymer brushes. As a result, chemical patterning of surfaces with polymer brushes traditionally requires iterative: i) initiator deposition, ii) pattern amplification via SI-CRP, and iii) polymer chain end deactivation. These multiple steps (plus related rinsing and cleaning steps) are repeated for each additional polymeric species, rapidly increasing the amount of required processing steps for even simple patterned surfaces. Such repetitive methodologies are therefore challenging,^[40] creating a demand for more efficient and less complicated fabrication strategies.

An ideal process would combine the benefits of: i) a synthetically facile, high throughput approach with ii) the ability to create multiple levels of patterning via a continuous process. In analogy with traditional photolithography, light represents a mild non-contact stimulus capable of mediating numerous chemical reactions.^[5,7–9,32,33,41–45] In tandem with a variety of additional post polymerization functionalization procedures,^[46] photochemistry also allows the spatially controlled incorporation and immobilization of an array of different functional units on surfaces.

Here, the combination of stopped-flow techniques^[47] and reduction photolithography is described,^[48] to engineer a modular platform for sequential photochemical reactions in a continuous manner. This facilitates chemical surface patterning through successive exchange of reactants within a stop-flow cell, while providing significant flexibility to exchange light sources, and/or spatially decoupled photomasks. **Scheme 1** illustrates such a photochemical sequence: Spatially controlled photopolymerization, followed by exchange of the solution within the stop-flow cell, and then secondary functionalization of polymer brushes, in this case by light-mediated removal of the active terminal bromine chain end. During this entire process, neither wafer nor photomask are moved, which allows spatial confinement of functionalization exclusively to regions where polymer brushes were previously grown. As a direct consequence, adjacent surface-grafted polymerization initiators remain untouched, affording hierarchical chemical patterning on uniformly functionalized

Dr. C. W. Pester, B. Narupai, K. M. Mattson,
E. H. Discekici, Prof. C. J. Hawker
Materials Research Laboratory (MRL)
University of California, Santa Barbara
Santa Barbara, CA 93106, USA
E-mail: pester@mrl.ucsb.edu; hawker@mrl.ucsb.edu



Dr. C. W. Pester, Prof. C. J. Hawker
Materials Department
University of California, Santa Barbara
Santa Barbara, CA 93106, USA

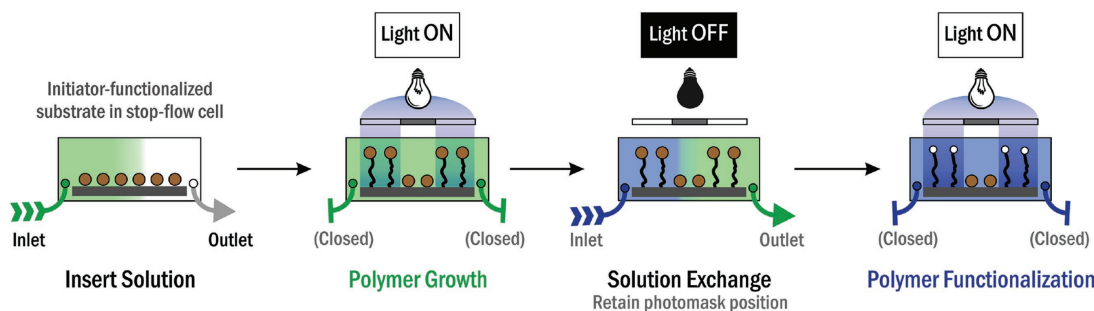
B. Narupai, K. M. Mattson, E. H. Discekici, Prof. C. J. Hawker
Department of Chemistry and Biochemistry
University of California, Santa Barbara
Santa Barbara, CA 93106, USA

Dr. D. P. Bothman
Department of Mechanical and Environmental Engineering
University of California, Santa Barbara
Santa Barbara, CA 93106, USA

Prof. D. Klinger
Institut für Pharmazie
Freie Universität Berlin
14195 Berlin, Germany

K. W. Lee
Department of Physics
University of California
Santa Barbara, CA 93106, USA

DOI: 10.1002/adma.201602900



Scheme 1. Concept of solution-exchange lithography. Enclosing a substrate in a stop-flow cell allows for in situ exchange of reactants and execution of successive chemical reactions at precisely the same location. Illustrated here is light-mediated growth of polymer brushes followed by solution exchange and subsequent, spatially controlled passivation of the active polymer chain ends.

substrates. This renders repetitive initiator deposition and related cleaning/treatment steps unnecessary and results in economic and environmental advantages. Ultimately, this solution-exchange lithography concept streamlines the production of chemically patterned surfaces and affords access to hierarchically structured substrates, all from uniform initiating layers.

The experimental setup involves an array of lenses to optically reproduce 1:1, magnify, or reduce and project an inkjet-printed photomask onto a substrate positioned inside a stop-flow cell (see Figure 1). This stop-flow cell was readily scaled to accommodate large wafers of $\varnothing = 7.6$ cm (3 in.) diameter, enhancing both the relevance and potential of this process, with the immediate proximity between cover glass and substrate allowing capillary forces to uniformly spread the reactants over the surface (see Figure S1, Supporting Information). This uniform spreading allows production of homogeneous uniform polymer brush films with thicknesses of up to 120 ± 2 nm as determined by optical reflectometry. Reduction projection reproduces the image from an original photomask on a surface with reduced size. This concept facilitates alignment and/or stacking of multiple patterns by eye, paving a path toward complex microscopic patterns from macroscopic photomasks. The ratio of the focal lengths of the two lenses (f_1 and f_2) determines the linear reduction factor (LRF) = f_1/f_2 , which could readily be adjusted by simply exchanging lenses. For this work, focal lengths of $f_1 = 500$ mm and $f_2 = 100$ mm were used, resulting in optical reduction by a factor of five (area reduction to 1/25th of the original photomask). This spatial decoupling (separating) of the photomask(s) from the substrate has a number of benefits. The noncontact-based nature allows use of inexpensively produced, inkjet-printed photomasks. If desired, simple x,y -translation of the substrate stage allows lateral repetition of either a single or multiple patterns. In addition, all processing steps, including chemical reactions, rinsing, and drying can be performed without removing the substrate from its original position. This allows successive, spatially well-defined (photo)chemical reactions to be performed sequentially from uniform initiating layers, including but not limited to both traditional^[10] and light-mediated controlled radical polymerization,^[5,7-9,32,33,41,42] dehalogenation,^[43] thiol-ene coupling,^[49,50] and atom transfer radical addition.^[44,45] As an added benefit, the stop-flow cell is sealed from the surrounding environment

and is readily filled via cannula transfer. This enables oxygen-sensitive reactions to be performed under simple conditions, without the need for a glove box or other Schlenk-technique related equipment (see the Experimental Section).

Figure 2 demonstrates the potential of this setup for the controlled radical photopolymerization^[8,13,32] growth of patterned poly(methyl methacrylate) (poly(MMA)) brushes with high spatial fidelity (see Figure 2b,e, and Figure S2, Supporting Information). The resulting topographical patterning was revealed

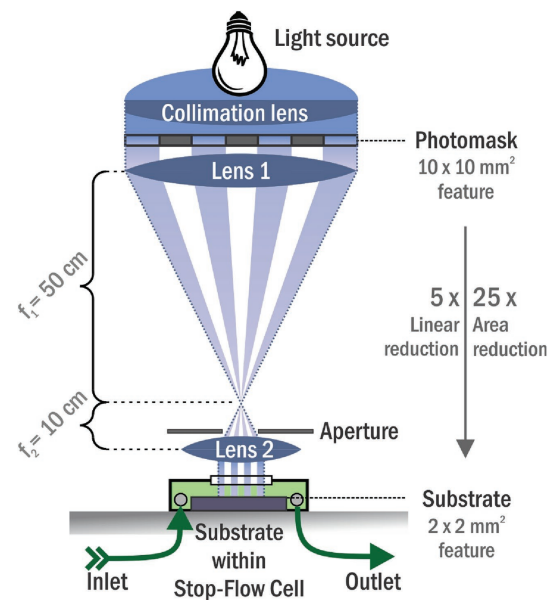


Figure 1. Schematic of solution-exchange lithography. An array of lenses is used to project the pattern of a photomask onto a substrate that is enclosed in a stop-flow cell. At focal lengths of $f_1 = 50$ cm and $f_2 = 10$ cm, this projector reduces features of the photomask image by a linear reduction factor of LRF = 5 (25 \times reduction in area) and reproduces them on the surface. Spatially decoupling the stop-flow cell from the photomask allows exchange of solutions while retaining the exact position of the photomask, enabling sequential stop-flow photochemistry.

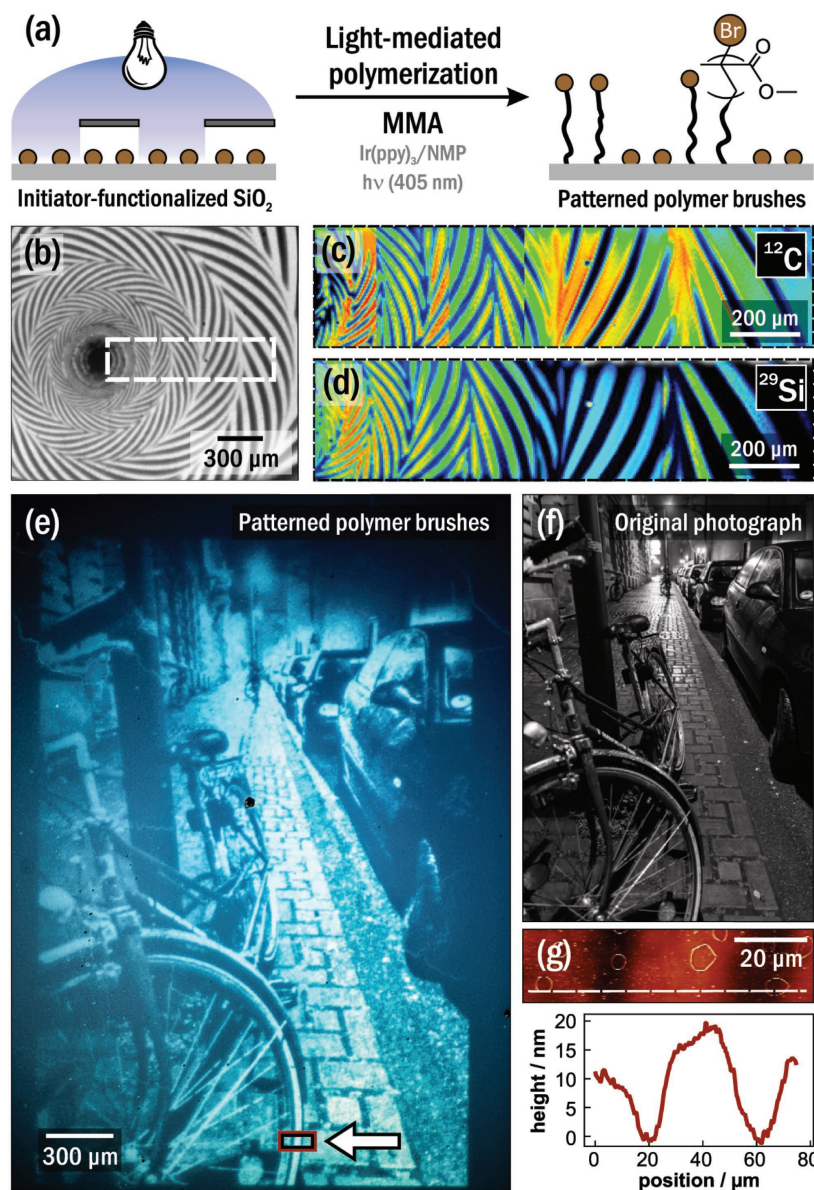


Figure 2. a) Schematic of light-mediated controlled radical polymerization of methyl methacrylate (MMA) by irradiation of an initiator-functionalized SiO₂ substrate through a binary photomask. The brown circles indicate the polymerization initiators. For clarity, both the detailed projection setup (see Figure 1) and the stop-flow cell (see Scheme 1) are omitted. b) Optical-microscopy image of poly(MMA) brushes (light) on SiO₂ (dark). The dashed rectangle in (b) indicates where the secondary-ion mass-spectrometry element maps of carbon ($m/z = 12$ (c)) and silicon ($m/z = 29$ (d)) fragments were obtained. e, f) A patterned poly(MMA) brush reproduction (e) of an original photograph (f), which was taken by C. W. Pester. The reproduction illustrates the achievable spatial resolution and complexity. The original photomask was reproduced on the substrate at 1/25th its original size, allowing for the production of multiple different polymer-brush-height gradients in close proximity and in a single polymerization step. g) Atomic force microscopy image of the square area indicated in (e), and the corresponding line cut (dashed line) indicates a polymer brush height of up to 20 nm.

by optical microscopy and atomic force microscopy (AFM), which showed a patterned polymer brush thickness of 20 nm after 30 min of light-mediated controlled radical polymerization

(see Figure 2g and the Experimental Section). In secondary-ion mass spectrometry (SIMS), carbon ($m/z = 12$, poly(MMA)) fragment maps further indicated successful reproduction of the

original photomask image (see Figure 2c). Correspondingly, silicon ($m/z = 29$) was detected exclusively in regions of the silicon dioxide (SiO_2) substrate where the photomask blocked the light and no polymer was grown (see Figure 2d). At LRF = 5, the total area of the resulting reduced pattern ($2 \text{ mm} \times 2 \text{ mm}$) was 4% of the original inkjet-printed photomask ($10 \text{ mm} \times 10 \text{ mm}$). The smallest obtainable line features are a function of both initial feature sizes and optical reduction. For the experiments described herein, features as small as $2 \mu\text{m}$ were obtained (see Figure 2b). As previously reported, simple variation of either polymerization time and/or photon flux may be used to target different brush heights, and a majority of polymer chain ends remain active for additional functionalization or further growth.^[13,32,33] The rate of polymer brush growth is a function of the distance between the substrate and light source (d_{LED}), as well as the intensity of the incident light.^[33] For the experiments depicted in this report, we utilized constant substrate-to-light source distances of $d_{\text{LED}} = f_1 + f_2 = 600 \text{ mm}$ (for the projection of patterns), or $d_{\text{LED}} = 15 \text{ mm}$ (for the growth of uniform polymer brush layers). At $d_{\text{LED}} = 600 \text{ mm}$, we could regulate light intensities between 6.88 and $173.6 \mu\text{W mm}^{-2}$ (confined to a spot size of 0.25 cm^2), which would allow for modulation of the polymerization kinetics if desired.^[33] The polymer brush patterns described in this contribution were all produced using an intensity of $5.6 \mu\text{W mm}^{-2}$ at $d_{\text{LED}} = 600 \text{ mm}$, which afforded linear polymer brush growth (see Figure S3, Supporting Information). This patterning approach was shown to be compatible with both conventional photomasks as well as with inkjet-printed overhead transparencies (see Figure 2b,e), affording the reproduction of arbitrarily complex patterns and manufacturing of surfaces combining numerous polymer brush height gradients on a single substrate.

The ability to exchange reactants in situ while retaining the position of the photomask is a significant advantage when chemically patterning polymer brushes. The use of sequential photochemical reactions allows preparation of chemically versatile surfaces, as demonstrated in the following by preparation of binary polymer brush patterns. Such binary patterned substrates offer lateral combination of different functional materials with contrasting physical properties and represent an intriguing pathway toward surfaces which selectively adapt to their environment.^[21] However, in conventional processes, the preparation of binary polymer brushes with microscale feature sizes requires tedious and iterative deposition of initiator patterns, subsequent pattern amplification (via SI-CRP), followed by chain end passivation (vide supra).^[38] To the best of our knowledge, no established method has been capable of fabricating binary patterned brushes from uniform initiator layers. In contrast, the setup described herein allows for the preparation of binary brushes from a uniform initiating layer via sequential stop-flow photochemistry. Eliminating the repetitive initiator deposition steps not only facilitates processing, but also prevents related chemical contamination. Figure 3a illustrates the formation of such a chemically patterned, binary surface with disparate wetting properties. Initially, patterned poly(ethylene glycol) methacrylate (PEGMA) brushes were grown by irradiation through a photomask. AFM indicated a thickness of the patterned polymer brushes of 13 nm after 15 min of irradiation at $\lambda = 405 \text{ nm}$ through

a photomask. Then, without moving the photomask, reactants within the stop-flow cell were exchanged and a solution of a highly reducing photocatalyst was inserted to promote spatially controlled dehalogenation of the polymer brush chain end.^[43] Because the photomask remains in its original position, this subsequent, light-mediated passivation reaction is locally confined to where the initial PEGMA polymerization occurred. The poly(PEGMA) brushes are therefore selectively deactivated and cannot participate in subsequent polymerizations. Surface-bound polymerization initiators that did not participate in the initial polymerization remain active and allow a third sequential reaction to be performed, i.e., growth of $1H,1H,2H,2H$ -perfluorooctyl methacrylate (PFOMA) polymer brushes via atom transfer radical polymerization (ATRP). Optical microscopy (Figure 3b–d) and SIMS (Figure 3e,f) confirmed the topographical and binary chemical nature of the resulting substrate with fluorine ($m/z = 19$, poly(PFOMA)) and oxygen ($m/z = 16$, poly(PEGMA)) fragment maps matching the positive and negative representation of the original photomask, respectively. These binary patterns were also accessible by substituting the dehalogenation step (cf. Figure 3a) with spatially controlled chain end passivation via atom transfer radical addition (see Figure S6, Supporting Information),^[44,45] highlighting the compatibility of this platform with a range of light-mediated reactions.

The preparation of binary hydrophilic poly(PEGMA) and hydrophobic poly(PFOMA) brushes from incompatible monomers further serves to demonstrate the breadth of accessible materials. Their significantly contrasting wetting properties are evident from their water contact angles, $\theta_{\text{PEGMA}} = 61^\circ$ and $\theta_{\text{PFOMA}} = 120^\circ$, which, according to the Young–Dupré equation, correspond to surface energies of $W_{\text{poly(PEGMA)}} = 0.11 \text{ J m}^{-2}$ and $W_{\text{poly(PFOMA)}} = 0.04 \text{ J m}^{-2}$, respectively (see Figure S5, Supporting Information).^[51] Spatially confined, hydrophilic poly(PEGMA) regions are observed to selectively swell upon rising humidity (see Figure 3c), increasing the poly(PEGMA) brush height and promoting localized water droplet formation, i.e., selective wetting (Figure 3d). The synthesis of such continuous binary patterns from uniform initiating layers offers significant opportunities and directly relies on the ability to exchange reactants in situ, allowing for sequential photochemical procedures while retaining the position of the photomask.

In addition to the exchange of solutions, the modular nature of this strategy also allows substitution of photomasks and/or light sources during the modification of a single substrate. This feature is illustrated by successively performing a series of photochemical reactions while exchanging both the photomask and the light source (i.e., the wavelength). Initially, a $51.1 \pm 0.5 \text{ nm}$ thick, homogeneous poly(PEGMA-co-VMA) (where VMA is vinyl methacrylate, 50:50 mol%) copolymer brush layer was grown by uniformly irradiating the substrate for 10 min . X-ray photoelectron spectroscopy (XPS) confirmed the targeted 50 mol% incorporation of vinyl functionalities (see the Supporting Information). Without changing the position of the substrate, the reactants within the stop-flow cell were exchanged and a subsequent thiol-ene coupling reaction was performed. Figure 4a illustrates radical addition of a hydrophobic $1H,1H,2H,2H$ -perfluorodecanethiol (PFDT) across

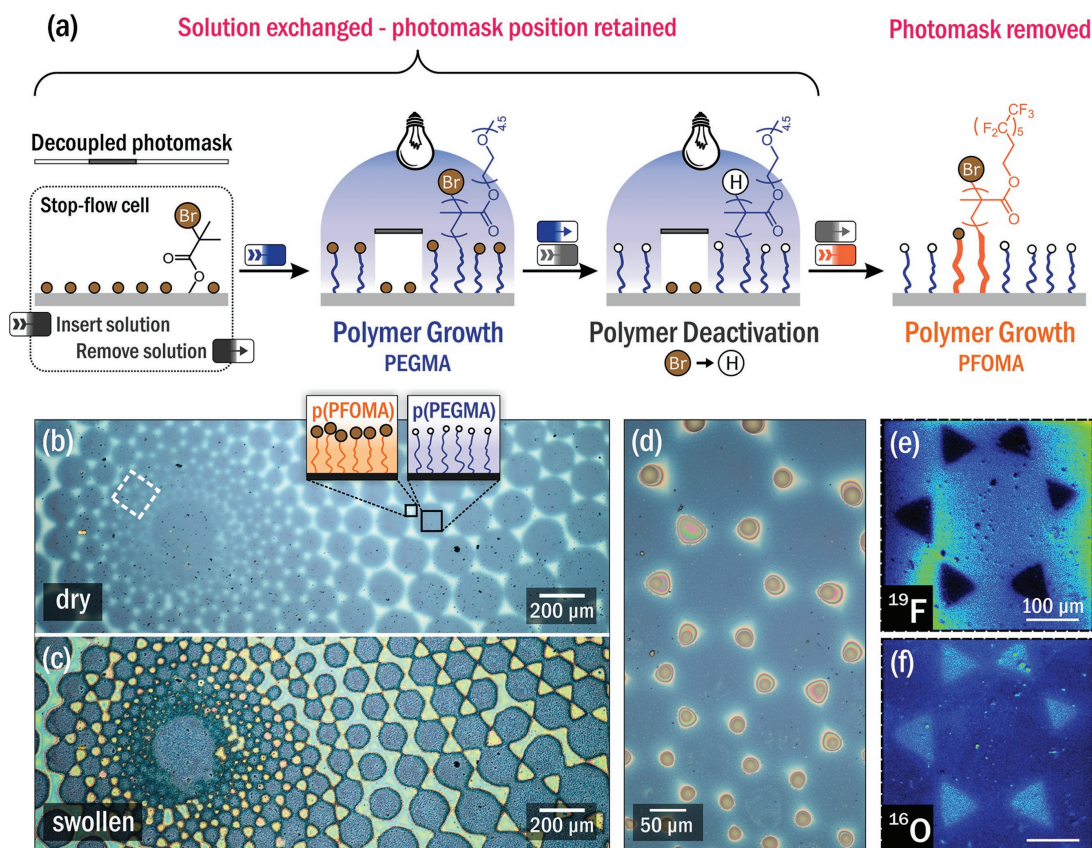


Figure 3. a) Formation of binary brushes via a cascade of sequential photochemical reactions. The substrate is enclosed in the stop-flow cell throughout this process. For clarity, we omitted displaying the stop-flow cell and the projection setup (compare with Figure 1). Photopolymerization of PEGMA is followed by light-mediated dehalogenation (local deactivation of polymer brush chain ends). The photomask remains in place while reactant solutions are exchanged. Lastly, the photomask is removed and PFOMA is polymerized via atom transfer radical polymerization. The color-coded boxes above the arrows indicate the experimental procedure of inserting or removing reactant solution. b) Optical bright-field image of dry binary polymer brushes. c) Lateral combination of hydrophilic and hydrophobic properties allows for selective swelling in a high humidity environment. d) Water droplets are formed exclusively in hydrophilic regions. e, f) Secondary-ion mass spectrometry indicates spatial confinement of fluorine (e) and oxygen (f) fragments, providing additional evidence for the chemically binary nature of the surface. The ^{16}O and ^{19}F maps obtained from the dashed white rectangular region in (b) represent the positive and negative of the original photomask, respectively.

the pendant vinyl functionalities present in the hydrophilic poly(PEGMA-co-VMA) copolymer brush. As a result, a novel surface-tethered bottle brush architecture with statistically distributed side arms of different polarities was obtained. XPS indicated the appearance of both fluorine and sulfur peaks and allowed quantitative determination of the efficiency of the thiol-ene reaction ($\approx 79\%$ yield) within the outermost 10 nm of the polymer brush (see Figure 4b–d and Supporting Information). Highlighting the ability of this modular platform to exchange light sources, thiol-ene coupling was successfully performed both under UV ($\lambda = 365\text{ nm}$)^[49] as well as under visible-light ($\lambda = 405\text{ nm}$) irradiation (see the Experimental Section).^[50]

Traditionally, patterning with materials of such distinctly dissimilar polarities, i.e., PEGMA and PFDT, is considered difficult. For example, the initial polymer brush may render the

substrate too hydrophobic (or hydrophilic) for uniform wetting and subsequent, spatially controlled functionalization. Here, this challenge is mitigated by the immediate proximity of the cover glass, which allows capillary action to serve as the driving force to uniformly spread the reactants over the substrate. Indeed, as illustrated in Figure 5a, PFDT is readily incorporated with spatial control by irradiation of a poly(PEGMA-co-VMA) coated substrate through a photomask. In optical microscopy (see Figure 5b), darker areas can be identified as PFDT-functionalized poly(PEGMA-co-VMA/PFDT) bottlebrushes. The addition of PFDT into the polymer brush backbone locally increases density (and brush height) to yield optical contrast. Optical reflectometry and AFM indicated a localized increase in polymer brush thickness from $60.2 \pm 3.0\text{ nm}$ to a total bottlebrush height of $70.0 \pm 3.1\text{ nm}$. Chemical patterning was

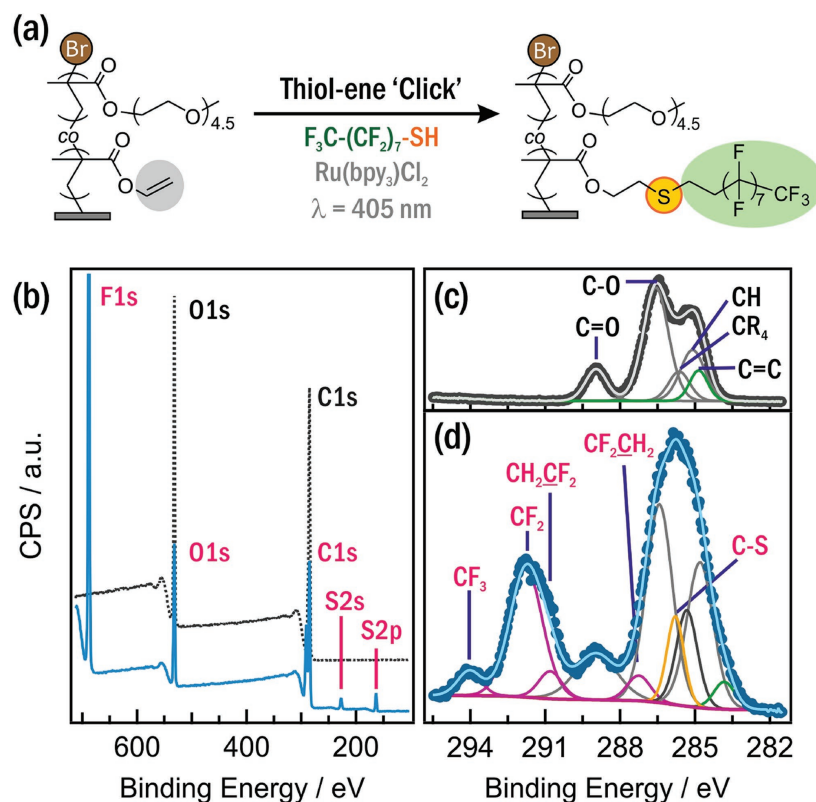


Figure 4. a) Light-mediated thiol-ene coupling of pendant vinyl groups in poly(PEGMA-co-VMA) polymer brushes with 1H,1H,2H,2H-perfluorodecanethiol (PFDT) to form bottlebrush architectures with hydrophilic and hydrophobic sidearms. b) Fluorine (F1s) and sulfur (S2s and S2p) peaks in the X-ray photoelectron spectrum indicate successful formation of poly(PEGMA-co-VMA/PFDT) bottlebrushes. The dashed gray and solid blue lines correspond to the initial and the thiol-ene treated film, respectively. High-resolution XPS carbon C1s scans of both c) the initial and d) thiol-ene functionalized film. A sum of Gaussian bell curves (solid lines) was used to fit experimental data (bullets) and quantify binding energies and ratios of individual chemical components.

verified by mapping fluorine ($m/z = 19$, Figure 5b, inset) fragments in SIMS, which were detected exclusively where PFDT was incorporated into the polymer brush.

A key advantage of this experimental setup is the capability to hierarchically pattern substrates from uniform initiator monolayers (vide supra). Notably, sequential functionalization is now also possible on previously grown (uniform or patterned) polymer brushes, enhancing the scope of accessible substrates and materials. This benefit is illustrated by chain-extending patterned poly(PEGMA-co-VMA/PFDT) bottlebrushes with methyl methacrylate (MMA) to form poly(PEGMA-co-VMA/PFDT)-*b*-poly(MMA) diblock architectures (see Figure 5a). Starting from the spiral pattern shown in Figure 5b, exchange of both the solution and the photomask allowed a second, different pattern to be fabricated on the initial polymer brush surface. Optical microscopy (Figure 5c) confirmed the presence of two patterns, corresponding to the initial thiol-ene patterned spiral (cf. Figure 5b), superimposed by poly(MMA) rectangles. Demonstrating the chemical and topographical possibilities, this surface combines three monomers, one thiol-ene

functionalization, and two different patterns. Significantly, the resulting four, distinct polymer brush architectures, each with discrete chemical properties, were obtained by only three sequential photochemical processing steps from a uniform initiating layer.

In conclusion, this contribution illustrates the versatility and modular nature of solution-exchange lithography as a novel platform for surface patterning. This approach circumvents the need for repetitive initiator deposition, as is common in many conventional techniques, and allows preparation of patterned surfaces with large topographical and chemical variety from uniform initiating monolayers. Key to these advances is the ability to exchange reaction solutions in situ, leading to homogeneous wetting of substrates with solutions of vastly contrasting polarity. Eliminating the necessity to remove the substrate between individual processing steps enables successive reactions to be performed in the same location with microscale resolution. In addition, all procedures, including oxygen-sensitive reactions, can now be performed in a closed stop-flow cell and without the necessity of a glove box, while

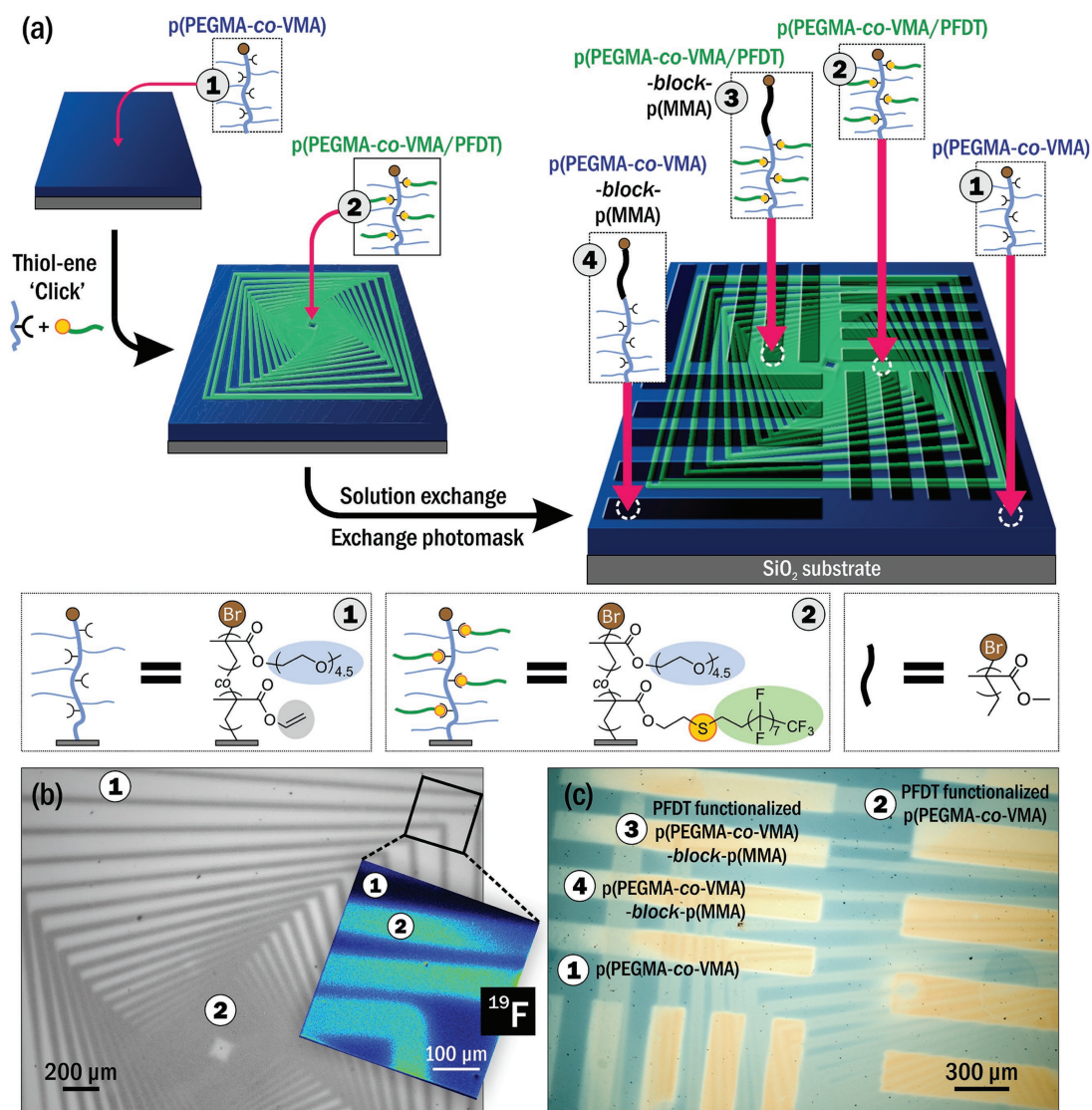


Figure 5. a) Schematic of sequential, different photochemical reactions performed without tampering with the substrate. A homogeneous poly(PEGMA-co-VMA) (1) copolymer layer was grown, then locally functionalized via thiol-ene "click" chemistry (see Figure 4) to form poly(PEGMA-co-VMA/PFDT) bottlebrushes (2). b) Both optical microscopy and ^{19}F secondary-ion mass spectrometry maps (inset) confirm the resulting chemical "spiral" pattern. The light and dark areas in the optical image correspond to the initial poly(PEGMA-co-VMA) brush layer and PFDT-functionalized bottlebrushes, respectively. Subsequently, while leaving the substrate in place, both the solution and the photomask were exchanged. Chain extension via spatially controlled photopolymerization of methyl methacrylate (MMA) results in a rectangular pattern of poly(PEGMA-co-VMA/PFDT)-*b*-poly(MMA) (3) and poly(PEGMA-co-VMA)-*b*-poly(MMA) (4) diblock regions. c) Optical microscopy showed the overlay of two distinctly dissimilar patterns and confirmed the formation of hierarchical 3D polymer brushes. The optical image of the resulting hierarchical 3D polymer brushes showed both the initial thiol-ene spiral pattern (cf. b), and the rectangular poly(MMA) pattern.

the decoupling of photomask and wafer allows the use of inexpensive, inkjet-printed overhead transparencies as photomasks, significantly reducing both time and cost related to fabrication of standard photomasks. We believe the platform described

herein offers a facile strategy for the highly reproducible and streamlined production of topographically- and chemically diverse patterned polymer brush surfaces from uniform initiating layers.

Experimental Section

General Reagent and Setup Information: Silicon substrates with 100 nm oxide were purchased from Silicon Quest International. Monomers and other chemicals were obtained from Sigma–Aldrich and, unless otherwise noted, used without further purification. The stop-flow cell was custom designed. All projector parts, including light source, posts, holders, and lenses were obtained by Thorlabs. Thorlabs Olympus BX & IX series ($\lambda = 365$ and 405 nm) collimated light-emitting diodes (LEDs) were used for all light-mediated reactions. LED light intensities were modulated by a Thorlabs LED D1B T-cube driver and measured by a Newport optical power/energy meter model 842 PE with a Newport 884-IGR OD3 attenuator.

General Procedure for Oxygen-Free Filling of the Cell: The reagent solution was placed in a reaction vial and degassed by passing a continuous stream of dry argon through the solution. The outlet was connected to the stop-flow cell, while simultaneously purging the reaction chamber. After 10 min of sparging both solution and the stop-flow cell, the reagent was transferred into the stop-flow cell via a cannula transfer process. The required time for this filling process can be adjusted by regulating the pressure of the inert gas. Experimentally, slow filling (approx. 30 s) has proven most successful for uniform substrate wetting. Finally, the outlet and inlet valves were closed (in that order) and the stop-flow cell was left to react for a given amount of time (with either the light source on or off). For multistep processes, the chamber was rigorously rinsed with 10 mL of *N*-methyl-2-pyrrolidone (NMP) and 20 mL dichloromethane (DCM) (unless noted otherwise) between individual steps.

Light-Mediated Polymerization and Dehalogenation: Wafer preparation and immobilization of α -bromoisobutyrate (initiating species) on silicon substrates was performed following previously published procedures.^[32] Unless otherwise noted, all light-mediated polymerizations were carried out at a light intensity of 5.6 $\mu\text{W mm}^{-2}$ and in a 1:4 v/v mixture of catalyst solution (1.2 mg mL⁻¹ tris[2-phenylpyridinato-C²,N]iridium(III) (*fac*-Ir(ppy)₃) in NMP) to monomer, as previously reported.^[32] Dehalogenation reactions were performed according to previously reported conditions^[43] by flooding the chamber with dehalogenation solution and irradiation for 4 h with $\lambda = 405$ nm light.

ATRP of 1H,1H,2H,2H-Perfluorodecyl Methacrylate: Inhibitor was removed from 1H,1H,2H,2H-perfluorooctyl methacrylate (PFOMA) by flowing the monomer through a short plug of basic alumina. PFOMA (708 μL , 2.45 mmol) and *N,N,N',N',N''*-pentamethyldiethylenetriamine (PMDETA) (63 μL , 0.3 mmol) were dissolved in 10 mL of *N,N*-dimethylformamide (DMF). The solution was sparged under stirring and argon flow for 30 min before transfer to a second, previously degassed vial containing 28 mg (0.2 mmol) copper(I) bromide (CuBr). The resulting PFOMA/PMDETA/CuBr/DMF solution was sparged for another 30 min before transfer into previously degassed vials containing the SiO₂ substrates. The polymerization was terminated by opening the vial to air, followed by repeated rinsing of the wafers with DMF and DCM.

UV Thiol-ene “Click” Reaction of 1H,1H,2H,2H-Perfluorodecanethiol: PEGMA (average $M_n = 300$ g mol⁻¹) and VMA were copolymerized (1:1 mol%) via Ir(ppy)₃-catalyzed polymerization on functionalized SiO₂ wafers according to the method described above. Thiol-ene coupling was carried out between the surface-anchored vinyl moieties in the backbone of the polymer brushes and 1H,1H,2H,2H-perfluorodecanethiol (PFDT) by flooding the stop-flow cell with a solution of PFDT (0.9 mL, 3.1 mmol), 2,2-dimethoxy-2-phenylacetophenone (DMPA) (30 mg, 0.12 mmol), and butylated hydroxytoluene (BHT) (15 mg, 0.07 mmol) in 1.35 mL chlorobenzene and irradiation with $\lambda = 365$ nm light for 2 h.

Visible-Light-Mediated Thiol-ene Click Reaction of 1H,1H,2H,2H-Perfluorodecanethiol: Modifying a previously published method,^[50] within the stop-flow cell, a uniformly covered a 50:50 mol% statistical copolymer brush composed of PEGMA and VMA (thickness 51.1 \pm 0.5 nm) with was covered with a solution of PFDT (0.8 mL, 2.8 mmol), tris(2,2'-bipyridyl) ruthenium(II)chloride hexahydrate (Ru(bpy)₃Cl₂ · 6H₂O, 0.6 mg, 0.8 mmol), and 4-decylniline (2 mg, 8.6 mmol) in 2.5 mL NMP. Irradiation with $\lambda = 405$ nm light afforded patterned substrates after 30 min at 79% yield (as determined by XPS, see Supporting Information).

Instrumentation and Analysis: Film thicknesses were measured with a Filmetrics F20 by setting silicon oxide (100 nm) as the first layer and the polymer brush as the second layer. Optical images were captured with a Nikon Ellipse E600 optical microscope. Tapping mode atomic force images were recorded using a MFP-3D system (Asylum Research, Santa Barbara, CA). The measurements were conducted using commercial Si cantilevers. XPS was performed using a Kratos Axis Ultra Spectrometer (Kratos Analytical, Manchester, UK) with a monochromatic aluminum K_α X-ray source (1486.6 eV) operating at 225 W under a vacuum of 10⁻⁸ Torr. Charge compensation was carried out by injection of low-energy electrons into the magnetic lens of the electron spectrometer. The analyzer pass energy was set at 20 eV for high-resolution spectra, and data were recorded at intervals of 0.05 eV. Survey spectra were recorded at 80 eV pass energy. Spectra were analyzed using CasaXPS v.2.3.16 software (Casa Software Ltd.). Unless noted otherwise, XPS spectra were normalized with respect to the carbonyl peak at a binding energy of 288.96 eV. SIMS imaging was performed using a Cameca IMS 7f system (Cameca SAS, Gennevilliers, France). A 10 kV Cs⁺ ion beam and 5 kV negative sample potential were used, for a total impact energy of 15 kV. The 150 pA primary beam was focused to a spot size of approximately 1 μm , and rastered over a 400 $\mu\text{m} \times 400 \mu\text{m}$ area. Images of negatively charged secondary ions were typically collected for 20 to 60 s, depending on signal strength. The approximate film etching rate during imaging was 4 Å min^{-1} . The reported contact angles were measured using an OCA 15Pro optical contact-angle measuring instrument (Dataphysics). A 1 μL droplet of deionized water was deposited on the samples and allowed to equilibrate for ≈ 10 s. Then, the shape of droplet was modeled as a truncated sphere. The reported contact angles are the angles between the tangent and the base of the truncated sphere at the liquid–solid–vapor triple line.

Supporting Information

Supporting Information is available from the Wiley Online Library or from the author.

Acknowledgements

The authors dedicate this work to the late Prof. Edward J. Kramer. C.W.P. acknowledges the Alexander von Humboldt Foundation for financial support. This work was in part supported by the MRSEC Program of the National Science Foundation under Award No. DMR 1121053, the Office of Naval Research (ONR) through Award No. N000141110325, and the Institute for Collaborative Biotechnologies through Grant No. W911NF-09-0001 from the U.S. Army Research Office. K.M.M. and E.H.D. thank the NSF Graduate Research Fellowship for funding. B.N. thanks the Development and Promotion of Science and Technology Talents Project, Royal Government of Thailand Fellowship for funding. B.N., K.M.M., and C.J.H. also thank the PREM program of the National Science Foundation (DMR-1205194) for partial support. The authors thank Dr. Thomas E. Mates for help with acquisition of SIMS data, and Dr. Yair Kaufmann for determination of contact angles. The authors also appreciate fruitful discussions with Dr. Lewis Manring and Prof. Ryan Hayward.

Received: June 1, 2016

Revised: July 14, 2016

Published online:

- [1] E. Almeida, T. C. Diamantino, O. de Sousa, *Prog. Org. Coatings* **2007**, *59*, 2.
- [2] H. Murata, B. J. Chang, O. Prucker, M. Dahm, J. Ruhe, *Surf. Sci.* **2004**, *570*, 111.
- [3] S. Liang, N. M. Neisius, S. Gaan, *Prog. Org. Coatings* **2013**, *76*, 1642.

- [4] K. Norrman, A. Ghanbari-Siahkali, N. B. Larsen, *Annu. Rep. Prog. Chem., Sect. C* **2005**, *101*, 174.
- [5] B. Zhao, W. J. Brittain, *Prog. Polym. Sci.* **2000**, *25*, 677.
- [6] R. Barbey, L. Lavanant, D. Paripovic, N. Schüwer, C. Sugnaux, S. Tugulu, H. Klok, *Chem. Rev.* **2009**, *109*, 5437.
- [7] F. A. Leibfarth, K. M. Mattson, B. P. Fors, H. A. Collins, C. J. Hawker, *Angew. Chem., Int. Ed.* **2013**, *52*, 199.
- [8] B. P. Fors, C. J. Hawker, *Angew. Chem., Int. Ed.* **2012**, *51*, 8850.
- [9] S. Dadashi-Silab, M. Atilla Tasdelen, Y. Yagci, *J. Polym. Sci., Part A: Polym. Chem.* **2014**, *52*, 2878.
- [10] K. Matyjaszewski, J. Xia, *Chem. Rev.* **2001**, *101*, 2921.
- [11] Z. Nie, E. Kumacheva, *Nat. Mater.* **2008**, *7*, 277.
- [12] O. Azzaroni, *J. Polym. Sci., Part A: Polym. Chem.* **2012**, *50*, 3225.
- [13] C. W. Pester, J. E. Poelma, B. Narupai, S. N. Patel, G. M. Su, T. E. Mates, Y. Luo, C. K. Ober, C. J. Hawker, E. J. Kramer, *J. Polym. Sci., Part A: Polym. Chem.* **2016**, *54*, 253.
- [14] B. Li, B. Yu, Q. Ye, F. Zhou, *Acc. Chem. Res.* **2015**, *48*, 229.
- [15] M. E. Welch, C. K. Ober, *J. Polym. Sci., Part B: Polym. Phys.* **2013**, *51*, 1457.
- [16] X. Zhou, X. Liu, Z. Xie, Z. Zheng, *Nanoscale* **2011**, *3*, 4929.
- [17] T. Chen, I. Amin, R. Jordan, *Chem. Soc. Rev.* **2012**, *41*, 3280.
- [18] U. Schmelmer, A. Paul, A. Küller, M. Steenackers, A. Ulman, M. Grunze, A. Götzhäuser, R. Jordan, *Small* **2007**, *3*, 459.
- [19] A. Olivier, F. Meyer, J. M. Raquez, P. Damman, P. Dubois, *Prog. Polym. Sci.* **2012**, *37*, 157.
- [20] T. Wu, K. Efimenko, J. Genzer, *J. Am. Chem. Soc.* **2002**, *124*, 9394.
- [21] S. Minko, D. Usov, E. Goreschnik, M. Stamm, *Macromol. Rapid Commun.* **2001**, *22*, 206.
- [22] E. Wischerhoff, K. Uhlig, A. Lankenau, H. G. Börner, A. Laschewsky, C. Duschl, J.-F. Lutz, *Angew. Chem., Int. Ed.* **2008**, *47*, 5666.
- [23] J. Buensow, T. S. Kelby, W. T. S. Huck, *Acc. Chem. Res.* **2010**, *43*, 466.
- [24] O. Azzaroni, B. Trappmann, P. Van Rijn, F. Zhou, B. Kong, W. T. S. Huck, *Angew. Chem., Int. Ed.* **2006**, *45*, 7440.
- [25] F. Zhou, P. M. Biesheuvel, E. Y. Choi, W. Shu, R. Poetes, U. Steiner, W. T. S. Huck, *Nano Lett.* **2008**, *8*, 725.
- [26] P. M. Mendes, *Chem. Soc. Rev.* **2008**, *37*, 2512.
- [27] N. Ayres, *Polym. Chem.* **2010**, *1*, 769.
- [28] Q. Wei, T. Becherer, S. Angioletti-Uberti, J. Dzubielka, C. Wischke, A. T. Neffe, A. Lendlein, M. Ballauff, R. Haag, *Angew. Chem., Int. Ed.* **2014**, *53*, 8004.
- [29] K. Wolski, M. Szuwarzyński, M. Kopec, S. Zapotoczny, *Eur. Polym. J.* **2015**, *65*, 155.
- [30] R. D. Piner, J. Zhu, F. Xu, S. Hong, C. A. Mirkin, *Science* **1999**, *283*, 661.
- [31] W. Eck, V. Stadler, W. Geyer, M. Zharnikov, A. Götzhäuser, M. Grunze, *Adv. Mater.* **2000**, *12*, 805.
- [32] J. E. Poelma, B. P. Fors, G. F. Meyers, J. W. Kramer, C. J. Hawker, *Angew. Chem., Int. Ed.* **2013**, *52*, 6844.
- [33] E. H. Discekici, C. W. Pester, N. J. Treat, J. Lawrence, K. M. Mattson, B. Narupai, E. P. Tourmaysan, Y. Luo, A. J. McGrath, P. G. Clark, J. Read de Alaniz, C. J. Hawker, *ACS Macro Lett.* **2016**, *5*, 258.
- [34] M. Kaholek, W. K. Lee, B. LaMattina, K. C. Caster, S. Zauscher, *Nano Lett.* **2004**, *4*, 373.
- [35] A. Rastogi, M. Y. Paik, M. Tanaka, C. K. Ober, *ACS Nano* **2010**, *4*, 771.
- [36] S. Sun, M. Montague, K. Critchley, M.-S. Chen, W. J. Dressick, S. D. Evans, G. J. Leggett, *Nano Lett.* **2006**, *6*, 29.
- [37] G. M. Whitesides, Y. Xia, *Angew. Chem., Int. Ed.* **1998**, *37*, 551.
- [38] F. Zhou, Z. Zheng, B. Yu, W. Liu, W. T. S. Huck, *J. Am. Chem. Soc.* **2006**, *128*, 16253.
- [39] S. Alom Ruiz, C. S. Chen, *Soft Matter* **2007**, *3*, 168.
- [40] M. Steenackers, R. Jordan, A. Küller, M. Grunze, *Adv. Mater.* **2009**, *21*, 2921.
- [41] P. Xiao, J. Zhang, F. Dumur, M. A. Tehfe, F. Morlet-Savary, B. Graff, D. Gigmes, J. P. Fouassier, J. Lalevée, *Prog. Polym. Sci.* **2015**, *41*, 32.
- [42] J. Lalevée, S. Telitel, P. Xiao, M. Lepeltier, F. Dumur, F. Morlet-Savary, D. Gigmes, J. P. Fouassier, *Beilstein J. Org. Chem.* **2014**, *10*, 863.
- [43] K. M. Mattson, C. W. Pester, W. R. Gutekunst, A. T. Hsueh, E. H. Discekici, Y. Luo, B. V. K. J. Schmidt, A. J. McGrath, P. G. Clark, C. J. Hawker, unpublished.
- [44] B. P. Fors, J. E. Poelma, M. S. Menyo, M. J. Robb, D. M. Spokoyny, J. W. Kramer, J. H. Waite, C. J. Hawker, *J. Am. Chem. Soc.* **2013**, *135*, 14106.
- [45] J. D. Nguyen, J. W. Tucker, M. D. Konieczynska, C. R. J. Stephenson, *J. Am. Chem. Soc.* **2011**, *133*, 4160.
- [46] R. M. Arnold, D. L. Patton, V. V. Popik, J. Locklin, *Acc. Chem. Res.* **2014**, *47*, 2999.
- [47] D. Dendukuri, S. S. Gu, D. C. Pregibon, T. A. Hatton, P. S. Doyle, *Lab Chip* **2007**, *7*, 818.
- [48] H. Wu, T. W. Odom, G. M. Whitesides, *Anal. Chem.* **2002**, *74*, 3267.
- [49] C. E. Hoyle, C. N. Bowman, *Angew. Chem., Int. Ed.* **2010**, *49*, 1540.
- [50] J. Xu, C. Boyer, *Macromolecules* **2015**, *48*, 520.
- [51] L. Makkonen, *Langmuir* **2000**, *16*, 7669.

Bibliography

- [1] K. Matyjaszewski and N. V. Tsarevsky, “Nanostructured functional materials prepared by atom transfer radical polymerization,” *Nature Chemistry*, vol. 1, pp. 276–288, June 2009.
- [2] G. Odian, *Principles of Polymerization*. John Wiley & Sons, 4 ed., 2004.
- [3] S. Yamago and Y. Nakamura, “Recent progress in the use of photoirradiation in living radical polymerization,” *Polymer*, vol. 54, pp. 981–994, Feb. 2013.
- [4] K. Matyjaszewski and N. V. Tsarevsky, “Macromolecular engineering by atom transfer radical polymerization,” *Journal of the American Chemical Society*, vol. 136, pp. 6513–6533, May 2014.
- [5] K. Matyjaszewski, “Atom Transfer Radical Polymerization (ATRP): Current Status and Future Perspectives,” *Macromolecules*, vol. 45, no. 10, pp. 4015–4039, 2012.
- [6] M. Destarac, “Controlled Radical Polymerization: Industrial Stakes, Obstacles and Achievements,” *Macromolecular Reaction Engineering*, vol. 4, no. 3-4, pp. 165–179, 2010.
- [7] H.-C. Kim, S.-M. Park, and W. D. Hinsberg, “Block copolymer based nanostructures: materials, processes, and applications to electronics,” *Chemical Reviews*, vol. 110, pp. 146–177, Jan. 2010.
- [8] G. H. Fredrickson and F. S. Bates, “Dynamics of block copolymers: theory and experiment,” *Annual Review of Materials Science*, 1996.
- [9] F. S. Bates and G. H. Fredrickson, “Block copolymer thermodynamics: theory and experiment,” *Annual Review of Physical Chemistry*, vol. 41, pp. 525–557, 1990.
- [10] A. Hirao, R. Goseki, and T. Ishizone, “Advances in Living Anionic Polymerization: From Functional Monomers, Polymerization Systems, to Macromolecular Architectures,” *Macromolecules*, vol. 47, pp. 1883–1905, Mar. 2014.
- [11] D. Baskaran and A. H. E. Müller, “Anionic vinyl polymerization - 50 years after Michael Szwarc,” *Progress in Polymer Science*, vol. 32, pp. 173–219, Feb. 2007.

- [12] W. A. Braunecker and K. Matyjaszewski, "Controlled/living radical polymerization: Features, developments, and perspectives," *Progress in Polymer Science*, vol. 32, pp. 93–146, Jan. 2007.
- [13] C. J. Hawker, "Molecular Weight Control by a "Living" Free-Radical Polymerization Process," *Journal of the American Chemical Society*, vol. 116, pp. 11185–11186, Nov. 1994.
- [14] J.-S. Wang and K. Matyjaszewski, "Controlled/"living" radical polymerization. Atom transfer radical polymerization in the presence of transition-metal complexes," *Journal of the American Chemical Society*, vol. 117, pp. 5614–5615, May 1995.
- [15] M. Kato, M. Kamigaito, M. Sawamoto, and T. Higashimura, "Polymerization of Methyl Methacrylate with the Carbon Tetrachloride/Dichlorotris- (triphenylphosphine)ruthenium(II)/Methylaluminum Bis(2,6-di-tert-butylphenoxide) Initiating System: Possibility of Living Radical Polymerization," *Macromolecules*, vol. 28, pp. 1721–1723, Sept. 1995.
- [16] J. Chiefari, Y. K. B. Chong, F. Ercole, J. Krstina, J. Jeffery, T. P. T. Le, R. T. A. Mayadunne, G. F. Meijs, C. L. Moad, G. Moad, E. Rizzardo, and S. H. Thang, "Living free-radical polymerization by reversible addition-fragmentation chain transfer: The RAFT process," *Macromolecules*, vol. 31, pp. 5559–5562, Aug. 1998.
- [17] M. K. Georges, R. P. N. Veregin, P. M. Kazmaier, and G. K. Hamer, "Narrow molecular weight resins by a free-radical polymerization process," *Macromolecules*, vol. 26, pp. 2987–2988, May 1993.
- [18] J. Nicolas, Y. Guillaneuf, C. Lefay, D. Bertin, D. Gigmes, and B. Charleux, "Nitroxide-mediated polymerization," *Progress in Polymer Science*, vol. 38, pp. 63–235, Jan. 2013.
- [19] D. Benoit, V. Chaplinski, R. Braslau, and C. J. Hawker, "Development of a Universal Alkoxyamine for "Living" Free Radical Polymerizations," *Journal of the American Chemical Society*, vol. 121, pp. 3904–3920, Apr. 1999.
- [20] R. B. Grubbs, "Nitroxide-Mediated Radical Polymerization: Limitations and Versatility," *Polymer Reviews*, vol. 51, pp. 104–137, Apr. 2011.
- [21] K. Matyjaszewski and J. Spanswick, "Controlled/living radical polymerization," *Materials Today*, vol. 8, pp. 26–33, Mar. 2005.
- [22] G. Moad, E. Rizzardo, and S. H. Thang, "Living Radical Polymerization by the RAFT Process – A Third Update," *Australian Journal of Chemistry*, vol. 65, pp. 985–1076, July 2012.

- [23] H. Willcock and R. K. O'Reilly, "End group removal and modification of RAFT polymers," *Polymer Chemistry*, vol. 1, no. 2, pp. 149–157, 2010.
- [24] F. Canturk, B. Karagoz, and N. Bicak, "Removal of the copper catalyst from atom transfer radical polymerization mixtures by chemical reduction with zinc powder," *Journal of Polymer Science Part A: Polymer Chemistry*, vol. 49, pp. 3536–3542, June 2011.
- [25] K. Matyjaszewski, T. Pintauer, and S. Gaynor, "Removal of Copper-Based Catalyst in Atom Transfer Radical Polymerization Using Ion Exchange Resins," *Macromolecules*, vol. 33, pp. 1476–1478, Feb. 2000.
- [26] T. Pintauer and K. Matyjaszewski, "Atom transfer radical addition and polymerization reactions catalyzed by ppm amounts of copper complexes," *Chemical Society Reviews*, vol. 37, no. 6, pp. 1087–1097, 2008.
- [27] Y. Kwak, A. J. D. Magenau, and K. Matyjaszewski, "ARGET ATRP of Methyl Acrylate with Inexpensive Ligands and ppm Concentrations of Catalyst," *Macromolecules*, vol. 44, pp. 811–819, Feb. 2011.
- [28] N. J. Treat, H. Sprafke, J. W. Kramer, P. G. Clark, B. E. Barton, J. Read de Alaniz, B. P. Fors, and C. J. Hawker, "Metal-Free Atom Transfer Radical Polymerization," *Journal of the American Chemical Society*, vol. 136, pp. 16096–16101, Nov. 2014.
- [29] X. Pan, C. Fang, M. Fantin, N. Malhotra, W. Y. So, L. A. Peteanu, A. A. Isse, A. Gennaro, P. Liu, and K. Matyjaszewski, "Mechanism of Photoinduced Metal-Free Atom Transfer Radical Polymerization: Experimental and Computational Studies," *Journal of the American Chemical Society*, vol. 138, pp. 2411–2425, Feb. 2016.
- [30] R. Barbey, L. Lavanant, D. Paripovic, N. Schüwer, C. Sugnaux, S. Tugulu, and H.-A. Klok, "Polymer brushes via surface-initiated controlled radical polymerization: synthesis, characterization, properties, and applications.," *Chemical Reviews*, vol. 109, pp. 5437–5527, Nov. 2009.
- [31] A. Olivier, F. Meyer, J.-M. Raquez, P. Damman, and P. Dubois, "Surface-initiated controlled polymerization as a convenient method for designing functional polymer brushes: From self-assembled monolayers to patterned surfaces," *Progress in Polymer Science*, vol. 37, pp. 157–181, Jan. 2012.
- [32] O. Azzaroni, "Polymer brushes here, there, and everywhere: Recent advances in their practical applications and emerging opportunities in multiple research fields," *Journal of Polymer Science Part A: Polymer Chemistry*, vol. 50, pp. 3225–3258, May 2012.

- [33] J. Choi, P. Schattling, F. D. Jochum, J. Pyun, K. Char, and P. Theato, "Functionalization and patterning of reactive polymer brushes based on surface reversible addition and fragmentation chain transfer polymerization," *Journal of Polymer Science Part A: Polymer Chemistry*, vol. 50, pp. 4010–4018, Oct. 2012.
- [34] S. Edmondson, V. L. Osborne, and W. T. S. Huck, "Polymer brushes via surface-initiated polymerizations," *Chemical Society Reviews*, vol. 33, no. 1, pp. 14–22, 2004.
- [35] M. Husseman, E. E. Malmström, M. McNamara, M. Mate, D. Mecerreyes, D. G. Benoit, J. L. Hedrick, P. Mansky, E. Huang, T. P. Russell, and C. J. Hawker, "Controlled Synthesis of Polymer Brushes by "Living" Free Radical Polymerization Techniques," *Macromolecules*, vol. 32, pp. 1424–1431, Mar. 1999.
- [36] K. Matyjaszewski, P. J. Miller, N. Shukla, B. Immaraporn, A. Gelman, B. B. Luokala, T. M. Siclovan, G. Kickelbick, T. Vallant, H. Hoffmann, and T. Pakula, "Polymers at Interfaces: Using Atom Transfer Radical Polymerization in the Controlled Growth of Homopolymers and Block Copolymers from Silicon Surfaces in the Absence of Untethered Sacrificial Initiator," *Macromolecules*, vol. 32, pp. 8716–8724, Dec. 1999.
- [37] E. H. Discekici, C. W. Pester, N. J. Treat, J. Lawrence, K. M. Mattson, B. Narupai, E. P. Toumayan, Y. Luo, A. J. McGrath, P. G. Clark, J. Read de Alaniz, and C. J. Hawker, "Simple Benchtop Approach to Polymer Brush Nanostructures Using Visible-Light-Mediated Metal-Free Atom Transfer Radical Polymerization," *ACS Macro Letters*, vol. 5, pp. 258–262, Feb. 2016.
- [38] F. A. Leibfarth, K. M. Mattson, B. P. Fors, H. A. Collins, and C. J. Hawker, "External regulation of controlled polymerizations," *Angewandte Chemie (International ed. in English)*, vol. 52, pp. 199–210, Jan. 2013.
- [39] B. P. Fors and C. J. Hawker, "Control of a Living Radical Polymerization of Methacrylates by Light," *Angewandte Chemie International Edition*, vol. 51, pp. 8850–8853, July 2012.
- [40] P. Xiao, J. Zhang, F. Dumur, M. A. Tehfe, F. Morlet-Savary, B. Graff, D. Gigmes, J. P. Fouassier, and J. Lalevée, "Visible light sensitive photoinitiating systems: Recent progress in cationic and radical photopolymerization reactions under soft conditions," *Progress in Polymer Science*, vol. 41, pp. 32–66, Feb. 2015.
- [41] M. Chen, M. Zhong, and J. A. Johnson, "Light-Controlled Radical Polymerization: Mechanisms, Methods, and Applications," *Chemical Reviews*, p. acs.chemrev.5b00671, Mar. 2016.

- [42] S. Chatani, C. J. Kloxin, and C. N. Bowman, "The power of light in polymer science: photochemical processes to manipulate polymer formation, structure, and properties," *Polymer Chemistry*, vol. 5, no. 7, pp. 2187–2201, 2014.
- [43] N. Corrigan, S. Shanmugam, J. Xu, and C. Boyer, "Photocatalysis in organic and polymer synthesis," *Chemical Society Reviews*, 2016.
- [44] X. Pan, M. A. Tasdelen, J. Laun, T. Junkers, Y. Yagci, and K. Matyjaszewski, "Photomediated Controlled Radical Polymerization," *Progress in Polymer Science*, July 2016.
- [45] J. T. Trotta and B. P. Fors, "Organic Catalysts for Photocontrolled Polymerizations," *Synlett*, vol. 27, no. 05, pp. 702–713–713, 2016.
- [46] X. Zhou, X. Liu, Z. Xie, and Z. Zheng, "3D-patterned polymer brush surfaces," *Nanoscale*, vol. 3, no. 12, pp. 4929–4939, 2011.
- [47] J. E. Poelma, B. P. Fors, G. F. Meyers, J. W. Kramer, and C. J. Hawker, "Fabrication of Complex Three-Dimensional Polymer Brush Nanostructures through Light-Mediated Living Radical Polymerization," *Angewandte Chemie International Edition*, vol. 52, pp. 6844–6848, June 2013.
- [48] M. Szwarc, "Living Polymers," *Nature*, vol. 178, no. 4543, pp. 1168–1169, 1956.
- [49] M. Szwarc, M. Levy, and R. Milkovich, "Polymerization initiated by electron transfer to monomer. A new method of formation of block polymers," *Journal of the American Chemical Society*, vol. 78, pp. 2656–2657, June 1956.
- [50] J. E. Moses and A. D. Moorhouse, "The growing applications of click chemistry," *Chemical Society Reviews*, vol. 36, no. 8, p. 1249, 2007.
- [51] U. Mansfeld, C. Pietsch, R. Hoogenboom, C. R. Becer, and U. S. Schubert, "Clickable initiators, monomers and polymers in controlled radical polymerizations – a prospective combination in polymer science," *Polymer Chemistry*, vol. 1, no. 10, p. 1560, 2010.
- [52] H. C. Kolb, M. G. Finn, and K. B. Sharpless, "Click Chemistry: Diverse Chemical Function from a Few Good Reactions," *Angewandte Chemie (International ed. in English)*, vol. 40, pp. 2004–2021, June 2001.
- [53] C. J. Hawker and K. L. Wooley, "The Convergence of Synthetic Organic and Polymer Chemistries," *Science*, vol. 309, pp. 1200–1205, Aug. 2005.
- [54] A. B. Lowe, "Thiol-yne 'click'/coupling chemistry and recent applications in polymer and materials synthesis and modification," *Polymer*, vol. 55, pp. 5517–5549, Oct. 2014.

- [55] C. E. Hoyle and C. N. Bowman, "Thiol-ene click chemistry," *Angewandte Chemie (International ed. in English)*, vol. 49, pp. 1540–1573, Feb. 2010.
- [56] C. E. Hoyle, A. B. Lowe, and C. N. Bowman, "Thiol-click chemistry: a multifaceted toolbox for small molecule and polymer synthesis," *Chemical Society Reviews*, vol. 39, no. 4, p. 1355, 2010.
- [57] M. J. Kade, D. J. Burke, and C. J. Hawker, "The power of thiol-ene chemistry," *Journal of Polymer Science Part A: Polymer Chemistry*, vol. 48, pp. 743–750, Feb. 2010.
- [58] C. E. Hoyle, T. Y. Lee, and T. Roper, "Thiol-enes: Chemistry of the past with promise for the future," *Journal of Polymer Science Part A: Polymer Chemistry*, vol. 42, no. 21, pp. 5301–5338, 2004.
- [59] S. P. S. Koo, M. M. Stamenović, R. A. Prasath, A. J. Inglis, F. E. Du Prez, C. Barner-Kowollik, W. Van Camp, and T. Junkers, "Limitations of radical thiol-ene reactions for polymer-polymer conjugation," *Journal of Polymer Science Part A: Polymer Chemistry*, vol. 48, pp. 1699–1713, Apr. 2010.
- [60] C. Barner-Kowollik, F. E. Du Prez, P. Espeel, C. J. Hawker, T. Junkers, H. Schlaad, and W. Van Camp, "'Clicking' Polymers or Just Efficient Linking: What Is the Difference?," *Angewandte Chemie International Edition*, vol. 50, pp. 60–62, Dec. 2010.
- [61] C. J. Hawker, A. W. Bosman, and E. Harth, "New Polymer Synthesis by Nitroxide Mediated Living Radical Polymerizations," *Chemical Reviews*, vol. 101, pp. 3661–3688, Dec. 2001.
- [62] G. Moad, E. Rizzardo, and S. H. Thang, "Radical addition–fragmentation chemistry in polymer synthesis," *Polymer*, vol. 49, pp. 1079–1131, Mar. 2008.
- [63] S. Perrier and P. Takolpuckdee, "Macromolecular design via reversible addition-fragmentation chain transfer (RAFT)/xanthates (MADIX) polymerization," *Journal of Polymer Science Part A: Polymer Chemistry*, vol. 43, no. 22, pp. 5347–5393, 2005.
- [64] O. Altintas, T. Josse, M. Abbasi, J. De Winter, V. Trouillet, P. Gerbaux, M. Wilhelm, and C. Barner-Kowollik, "ATRP-based polymers with modular ligation points under thermal and thermomechanical stress," *Polymer Chemistry*, vol. 6, no. 15, pp. 2854–2868, 2015.
- [65] Y. K. Chong, G. Moad, E. Rizzardo, and S. H. Thang, "Thiocarbonylthio End Group Removal from RAFT-Synthesized Polymers by Radical-Induced Reduction," *Macromolecules*, vol. 40, pp. 4446–4455, June 2007.

- [66] J. Bibiao, F. Jianbo, Y. Yang, R. Qiang, W. Wenyun, and H. Jianjun, "Modification of the halogen end groups of polystyrene prepared by ATRP," *European Polymer Journal*, vol. 42, pp. 179–187, Jan. 2006.
- [67] V. Coessens and K. Matyjaszewski, "Dehalogenation of polymers prepared by atom transfer radical polymerization," *Macromolecular Rapid Communications*, vol. 20, pp. 66–70, Feb. 1999.
- [68] T. Chen, I. Amin, and R. Jordan, "Patterned polymer brushes," *Chemical Society Reviews*, vol. 41, no. 8, pp. 3280–3296, 2012.
- [69] A. Rastogi, M. Y. Paik, M. Tanaka, and C. K. Ober, "Direct Patterning of Intrinsically Electron Beam Sensitive Polymer Brushes," *ACS Nano*, vol. 4, pp. 771–780, Feb. 2010.
- [70] S. Tugulu, M. Harms, M. Fricke, D. Volkmer, and H.-A. Klok, "Polymer Brushes as Ionotropic Matrices for the Directed Fabrication of Microstructured Calcite Thin Films," *Angewandte Chemie International Edition*, vol. 45, pp. 7458–7461, Nov. 2006.
- [71] O. Prucker, M. Schimmel, G. Tovar, W. Knoll, and J. Ruhe, "Microstructuring of Molecularly Thin Polymer Layers by Photolithography," *Advanced Materials*, vol. 10, pp. 1073–1077, Oct. 1998.
- [72] S. Sun, M. Montague, K. Critchley, M.-S. Chen, W. J. Dressick, S. D. Evans, and G. J. Leggett, "Fabrication of Biological Nanostructures by Scanning Near-Field Photolithography of Chloromethylphenylsiloxane Monolayers," *Nano Letters*, vol. 6, pp. 29–33, Jan. 2006.
- [73] F. Zhou, L. Jiang, W. Liu, and Q. Xue, "Fabrication of Chemically Tethered Binary Polymer-Brush Pattern through Two-Step Surface-Initiated Atomic-Transfer Radical Polymerization," *Macromolecular Rapid Communications*, vol. 25, pp. 1979–1983, Dec. 2004.
- [74] B. P. Fors, J. E. Poelma, M. S. Menyo, M. J. Robb, D. M. Spokoyny, J. W. Kramer, J. H. Waite, and C. J. Hawker, "Fabrication of Unique Chemical Patterns and Concentration Gradients with Visible Light," *Journal of the American Chemical Society*, vol. 135, no. 38, pp. 14106–14109, 2013.
- [75] C. W. Pester, J. E. Poelma, B. Narupai, S. N. Patel, G. M. Su, T. E. Mates, Y. Luo, C. K. Ober, C. J. Hawker, and E. J. Kramer, "Ambiguous anti-fouling surfaces: Facile synthesis by light-mediated radical polymerization," *Journal of Polymer Science Part A: Polymer Chemistry*, vol. 54, pp. 253–262, Aug. 2015.

- [76] E. H. Discekici, N. J. Treat, S. O. Poelma, K. M. Mattson, Z. M. Hudson, Y. Luo, C. J. Hawker, and J. R. de Alaniz, "A highly reducing metal-free photoredox catalyst: design and application in radical dehalogenations," *Chemical Communications*, vol. 51, no. 58, pp. 11705–11708, 2015.
- [77] S. O. Poelma, G. L. Burnett, E. H. Discekici, K. M. Mattson, N. J. Treat, Y. Luo, Z. M. Hudson, S. L. Shankel, P. G. Clark, J. W. Kramer, C. J. Hawker, and J. Read de Alaniz, "Chemoselective Radical Dehalogenation and C–C Bond Formation on Aryl Halide Substrates Using Organic Photoredox Catalysts," *The Journal of Organic Chemistry*, vol. 81, pp. 7155–7160, Aug. 2016.
- [78] X. Huang and M. J. Wirth, "Surface-Initiated Radical Polymerization on Porous Silica," *Analytical Chemistry*, vol. 69, pp. 4577–4580, Nov. 1997.
- [79] F. Zhou, Z. Zheng, B. Yu, W. Liu, and W. T. S. Huck, "Multicomponent polymer brushes," *Journal of the American Chemical Society*, vol. 128, pp. 16253–16258, Dec. 2006.
- [80] T. Chen, R. Jordan, and S. Zauscher, "Extending micro-contact printing for patterning complex polymer brush microstructures," *Polymer*, vol. 52, pp. 2461–2467, May 2011.
- [81] N. Balachander and C. N. Sukenik, "Monolayer transformation by nucleophilic substitution: Applications to the creation of new monolayer assemblies," *Langmuir*, vol. 6, pp. 1621–1627, Nov. 1990.
- [82] B. V. K. J. Schmidt, M. Hetzer, H. Ritter, and C. Barner-Kowollik, "Cyclodextrin-Complexed RAFT Agents for the Ambient Temperature Aqueous Living/Controlled Radical Polymerization of Acrylamido Monomers," *Macromolecules*, vol. 44, pp. 7220–7232, Sept. 2011.
- [83] J. Skey and R. K. O'Reilly, "Facile one pot synthesis of a range of reversible addition–fragmentation chain transfer (RAFT) agents," *Chemical Communications*, no. 35, p. 4183, 2008.
- [84] S. Yamago, "Precision Polymer Synthesis by Degenerative Transfer Controlled/Living Radical Polymerization Using Organotellurium, Organostibine, and Organobismuthine Chain-Transfer Agents," *Chemical Reviews*, vol. 109, pp. 5051–5068, Nov. 2009.
- [85] A. Debuigne, R. Poli, C. Jérôme, R. Jérôme, and C. Detrembleur, "Overview of cobalt-mediated radical polymerization: Roots, state of the art and future prospects," *Progress in Polymer Science*, vol. 34, pp. 211–239, Mar. 2009.

- [86] A. Goto, Y. Tsujii, and T. Fukuda, "Reversible chain transfer catalyzed polymerization (RTCP): A new class of living radical polymerization," *Polymer*, vol. 49, pp. 5177–5185, Nov. 2008.
- [87] M. Ouchi, T. Terashima, and M. Sawamoto, "Transition Metal-Catalyzed Living Radical Polymerization: Toward Perfection in Catalysis and Precision Polymer Synthesis," *Chemical Reviews*, vol. 109, pp. 4963–5050, Nov. 2009.
- [88] J. A. M. Hepperle, H. Luftmann, and A. Studer, "Controlled nitroxide-mediated radical polymerization of methyl and phenyl vinyl ketone," *Journal of Polymer Science Part A: Polymer Chemistry*, vol. 50, pp. 2150–2160, Mar. 2012.
- [89] P. J. M. Stals, T. N. T. Phan, D. Gigmes, T. F. E. Paffen, E. W. Meijer, and A. R. A. Palmans, "Nitroxide-mediated controlled radical polymerizations of styrene derivatives," *Journal of Polymer Science Part A: Polymer Chemistry*, vol. 50, pp. 780–791, Nov. 2011.
- [90] E. Groison, S. Brusseau, F. D'Agosto, S. Magnet, R. Inoubli, L. Couvreur, and B. Charleux, "Well-Defined Amphiphilic Block Copolymer Nanoobjects via Nitroxide-Mediated Emulsion Polymerization," *ACS Macro Letters*, vol. 1, pp. 47–51, Jan. 2012.
- [91] D. Benoit, S. Grimaldi, S. Robin, J.-P. Finet, P. Tordo, and Y. Gnanou, "Kinetics and Mechanism of Controlled Free-Radical Polymerization of Styrene and n-Butyl Acrylate in the Presence of an Acyclic β -Phosphonylated Nitroxide," *Journal of the American Chemical Society*, vol. 122, pp. 5929–5939, June 2000.
- [92] X. G. Qiao, M. Lansalot, E. Bourgeat-Lami, and B. Charleux, "Nitroxide-Mediated Polymerization-Induced Self-Assembly of Poly(poly(ethylene oxide) methyl ether methacrylate-co-styrene)-b-poly(n-butyl methacrylate-co-styrene) Amphiphilic Block Copolymers," *Macromolecules*, vol. 46, pp. 4285–4295, June 2013.
- [93] X. G. Qiao, P. Y. Dugas, B. Charleux, M. Lansalot, and E. Bourgeat-Lami, "Synthesis of Multipod-like Silica/Polymer Latex Particles via Nitroxide-Mediated Polymerization-Induced Self-Assembly of Amphiphilic Block Copolymers," *Macromolecules*, vol. 48, pp. 545–556, Feb. 2015.
- [94] A. C. Greene and R. B. Grubbs, "Synthesis and Evaluation of N-Phenylalkoxyamines for Nitroxide-Mediated Polymerization," *Macromolecules*, vol. 42, pp. 4388–4390, July 2009.
- [95] A. C. Greene and R. B. Grubbs, "Nitroxide-Mediated Polymerization of Methyl Methacrylate and Styrene with New Alkoxyamines from 4-Nitrophenyl 2-Methylpropionat-2-yl Radicals," *Macromolecules*, vol. 43, pp. 10320–10325, Dec. 2010.

- [96] Y. Guillaneuf, D. Gigmes, S. R. A. Marque, P. Astolfi, L. Greci, P. Tordo, and D. Bertin, "First Effective Nitroxide-Mediated Polymerization of Methyl Methacrylate," *Macromolecules*, vol. 40, pp. 3108–3114, May 2007.
- [97] J. D. Druliner, "Living radical polymerization involving oxygen-centered species attached to propagating chain ends," *Macromolecules*, vol. 24, pp. 6079–6082, Nov. 1991.
- [98] T. C. Chung, W. Janvikul, and H. L. Lu, "A novel "stable" radical initiator based on the oxidation adducts of alkyl-9-BBN," *Journal of the American Chemical Society*, vol. 118, no. 3, pp. 705–706, 1996.
- [99] M. Steenbock, M. Klapper, and K. Müllen, "Triazoliny radicals – new additives for controlled radical polymerization," *Macromolecular Chemistry and Physics*, vol. 199, pp. 763–769, May 1998.
- [100] A. Dasgupta, M. Klapper, and K. Müllen, "Controlled Polymerization of N-trimethylsilyl Methacrylamide: A New Polymethacrylamide Precursor," *Polymer Bulletin*, vol. 60, no. 2-3, pp. 199–210–210, 2008.
- [101] A. Dasgupta, T. Brand, M. Klapper, and K. Müllen, "Triazoliny-controlled radical polymerization as innovative route to poly(hydroxyethyl methacrylate)," *Polymer Bulletin*, vol. 46, no. 2-3, pp. 131–138, 2001.
- [102] S. N. Khelfallah, M. Peretolchin, M. Klapper, and K. Müllen, "Controlled radical polymerization of N,N-dimethylaminoethyl methacrylate using triazoliny as counter radical," *Polymer Bulletin*, vol. 53, no. 5, pp. 295–304, 2005.
- [103] E. K. Y. Chen, S. J. Teertstra, D. Chan-Seng, P. O. Otieno, R. G. Hicks, and M. K. Georges, "Verdazyl-Mediated Living-Radical Polymerization of Styrene and n-Butyl Acrylate," *Macromolecules*, vol. 40, pp. 8609–8616, Nov. 2007.
- [104] S. J. Teertstra, E. Chen, D. Chan-Seng, P. O. Otieno, R. G. Hicks, and M. K. Georges, "Verdazyl-Mediated Polymerization of Styrene," *Macromolecular Symposia*, vol. 248, pp. 117–125, Feb. 2007.
- [105] G. Rayner, T. Smith, W. Barton, M. Newton, R. J. Deeth, I. Prokes, G. J. Clarkson, and D. M. Haddleton, "A comparison of verdazyl radicals modified at the 3-position as mediators in the living radical polymerisation of styrene and n-butyl acrylate," *Polymer Chemistry*, vol. 3, no. 8, p. 2254, 2012.
- [106] B. Yamada, Y. Nobukane, and Y. Miura, "Radical polymerization of styrene mediated by 1,3,5-triphenylverdazyl," *Polymer Bulletin*, vol. 41, pp. 539–544, Nov. 1998.

- [107] B. D. Koivisto and R. G. Hicks, "The magnetochemistry of verdazyl radical-based materials," *Coordination Chemistry Reviews*, vol. 249, pp. 2612–2630, Dec. 2005.
- [108] H. M. Blatter and H. Lukaszewski, "A new stable free radical," *Tetrahedron Letters*, vol. 9, pp. 2701–2705, Jan. 1968.
- [109] M. Demetriou, A. A. Berezin, P. A. Koutentis, and T. Krasia-Christoforou, "Benzotriazinyl-mediated controlled radical polymerization of styrene," *Polymer International*, vol. 63, pp. 674–679, Apr. 2014.
- [110] P. Koutentis and D. Lo Re, "Catalytic Oxidation of N-Phenylamidrazones to 1,3-Diphenyl-1,4-dihydro-1,2,4-benzotriazin-4-yls: An Improved Synthesis of Blatter's Radical," *Synthesis*, vol. 2010, pp. 2075–2079, May 2010.
- [111] M. Beija, M.-T. Charreyre, and J. M. G. Martinho, "Dye-labelled polymer chains at specific sites: Synthesis by living/controlled polymerization," *Progress in Polymer Science*, vol. 36, pp. 568–602, Apr. 2011.
- [112] R. Mchale, F. Aldabbagh, and P. B. Zetterlund, "The role of excess nitroxide in the SG1 (N-tert-butyl-N-[1-diethylphosphono-(2,2-dimethylpropyl)] nitroxide)-mediated polymerization of methyl methacrylate," *Journal of Polymer Science Part A: Polymer Chemistry*, vol. 45, no. 11, pp. 2194–2203, 2007.
- [113] L. Li, L. Zhu, D. Chen, X. Hu, and R. Wang, "Use of Acylhydrazine- and Acylhydrazone-Type Ligands to Promote CuI-Catalyzed C–N Cross-Coupling Reactions of Aryl Bromides with N-Heterocycles," *European Journal of Organic Chemistry*, vol. 2011, pp. 2692–2696, May 2011.
- [114] C.-Y. Zhang, X.-H. Liu, B.-L. Wang, S.-H. Wang, and Z.-M. Li, "Synthesis and Antifungal Activities of New Pyrazole Derivatives via 1,3-dipolar Cycloaddition Reaction," *Chemical Biology & Drug Design*, vol. 75, pp. 489–493, May 2010.
- [115] C. Fruijtier-Pöllöth, "Safety assessment on polyethylene glycols (PEGs) and their derivatives as used in cosmetic products," *Toxicology*, vol. 214, pp. 1–38, Oct. 2005.
- [116] R. B. Greenwald, Y. H. Choe, J. McGuire, and C. D. Conover, "Effective drug delivery by PEGylated drug conjugates," *Advanced Drug Delivery Reviews*, vol. 55, pp. 217–250, Feb. 2003.
- [117] B. Obermeier, F. Wurm, C. Mangold, and H. Frey, "Multifunctional Poly(ethylene glycol)s," *Angewandte Chemie International Edition*, vol. 50, pp. 7988–7997, July 2011.
- [118] S. J. Sofia, V. Premnath, and E. W. Merrill, "Poly(ethylene oxide) Grafted to Silicon Surfaces: Grafting Density and Protein Adsorption," *Macromolecules*, vol. 31, pp. 5059–5070, July 1998.

- [119] A. Halperin, “Polymer Brushes that Resist Adsorption of Model Proteins: Design Parameters,” *Langmuir*, vol. 15, pp. 2525–2533, Mar. 1999.
- [120] R.-V. Ostaci, D. Damiron, S. Al Akhrass, Y. Grohens, and E. Drockenmuller, “Poly(ethylene glycol) brushes grafted to silicon substrates by click chemistry: influence of PEG chain length, concentration in the grafting solution and reaction time,” *Polymer Chemistry*, vol. 2, no. 2, pp. 348–354, 2011.
- [121] K. Knop, R. Hoogenboom, D. Fischer, and U. S. Schubert, “Poly(ethylene glycol) in Drug Delivery: Pros and Cons as Well as Potential Alternatives,” *Angewandte Chemie International Edition*, vol. 49, pp. 6288–6308, July 2010.
- [122] V. S. Wilms, H. Bauer, C. Tonhauser, A.-M. Schilman, M.-C. Müller, W. Tremel, and H. Frey, “Catechol-initiated polyethers: multifunctional hydrophilic ligands for PEGylation and functionalization of metal oxide nanoparticles,” *Biomacromolecules*, vol. 14, pp. 193–199, Jan. 2013.
- [123] B. P. Lee, P. B. Messersmith, J. N. Israelachvili, and J. H. Waite, “Mussel-Inspired Adhesives and Coatings,” *Annual Review of Materials Research*, vol. 41, pp. 99–132, July 2011.
- [124] J. H. Waite and M. L. Tanzer, “Polyphenolic Substance of *Mytilus edulis*: Novel Adhesive Containing L-Dopa and Hydroxyproline,” *Science*, vol. 212, pp. 1038–1040, May 1981.
- [125] H. J. Meredith, C. L. Jenkins, and J. J. Wilker, “Enhancing the Adhesion of a Biomimetic Polymer Yields Performance Rivaling Commercial Glues,” *Advanced Functional Materials*, vol. 24, no. 21, pp. 3259–3267, 2014.
- [126] S. Hong, K. Yang, B. Kang, C. Lee, I. T. Song, E. Byun, K. I. Park, S. W. Cho, and H. Lee, “Hyaluronic Acid Catechol: A Biopolymer Exhibiting a pH-Dependent Adhesive or Cohesive Property for Human Neural Stem Cell Engineering,” *Advanced Functional Materials*, vol. 23, no. 14, pp. 1774–1780, 2013.
- [127] J. Yu, W. Wei, M. S. Menyo, A. Masic, J. H. Waite, and J. N. Israelachvili, “Adhesion of mussel foot protein-3 to TiO₂ surfaces: the effect of pH,” *Biomacromolecules*, vol. 14, pp. 1072–1077, Apr. 2013.
- [128] G. Bilic, C. Brubaker, P. B. Messersmith, A. S. Mallik, T. M. Quinn, C. Haller, E. Done, L. Gucciardo, S. M. Zeisberger, R. Zimmermann, J. Deprest, and A. H. Zisch, “Injectable candidate sealants for fetal membrane repair: bonding and toxicity in vitro,” *American Journal of Obstetrics & Gynecology*, vol. 202, pp. 85.e1–85.e9, Jan. 2010.

- [129] K. J. Winstanley, A. M. Sayer, and D. K. Smith, "Anion binding by catechols—an NMR, optical and electrochemical study," *Organic & Biomolecular Chemistry*, vol. 4, no. 9, pp. 1760–1767, 2006.
- [130] B. Mizrahi, X. Khoo, H. H. Chiang, K. J. Sher, R. G. Feldman, J.-J. Lee, S. Irusta, and D. S. Kohane, "Long-lasting antifouling coating from multi-armed polymer," *Langmuir*, vol. 29, pp. 10087–10094, Aug. 2013.
- [131] Y. Ai, Y. Wei, J. Nie, and D. Yang, "Study on the synthesis and properties of mussel mimetic poly(ethylene glycol) bioadhesive," *Journal of Photochemistry and Photobiology. B, Biology*, vol. 120, pp. 183–190, Mar. 2013.
- [132] B.-H. Im, J.-H. Jeong, M. R. Haque, D. Y. Lee, C.-H. Ahn, J. E. Kim, and Y. Byun, "The effects of 8-arm-PEG-catechol/heparin shielding system and immunosuppressive drug, FK506 on the survival of intraportally allotransplanted islets," *Biomaterials*, vol. 34, pp. 2098–2106, Mar. 2013.
- [133] S. Mondini, C. Drago, A. M. Ferretti, A. Puglisi, and A. Ponti, "Colloidal stability of iron oxide nanocrystals coated with a PEG-based tetra-catechol surfactant," *Nanotechnology*, vol. 24, p. 105702, Feb. 2013.
- [134] T. Kotsokechagia, N. M. Zaki, K. Syres, P. d. Leonardis, A. Thomas, F. Cellisi, and N. Tirelli, "PEGylation of Nanosubstrates (Titania) with Multifunctional Reagents: At the Crossroads between Nanoparticles and Nanocomposites," *Langmuir*, vol. 28, pp. 11490–11501, Aug. 2012.
- [135] T. Gillich, E. M. Benetti, E. Rakhmatullina, R. Konradi, W. Li, A. Zhang, A. D. Schlüter, and M. Textor, "Self-assembly of focal point oligo-catechol ethylene glycol dendrons on titanium oxide surfaces: adsorption kinetics, surface characterization, and nonfouling properties," *Journal of the American Chemical Society*, vol. 133, pp. 10940–10950, July 2011.
- [136] C. E. Brubaker, H. Kissler, L.-J. Wang, D. B. Kaufman, and P. B. Messersmith, "Biological performance of mussel-inspired adhesive in extrahepatic islet transplantation," *Biomaterials*, vol. 31, pp. 420–427, Jan. 2010.
- [137] A. Statz, J. Finlay, J. Dalsin, M. Callow, J. A. Callow, and P. B. Messersmith, "Algal antifouling and fouling-release properties of metal surfaces coated with a polymer inspired by marine mussels," *Biofouling*, vol. 22, pp. 391–399, Jan. 2006.
- [138] J. L. Dalsin, L. Lin, S. Tosatti, J. Vörös, M. Textor, and P. B. Messersmith, "Protein Resistance of Titanium Oxide Surfaces Modified by Biologically Inspired mPEG-DOPA," *Langmuir*, vol. 21, pp. 640–646, Jan. 2005.

- [139] B. P. Lee, J. L. Dalsin, and P. B. Messersmith, "Synthesis and gelation of DOPA-Modified poly(ethylene glycol) hydrogels," *Biomacromolecules*, vol. 3, no. 5, pp. 1038–1047, 2002.
- [140] J. Sedó, J. Saiz Poseu, F. Busqué, and D. Ruiz Molina, "Catechol-based biomimetic functional materials," *Advanced Materials*, vol. 25, pp. 653–701, Feb. 2013.
- [141] H. Lee, K. D. Lee, K. B. Pyo, S. Y. Park, and H. Lee, "Catechol-Grafted Poly(ethylene glycol) for PEGylation on Versatile Substrates," *Langmuir*, vol. 26, no. 6, pp. 3790–3793, 2010.
- [142] W. Wei, J. Yu, M. A. Gebbie, Y. Tan, N. R. Martinez Rodriguez, J. N. Israelachvili, and J. H. Waite, "Bridging Adhesion of Mussel-Inspired Peptides: Role of Charge, Chain Length, and Surface Type," *Langmuir*, vol. 31, pp. 1105–1112, Jan. 2015.
- [143] M. Yu and T. J. Deming, "Synthetic Polypeptide Mimics of Marine Adhesives," *Macromolecules*, vol. 31, pp. 4739–4745, July 1998.
- [144] V. Ball, D. D. Frari, V. Toniazzo, and D. Ruch, "Kinetics of polydopamine film deposition as a function of pH and dopamine concentration: Insights in the polydopamine deposition mechanism," *Journal of Colloid And Interface Science*, vol. 386, pp. 366–372, Nov. 2012.
- [145] C. R. Matos-Pérez, J. D. White, and J. J. Wilker, "Polymer composition and substrate influences on the adhesive bonding of a biomimetic, cross-linking polymer," *Journal of the American Chemical Society*, vol. 134, pp. 9498–9505, June 2012.
- [146] C. L. Jenkins, H. J. Meredith, and J. J. Wilker, "Molecular Weight Effects upon the Adhesive Bonding of a Mussel Mimetic Polymer," *ACS Applied Materials & Interfaces*, vol. 5, pp. 5091–5096, June 2013.
- [147] J. Yu, W. Wei, E. Danner, R. K. Ashley, J. N. Israelachvili, and J. H. Waite, "Mussel protein adhesion depends on interprotein thiol-mediated redox modulation," *Nature Chemical Biology*, vol. 7, pp. 588–590, Sept. 2011.
- [148] H. Lee, N. F. Scherer, and P. B. Messersmith, "Single-molecule mechanics of mussel adhesion," *Proceedings of the National Academy of Sciences of the United States of America*, vol. 103, no. 35, pp. 12999–13003, 2006.
- [149] K. H. Tan and R. Nishida, "Methyl eugenol: Its occurrence, distribution, and role in nature, especially in relation to insect behavior and pollination," *Journal of Insect Science*, vol. 12, pp. 1–74, 2012.
- [150] R. D. Crouch, "Selective deprotection of silyl ethers," *Tetrahedron*, vol. 69, pp. 2383–2417, Mar. 2013.

- [151] J. Heo, T. Kang, S. G. Jang, D. S. Hwang, J. M. Spruell, K. L. Killops, J. H. Waite, and C. J. Hawker, "Improved Performance of Protected Catecholic Polysiloxanes for Bioinspired Wet Adhesion to Surface Oxides," *Journal of the American Chemical Society*, vol. 134, no. 49, pp. 20139–20145, 2012.
- [152] J. K. Sprafke, J. M. Spruell, K. M. Mattson, D. Montarnal, A. J. McGrath, R. Pöttsch, D. Miyajima, J. Hu, A. A. Latimer, B. I. Voit, T. Aida, and C. J. Hawker, "Revisiting thiol-yne chemistry: Selective and efficient monoaddition for block and graft copolymer formation," *Journal of Polymer Science Part A: Polymer Chemistry*, vol. 53, pp. 319–326, Aug. 2014.
- [153] B. F. Lee, M. Wolffs, K. T. Delaney, J. K. Sprafke, F. A. Leibfarth, C. J. Hawker, and N. A. Lynd, "Reactivity Ratios and Mechanistic Insight for Anionic Ring-Opening Copolymerization of Epoxides," *Macromolecules*, vol. 45, pp. 3722–3731, May 2012.
- [154] J. D. White and J. J. Wilker, "Underwater Bonding with Charged Polymer Mimics of Marine Mussel Adhesive Proteins," *Macromolecules*, vol. 44, pp. 5085–5088, July 2011.